Regulation of expression, purification and structural determination of the cross-wall splitting protein PcsB in *Streptococcus pneumoniae*

Regulering av ekspresjon, rensing og strukturbestemmelse av PcsB, enzymet som kløyver septal cellevegg hos *Streptococcus pneumoniae*

Philosophiae Doctor (PhD) Thesis

Gro Anita Stamsås

Department of Chemistry, Biotechnology and Food Science
Faculty of Veterinary Medicine and Bioscience
Norwegian University of Life Sciences

Ås 2015

Thesis number 2015:8
ISSN 1894-6402
ISBN 978-82-575-1265-1

Table of Contents

Acknowledgements

The present work was carried out in the Molecular Microbiology group, Department of Chemistry, Biotechnology and Food Science at The Norwegian University of Life Sciences from 2010 to 2015. The work was supported by the Research Council of Norway.

First of all, I would like to thank my supervisor Professor Leiv Sigve Håvarstein. Your dedication to your field is very inspiring. Thank you for always being available and for patiently answering all my questions and sharing your knowledge with me. Thanks for giving me the opportunity to learn so much from you.

I would also like to express my gratefulness to my co-supervisor Dr. Daniel Straume. Thank you for never giving up on me, and for your patient guidance. Thank you for always having suggestions on how to improve my experiments, and explanations for why experiments went wrong. Your lab skills are truly impressive, and I have learned so much from you. You have been a great support, and I could not have done this without you.

Zhian Salehian, thank you for all the help in the lab. Your famous quotes as "If I don`t have time, I will make time" and "I am not stressed, I am just harmoniously stressed" describes your positive personality very well. Your everyday high spirits affects everyone in your presence, and you have become a highly valued colleague and friend.

Dr. Kari Helene Berg has been a tremendous support the last four and a half years. Thank you, for not only sharing your lab expertise with me, but also for becoming a very close friend. I hope that we will continue our traditions involving "dansband-weekends" at sea, calm dinners in "Brattbakken" and cooking of insane amounts of caramel. Our risky mountain expeditions would be impossible to perform without your famous pressure therapy, red wine and your mum`s homemade "mjølkekaker".

Sergio Bartual deserves to be acknowledged for not only contributing to our joint paper, but also for explaining me the basics in crystallography.

Elin Ørmen and Hilde Kolstad at the Imaging Centre has contributed during SEM and TEM imaging. Your help is highly appreciated.

Finally, thanks to my family and friends for all your support during these years.

Ås, January 2015

Gro Anita Stamsås

Summary

The human pathogen *Streptococcus pneumoniae* causes approximately 1.6 million deaths per year. Hence, it is of great concern that the bacterium`s resistance against antibiotics has increased dramatically in recent decades. If this development continues, currently prescribed antibiotics might become useless. For this reason, it is important to identify new drug targets and antibiotics that can be used to fight pneumococcal infections. The cell wall synthesis machinery and the cell division apparatus are attractive targets for development of new antimicrobial agents. However, much remains to be learned about these processes in *S. pneumoniae* and other bacteria. Further research on bacterial cell division and cell wall synthesis is therefore needed.

The integrity of the cell wall protects bacterial cells from turgor pressure-induced lysis during cell division. The synthesis and splitting of the new cross wall are two operations that must be carefully coordinated. The two-component regulatory system WalRK is believed to play a central coordinating role in these processes. The gene *pcsB*, which is under WalRK control, encodes an enzyme that has been predicted to split the septal cross wall during cell division.

In the present work a tandem affinity tag was designed in order to purify large amounts of recombinant PcsB to a high degree of purity. A successful crystallization of the protein was achieved, and its unique 3D structure was solved. The structure revealed an N-terminal coiled-coil domain consisting of five helices, attached to the C-terminal catalytic cysteine-histidine-dependent amidohydrolase/peptidase (CHAP) domain via an alanine-rich linker. Strikingly, PcsB adopts a dimeric structure in which the catalytic domains are facing each other, and the V-shaped coiled-coil domains acts as molecular “tweezers” locking the catalytic domain of each monomer in an inactive configuration. In fact, the CHAP domain of one PcsB monomer is inserted into the internal cavity of the coiled-coil domain of the other. PcsB exists as a mixture of dimers and monomers in solution. Analytical ultracentrifugation and SAXS (small-angle X-ray scattering) experiments showed that in solution, monomeric PcsB is in an inactive conformation with the CHAP domain inserted in its own coiled-coil domain. Once this became clear we were able to demonstrate that PcsB has enzymatic activity by expressing and purifying a recombinant protein consisting only of

the CHAP domain. Thus, for the first time, *in vitro* muralytic activity was detected for PcsB, settling the long-standing question of whether it is a cell wall hydrolase or not.

The dimeric structure, in which the two monomers are locked "head to head" in an inactive state, led us to propose a model describing how PcsB might function during cell division. In order to become active, the CHAP domains have to be released, probably by conformational changes within the coiled-coil domain. The energy needed for this conformational change is probably provided by the ATPase FtsE. FtsE and its partner FtsX form a complex that has been previously shown to directly interact with PcsB. Furthermore, since PcsB forms a linear dimer of 164 Å in length, it should be long enough to extend across the septal cross wall and reach the transmembrane FtsX protein in each daughter cell. This suggests that splitting of the septal cross wall is a cooperative process that requires the coordinated participation of both cells.

Transcription of the *pcsB* gene is known to be controlled by the WalRK two-component regulatory system. However, the signal(s) sensed by the WalK histidine kinase has been a mystery for decades. In contrast to most low-GC Gram-positive bacteria, the WalK protein of *S. pneumoniae* and other streptococci does not contain an extracellular sensor domain. Hence, it has been speculated that pneumococcal WalK senses an intracellular signal, and that the single transmembrane segment only serves as a membrane anchor. By using alanine substitution mutagenesis and domain swapping between *S. pneumoniae* and *Streptococcus thermophilus* WalK proteins, we have obtained strong evidence indicating that the single transmembrane segment of WalK senses or relays a signal that regulates its kinase and/or phosphatase activity. Furthermore, we verified previous findings that deletion of a eukaryotic-type serine/threonine protein kinase called StkP, leads to decreased expression of the *pcsB* gene. Interestingly, our results suggest that StkP does not regulate *pcsB* expression by phosphorylating WalR as previously assumed. Instead, we obtained evidence that this regulation depends on WalK, and that StkP might be able to influence the kinase and/or phosphatase activity of WalK through direct physical interaction.

Sammendrag

Den humanpatogene *Streptococcus pneumoniae* forårsaker omtrent 1,6 millioner dødsfall hvert år. Derfor er det knyttet stor bekymring til at bakteriens resistens mot antibiotika har økt dramatisk de siste tiårene. Dersom denne utviklingen fortsetter vil trolig dagens antibiotika ikke lenger fungere. For å kunne behandle infeksjoner forårsaket av bakterien i fremtiden, er det derfor viktig å identifisere nye mål for antibiotika. Cellevegg-syntesemaskineriet og celledelingsapparatet er attraktive mål i utviklingen av nye antibiotika. Dessverre er disse prosessene fremdeles dårlig karakterisert i *S. pneumoniae* og i andre bakterier. Derfor trengs det mer forskning på celledeling og celleveggsyntese i bakterier.

Celleveggen beskytter bakteriene fra lysis forårsaket av turgor trykket under celledeling. Derfor må syntese og kløyving av septal cellevegg være to finkoordinerte prosesser. To-komponent systemet WalRK spiller trolig en sentral rolle i denne koordineringen. Genet *pcsB,* som er regulert av WalRK, koder for et enzym som er antatt å kløyve septal cellevegg under celledeling.

I dette arbeidet ble en tandem affinitetsmarkør utviklet for å rense store mengder rekombinant PcsB til en høy grad av renhet. En suksessfull krystallisering av proteinet ble oppnådd og dets unike 3D struktur ble løst. Strukturen avslørte at det N-terminale «coiled-coil»-domenet, som bestod av fem helikser, var festet til det C-terminale katalytiske cystein-histidin-avhengige amidohydrolase/peptidase (CHAP)-domenet med en «linker» rik på alanin. Overraskende fant vi at PcsB foreligger som dimerer med de katalytiske domenene vendt mot hverandre. De V-formede «coiled-coil»-domenene foreligger som molekylære «pinsetter» som stenger det katalytiske domenet fra hver monomer i en inaktiv konfigurasjon. CHAP-domenet fra én PcsB monomer er satt inn og blokkert i «coiled-coil» domenet fra den andre. PcsB foreligger som en blanding av monomerer og dimerer i løsning. Analytisk ultrasentrifugering og SAXS (small-angle X-ray scattering) eksperimenter viste at monomerer i løsning foreligger i en inaktiv konformasjon med CHAP-domenet satt inn og blokkert i sitt eget «coiled-coil» domene. Da disse observasjonene ble gjort kunne enzymatisk aktivitet påvises ved å uttrykke et rekombinant protein kun bestående av

CHAP-domenet. Dermed kunne *in vitro* enzymatisk aktivitet for første gang bli påvist for PcsB, og spørsmålet om PcsB var en cellevegg hydrolase eller ikke endelig besvares.

Dimerstrukturen hvor to monomerer foreligger «hode mot hode» og låst i en inaktiv konformasjon i hverandres «coiled-coil» domene, er grunnlaget for vår modell som trolig beskriver PcsB sin rolle under celledeling. For å kunne bli aktiv må CHAP-domenet slippes fri. Trolig skjer dette via konformasjonsendringer i «coiled-coil»-domenet. Energien som denne konformasjonsendringen krever, kommer trolig av ATPase aktivitet fra FtsE. FtsE og dens partner FtsX danner et kompleks som tidligere er vist å interagere med PcsB. Siden PcsB danner en lineær dimer på 164 Å i lengde, burde dette være langt nok til å rekke over den septale celleveggen og nå det transmembrane FtsX proteinet i hver dattercelle. Kløyving av septal cellevegg foreslås derfor å være en samarbeidsprosess som krever koordinert deltagelse fra begge celler.

Det er kjent at transkripsjon av genet *pcsB* er kontrollert av to-komponentsystemet WalRK, men signalet eller signalene som WalRK mottar har vært et mysterium i flere tiår. I motsetning til andre Gram-positive bakterier med lavt GC-innhold så har ikke WalK proteinet i *S. pneumoniae* og andre streptokokker noe ekstracellulært sensordomene. Derfor har det blitt spekulert i at WalK i *S. pneumoniae* mottar et signal intracellulært, og at det enslige transmembrane segmentet kun fungerer som et membrananker. Ved å bruke alanin substitusjons-mutagenese og bytting av domener mellom WalK proteinene i *S. pneumoniae* og *Streptococcus thermophilus,* har vi samlet sterke data som tyder på at WalK sitt enslige transmembransegment enten mottar eller videresender et signal som regulerer kinase- eller fosfatase-aktiviteten. Videre har vi verifisert tidligere funn hvor delesjon av en eukaryot type serin/treonin protein kinase ved navn StkP forårsaker nedregulering av *pcsB*-ekspresjon. Resultatene våre indikerer at StkP ikke regulerer *pcsB*-ekspresjon ved å fosforylere WalR, som tidligere er foreslått. I stedet tyder våre resultater på at StkP mediert regulering av *pcsB* avhenger av WalK, og at StkP kanskje kan interagere direkte med WalK og påvirke kinase/fosfatase aktiviteten til WalK.

List of papers

List of papers included in the thesis

Paper I

Stamsås GA, Håvarstein LS and Straume D (2013) CHiC, a new tandem affinity tag for the protein purification toolbox. Journal of Microbiological Methods 92(1): 59-63.

Paper II

Bartual SG, Straume D, **Stamsås GA**, Muñoz IG, Alfonso C, Martínez-Ripoll M, Håvarstein LS and Hermoso JA (2014) Structural basis of PcsB-mediated cell separation in *Streptococcus pneumoniae*. Nature Communications 5: 3842

Paper III

Stamsås GA, Straume D, Salehian Z and Håvarstein LS. The single transmembrane segment of pneumococcal WalK is required for the perception of an intramembrane or extracellular signal. (Manuscript)

Other papers by the author, not included in the thesis

Berg KH, **Stamsås GA**, Straume D and Håvarstein LS (2013) The effect of low PBP2b levels on cell morphology and peptidoglycan composition in *Streptococcus pneumoniae* R6. Journal of Bacteriology 195(19): 4342-4354.

Straume D, **Stamsås GA** and Håvarstein LS (2014) Natural transformation and genome evolution in *Streptococcus pneumoniae*. Infection, Genetics and Evolution (2014).

1. Introduction

Almost all bacteria are surrounded by a cell wall that protects the cell from its internal turgor pressure and gives the bacterium its shape. In order to divide, bacteria must synthesize a new septal cell wall (also called cross-wall) that separates the two daughter cells. This cross-wall needs to be split down the middle by cell wall hydrolases for the bacteria to divide, but the precise mechanism underlying this fundamental process is still poorly understood. In the important human pathogen *Streptococcus pneumoniae* the putative cell wall hydrolase PcsB is predicted to be a key player in this operation. The work in this thesis has focused on characterizing the activity and structure of PcsB, and how expression of this protein is regulated.

1.1 *Streptococcus pneumoniae*

S. pneumoniae is a Gram-positive bacterium belonging to the Mitis group of streptococci together with 11 other species [1]. It colonizes the human nasopharynx, and can cause diseases ranging from mild respiratory infections to more severe life threatening conditions like meningitis or bacteremia [2, 3]. The World Health Organization (WHO) has estimated that this bacterium is responsible for 1.6 million human deaths per year, with the majority being children and elderly in developing countries [4]. Humans of any age can be colonized by *S. pneumoniae*, however it is most common during infancy. In adults, median duration of carriage is 31 days while it is 60 days for children [3]. The main reason for pneumococcal transmission between people is the carriage of this bacterium by young children [2]. *S. pneumoniae* is a polysaccharide-encapsulated bacterium. The capsule functions as an important virulence factor that helps the bacterium to establish an infection and to evade the host immune system [5]. More than 90 different serotypes are identified, all different in their chemical composition of the capsule. [2]. According to WHO, the present pneumococcal vaccines are based on the polysaccharide capsule from 7, 10, 13 and 23 different serotypes.

When a person is infected with *S. pneumoniae*, he or she is treated with antibiotics, primarily β-lactam antibiotics such as penicillin. β-lactams bind to and inhibit the active transpeptidase site of

so-called penicillin binding proteins (PBPs) [6], which are responsible for polymerization of the peptidoglycan layer that surrounds the cytoplasmic membrane of most bacteria. When peptidoglycan synthesis is inhibited, the cells can no longer grow and divide and the infection is treated. However, resistance against many of the most commonly used penicillins is starting to become a medical concern worldwide [7-9]. Penicillin resistance in pneumococci is caused by alterations in the transpeptidase domain of the PBPs, which decrease their affinity for β-lactams [9]. As *S. pneumoniae* is a natural competent bacterium, the high plasticity of its genome combined with the use of penicillins to treat infections contribute extensively to the spread of PBPs with low β-lactam affinity among pneumococcal strains [7]. The increased number of antibiotic resistant isolates that has been reported in recent years has resulted in more research aimed at learning more about bacterial cell division and their cell wall metabolism. This is very important not only for the academic interest of understanding these fundamental processes in the bacterial life cycle, but it will also provide valuable information with respect to antibiotic resistance and drug target discovery.

1.2 Structure of the pneumococcal cell wall

1.2.1 Pneumococcal peptidoglycan structure

Peptidoglycan is the main cell wall polymer that envelopes the cytoplasmic membrane. This giant molecule, called the sacculus, protects the cell from lysis due to turgor pressure, gives the cell its shape and functions as an anchoring point for other cell wall components [10, 11]. The backbone of peptidoglycan consists of alternating N-acetylglucosamine (GlcNAc) and N-acetylmuramic acid (MurNAc) residues. The MurNAc residue has a pentapeptide called stem peptide attached to it. In *S. pneumoniae*, the amino acid sequence of the stem peptide is L-Ala-D-*i*Gln-L-Lys-D-Ala-D-Ala where the L-Ala residue is attached to the MurNAc (Figure 1) [10, 12]. This pentapeptide can be crosslinked with neighboring stem peptides by PBPs or cleaved by carboxypeptidases [13]. Crosslinking occurs between the ε-amino group of L-Lys in position three of one peptide, and the carboxyl group of the D-Ala residue at position four of the other peptide [10]. The energy needed for performing this reaction is provided by the release of the terminal D-Ala residue of the donor peptide [14]. Some of the peptides contain an interpeptide bridge, either L-Ser-L-Ala or L-Ala-L-

Ala linked to their lysine residue (Figure 1) [13]. Hence, the peptidoglycan contains a mixture of non-cross-linked stem peptides and peptides that are cross-linked directly or via interpeptide bridges.

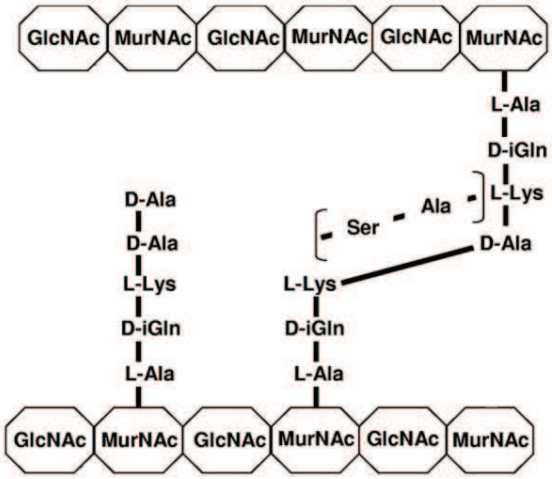

Figure 1. **Peptidoglycan structure in *S. pneumoniae.*** Alternating units of N-acetylglucosamine (GlcNAc) and N-acetylmuramic acid (MurNAc) make up the glycan chains, which are connected via stem peptides. The stem peptides are attached to MurNAc and can be crosslinked either directly or indirectly via an interpeptide bridge consisting of L-Ala-L-Ala or L-Ser-L-Ala. The figure is modified from Barendt et al. [15] and reprinted with permission from American Society for Microbiology.

Two models have been proposed with respect to the orientation of the glycan strands in the peptidoglycan layer. One model presents the glycan strands standing perpendicular to the cell surface and the other most preferred model presents the glycan chains lying parallel to the cell surface [10, 16-22]. The "inside-to-outside" model for cell wall synthesis suggests that new peptidoglycan is inserted at the inner surface of the cell wall, parallel to the cell surface, in a non-stretched form. The outer stretched layers of peptidoglycan are thought to be subjected to hydrolytic activity, resulting in an outwards movement of the inner peptidoglycan layers [14].

The length of the glycan chains varies between different bacterial species. For *Bacillus subtilis*, the chain length has been reported to be in the range of 50-250 disaccharide units [10, 13], while others report chains up to 5000 disaccharides in length [17]. In *Staphylococcus aureus*, the chain length is estimated to be much shorter, approximately 18 disaccharide units long [10, 13]. The length of glycan chains in *S. pneumoniae* is predicted to be more similar to those in *B. subtilis* than

S. aureus [13]. The biological purpose of different glycan chain lengths among bacteria is not known.

1.2.2 Teichoic acid, an essential cell wall polymer in *S. pneumoniae*

The cell wall of *S. pneumoniae* contains a polymer called teichoic acid. Two types of this polymer are present in *S. pneumoniae*, wall teichoic acid (WTA) and lipoteichoic acid (LTA). WTA is bound to MurNAc whereas LTA is attached to a lipid anchor. In most species, WTA and LTA differ in their primary structure, while for *S. pneumoniae* the repeating units of WTA and LTA are identical [13, 23-26]. Teichoic acids are essential in *S. pneumoniae* [23, 27], and play an important role in processes like regulation of cell wall hydrolases, transformability, resistance towards antimicrobial peptides and cell division [23-25]. The repeating unit of teichoic acids in *S. pneumoniae* consists of a 2-acetamido-4-amino-2,4,6-trideoxygalactose that is attached to a glucose residue, followed by a ribitol phosphate and two N-acetylgalactosamine residues that each carry a phosphorylcholine (Figure 2) [13, 24, 28, 29].

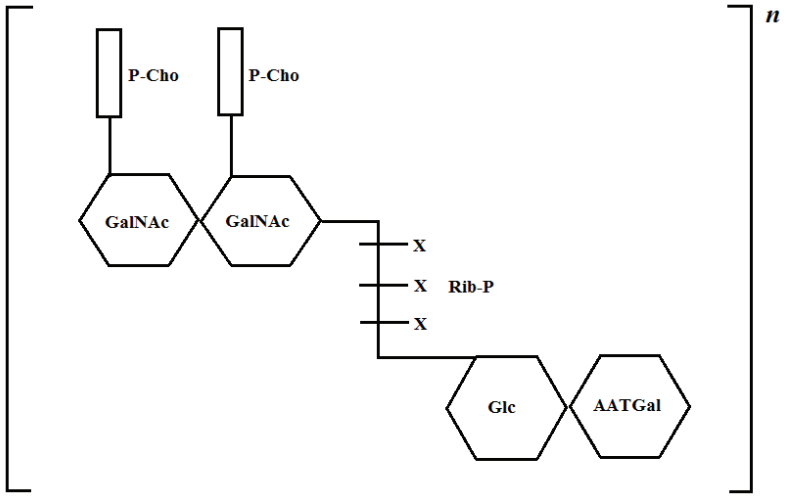

Figure 2. The repeating unit of teichoic acid in *S. pneumoniae*. The repeating unit that forms the teichoic acids consists of 2-acetamido-4-amino-2,4,6-trideoxygalactose (AATGal), glucose (Glc), ribitiol phosphate (Rib-P), two N-acetylgalactosamine residues (GalNAc) that carry a phosphorylcholine (P-Cho) each. Ribitol can be decorated with D-Ala or GalNAc residues, marked X in the figure [24].

Synthesis of the repeating unit of teichoic acids requires the gene products of at least 16 genes. These include the gene products of *licABC,* that perform uptake and activation of choline, while

the gene products of the *tarIJ* genes synthesize activated ribitol (CDP-ribitol) [24]. The transporter TacF transfers the precursor across the cell membrane. TacF is only able to transport teichoic acid precursors containing choline [24, 30]. Hence, absence of choline results in a situation where the teichoic acid precursor remains attached to the carrier lipid anchor, making this carrier unavailable for peptidoglycan precursors, thereby inhibiting cell wall synthesis [31, 32].

1.3 Peptidoglycan synthesis and cell division in *S. pneumoniae*

1.3.1 Peptidoglycan synthesis

The synthesis of peptidoglycan can be divided into three major steps: (i) the synthesis of precursors in the cytoplasm, (ii) the synthesis of lipid-linked intermediates and (iii) extracellular polymerization. In the cytoplasm, uridine diphosphate-GlcNAc (UDP-GlcNAc) is synthesized from fructose-6-phosphate. UDP-MurNAc is then synthesized from UDP-GlcNAc by the two enzymes MurA and MurB. MurC, D, E and F are responsible for assembly and attachment of the stem peptide, which leads to the UDP-MurNAc-pentapeptide [33, 34]. The synthesis of the lipid-linked intermediates starts with the transfer of the UDP-MurNAc-pentapeptide to the membrane-bound undecaprenyl phosphate also called bactoprenol. This reaction is carried out by MraY, and results in the formation of undecaprenyl-pyrophosphoryl-MurNAc-pentapeptide, also called lipid I. The transfer of UDP-GlcNAc to lipid I, by MurG, gives rise to lipid II (undecaprenyl-pyrophosphoryl-MurNAc-pentapeptide-GlcNAc). Several modifications of the precursor can occur at the lipid II level. Two examples are the attachment of an interpeptide bridge to the stem peptide by MurM and MurN, and amidation of the D-Glu residue in position two in the stem peptide by MurT and GatD, creating D-*i*Gln [14, 34-36]. Interestingly, about 98% of the crosslinked stem peptides in the pneumococcal cell wall are found to have D-*i*Gln instead of D-Glu [13]. In fact, assembly of peptidoglycan performed *in vitro* shows that this residue has to be amidated into iso-glutamine for efficient crosslinking to occur [36]. Lipid II is then translocated to the extracellular side of the membrane by an unknown mechanism, however FtsW and RodA are thought to function as lipid II flippases [14, 34, 35].

During extracellular polymerization of peptidoglycan, PBPs catalyze both transglycosylation and transpeptidation of peptidoglycan, using lipid II as substrate. The genome of *S. pneumoniae* encodes six PBPs. Three class A PBPs called PBP1a, PBP1b and PBP2a are able to catalyze both transglycosylation and transpeptidation, while the two class B PBPs named PBP2b and PBP2x are only able to catalyze transpeptidation [34, 36-39]. PBP3 is a carboxypeptidase that removes the terminal D-Ala residue of the pentapeptide, resulting in a tetrapeptide [39, 40]. *S. pneumoniae* also possesses another carboxypeptidase DacB that removes the amino acid in position four, creating a tripeptide [38, 39]. Removal of both terminal D-Ala residues results in a stem peptide unavailable for transpeptidation [37]. These two carboxypeptidases regulate the amount of substrate available for transpeptidation performed by the other PBPs [39]. β-lactam antibiotics inhibit the transpeptidase activity of PBPs due to structural resemblance to their natural D-Ala-D-Ala stem peptide substrate. β-lactams bind within the active site to form a covalent adduct that results in inhibition of PBP activity [6, 37, 41].

In contrast to coccoid bacteria like *S. aureus,* which are thought to only possess septal peptidoglycan synthesis, the ovococcal *S. pneumoniae* most likely performs both peripheral and septal peptidoglycan synthesis. The pneumococcal peptidoglycan synthesis machinery therefore resembles the machinery found in rod shaped bacteria [14, 42]. Two models are proposed that explain how septal and peripheral cell wall synthesis occur. One model suggests formation of only one protein complex that performs both actions. The other model presents two independent protein complexes; one called the divisome, and the other elongasome [36, 38, 43]. Three proteins named StkP, DivIVA and GpsB are thought to be part of a molecular switch that guides the cell between septal and peripheral cell wall synthesis. The kinase StkP localizes to midcell where it phosphorylates, and thereby modulates the activity of DivIVA. While unphosphorylated DivIVA is thought to stimulate peripheral cell wall synthesis, phosphorylated DivIVA does not promote this. The DivIVA paralog GpsB counteracts peripheral cell wall synthesis by stimulating StkP phosphorylation of DivIVA [43]. How this switch is timed and regulated during cell division is still an open question.

1.3.2 Pneumococcal cell division

For normal bacterial cell division to occur, membrane invagination, cell wall synthesis and chromosome segregation must be coordinated [44]. The sacculus must grow and divide in a manner that still protects the cells from lysis due to turgor pressure [11, 34]. In Gram-negative bacteria, the septum synthesis, membrane invagination and cell separation are thought to occur simultaneously. In contrast, cell division in Gram-positive bacteria consists of two separate events: septation and daughter cell separation. The septal cross-wall is often fully synthesized before it is cleaved down the middle [45]. In *S. aureus,* this septal wall consists of two layers of peptidoglycan and a mid-zone. This mid-zone is thought to contain active hydrolytic enzymes, which cleave the septal wall down the middle to separate the two daughter cells [45, 46]. In *Streptococcus gordonii* and *S. pneumoniae,* this cleavage seems to occur simultaneously as synthesis of the new cross wall progresses [44, 47, 48].

The exact order in which cell division proteins are recruited to the division site in *S. pneumoniae* is not well understood. What we do know is that early in the division process the membrane protein MapZ (also called LocZ) localizes to mid-cell to form a ring-like structure at the cell`s equator (Figure 3) [49, 50]. MapZ finds the mid-cell position via its extracellular domain, and it is believed that it recognizes a mid-cell specific structure in the peptidoglycan such as the equatorial mark, which can be seen on the cell surface. Once formed, the MapZ ring recruits the tubulin-like FtsZ protein to the division site, which then polymerizes into a Z-ring [38, 44, 49]. Many cell division proteins, like DivIVA, PBP1a and PBP2x, do not localize to the septum until the FtsZ-ring is completely assembled [14, 38]. Evidence suggest that cytokinesis is driven by constriction of the Z-ring [51, 52]. Noteworthy, MapZ can be phosphorylated by the kinase StkP [53], but the significance of this is unclear since it does not seem to be crucial for MapZ function [50].

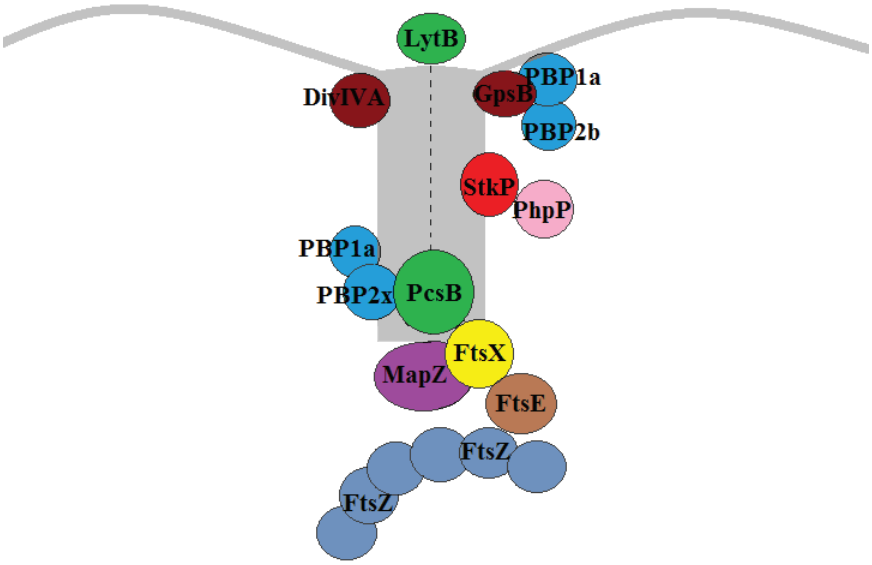

Figure 3. Simplified model of pneumococcal cell division. MapZ guides FtsZ to mid-cell before the FtsZ-ring recruits approximately 20 other proteins [49, 54]. PBP2x most probably contributes during cross wall synthesis while PBP2b contributes to peripheral peptidoglycan synthesis [55, 56]. StkP, DivIVA and GpsB are believed to function as a switch between septal and peripheral cell wall synthesis [43]. The putative cell wall hydrolase PcsB interacts with the FtsEX complex, and is assumed to take part in cross wall splitting [57]. The cell wall hydrolase LytB is responsible for the last step in daughter cell separation [58]

Two other proteins called FtsE and FtsX form a complex in the septum that are essential for normal cell division in *S. pneumoniae* [57]. Although the FtsEX complex resembles a transporter, the lack of charged residues in the transmembrane segments of FtsX suggests a different function. In *Escherichia coli,* FtsE interacts with FtsZ, and ATP-hydrolysis by FtsE contributes to constriction of the FtsZ ring [59-61]. Such a mechanism has never been found in *S. pneumoniae*. Instead, the pneumococcal FtsEX complex has been shown to interact with the putative cell wall hydrolase PcsB that is essential for normal cell division (Figure 3). When the cells divide, they must synthesize a septal cross-wall, and a crucial step is to split this cross-wall down the middle to separate the two daughter cells. How this is accomplished is poorly understood, but PcsB is proposed to be responsible for the cross-wall cleavage, and FtsEX most probably regulate its activity [57, 62]. The two daughter cells are finally released from each other by the enzyme LytB, which performs the final cuts in the cell wall between them [58].

1.4 Cell wall hydrolases in *S. pneumoniae*

Almost all bacteria possess cell wall hydrolases (also called murein hydrolases) that cleave covalent bonds in the peptidoglycan. This is essential in order to incorporate newly made peptidoglycan into the sacculus during cell division [11, 63, 64]. The crucial role of murein hydrolases during cell division has resulted in a high degree of redundancy in their hydrolytic activity [64, 65]. For example, seven different hydrolases can be removed simultaneously without affecting the growth rate in *E. coli* [66]. Being able to cleave the cell wall, these enzymes can potentially be lethal to the cells. Hence, the activity of cell wall hydrolases must be kept under tight control. This control occurs at both the transcriptional, translational and post-translational level [64, 67].

Cell wall hydrolases usually consist of two domains. One domain responsible for binding to the cell surface, while the other possesses hydrolytic activity [68]. In many cases, the binding domain has conserved repeating motifs in order to attach to the cell surface, for example lysM domains and choline-binding domains [64]. New enzymes have often evolved due to new combinations of binding-modules and hydrolytic-modules, so called domain shuffling [68-70]. One example is the major cell-separation enzyme in *Streptococcus thermophilus* called Cse, in which the cell wall binding LysM-domain from a protein encoded by a gene called *sip* was combined with the hydrolytic cysteine-histidine-dependent amidohydrolase/peptidase (CHAP) domain of PcsB [69].

Peptidoglycan hydrolases can be classified based on which bond in the peptidoglycan the enzyme cleaves. Different groups of hydrolytic enzymes include glycosidases, amidases and endopeptidases [63, 64, 71]. The glycosidases cleave the glycosidic β-1,4 bond between MurNAc and GlcNAc. This group includes both β-N-acetylmuramidases (lysozymes) and β-N-acetylglucosaminidases. The amidases constitute a group of enzymes that cleave the bond between the MurNAc and the first amino acid (L-Ala) in the stem peptide, whereas endopeptidases cut a peptide bond within the stem peptide of the peptidoglycan [63, 64, 68].

In *S. pneumoniae*, peptidoglycan hydrolases are important not only during cell division, they also affect several important processes like autolysis and fratricide. The best studied pneumococcal cell

wall hydrolase is its major autolysin LytA. It is an N-acetylmuramoyl-L-alanine amidase, which cleaves between L-Ala and MurNAc. It contributes to release of the pneumococcal cytolysin called pneumolysin during infection and to target cell lysis during fratricide. It consists of a choline-binding domain and a hydrolytic domain. In order to introduce cuts in the peptidoglycan, LytA depends on binding to the choline-decorated teichoic acids in the pneumococcal cell wall [72-76]. Interestingly, the strong affinity of the choline-binding domain to choline can be exploited in the purification of recombinant proteins. Since choline-binding domains bind the structure of tertiary alkylamines, proteins having this domain can be purified by affinity chromatography using a solid phase of diethylaminoethanol [77-79].

Other important cell wall hydrolases in *S. pneumoniae* include LytB, LytC and CbpD, which are all secreted choline-binding proteins. The enzyme LytB functions as an endo-β-N-acetylglucosaminidase responsible for cleaving peptidoglycan in the final step of daughter cell separation during cell division (see section 1.3.2). A LytB mutant therefore forms long chains of cells that are connected by a thin peptidoglycan filament [58, 71, 80, 81]. LytC is a lysozyme that performs hydrolytic activity on cell walls in which cuts have already been made by other cell wall hydrolases or on cell walls with non-crosslinked peptides [82]. The biological role of LytC is uncertain, although LytC has been shown to contribute both to autolysis at 30ºC and to cell lysis during fratricide [74, 83, 84]. CbpD is the key enzyme responsible for cell lysis during fratricide. It possesses a CHAP domain that introduces cuts in the cell wall of target cells, leading to cell lysis [74, 85, 86]. Even though many of the pneumococcal cell wall hydrolases play important roles in *S. pneumoniae*, only the putative cell wall hydrolase PcsB is reported to be essential (see section 1.3.2). Its function is not known, but it is required for normal cell division and is considered being the enzyme responsible for septal cross wall splitting.

1.5 PcsB, an essential putative cell wall hydrolase in *S. pneumoniae*

PcsB was first identified in *Streptococcus agalactiae* as a protein found to dominate in the supernatant. Homology searches show that PcsB is highly conserved among streptococci and

lactococci, while a partial homologue is found in some enterococci. The name PcsB, short for "protein required for cell separation in group B Streptococcus", derives from the observation that *pcsB* deletion mutants of *S. agalactiae* grew in clusters comprising many cells instead of chains as in wild-type cells. New septa were not initiated at mid-cell but at random positions and angles in the *pcsB* mutant, and unseparated cells continued to form new septa. The *pcsB* gene could only be removed in the presence of an osmoprotectant, indicating that the cells became sensitive towards osmotic pressure [87]. Overexpression of *pcsB* did not lead to elevated levels of PcsB in the supernatant. Therefore, the amount of secreted PcsB must be regulated either at the level of translation or secretion [88].

The initial studies on *pcsB* in *S. pneumoniae* suggested that it was an essential gene in this bacterium. Since *S. pneumoniae* only contains one copy of *pcsB*, while *S. agalactiae* contains several *pcsB* paralogues, it is speculated that this redundancy might be the reason for the non-essential role of *pcsB* in *S. agalactiae* [89-92]. However, subsequent studies could report *pcsB* as non-essential in four different genetic backgrounds of *S. pneumoniae,* among them the virulent TIGR4 strain. Removal of *pcsB* in TIGR4 resulted in a similar phenotype as described for *S. agalactiae*. In addition to the formation of large cell aggregates, it developed misplaced septa that were synthesized at abnormal angles relative to the old cell wall (Figure 4) [93, 94]. For the pneumococcal strains D39 (serotype 2) and R6 (descendant of serotype 2) *pcsB* is reported to be essential. The reason why TIGR4 can survive without *pcsB,* while the D39 and R6 strains cannot, is not known. A six days incubation at 37°C, however, allowed viable *pcsB* mutants of D39 to grow. It can therefore be argued that *pcsB* mutants in the virulent TIGR4 strain were obtained upon high selective pressure and accumulation of suppressor mutations [90].

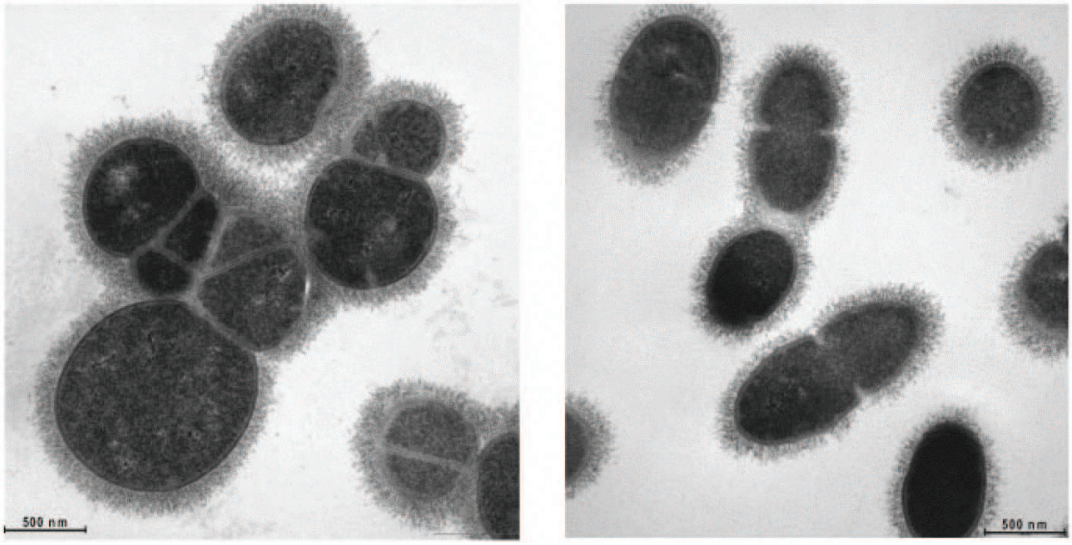

Figure 4. Morphology of a *pcsB* mutant of *S. pneumoniae* TIGR4. The left panel shows a *pcsB* mutant with unseparated cells growing in clusters with disrupted division angels. The panel to the right shows a *pcsB* mutant in which the *pcsB* expression has been restored by a plasmid containing the *pcsB* gene [94]. The figure is reprinted from Giefing-Kroll et al. [94] with permission from the Society for General Microbiology (SGM).

PcsB consists of four parts; (i) an N-terminal secretory signal peptide, (ii) a coiled-coil domain containing a leucine zipper motif, (iii) a linker and (iv) a C-terminal CHAP domain (Figure 5) [91, 94].

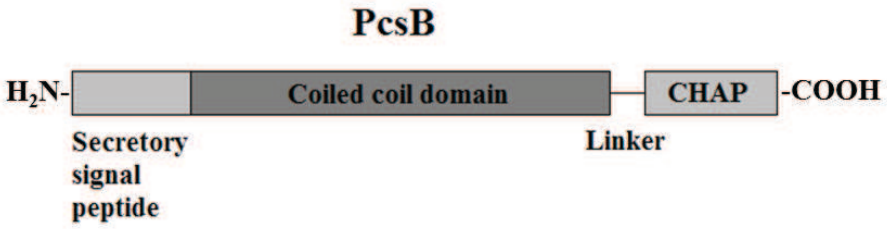

Figure 5. Predicted domain organization of pneumococcal PcsB. The N-terminal part consists of a secretory signal peptide. The coiled-coil domain is predicted to contain a leucine zipper motif. There is a linker between the coiled-coil domain and the predicted CHAP domain [91, 94].

PcsB is shown to localize to the septum and to the equatorial lines where ongoing cell wall synthesis occurs in *S. pneumoniae*, where it interacts with the FtsEX complex [57]. PcsB is very abundant in *S. pneumoniae*, estimated to be present at approximately 5000 monomers in each cell. However, the synthesis of PcsB must be even higher due to the high amount of PcsB that is found in the supernatant as well [90]. The reason why PcsB is needed in such high amounts is not clear, but normal cell growth is completely dependent on this high expression level. Only a small reduction in *pcsB* expression leads to severe defects in cell division [90]. Interestingly, PcsB is only detected in the supernatant and the membrane fractions of *S. pneumoniae,* but not in the cell wall fraction where it is predicted to act as a murein hydrolase [57, 95].

Transcriptional analyses of a TIGR4 *pcsB* mutant strain have shown altered expression of several genes. Of particular interest is the increased expression of two genes encoding so called LysM-domain proteins. Elevated expression of the corresponding genes, *spr0096* and *spr1875*, was also identified in a *pcsB* depleted R6 strain. Since LysM domains are cell wall binding modules, it is thought that these two proteins participate in cell wall metabolism. An up-regulation of these LysM-containing proteins might partially compensate for the loss of PcsB [90, 94].

1.5.1 Activation of cell wall hydrolases by the FtsEX complex during cell division

Many murein hydrolases involved in bacterial cell division are regulated by a protein complex consisting of FtsE and FtsX, as reported for *E. coli* and *B. subtilis*. FtsE is a cytoplasmic ATPase that interacts with FtsX which is embedded in the cytoplasmic membrane. In *E. coli*, the FtsEX complex contributes to constriction of the Z-ring during cell division [59-61]. In this bacterium, the proteins EnvC and NlpD activate three redundant amidases called AmiA, AmiB and AmiC that are responsible for septal cross-wall splitting during cell division. EnvC is shown to interact with a periplasmic loop of FtsX, and is only able to activate the amidases AmiA and AmiB when the FtsEX complex performes cytoplasmic ATP-hydrolysis. It is therefore believed that ATP-hydrolysis by FtsE results in a conformational change in FtsX that is transmitted to EnvC, leading to activation of the amidases AmiA and AmiB. This is an elegant way of controlling that these amidases are activated at the right place in the cell and not until assembly of the cytokinetic Z-ring is completed [96-99]. Similarly, a cell wall hydrolase called CwlO, needed for cell wall elongation

in *B. subtilis*, is shown to interact with FtsX, and its activation depends on ATP-hydrolysis by FtsE as well [100, 101].

The regulatory role of the FtsEX complex in the control of murein hydrolase activity is also seen in *S. pneumoniae*. As previously mentioned, the putative murein hydrolase PcsB is shown to interact with FtsX [57, 62]. The coiled-coil domain of PcsB interacts with the two extracellular loops ECL1 and ECL2 of FtsX (Figure 6). Because of the fact that FtsE, FtsX and PcsB all are essential in pneumococcal cell division, and that depletion of *ftsX* or *ftsE* gives rise to a Δ*pcsB* phenotype, it is believed that activation of PcsB requires interaction with FtsX. The energy derived from ATP-hydrolysis by FtsE probably induces a conformational change in FtsX that is transmitted to PcsB, which then becomes active. However, it is not known whether PcsB functions as a murein hydrolase, a scaffolding protein or as a regulator of another cell wall hydrolase [57, 62].

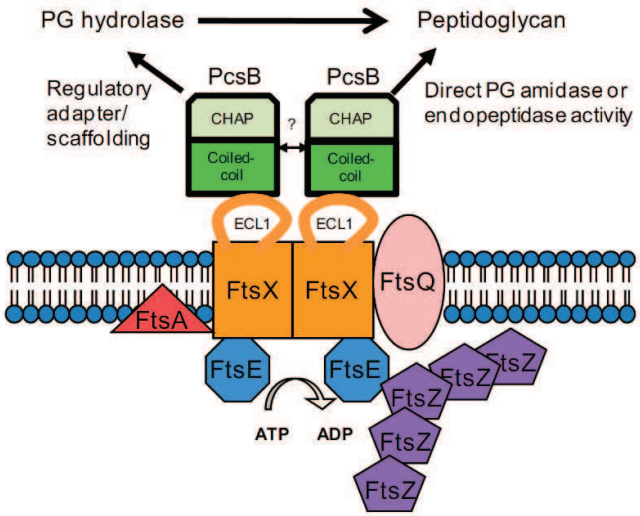

Figure 6. **Predicted model of PcsB activation in *S. pneumoniae*.** Membrane embedded FtsX interacts with the coiled-coil domain of PcsB via its extracellular loops ECL1 and ECL2 (ECL2 is not shown in the figure). Hydrolysis of ATP by FtsE in the cytoplasm most probably induces a conformational change in FtsX that is transferred via the ECL1 and ECL2 loops to PcsB, which then becomes active [57, 62]. The figure is reprinted from Sham et al. [57] with permission from PNAS.

1.5.2 Evidence for muralytic activity of PcsB are lacking

PcsB contains a CHAP domain, which is predicted to possess peptidoglycan hydrolytic activity. Other examples of proteins carrying this domain are CbpD from *S. pneumoniae* (see section 1.4), the cell separation enzyme Cse from *S. thermophilus* and the competence induced murein hydrolase LytF from *S. gordonii* [102-104]. CHAP domains have been shown to possess either amidase activity or endopeptidase activity resulting in cleavage of stem peptides in the peptidoglycan [68]. All members of the CHAP superfamily are predicted to possess the same hydrolytic mechanism, but very few CHAP-containing enzymes have been characterized with respect to their site of cleavage within the stem peptide [68, 102]. The active site comprises a catalytic triad where a cysteine performs a nucleophilic attack, a histidine residue functions as a proton donor, and a polar residue, usually asparagine or aspartic acid, contributes by orienting the histidine residue in the correct position [102].

Hydrolytic activity of PcsB has never been detected. Several attempts to demonstrate its activity have been conducted, but not one has yet succeeded. Even when the pneumococcal PcsB was tested in the presence of a recombinant ECL1 extracellular loop of FtsX, no muralytic activity was seen [57, 87, 88]. Furthermore, addition of recombinant PcsB into the medium of a *pcsB* mutant of *S. pneumoniae* TIGR4 did not restore wild-type phenotype [94]. These observations have led to speculations that PcsB does not function as a cell wall hydrolase after all, but rather as a scaffolding protein or as an activator of another cell wall hydrolase [57, 93-95]. However, the point mutations C292A or H343A in the predicted active site of the CHAP domain are lethal, indicating that enzymatic activity of the CHAP domain is required for cell viability [91].

1.6 PcsB expression is controlled by the essential two-component system WalRK

Two-component systems are found in almost all bacterial genomes, and are used by the bacteria to monitor and adapt to changes in its environment. A typical two-component system comprises a membrane bound sensor kinase and a cytoplasmic response regulator. The function of the membrane associated kinase is normally to sense environmental stimuli and to function as a signal

transducer. This signal is then transferred from the kinase to the cytoplasmic response regulator, which then becomes active and modulates expression of specific sets of genes [105-108].

A two-component system called WalRK (other names used for this system are VicRK, YycFG, MicAB) has been shown to be essential in *B. subtilis*, *S. aureus*, and *S. pneumoniae.* For *B. subtilis* and *S. aureus*, deletion of *walK* alone is lethal [109, 110]. In *S. pneumoniae*, on the other hand, a *walK* deletion mutant can be obtained, although the cells become quite stressed. A double knockout deleting both *walK* and *walR*, however, is not tolerated by the cells [111]. The WalRK system was first identified in *B. subtilis* and is highly conserved among low G+C Gram-positive bacteria. Phosphorylation of the response regulator WalR by the histidine kinase WalK leads to activation of genes in the WalRK regulon. When *walK* is removed from the *S. pneumoniae* genome, the level of gene expression in the WalRK regulon drops fivefold, indicating that WalK has a high kinase activity upon WalR [92, 112]. For all WalRK regulons identified, the majority of the genes encode peptidoglycan hydrolases that participate during cell division [110, 112-114].

WalRK regulated genes are only transcribed during early exponential growth phase and transcription is shut off when cells enter stationary phase. Even when the *walRK* genes are constitutively expressed in *B. subtilis*, the transcription of genes in the WalRK regulon follows the same pattern. This suggests that the WalRK system responds to a signal that is not part of the WalRK regulon. The signal that activates the WalRK two-component system remains a mystery, but it is generally accepted among researchers within the field that this system monitors the status of cell wall synthesis in the bacterium [110, 115-117]. Moreover, the system is thought to coordinate cell division with peptidoglycan synthesis, and to carry out an overall regulation of the cell wall metabolism with many partially redundant genes involved [109, 113, 114, 118, 119]. The reason why the WalRK system is essential in *B. subtilis* and *S. aureus* is not clear since deletion of any gene positively regulated by WalRK is tolerated. It is discussed that removal of this system could cause a lethal imbalance between cell wall synthesis and the lytic activity of cell wall hydrolases [110, 120]. In *S. pneumoniae,* the essential nature of WalRK is easily explained by its positive regulation of the putative cell wall hydrolase PcsB [89].

Microarray analysis of *S. pneumoniae* during *walR* depletion in a *ΔwalK* background revealed altered transcription of 49 genes [89]. The most affected genes were *pspA, pcsB, lytB* and two genes encoding the LysM-containing proteins mentioned in section 1.5 [89, 92]. Only two LysM-

containing proteins (Spr0096 and Spr1875) are found in *S. pneumonia*e and expression of both is controlled by the WalRK system [15, 89, 92]. The LysM motif displays interactions towards peptidoglycan and is often found in cell wall hydrolases [121, 122]. One of these two LysM-containing proteins is predicted to possess a cell wall hydrolase domain resembling that of a lysozyme. Removal of the gene (*spr1875*) encoding this protein does not alter cell growth nor muropeptide pattern of the peptidoglycan [15]. However, a Δ*spr1875* mutant displayed an overall thickening of the cell wall [94]. Both virulence and lipid integrity may also be under the control of the WalRK system in *S. pneumoniae*, although the latter is suspected to be an indirect effect from WalRK`s ability to affect cell wall metabolism [92, 110, 123, 124].

1.6.1 Organization and transcription of the *wal* operon in *S. pneumoniae*

The *wal* operon is organized differently between bacterial species. The pneumococcal *wal* operon consists of three genes, *walR*, *walK* and *walJ* (Figure 7), encoding the response regulator WalR, the histidine kinase WalK and a protein with unknown function called WalJ. In *B. subtilis* the *wal* operon consists of six genes (*walR*, *walK*, *yycH*, *yycI*, *walJ* and *yycK*). The genes *yycH* and *yycI* encode proteins that regulate the kinase activity of WalK, whereas *yycK* encodes a protein of unknown function. Only one mRNA corresponding to the whole 2.9 kb *wal* operon has been detected in *S. pneumoniae* [110, 125, 126]. In *B. subtilis*, on the other hand, three transcripts have been identified; One 7.4 kb long mRNA covering all six genes, one 2.4 kb transcript covering only *walR* and *walK* and a small 1.4 kb transcript containing the *yycK* gene [109, 110].

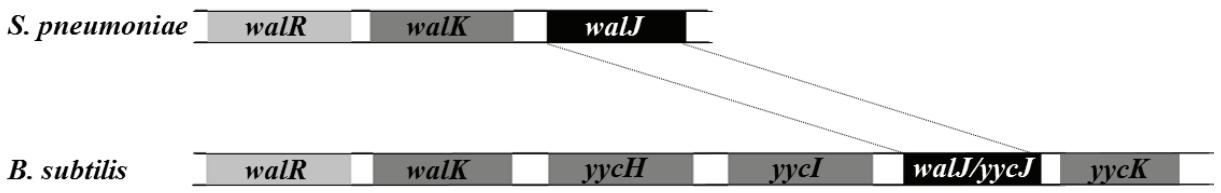

Figure 7. The *wal* operon is organized differently in *S. pneumoniae* and *B. subtilis*. The *wal* operon in *S. pneumoniae* contains only three genes, whereas the *B. subtilis wal* operon contains six genes [110].

It exists conflicting results with respect to auto-regulation of the *wal* operon in *S. pneumonaie*. One study detected elevated transcription of the chromosomal *walRK* genes when an extra copy of the *walR* gene was over-expressed, indicating an auto-regulatory circuit. However, a WalR DNA binding site has never been identified upstream the pneumococcal *wal* operon [92, 124]. Furthermore, auto-regulation of the WalRK system would require WalR promoted expression of an inducer signal, which activates WalK. Such an inducer has not been identified. Neither in *B. subtilis*, has an auto-regulation of the *wal* operon has been detected [113]. The *B. subtilis walRK* genes are only expressed during early exponential growth phase. When the cells enter the stationary phase, transcription is dramatically reduced [113]. The gene products WalR and WalK on the other hand, are present throughout growth [118, 127].

1.6.2 The histidine kinase WalK

All WalK homologues contain a so-called HAMP domain (histidine kinases, adenylyl cyclases, methyl-accepting proteins and phosphatases), a PAS domain (Per-Arnt-Sim, named after the first three proteins in which it was identified), dimerization and histidine phosphorylation domain (DHp) and a catalytic ATPase domain (CA) (Figure 8) [106, 126, 128]. The function of PAS and HAMP domains is not well understood. However, some evidence suggest that PAS domains have the ability to monitor the presence of oxygen, light, or redox potential. It has also been suggested to be a protein-protein interaction domain, or being responsible for the binding of a specific, but unknown ligand [129-131]. HAMP domains are believed to detect and relay changes in protein conformation upon ligand binding [132]. An in-line mechanism has been proposed for PAS and HAMP signaling, rather than a direct interaction between the two domains [133]. The crystal structure of WalK from *Streptococcus mutans* suggests that the HAMP domain in principle could transfer a conformational change to the PAS domain via a helical structure that is stabilized by a leucine zipper motif [131]. Phosphorylated DHp domains function as a high affinity substrate for their cognate non-phosphorylated response regulators [134].

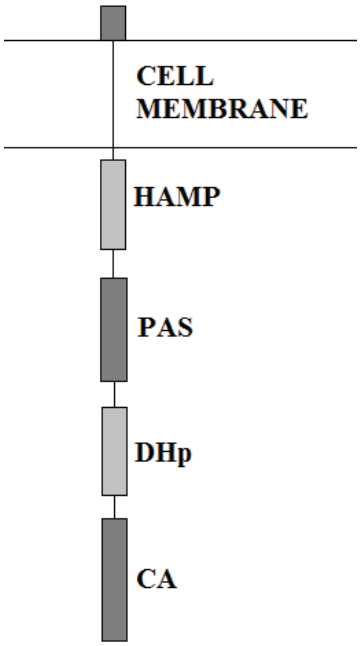

Figure 8. Domain organization of the pneumococcal WalK. In *S. pneumoniae*, WalK possesses only one transmembrane segment. The first 12 amino acids at the N-terminus are predicted to be located extracellularly [112]. The HAMP region is located adjacent to the cell membrane followed by the PAS domain, the DHp domain and the CA domain at the C-terminal end [110].

WalK contains, in most cases, two transmembrane segments connected by an extracellular loop. This loop consists of approximately 150 amino acids. The streptococcal WalK, on the other hand, contains only one transmembrane segment with an extracellular tail of 4 to 12 amino acids [128]. The pneumococcal WalK is predicted to have 12 amino acids extracelluarly [112]. The role of the transmembrane segment was originally thought to function simply as a membrane anchoring device. However, *in vitro* studies of WalK autophosphorylation and phosphoryl transfer, give rise to conflicting results. It has been demonstrated in both *S. pneumoniae* and *S. aureus* that WalK without its transmembrane segment can autophosphorylate and transfer its phosphoryl group rapidly to WalR *in vitro.* Full-length WalK in *S. aureus*, on the other hand, showed much lower kinase activity when tested in a detergent-micelle-model that resembles a cell membrane [116, 130, 135, 136]. In contradiction, another study could only detect autophosphorylation for full-length pneumococcal WalK when embedded in membrane vesicles [125]. Therefore, it is discussed whether the transmembrane part can affect the kinase activity of WalK or not. It has been suggested that the transmembrane segment provides a conformation of WalK with lower kinase activity, but that an activating signal can interact with the transmembrane segment and elevate the kinase activity [135].

Localization studies of WalK in *S. pneumoniae* show that it is not present in the septum area but rather distributed in foci throughout the cell surface [126]. This is in contrast to WalK in *B. subtilis,* which localizes to the septum of dividing cells and interacts with the divisome [117, 137, 138]. However, since the localization data for the pneumococcal WalK are less convising, conclusions about its exact localization should be considered with precautions.

1.6.3 The response regulator WalR

WalR consists of a reciever domain and a DNA-binding domain. The reciever domain will upon phosphorylation induce a conformational change that increases WalR`s ability to promote transcription from a selected set of promoters. These promoters contain a specific DNA sequence that is recognized by WalR. The DNA-binding domain of WalR belongs to the OmpR family, which members have a conserved DNA-binding module [139, 140]. The DNA recognition site of WalR was first identified in *B. subtilis*, and consists of two 6 bp tandem repeats separated by a 5 basepair spacer [115]. Since the DNA-binding domain of WalR is almost invariant between *B. subtilis*, *S. pneumoniae* and *S. aureus*, the regulator most probably recognizes similar DNA-binding sites. Indeed, the same DNA consensus found in *B. subtilis* was later identified as the WalR recognition site in *S. aureus* [116]. In *S. pneumoniae* the WalR consensus sequence is 5`-TGT (A/C/T) A (A/G/C) N5 (G/T/C) GT (A/C) A (T/C) - 3`, and it is higly similar to the consensus sequence identified in *B. subtilis* and *S. aureus* [92].

1.7 Contributing factors to crosstalk in WalRK signaling

Signal transduction from a histidine kinase to a response regulator can be embedded in a regulatory network, also involving accessory proteins and serine/threonine kinases [141, 142]. Deletion of *walK* in *S. pneumoniae* is tolerated, although the cells become quite stressed [111]. For *B. subtilis* and *S. aureus*, deletion of *walK* is lethal [109]. The reason why *S. pneumoniae* can survive without *walK* is not known, however, the non-essential role of WalK in *S. pneumoniae* was initially thought to depend on the phosphorylation of WalR by acetyl-phosphate [143, 144]. The cellular amount of

acetyl-phosphate is thought to reflect the metabolic state of the cell and affects gene expression through two-component systems [143, 145-147]. *In vitro* experiments did show that acetyl-phosphate could phosphorylate WalR from both *S. pneumoniae* and *B. anthracis* [92, 136, 148]. However, *in vivo* removal of acetyl-phosphate in *S. pneumoniae* caused only a moderate reduction in expression of the WalRK regulon [143, 144]. Removal of both acetyl-phosphate and WalK simultaneously, on the other hand, resulted in an additive decrease in the regulon expression. Hence, acetyl-phosphate can probably phosphorylate WalR *in vivo,* but the biological significance of acetyl-phosphate in this context is questionable [144]. An alternative explanation for the non-essential nature of the pneumococcal WalK might be that unphosphorylated WalR itself initiates sufficient transcription of the WalRK regulon for the cells to survive [112].

Another phosphorylation source that might affect signaling in the WalRK two-component system is the eukaryotic-type serine-threonine kinase StkP [149]. StkP and its cognate phosphatase PhpP are shown to phosphorylate and dephosphorylate, respectively, the two response regulators RR06 and RitR in *S. pneumoniae*. RR06 and the orphan response regulator RitR are both activated upon phoshorylation by StkP [150, 151]. WalR has never been indentified as a substrate for StkP [152, 153], however, an *stkP* mutant displays a clear decrease in expression of the WalRK regulon, without altering the expression of the *walRKJ* operon itself. These conflicting data therefore raise the question whether StkP can phosphorylate WalR directly, or if StkP somehow indirectly stimulates activation of WalR [149]. Evidence for a direct modulation of WalR by a serine-threonine kinase has only been demonstrated in *Streptococcus pyogenes* [154, 155], but this type of crosstalk between WalR and a serine-theronine kinase is also discussed in *B. subtilis* [156].

The genome of *S. pneumoniae* encodes 13 histidine kinases and 14 response regulators [111], and the level of crosstalk between these two-component systems is believed to be very low [157]. Still, crosstalk does occur. Three non-cognate histidine kinases were able to phosphorylate WalR *in vitro*, but they were not kinetically favoured compared to WalK`s ability to phosphorylate WalR. One of these non-cognate kinases, PnpS (invloved in phosphate uptake), could phosphorylate WalR also *in vivo*, but only when both WalK and the cognate regulator of PnpS (PnpR) were removed [112]. The extent of this crosstalk *in vivo* and its biological significance are not determined. Many of the histidine kinases studied are found to be bifunctional, working as both kinases and phosphatases [134, 158-160]. Interestingly, crosstalk between two-component systems

have only been subjected to their kinase activity. A histidine kinase has never been reported to perform phosphatase activity upon a non-cognate response regulator. The reason might be that a stronger interaction is needed between the kinase and the response regulator for phosphatase activity to occur than for phosphorylation [134]. Pneumococcal WalK is reported to possess a strong phosphatase activity towards phosphorylated WalR. It has even been suggested that the phosphatase activity might predominate over the kinase activity [112, 136]. This could be the reason why the contributions by other phosphodonors play a minor part in the pool of phosphorylated WalR.

1.8 Signal sensing by WalK is still an unsolved question

The signal(s) sensed by the WalRK two-component system remains a mystery [110, 117]. Since the predicted sensing domain of WalK is located outside the cell membrane, lipid II has been proposed as a candidate for triggering the WalRK system. This model, however, struggles to explain the situation in streptococci where the extracellular domain of WalK is absent [110]. Streptococcal WalK is therefore classified as an intramembrane-sensing histidine kinase (IM-HK), often found in Firmicutes. Due to their lack of an extracellular domain, it was initially thought that the IM-HK most likely senses a signal within the membrane or intracellularly [161]. Since no ligand has been found, some believe that IM-HKs are not able to sense a signal directly, but rather transfer a signal from an accessory protein that functions as the true sensor [142, 162-164]. This indirect sensing mechanism has been suggested for WalK in *B. subtilis*, despite the presence of an extracellular domain. YycH and YycI control the activity of *B. subtilis* WalK by interaction via their transmembrane helices [165]. The signal could be detected by YycH and YycI, and transferred to WalK [163]. A possible role of the transmembrane part of WalK kinases could therefore be to make interactions with signal sensing accessory protein(s) [164]. Perhaps this is why neither the sensing domains, nor the signals that activate them are known for the majority of these histidine kinases [106].

2. Aims of the study

When this work was initiated, the major cell-disconnecting peptidoglycan hydrolase had not been identified in *S. pneumoniae*. None of the known peptidoglycan hydrolases produced by *S. pneumoniae* were found to be essential. Furthermore, only one peptidoglycan hydrolase, LytB, seemed to play a role in the separation of daughter cells. LytB deficient pneumococcal cells form long chains in which the daughter cells remain attached to each other through thin peptidoglycan filaments. However, this peptidoglycan hydrolase is only responsible for the ultimate separation of daughter cells, and has no role in splitting of the septal cross wall. A protein called PcsB, appeared to be a better candidate for this role. PcsB is essential in *S. pneumoniae* strain R6 and other serotype 2 strains, while its absence causes severe growth defects, abnormal morphology and misplaced septa in other pneumococcal serotypes. Interestingly, PcsB contains a CHAP domain at its C-terminal end. Members of the CHAP superfamily are often found as catalytic domains in peptidoglycan hydrolases, and can possess amidase or endopeptidase activity. However, in spite of this, all attempts to demonstrate that PcsB possesses muralytic activity had failed.

The objective of this study was to learn more about the function of PcsB. In particular, we aimed at verifying or disproving the hypothesis that PcsB is responsible for splitting the septal cross wall in *S. pneumoniae*. To achieve this, a two-pronged strategy was employed. In one line of research, we sought to purify, characterize, crystallize and determine the three-dimensional structure of PcsB (Papers I and II). Our hope was that this might provide new information that would help us elucidate the biological function of PcsB. In another line of research, the strategy was to learn more about the biological function of PcsB by studying WalK, the histidine kinase sensor that regulates expression of *pcsB* in response to unknown external and/or internal signals (Paper III).

3. Main results and discussion

3.1 Paper I

CHiC, a new tandem affinity tag for the protein purification toolbox

During cell division in *S. pneumoniae* the septal cross wall, which separates the two daughter cells, must be split down the middle by one or more peptidoglycan hydrolases. It is of great interest to identify the key player(s) in this process. It might also be of practical importance, as the enzyme(s) involved can be a valuable drug target. Over the years, several peptidoglycan hydrolases has been suggested to contribute to daughter cell separation. Only LytB has a role in the process, as it is required for dispersal of pneumococcal chains [58]. In recent years, the putative murein hydrolase PcsB has emerged as the leading candidate for the major cross wall splitting enzyme in *S. pneumoniae*. However, attempts to demonstrate that PcsB is a peptidoglycan hydrolase have so far failed [57, 94]. Before the present study was started, it was known that PcsB interacts with and probably is controlled by the transmembrane FtsEX complex [57, 62]. This could mean that PcsB must be activated by FtsEX *in vivo*, and that purified recombinant PcsB is inactive because it adopts the "wrong" conformation *in vitro*. Another possibility was that the lack of detectable enzymatic activity was due to other factors such as the purification procedure or the assay conditions used. To address these questions, it was decided to express PcsB in *E. coli* and purify it to near homogeneity. This would allow us to characterize the properties of PcsB, and test its activity under different assay conditions. Another important goal was to produce sufficient amounts of PcsB for crystallization studies and structure determination. For this purpose we needed a procedure that would make it possible to purify PcsB in milligram quantities. Purification of PcsB has previously been shown to be challenging due to the fact that overexpressed native PcsB ends up in inclusion bodies which are difficult to refold [87, 94]. With this in mind, we chose a different approach. We designed a tandem affinity tag based on the choline-binding domain of CbpD. It has been shown previously that pneumococcal proteins with choline-binding domains bind strongly to the diethylaminoethanol groups of DEAE cellulose, and that such domains can be used as an affinity tag when fused to other proteins [77, 78]. In the original description of the system, the choline-binding domain of LytA, which contains six choline-binding sites [76] was

used. The choline-binding domain of CbpD is shorter and contains fewer choline-binding sites. The reason I chose the choline-binding domain from CbpD instead of the corresponding domain from LytA was that it is smaller and therefore might interfere less with the folding of the fusion partner. Besides, I knew it worked well, because other members of the research group had already used it as a "natural" affinity tag for the purification of CbpD itself.

In addition to the choline-binding domain of CbpD, the new 16.5 kDa affinity tag termed CHiC was constructed with an N-terminal conventional 6xHis-tag and a proteolytic site specific for the TEV (tobacco etch virus) endopeptidase at the C-terminus. The purposes of the 6xHis-tag are to both be able to perform immobilized metal affinity chromatography (IMAC) before treatment with the TEV protease, and to facilitate the removal of the CHiC-tag after digesting the affinity-purified fusion protein with His-tagged TEV protease (AcTEV^{TM} protease, Invitrogen). By using IMAC, undigested fusion protein, free CHiC-tag and AcTEV^{TM} protease can be separated from the purified target protein in a single step.

For the expression of PcsB and the extracellular domain (ECL1) of FtsX, two pRSET A (Invitrogen) based plasmids, pGS01 (PcsB) and pGS02 (ECL1), were constructed. In both cases the CHiC-tag was inserted at the N-terminal end of the target protein. Expression of the fusion proteins, which is driven by the lacT7 promoter, was induced by isopropyl-β-D-thiogalactopyranoside (IPTG). After the first purification step on DEAE cellulose, one liter of cell culture yielded 5-8 mg of CHiC-PcsB and CHiC-ECL1 with a purity of approximately 90-95%. Further purification by IMAC resulted in more than 95% pure protein, with negligible loss of protein during the purification process. The successful use of the CHiC-tag for purification of PcsB and ECL1 demonstrates that it has the potential to be a valuable new tool for affinity purification of recombinant proteins.

A major Achilles' heel of the fusion approach is that the affinity tag in most cases has to be removed after purification of the fusion protein. Although highly specific endopeptidases, such as the TEV protease, have solved the problem of nonspecific cleavage, incomplete processing is still a large problem. Processing efficiency will vary from one fusion protein to another, but in most cases a fraction will remain resistant to digestion. This undigested fraction is easy to remove when using the CHiC-tag system in combination with a His-tagged TEV protease. Another advantage of using the CHiC-tag is that highly purified target protein is obtained in just a few steps, minimizing

loss of material and manipulations that can result in denaturation of the protein. Furthermore, since large amounts of CHiC-PcsB was obtained in the soluble protein fraction, while previous attempts to purify PcsB mainly gave rise to inclusion bodies, the CHiC-tag has enhanced the solubility of PcsB. Regardless of their origin, more than half of all recombinant proteins overexpressed in *E. coli* accumulate in the form of insoluble inclusion bodies [166]. Thus, if the CHiC-tag functions as a general solubility enhancer, by inhibiting aggregation and/or promoting proper folding of its fusion partner, it will help mitigate a major obstacle in recombinant protein production.

3.2 Paper II

Structural basis of PcsB-mediated cell separation in *Streptococcus pneumoniae*

PcsB is essential in *S. pneumoniae* serotype 2 strains (e.g. R6 and D39), but not in other pneumococcal strains tested so far [62, 94]. However, deletion of the *pcsB* gene has dramatic consequences even in the strains in which PcsB is not essential. A complete loss of virulence is observed in these strains, and their growth rate are greatly reduced *in vitro*. Furthermore, they grow in clusters, and their division septa form in different planes [93, 94]. As already mentioned above, these phenotypic alterations and the presence of a putative muralytic domain, made PcsB the prime candidate for the major cross wall splitting enzyme in *S. pneumoniae*. The lack of *in vitro* muralytic activity led to speculations that PcsB might rather function as a scaffolding protein or as an activator of other peptidoglycan-processing enzymes. Arguing against this, however, was the fact that point mutations that change the putative catalytic cysteine or histidine residue in the CHAP domain of PcsB in strain R6, is lethal. This finding strongly indicates that PcsB possesses enzymatic activity [91]. In paper II of the present study, we sought to further elucidate the biological role of PcsB by using a crystallography based structural approach in combination with biochemical, genetic and electron microscopic analyses.

Electron microscopic examination of PcsB-depleted *S. pneumoniae* R6 cells.

In 2001, Reinscheid and co-workers used scanning and transmission electron microscopy to examine the morphology of *S. agalactiae* lacking the *pcsB* gene. They observed grossly abnormal cells growing in clumps, and severe defects in septum placement and cell separation. Corresponding studies of pneumococcal strains that are able to grow without PcsB showed essentially the same defects [93, 94]. To examine the effect of PcsB-stress in *S. pneumoniae* R6, PcsB must be gradually depleted. In 2004, Ng and co-workers used a fucose-regulated promoter to gradually downregulate the level of *pcsB* transcription in R6 cells. Using light and epifluorescence microscopy they observed chain formation in R6 cells subjected to reduced expression of PcsB, and misplaced septa in strongly depleted cells stained with FI-Van (fluorescent vancomycin). Detailed electron microscopy studies of PcsB-depleted R6 cells, however, had not

been reported previously. Hence, we decided to examine partially and strongly depleted R6 cells by transmission electron microscopy to determine how this treatment affects septum synthesis, placement and processing. To deplete PcsB in strain R6 we used the ComRS system, which was developed previously in our laboratory [27]. According to the literature, the septal cross wall of Gram-positive bacteria is fully synthesized before it is split down the middle to separate the daughter cells [167]. In contrast, synthesis and splitting of the new cross wall takes place in close succession in Gram-negative bacteria, and consequently appears to be coupled processes. Our results showed that R6 cells subjected to intermediate PcsB depletion have fully synthesized and apparently normal cross walls (supplementary Figure 1B, paper II). However, short chains of cells were observed in which the cross wall of the first-generation daughter cells remained uncleaved even though the cross walls of the second-generation daughter cells were fully formed. This result is in complete agreement with the idea that PcsB is a cross wall splitting hydrolase. In cells subjected to severe PcsB depletion misplaced septa were observed (supplementary Figure 1C, paper II). This is in accordance we previous reports [87, 93, 94], and suggests that PcsB might have a role in determining the subcellular location at which new septa are initiated.

Studies of the muralytic activity of PcsB

Having obtained milligram quantities of purified PcsB, we set out to develop an assay that would enable us to prove that PcsB possesses muralytic activity. Two different approaches were chosen. In one series of experiments, purified pneumococcal peptidoglycan, with or without teichoic acids, was used as substrate. To obtain teichoic-free peptidoglycan, it was treated with 48% hydrofluoric acid for 48 hours at 4 ^{o}C. After digesting this material with PcsB, or with PcsB in combination with mutanolysin, it was analysed by reversed-phase HPLC according to standard protocols. No significant difference in the chromatographic profiles of samples treated with or without PcsB was detected. In another series of experiments, the muralytic activity of purified PcsB protein was examined in zymogram gels. Whole pneumococcal cells were incorporated into the SDS-PAGE resolving gel as substrate. Also in this case the result was negative. No clearing zones were detected in the gel after it had been washed and incubated in refolding buffer. In sum, the results were in accordance with the negative results already reported by others [57, 87, 88].

Next, we speculated that the CHAP domain alone might be more active than the complete enzyme. This could be the case if the large N-terminal domain of PcsB somehow interferes with the activity of the catalytic domain *in vitro*. To facilitate purification, a 6xHis-tag was added to the N-terminal end of the CHAP domain (His-$CHAP_{PcsB}$). In parallel, a negative control, in which the predicted active site cysteine had been substituted by an alanine, was constructed (His-$CHAP_{PcsB(C292A)}$). The assays described above, which were negative for PcsB, were repeated with the CHAP domain. The assays carried out in solution and analysed by HPLC were negative. However, the zymogram assay exhibited distinct clearing zones resulting from the activity of His-$CHAP_{PcsB}$. In contrast, no clearing zones were detected in the lanes loaded with identical amounts of the His-$CHAP_{PcsB(C292A)}$ mutant protein (Figure 3A and B, paper II). Whole *S. pneumoniae* RH14 cells were incorporated as substrate in the 13% SDS-PAGE resolving gel. The RH14 strain was used because it lacks the LytA autolysin. If present, LytA would have completely digested all of the peptidoglycan substrate in the gel, making it impossible to detect the activity of other peptidoglycan hydrolases.

To gather additional evidence for the muralytic activity of $CHAP_{PcsB}$, we took advantage of the fact that $CHAP_{PcsB}$ and a corresponding domain in LytF, a protein produced by *S. gordonii* strain Challis, are 70% identical at the amino acid sequence level. LytF is a murein hydrolase that is produced only when *S. gordonii* cells are competent for natural genetic transformation. Evidence indicate that the bacteria produce this enzyme to attack and lyse related streptococcal strains and species in order to release DNA that can be taken up by the competent attacker cells [104]. Although the $CHAP_{PcsB}$ and $CHAP_{LytF}$ domains are highly homologous, their N-terminal domains are unrelated. In the case of LytF, it has been shown that the N-terminal domain targets the enzyme to the equatorial and septal regions of intact cells and peptidoglycan sacculi [104]. We constructed chimeras consisting of the N-terminal domain of LytF fused to the CHAP domain of PcsB (LytF-$CHAP_{PcsB}$) and vice versa (PcsB-$CHAP_{LytF}$). The former were expressed in pneumococcal cells from the ComS-inducible P_{comX} promoter [27]. Extracts of these cells were subjected to zymography with whole *S. gordonii* cells incorporated in the resolving gel as substrate. Clearing zones corresponding to the molecular mass of LytF-$CHAP_{PcsB}$ were observed, demonstrating that $CHAP_{PcsB}$ is able to hydrolyze *S. gordonii* peptidoglycan when fused to the cell wall targeting domain of LytF (Figure 3d, paper II). This interesting result suggests that the N-terminal domain of PcsB might suppress the muralytic activity of its cognate CHAP domain. Even more interesting was the discovery that pneumococcal cells, in which the gene encoding PcsB had been replaced

by a chimeric construct encoding PcsB-CHAP$_{LytF}$, are viable. Comparison of the growth kinetics of wild-type and mutant cells expressing PcsB-CHAP$_{LytF}$ showed that the mutant cells grow somewhat slower than wild-type cells. Moreover, light microscopy revealed that some of the mutant cells are morphologically abnormal (supplementary Figure 14, paper II). Nevertheless, the fact that CHAP$_{LytF}$ can substitute for the corresponding domain in PcsB, and give rise to a protein that is functional (although suboptimally), provides strong evidence that the CHAP$_{PcsB}$ domain functions as a peptidoglycan hydrolase.

The results outlined above strengthened our conviction that PcsB is the major cell disconnecting peptidoglycan hydrolase in *S. pneumoniae*. However, as we sought to determine the cleavage site of PcsB, it was a disappointment that no muralytic activity could be observed when peptidoglycan was digested with His-CHAP$_{PcsB}$ in aqueous solution. A lot of work was carried out in an attempt to identify reaction conditions that would give rise to detectable cleavage products. Physico-chemical conditions such as pH, temperature and solvent composition were varied, and the strong reducing agent dithiothreitol (DTT) was added to the reaction mixture to protect the active-site cysteine of the CHAP domain against possible oxidation. However, we did not succeed.

The lack of activity observed for PcsB in aqueous solution is also seen for other muralytic enzymes containing CHAP domains. Pneumococcal CbpD is a competence induced peptidoglycan hydrolase with an N-terminal CHAP domain that is only distantly related to CHAP$_{PcsB}$. It was found to be active in zymograms, and in lysing pneumococci in growing cultures [85]. Furthermore, transmission electron micrographs of lysed pneumococcal cells showed that CbpD causes the cells to rupture in the division zone [85]. However, no cleavage products could be detected after digesting purified peptidoglycan from *S. pneumoniae* with purified CbpD *in vitro* (Daniel Straume, unpublished results). Similar to CbpD, PcsB is localized to equators and septal regions of pneumococcal cells [57, 85]. Thus, a possible explanation for the “missing” cleavage products could be that CbpD as well as PcsB only cleaves a limited number of cross-linked stem peptides located in the septal region. Although perhaps unlikely, it cannot be ruled out that the active site of CHAP$_{PcsB}$ recognizes structural features around the scissile bond that only occurs in the interior of the septal cross wall. If only a small number of bonds are cleaved, the amount of products released could be below the detection limit of our assay.

The assumption that PcsB only cleaves a limited number of unique bonds, exclusively present in the pneumococcal cross wall, might explain why we were unable to detect cleavage products in our *in vitro* experiments. However, if true, this property should also limit digestion of the pneumococcal cell wall in the zymogram assays. So why do we observe clearing zones? When pneumococci are incorporated in the SDS-PAGE resolving gel, the SDS present will dissolve their cytoplasmic membranes and cause the cells to collapse due to loss of turgor pressure. It is conceivable, but entirely speculative, that the septal cross walls of these cells will be digested where there is His-$CHAP_{PcsB}$ protein present in the gel, thereby cleaving the sacculi into smaller fragments. Due to their smaller size, these fragments might diffuse more easily out of the polyacrylamide matrix. Another explanation might be that when purified fragmented peptidoglycan are incorporated into a SDS-PAGE gel, these gels are much more transparent than those with whole cells incorporated. It could be that the clearing zones observed in zymogram experiments, might be transparent areas with the presence of fragmented peptidoglycan instead of whole cells.

Crystallization and three-dimensional structure determination

Having developed a method to obtain large amounts of pure recombinant PcsB (by the use of CHiC-tag presented in paper I), we were in a good position to get PcsB crystals. This was obtained using the sitting-drop vapour diffusion method at 4 °C. To be able to solve the structure of PcsB at 2.5 Å resolution, selenomethionine (SeMet) had to be introduced at 4 different positions to solve the phase problem. Since mature PcsB, which consists of 365 amino acids, only contains two methionines (M140 and M150), two additional methionines had to be introduced (Q180M and L250M). The resulting protein was termed CHiC-PcsBmut. Purification of selenomethionine-derivatized CHiC-PcsBmut, termed SeMet-PcsB, turned out to be a challenge. When expressing SeMet-labelled PcsB, *E. coli* has to be grown in a special M9 minimal medium supplemented with selenomethionine. Under these conditions, recombinant SeMet-PcsB was insoluble and formed inclusion bodies. The problem was solved by adding 50 mM choline chloride to the growth medium. Presumably, choline taken up by the bacteria increased the solubility of SeMet-PcsB by binding to the choline-binding sites present in the CHiC-tag. The presence of choline probably

inhibited aggregation by promoting the correct folding of the choline-binding domain, which constitutes the major part of the tag.

Unexpectedly, the solution of the three-dimensional crystal structure of mature PcsB revealed that it adopts a 164 Å long dimeric structure in which the catalytic CHAP domain of each monomer is inserted in the internal cavity of the coiled-coil domain of the other (Figure 9C). This dimeric arrangement partially occludes the active site of the CHAP domain and consequently locks it in an inactive configuration. The coiled-coil domain is composed of three long (α1, α3 and α4) and two short helices (α2 and α5). The last of these, α5, connects the coiled-coil domain to the globular CHAP domain via an alanine-rich linker (Figure 9A). The structure of the coiled-coil domain shows a novel architecture that has no close structural homologs in the Protein Data Bank. The unusual dimeric structure adopted by PcsB in the crystal, where each V-shaped coiled-coil domain locks the CHAP domain of its dimeric partner in an inactive configuration, points to a regulatory function. It is reasonable to assume, that in order to get access to their substrate *in vivo*, the CHAP domains must be released by coordinated movements of the α-helices that make up the coiled-coil domains. In all likelihood, the energy required to drive these conformational changes comes from hydrolysis of ATP by the FtsE protein. FtsE, which is located at the cytoplasmic face of the membrane, forms a complex with the transmembrane protein FtsX [60]. Recent studies in *E. coli* suggest that ATP-hydrolysis by FtsE drives conformational changes in FtsX that via EnvC activates the AmiA and AmiB amidases so that they can cleave the septal peptidoglycan [98, 99]. Sham and co-workers (2011 and 2013) have shown that the large (ECL1) and the small (ECL2) extracellular loops of the pneumococcal FtsX transmembrane protein, interacts with the coiled-coil domain of PcsB. In addition, they isolated strains with temperature sensitive mutations in the coiled-coil domain of PcsB that were suppressed by amino acid changes in the extracellular loops of FtsX [62]. The locations of these amino acid changes point to specific interactions between the FtsX loops and the α1, α3 and α4 helices of PcsB (supplementary, Figure 15, paper II). Apparently, the FtsEX protein complexes in *E. coli* and *S. pneumoniae* sense the progress of cell division and regulates the activity of extracellular peptidoglycan hydrolases accordingly. In *E. coli*, FtsX controls AmiA and AmiB indirectly, through the periplasmic scaffold protein EnvC, whereas in *S. pneumoniae* there is a direct contact between FtsX and the cross wall splitting hydrolase [57].

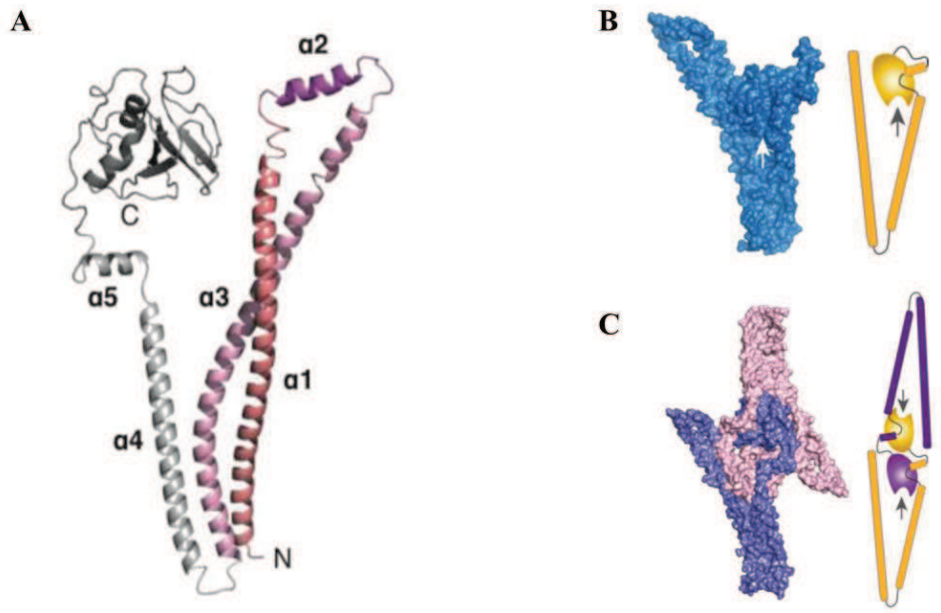

Figure 9. The crystal structure of PcsB. PcsB is shaped like a triangle consisting of a coiled-coil domain, a linker and a CHAP domain. Panel **A** shows how the coiled-coil domain consists of five helices, three long (α1, α3 and α4) and to short (α2 and α5). A linker connects the α5 helix with the catalytic CHAP domain. The CHAP domain possesses an exposed active site. When found in the monomeric form, panel **B**, the catalytic CHAP domain is inserted into its own coiled-coil domain. However, when found as a dimer, panel **C**, the CHAP domains are swapped between the monomers, so that the coiled-coil domain of one molecule blocks the CHAP domain of its dimeric partner [168].

The finding that PcsB adopts a linear dimeric structure in the crystal was unexpected. Thus, a pertinent question is whether this dimeric structure is relevant for the *in vivo* function of PcsB. As discussed in the paragraph above, the occlusion of the active site of the CHAP domain by the partner's coiled-coil domain suggests an interesting and plausible mechanism by which the potentially lethal activity of PcsB might be controlled. This control mechanism also fits very well with the results of Sham and co-workers (2011 and 2013), which showed that there is a direct interaction between the periplasmic parts of FtsX and the coiled-coil domain of PcsB. In all systems investigated, the FtsEX complexes regulates the activity of their cognate cross wall splitting peptidoglycan hydrolases [62, 98, 100, 169]. The sizes and shapes of the PcsB dimer and monomer provide additional clues to how PcsB might function in the *in vivo* situation. Analytical ultracentrifugation and SAXS experiments strongly indicated that the CHAP domain in the monomer is inserted in its own coiled-coil domain. Thus, the monomer is secreted into the periplasm in an inactive configuration. Another clue is that the length of the dimer (16.4 nm) and

the thickness of the septal cross wall (17-25 nm) is similar. This led us to propose the model presented in Figure 10, in which a monomer from each of the daughter cells meet in the middle of the septal cross wall to form an inactive dimer. When the daughter cells are ready to separate, some signal will activate the FtsEX complexes in each cell. This will induce conformational changes in the PcsB dimer that release and activate the CHAP domains. An intriguing property of this model is that it suggests that the daughter cells must cooperate to split their common cross wall. It makes biological sense that both cells must give an "all-is-ready" signal before digestion of the cross wall peptidoglycan is initiated. Because of the mesh-like structure of bacterial peptidoglycan, the PcsB-dimer is probably not able to move sideways. Thus, it is likely that it acts locally, and only cleaves the peptide bridges that are within reach from where it was originally inserted in the cross wall. After PcsB has performed its function, it is probably discarded. This is in accordance with the fact that large amounts of PcsB is present in the medium of exponentially growing pneumococcal cultures [90]. The released PcsB is most likely not able to do any damage on the cell wall both due to the adoption of the inactive monomeric form, and that the coiled-coil domain is not able to bind to the cell wall.

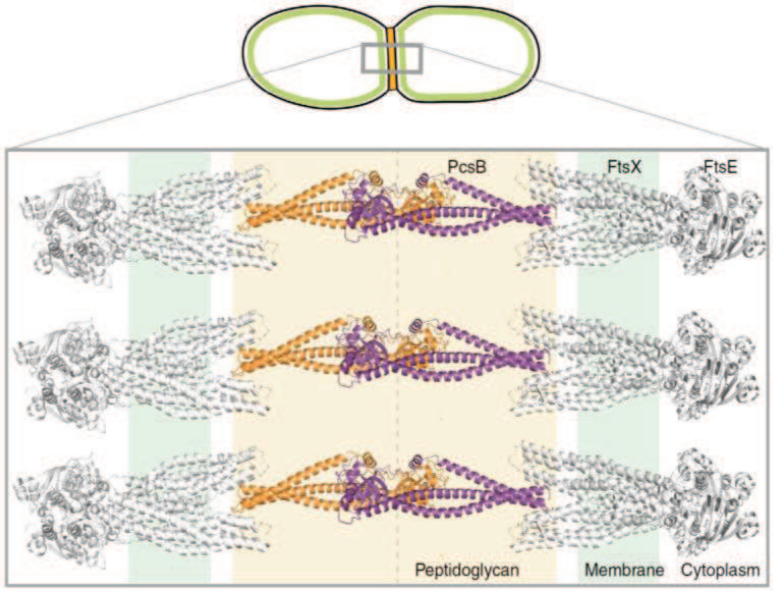

Figure 10. Regulation of the muralytic activity of PcsB. A proposed model on how PcsB is activated to perform muralytic activity on the cross wall in dividing pneumococcal cells. FtsX is responsible for the septum localization of PcsB. There PcsB exists as an inactive dimer, until the ATPase activity of FtsE induces an allosteric change that reaches PcsB through FtsX. This results in release of the CHAP domain from the coiled-coil domain and hydrolysis of the peptidoglycan. The two PcsB monomers found in a dimer, linear and with their CHAP domains in the middle, might be attached to each of the daughter cells. In this way the catalytic CHAP domain will be located in the middle of the septal cross wall.

As described above, our attempts to determine the cleavage site of the CHAP domain by biochemical methods failed. Unfortunately, all attempts to obtain crystals of complexes between PcsB and peptidoglycan analogs also failed. The three-dimensional structure of the CHAP domain revealed that it has an open active site consisting of a large groove that is about 31 Å long and 7 Å wide. However, the active site might not be easily accessible to the analog because it is probably occluded by the coiled-coil domain. To gain insight into the substrate recognition by PcsB, docking calculations using a peptide stem fragment was performed. The best fit placed the scissile bond between *i*Gln and L-Lys. The validity of this result will of course have to be verified experimentally in future studies.

3.3 Paper III

The single transmembrane segment of pneumococcal WalK is required for the perception of an intramembrane or extracellular signal

The essential two-component regulatory system WalRK is highly conserved among low-GC Gram-positive bacteria [110, 170]. The response regulator WalR is essential in all species tested, except for *S. pyogenes* [171]. Hence, WalR has emerged as a promising new drug target for combating infections caused by Gram-positive low-GC pathogens. In contrast to WalR, the membrane-anchored histidine kinase WalK is dispensable in *S. pneumoniae.* However, compared to wild-type strains, pneumococcal *walK* mutants are less virulent and have strongly reduced growth rates [125]. The biological function of WalRK has remained obscure since it was discovered in *B. subtilis* in 1998 [113], but a number of recent reports have revealed that it plays an important role in cell wall metabolism. The genes controlled by the WalRK system varies somewhat between species, but peptidoglycan hydrolases involved in cell growth and division are part of all characterized WalRK regulons [92, 110, 114, 116, 172].

In *S. pneumoniae*, WalR exerts strong positive regulation of the four cell wall associated proteins PcsB, LytB, Spr0096 and Spr1875 [89]. The two peptidoglycan hydrolases, PcsB and LytB, are required for cross wall splitting and chain dispersion, respectively [58, 168]. Spr0096 and Spr1875 both contain a LysM motif, a small domain known to bind peptidoglycan. The specific functions of Spr0096 and Spr1875, however, remains unknown. As the WalRK system controls the expression of PcsB and LytB, its major function could be to regulate proteins required to split the peptidoglycan cross wall during daughter cell separation. Thus, WalK might monitor the progress of the cell division process through direct interaction with other components of the divisome or by sensing specific signals. So far, however, no signal or signals sensed by WalK have been identified in any species.

In *B. subtilis*, *S. aureus* and other low-GC Gram-positive bacteria, WalK contains two putative sensor domains. One is a large extracellular loop flanked by two transmembrane segments. The loop consists of 150 amino acids, and is predicted to adopt a PAS-like fold [173]. The signal

perceived by this extracellular domain is probably relayed to the HAMP domain immediately inside of the cytoplasmic membrane by the transmembrane segment connecting these two domains. HAMP domains function as input-output modules for signal transduction, and are typically located between the membrane anchor and the DHp (dimerization and histidine phosphorylation domain) and CA (C-terminal catalytic and ATP-binding domain) domains of histidine kinases. The other possible sensor domain in WalK is a PAS domain located between the HAMP and DHp domains. PAS domains are found in diverse bacterial proteins, where they function in sensing and signal transduction. In contrast to other low-GC Gram-positive bacteria, the WalK kinases of streptococci are anchored to the cytoplasmic membrane via a single N-terminal transmembrane segment and their extracellular domains are very small. Hence, it has been speculated that streptococcal WalK kinases has lost the extracellular sensor domain, and that the remaining transmembrane segment only serves to anchor the protein to the inside of the membrane. In paper III we set out to investigate whether this supposition is true.

The transmembrane segment and immediate flanking regions of WalK contain conserved, functionally important amino acids

Comparison of the WalK sequences from 30 different streptococcal species revealed different patterns of conserved amino acids in the transmembrane segment and immediate flanking regions (Figure 1, paper III). Based on these differences the sequences were assigned to three groups. The transmembrane segment of pneumococcal WalK, which belongs to group III, contains four fully conserved amino acid residues. Two of these, F14 and F16, are located close to the external face of the cytoplasmic membrane, while the other two, G22 and F23, are situated in the middle. The fully conserved cytoplasmic amino acids, E33, R36 and D37, are located close to the inner face of the membrane, while a negatively charged residue is often found at the interface between the membrane and the external medium (position 13). To determine if these conserved amino acids are functionally important, a number of mutant strains were constructed in which one or more of the conserved amino acid residues were substituted with an alanine. Futhermore, several WalK chimera were constructed where the external, transmembrane and HAMP domains were swapped with the corresponding WalK domains from *S. thermophilus*. The WalK histidine kinase from *S. thermophilus* belongs to group II (Figure 1, paper III). With the exception of the semiconserved

amino acid in position 13, group II and III sequences does not share any fully conserved positions in their transmembrane segments or immediate flanking regions. To be able to monitor the effect of these mutations, a luciferase (*luc*) reporter gene driven by the *pcsB* promoter was inserted into a neutral site on the *S. pneumoniae* genome. The firefly luciferase protein is very rapidly degraded in *S. pneumoniae*, and is therefore well suited as a reporter for monitoring gene expression in this species [27]. To measure reporter gene expression, cultures of mutant strains were grown in 96-well microtiter plates at 37 ^{o}C inside a luminometer. Light emission resulting from luciferase expression was measured automatically every 5 minutes throughout the experiments.

The results showed that light emission by the WalK^{G22A} and WalK^{F23A} strains is strongly reduced. If the Δ*walK* background activity is subtracted, reporter gene expression in WalK^{G22A} and WalK^{F23A} strains is reduced by about 36% and 48%, respectively, compared to wild-type (Figure 2, paper III). This result is striking in itself, as it suggests that small conformational changes in the transmembrane segment are relayed to the output domain of the histidine kinase. Alternatively, the conservative G to A or F to A substitution could affect the ability of the transmembrane segment to anchor WalK to the inside of the cytoplasmic membrane. To check the possibility that these mutations prevents membrane insertion of the WalK^{G22A} and WalK^{F23A} transmembrane segments, a strain expressing a mutant WalK protein lacking the external and transmembrane domains was constructed. Reporter gene expression in the resulting WalKΔTM strain was at the background level, i.e. identical to that of the ΔWalK strain, demonstrating that the WalK^{G22A} and WalK^{F23A} proteins must be anchored to the membrane (Figure 2, paper III). WalK can function both as a histidine kinase and a phosphatase. Unfortunately, the reporter assay does not discriminate between these activities. Consequently, we do not know whether the decreased light emission observed with the WalK^{G22A} and WalK^{F23A} strains is due to decreased phosphorylation or increased dephosphorylation of WalR.

Alanine substitution of the conserved amino acids on the inner and outer face of the cytoplasmic membrane affected the activity of WalK in an unexpected way. All substitutions on the inner face (E33A, E33A/N34A, and R36A/D37A) significantly reduced reporter gene expression. The R12A/D13A substitutions had no effect, but when combined with the R36A/D37A mutations the resulting WalK$^{R12A/D13A/R36A/D37A}$ mutant strain emitted notably more light than the wild-type control (Figure 2, paper III). The finding that the R12A/D13A substitutions have little effect in a

wild-type background, but a strong effect in the R36A/D37A background, strongly indicates that the extracellular and/or transmembrane domain are involved in regulating the WalK output domain. To determine if one or both of these domains influence WalK activity, we performed a domain swapping analysis in which the extracellular, transmembrane and HAMP domains were exchanged with the corresponding domains from *S. thermophilus*. A reduction in reporter activity was observed in all cases where the transmembrane segment had been exchanged, while swapping of the external domains had no effect. Together, the alanine substitution and domain swapping analyses show that alterations in the transmembrane segment of WalK influences its kinase or phosphatase activity resulting in altered expression of PcsB and presumably other members of the WalRK regulon. It is highly unlikely that this would be the case if the transmembrane segment only served to anchor WalK to the cytoplasmic membrane. Thus, we concluded that the transmembrane segment functions as a sensor domain in WalK. We still have no clue as to the nature of the signal perceived by this sensor domain, but it is likely that the signal is sensed through intramembrane contact with another transmembrane protein. In *B. subtilis* it has been shown that the YycH and YycI proteins, which are located on the same transcription unit as YycG (WalK), serve as negative regulators of YycG activity [138, 165]. YycH and YycI are extracellular proteins, which are attached to the cytoplasmic membrane via single N-terminal transmembrane sequences. Studies show that YycH, YycI and YycG interact through their transmembrane helices, and that the activity of YycG is modulated by subtle alterations in the structure of this ternary transmembrane complex [165]. Although no close homologs of YycH and YycI are encoded in the *S. pneumoniae* genome, it is conceivable that pneumococcal WalK is regulated in a similar manner, i.e. through intramembrane contact between its transmembrane domain and the corresponding domains of other transmembrane proteins.

Is StkP regulating the activity of WalK?

Interestingly, the eukaryotic-type serine/threonine protein kinase StkP positively regulates the transcription of the genes encoding PcsB, LytB and Spr0096 [149]. It has been proposed in the literature that the WalK and StkP signal transduction pathways converge on the response regulator WalR [149], and some experimental evidence seem to support this idea [155]. In addition, it has been reported that the response regulators RR06 and RitR can be activated through StkP-mediated

threonine phosphorylation in *S. pneumoniae* [150, 151]. However, the results obtained in the present study do not easily fit into the proposed model. If StkP directly phosphorylates WalR to increase its ability to drive expression from cognate promoters, it would be expected that it is able to do so independently of WalK. Contrary to this, our results indicate that the effect of StkP depends on whether WalK is present or not. In the presence of WalK, deletion of the *stkP* gene reduces reporter gene expression by about 50% (Figure 4, paper III). In a Δ*walK* background, however, deletion of *stkP* has no effect at all. Even though the luciferase activity in a strain lacking *walK* is low, it is well above the detection limit of the reporter assay. Thus, if StkP is operating independently of WalK, a further reduction should have been observed in the *stkP*/*walK* double mutant. Similarly, when *stkP* was deleted in a $WalK^{T222A}$ background, no reduction in reporter gene expression was observed (Figure 4, paper III). The T222A mutation is reported to abolish the phosphatase activity of WalK, and lock it permanently in the kinase mode [112]. Thus, in this case, WalK is operating at maximum efficiency, and may therefore mask the effect of deleting *stkP*. We also investigated whether deleting *stkP* affected the crosstalk between the histidine kinase PnpS (HK04) and WalR in *S. pneumoniae*. PnpS only phosphorylates WalR when the genes encoding its cognate response regulator PnpR (RR04) and WalK have been deleted [112]. Our results show that reporter gene expression does not change when *stkP* is deleted in a *pnpR*/*walK* double mutant (Figure 4, paper III). Curiously, in all of the examples described above, StkP does not have a positive effect on reporter gene expression when WalK is absent, while its contribution is considerable in the presence of WalK (Figure 4, paper III). These observations led us to suspect that StkP stimulates PcsB expression by stimulating the kinase or inhibiting the phosphatase activity of WalK.

To further explore this possibility we wanted to determine if StkP's ability to upregulate PcsB expression depends on its kinase activity. To construct a strain producing an inactive kinase (SPH317), the invariant catalytic lysine residue (K42) of StkP was replaced by a methionine [174]. Immunoblotting with a phosphothreonine-specific antibody revealed two strong bands in the positive control (SPH261), but no bands in the samples prepared from the SPH317 ($StkP^{K42M}$) and SPH307 (ΔStkP) strains (Figure 5B, paper III). Intriguingly, the $StkP^{K42M}$ mutant showed significantly higher reporter gene expression than the ΔStkP mutant (Figure 5A, paper III). Compared to the SPH261 wild-type strain, light emission in strain SPH317 was somewhat reduced, but the reduction was much stronger in the SPH307 strain. This result clearly shows that the

presence of an inactive StkP protein has a positive effect on reporter gene expression. Hence, the hypothesis that the WalK and StkP signal transduction pathways converge on the response regulator WalR, and that StkP positively regulates PcsB by phosphorylating WalR, cannot be the whole truth.

Is it possible that StkP regulates the activity of WalK through direct protein-protein interaction? Fukushima and co-workers (2010) showed that the cytoplasmic PAS domain of *B. subtilis* YycG (WalK) is required to direct the protein to the septum. Using two-hybrid analysis they showed that YycG probably interacts with the later-stage cell division proteins DivIB, Pbp2B, FtsL and possibly FtsW. Furthermore, their results indicated that the interaction of YycG with the divisome proteins may serve a regulatory rather than localization function. Thus the idea that WalK can be regulated through direct interaction with other proteins are not unprecedented. However, in contrast to YycG from *B. subtilis,* which is localized at division septa, pneumococcal WalK is reported to have a patchy localization throughout the membrane [126]. StkP on the other hand, co-localize with the cell division apparatus [175, 176]. This suggests that WalK and StkP may not co-localize at the septum. Two attempts were made to verify the reported localization pattern of pneumococcal WalK either fusing green-fluorescent protein (GFP), or a FLAG-tag to the C-terminal end of WalK via a linker. However, no signal was detected when pneumococcal cells expressing either the WalK-GFP fusion protein or the WalK-FLAG fusion protein were examined in a fluorescence microscope (results not shown). These results suggest that WalK is expressed in small amounts, and that localization studies of WalK might be prone to artifacts. It does not make sense that WalK, which is thought to coordinate splitting of the septal cross wall with the cell division process, should be localized to the cell surface periphery. Further studies are needed to verify the localization of WalK in *S. pneumoniae*, and to verify or disprove the proposed interaction between WalK and StkP.

4. Concluding remarks and future perspectives

The present work has focused on the function and regulation of PcsB in *S. pneumoniae*. Before the work was started, several lines of evidence suggested that PcsB is involved in daughter cell separation in *S. pneumoniae* and other streptococci, but conclusive evidence was lacking. The new data provided in paper II leave little doubt that PcsB is the major cell disconnecting peptidoglycan hydrolase in these species. In addition, the structural data gave rise to a model that explains how PcsB might be regulated and perform its function *in vivo*. However, several important questions remain unanswered. A particularly interesting one is this: why is PcsB not essential in all pneumococcal strains? The strains that survive without PcsB is clearly very sick, but they still manage to grow and divide. The only explanation I can come up with is that these strains have a backup system that is missing or nonfunctional in the R6 and D39 strains. Three largely redundant amidases, AmiA, AmiB and AmiC, are involved in daughter cell separation in *E. coli*. All three must be deleted before *E. coli* cells fail to split their septal cross walls [99]. Considering the importance of the cell separation process, it is not surprising that bacteria have evolved more than one system that can carry out this function. An interesting topic for future research should therefore be to search for the peptidoglycan hydrolase(s) that allows some pneumococcal strains to survive without PcsB. Another important question that arise from the present study is how the FtsEX-PcsB complex is regulated. Even though ATP-hydrolysis probably drives the conformational change required to activate PcsB, some mechanism needs to control the activation of the FtsE ATPase. In addition, further research are required to identify the exact cleavage site of PcsB, and to explore and test the FtsEX-PcsB model proposed in paper II.

The data presented in paper III, represent strong evidence that the transmembrane segment of WalK functions as a sensor domain. An obvious question that follows is: what is the nature of the signal sensed? Although we were unable to answer this question in the present study, our results suggest that the sensor domain of WalK senses the presence of another transmembrane protein through direct contact between their transmembrane segments. StkP, which is a transmembrane protein, is a possible candidate for the unknown protein predicted to be sensed by WalK. Our data suggest that StkP's positive regulation of PcsB expression depends on the presence of WalK. Furthermore, we showed that most of this positive regulation is independent of the protein kinase

activity of StkP. Thus, it is possible that WalK senses the presence of StkP through its transmembrane segment or cytoplasmic PAS domain. StkP contains extracellular PASTA domains that have been shown to bind muropeptides in *S. pneumoniae* [177]. Homologous of StkP, PknB in *Mycobacterium tuberculosis* and PrkC in *B. subtilis* is also shown to bind muropeptides [178, 179]. Perhaps, StkP monitor the progress of cross wall synthesis and cell division via its extracellular PASTA domains and relays this information to WalK through direct interaction. This hypothesis should be tested in future studies.

5. References

1. Kilian, M., et al., *Evolution of* Streptococcus pneumoniae *and its close commensal relatives.* PLoS One, 2008. **3**(7): p. e2683.
2. Simell, B., et al., *The fundamental link between pneumococcal carriage and disease.* Expert Rev Vaccines, 2012. **11**(7): p. 841-55.
3. Shak, J.R., J.E. Vidal, and K.P. Klugman, *Influence of bacterial interactions on pneumococcal colonization of the nasopharynx.* Trends Microbiol, 2013. **21**(3): p. 129-35.
4. Levine, O.S., et al., *Pneumococcal vaccination in developing countries.* Lancet, 2006. **367**(9526): p. 1880-2.
5. Henriques-Normark, B. and E.I. Tuomanen, *The pneumococcus: epidemiology, microbiology, and pathogenesis.* Cold Spring Harb Perspect Med, 2013. **3**(7).
6. Wise, E.M., Jr. and J.T. Park, *Penicillin: its basic site of action as an inhibitor of a peptide cross-linking reaction in cell wall mucopeptide synthesis.* Proc Natl Acad Sci U S A, 1965. **54**(1): p. 75-81.
7. Cornick, J.E. and S.D. Bentley, Streptococcus pneumoniae*: the evolution of antimicrobial resistance to beta-lactams, fluoroquinolones and macrolides.* Microbes Infect, 2012. **14**(7-8): p. 573-83.
8. Riedel, S., et al., *Antimicrobial use in Europe and antimicrobial resistance in* Streptococcus pneumoniae*.* Eur J Clin Microbiol Infect Dis, 2007. **26**(7): p. 485-90.
9. Zapun, A., C. Contreras-Martel, and T. Vernet, *Penicillin-binding proteins and beta-lactam resistance.* FEMS Microbiol Rev, 2008. **32**(2): p. 361-85.
10. Vollmer, W., D. Blanot, and M.A. de Pedro, *Peptidoglycan structure and architecture.* FEMS Microbiol Rev, 2008. **32**(2): p. 149-67.
11. Vollmer, W., *Bacterial growth does require peptidoglycan hydrolases.* Mol Microbiol, 2012. **86**(5): p. 1031-5.
12. Garcia-Bustos, J.F., B.T. Chait, and A. Tomasz, *Structure of the peptide network of pneumococcal peptidoglycan.* J Biol Chem, 1987. **262**(32): p. 15400-5.
13. Bui, N.K., et al., *Isolation and analysis of cell wall components from* Streptococcus pneumoniae*.* Anal Biochem, 2012. **421**(2): p. 657-66.
14. Scheffers, D.J. and M.G. Pinho, *Bacterial cell wall synthesis: new insights from localization studies.* Microbiol Mol Biol Rev, 2005. **69**(4): p. 585-607.

15. Barendt, S.M., L.T. Sham, and M.E. Winkler, *Characterization of mutants deficient in the L,D-carboxypeptidase (DacB) and WalRK (VicRK) regulon, involved in peptidoglycan maturation of* Streptococcus pneumoniae *serotype 2 strain D39.* J Bacteriol, 2011. **193**(9): p. 2290-300.
16. Vollmer, W. and J.V. Holtje, *The architecture of the murein (peptidoglycan) in gram-negative bacteria: vertical scaffold or horizontal layer(s)?* J Bacteriol, 2004. **186**(18): p. 5978-87.
17. Hayhurst, E.J., et al., *Cell wall peptidoglycan architecture in* Bacillus subtilis. Proc Natl Acad Sci U S A, 2008. **105**(38): p. 14603-8.
18. Popham, D.L., *Visualizing the production and arrangement of peptidoglycan in Gram-positive cells.* Mol Microbiol, 2013. **88**(4): p. 645-9.
19. Vollmer, W. and S.J. Seligman, *Architecture of peptidoglycan: more data and more models.* Trends Microbiol, 2010. **18**(2): p. 59-66.
20. Dmitriev, B.A., et al., *Tertiary structure of bacterial murein: the scaffold model.* J Bacteriol, 2003. **185**(11): p. 3458-68.
21. Dmitriev, B., F. Toukach, and S. Ehlers, *Towards a comprehensive view of the bacterial cell wall.* Trends Microbiol, 2005. **13**(12): p. 569-74.
22. Beeby, M., et al., *Architecture and assembly of the Gram-positive cell wall.* Mol Microbiol, 2013. **88**(4): p. 664-72.
23. Baur, S., et al., *Synthesis of CDP-activated ribitol for teichoic acid precursors in* Streptococcus pneumoniae. J Bacteriol, 2009. **191**(4): p. 1200-10.
24. Denapaite, D., et al., *Biosynthesis of teichoic acids in* Streptococcus pneumoniae *and closely related species: lessons from genomes.* Microb Drug Resist, 2012. **18**(3): p. 344-58.
25. Fischer, W., *Phosphocholine of pneumococcal teichoic acids: role in bacterial physiology and pneumococcal infection.* Res Microbiol, 2000. **151**(6): p. 421-7.
26. Fischer, W., et al., *Teichoic acid and lipoteichoic acid of* Streptococcus pneumoniae *possess identical chain structures. A reinvestigation of teichoid acid (C polysaccharide).* Eur J Biochem, 1993. **215**(3): p. 851-7.
27. Berg, K.H., et al., *Peptide-regulated gene depletion system developed for use in* Streptococcus pneumoniae. J Bacteriol, 2011. **193**(19): p. 5207-15.
28. Hakenbeck, R., et al., *Versatility of choline metabolism and choline-binding proteins in* Streptococcus pneumoniae *and commensal streptococci.* FEMS Microbiol Rev, 2009. **33**(3): p. 572-86.
29. Seo, H.S., et al., *A new model of pneumococcal lipoteichoic acid structure resolves biochemical, biosynthetic, and serologic inconsistencies of the current model.* J Bacteriol, 2008. **190**(7): p. 2379-87.

30. Damjanovic, M., et al., *The essential tacF gene is responsible for the choline-dependent growth phenotype of* Streptococcus pneumoniae. J Bacteriol, 2007. **189**(19): p. 7105-11.
31. Kharat, A.S. and A. Tomasz, *Drastic reduction in the virulence of* Streptococcus pneumoniae *expressing type 2 capsular polysaccharide but lacking choline residues in the cell wall.* Mol Microbiol, 2006. **60**(1): p. 93-107.
32. Fischer, H. and A. Tomasz, *Production and release of peptidoglycan and wall teichoic acid polymers in pneumococci treated with beta-lactam antibiotics.* J Bacteriol, 1984. **157**(2): p. 507-13.
33. Barreteau, H., et al., *Cytoplasmic steps of peptidoglycan biosynthesis.* FEMS Microbiol Rev, 2008. **32**(2): p. 168-207.
34. Egan, A.J. and W. Vollmer, *The physiology of bacterial cell division.* Ann N Y Acad Sci, 2013. **1277**: p. 8-28.
35. Bouhss, A., et al., *The biosynthesis of peptidoglycan lipid-linked intermediates.* FEMS Microbiol Rev, 2008. **32**(2): p. 208-33.
36. Zapun, A., et al., *In vitro reconstitution of peptidoglycan assembly from the Gram-positive pathogen* Streptococcus pneumoniae. ACS Chem Biol, 2013. **8**(12): p. 2688-96.
37. Sauvage, E., et al., *The penicillin-binding proteins: structure and role in peptidoglycan biosynthesis.* FEMS Microbiol Rev, 2008. **32**(2): p. 234-58.
38. Massidda, O., L. Novakova, and W. Vollmer, *From models to pathogens: how much have we learned about* Streptococcus pneumoniae *cell division?* Environ Microbiol, 2013. **15**(12): p. 3133-57.
39. Morlot, C., et al., *Crystal structure of a peptidoglycan synthesis regulatory factor (PBP3) from* Streptococcus pneumoniae. J Biol Chem, 2005. **280**(16): p. 15984-91.
40. Severin, A., et al., *Altered murein composition in a DD-carboxypeptidase mutant of* Streptococcus pneumoniae. J Bacteriol, 1992. **174**(15): p. 5152-5.
41. Tipper, D.J. and J.L. Strominger, *Mechanism of action of penicillins: a proposal based on their structural similarity to acyl-D-alanyl-D-alanine.* Proc Natl Acad Sci U S A, 1965. **54**(4): p. 1133-41.
42. Pinho, M.G., M. Kjos, and J.W. Veening, *How to get (a)round: mechanisms controlling growth and division of coccoid bacteria.* Nat Rev Microbiol, 2013. **11**(9): p. 601-14.
43. Fleurie, A., et al., *Interplay of the serine/threonine-kinase StkP and the paralogs DivIVA and GpsB in pneumococcal cell elongation and division.* PLoS Genet, 2014. **10**(4): p. e1004275.
44. Zapun, A., T. Vernet, and M.G. Pinho, *The different shapes of cocci.* FEMS Microbiol Rev, 2008. **32**(2): p. 345-60.

45. Matias, V.R. and T.J. Beveridge, *Cryo-electron microscopy of cell division in* Staphylococcus aureus *reveals a mid-zone between nascent cross walls.* Mol Microbiol, 2007. **64**(1): p. 195-206.
46. Matias, V.R. and T.J. Beveridge, *Native cell wall organization shown by cryo-electron microscopy confirms the existence of a periplasmic space in* Staphylococcus aureus. J Bacteriol, 2006. **188**(3): p. 1011-21.
47. Zuber, B., et al., *Granular layer in the periplasmic space of gram-positive bacteria and fine structures of* Enterococcus gallinarum *and* Streptococcus gordonii *septa revealed by cryo-electron microscopy of vitreous sections.* J Bacteriol, 2006. **188**(18): p. 6652-60.
48. Schuster, C., B. Dobrinski, and R. Hakenbeck, *Unusual septum formation in* Streptococcus pneumoniae *mutants with an alteration in the D,D-carboxypeptidase penicillin-binding protein 3.* J Bacteriol, 1990. **172**(11): p. 6499-505.
49. Fleurie, A., et al., *MapZ marks the division sites and positions FtsZ rings in* Streptococcus pneumoniae. Nature, 2014. **516**(7530): p. 259-62.
50. Holeckova, N., et al., *LocZ Is a New Cell Division Protein Involved in Proper Septum Placement in* Streptococcus pneumoniae. MBio, 2014. **6**(1).
51. Morlot, C., et al., *Growth and division of* Streptococcus pneumoniae*: localization of the high molecular weight penicillin-binding proteins during the cell cycle.* Mol Microbiol, 2003. **50**(3): p. 845-55.
52. Strauss, M.P., et al., *3D-SIM super resolution microscopy reveals a bead-like arrangement for FtsZ and the division machinery: implications for triggering cytokinesis.* PLoS Biol, 2012. **10**(9): p. e1001389.
53. Novakova, L., et al., *Identification of multiple substrates of the StkP Ser/Thr protein kinase in* Streptococcus pneumoniae. J Bacteriol, 2010. **192**(14): p. 3629-38.
54. Harry, E.J., *Microbiology: A beacon for bacterial tubulin.* Nature, 2014. **516**(7530): p. 175-6.
55. Berg, K.H., et al., *Effects of low PBP2b levels on cell morphology and peptidoglycan composition in* Streptococcus pneumoniae *R6.* J Bacteriol, 2013. **195**(19): p. 4342-54.
56. Sham, L.T., et al., *Recent advances in pneumococcal peptidoglycan biosynthesis suggest new vaccine and antimicrobial targets.* Curr Opin Microbiol, 2012. **15**(2): p. 194-203.
57. Sham, L.T., et al., *Essential PcsB putative peptidoglycan hydrolase interacts with the essential FtsXSpn cell division protein in* Streptococcus pneumoniae *D39.* Proc Natl Acad Sci U S A, 2011. **108**(45): p. E1061-9.
58. Garcia, P., et al., *LytB, a novel pneumococcal murein hydrolase essential for cell separation.* Mol Microbiol, 1999. **31**(4): p. 1275-81.

59. Arends, S.J., R.J. Kustusch, and D.S. Weiss, *ATP-binding site lesions in FtsE impair cell division.* J Bacteriol, 2009. **191**(12): p. 3772-84.
60. Schmidt, K.L., et al., *A predicted ABC transporter, FtsEX, is needed for cell division in* Escherichia coli. J Bacteriol, 2004. **186**(3): p. 785-93.
61. Corbin, B.D., et al., *Interaction between cell division proteins FtsE and FtsZ.* J Bacteriol, 2007. **189**(8): p. 3026-35.
62. Sham, L.T., et al., *Involvement of FtsE ATPase and FtsX extracellular loops 1 and 2 in FtsEX-PcsB complex function in cell division of* Streptococcus pneumoniae *D39.* MBio, 2013. **4**(4).
63. Lopez, R. and E. Garcia, *Recent trends on the molecular biology of pneumococcal capsules, lytic enzymes, and bacteriophage.* FEMS Microbiol Rev, 2004. **28**(5): p. 553-80.
64. Vollmer, W., et al., *Bacterial peptidoglycan (murein) hydrolases.* FEMS Microbiol Rev, 2008. **32**(2): p. 259-86.
65. Wyckoff, T.J., J.A. Taylor, and N.R. Salama, *Beyond growth: novel functions for bacterial cell wall hydrolases.* Trends Microbiol, 2012. **20**(11): p. 540-7.
66. Heidrich, C., et al., *Effects of multiple deletions of murein hydrolases on viability, septum cleavage, and sensitivity to large toxic molecules in* Escherichia coli. J Bacteriol, 2002. **184**(22): p. 6093-9.
67. Singh, S.K., et al., *Three redundant murein endopeptidases catalyse an essential cleavage step in peptidoglycan synthesis of* Escherichia coli *K12.* Mol Microbiol, 2012. **86**(5): p. 1036-51.
68. Layec, S., B. Decaris, and N. Leblond-Bourget, *Diversity of Firmicutes peptidoglycan hydrolases and specificities of those involved in daughter cell separation.* Res Microbiol, 2008. **159**(7-8): p. 507-15.
69. Borges, F., et al., *cse, a Chimeric and variable gene, encodes an extracellular protein involved in cellular segregation in* Streptococcus thermophilus. J Bacteriol, 2005. **187**(8): p. 2737-46.
70. Lopez, R., et al., *The pneumococcal cell wall degrading enzymes: a modular design to create new lysins?* Microb Drug Resist, 1997. **3**(2): p. 199-211.
71. De Las Rivas, B., et al., *Purification and polar localization of pneumococcal LytB, a putative endo-beta-N-acetylglucosaminidase: the chain-dispersing murein hydrolase.* J Bacteriol, 2002. **184**(18): p. 4988-5000.
72. Mosser, J.L. and A. Tomasz, *Choline-containing teichoic acid as a structural component of pneumococcal cell wall and its role in sensitivity to lysis by an autolytic enzyme.* J Biol Chem, 1970. **245**(2): p. 287-98.
73. Giudicelli, S. and A. Tomasz, *Attachment of pneumococcal autolysin to wall teichoic acids, an essential step in enzymatic wall degradation.* J Bacteriol, 1984. **158**(3): p. 1188-90.

74. Eldholm, V., et al., *Fratricide in* Streptococcus pneumoniae*: contributions and role of the cell wall hydrolases CbpD, LytA and LytC.* Microbiology, 2009. **155**(Pt 7): p. 2223-34.
75. Briese, T. and R. Hakenbeck, *Interaction of the pneumococcal amidase with lipoteichoic acid and choline.* Eur J Biochem, 1985. **146**(2): p. 417-27.
76. Mellroth, P., et al., *Structural and functional insights into peptidoglycan access for the lytic amidase LytA of* Streptococcus pneumoniae. MBio, 2014. **5**(1): p. e01120-13.
77. Sanz, J.M., R. Lopez, and J.L. Garcia, *Structural requirements of choline derivatives for 'conversion' of pneumococcal amidase. A new single-step procedure for purification of this autolysin.* FEBS Lett, 1988. **232**(2): p. 308-12.
78. Sanchez-Puelles, J.M., et al., *Immobilization and single-step purification of fusion proteins using DEAE-cellulose.* Eur J Biochem, 1992. **203**(1-2): p. 153-9.
79. Ortega, S., et al., *Single-step purification on DEAE-sephacel of recombinant polypeptides produced in* Escherichia coli. Biotechnology (N Y), 1992. **10**(7): p. 795-8.
80. Garcia, P., et al., *Purification and characterization of the autolytic glycosidase of* Streptococcus pneumoniae. Biochem Biophys Res Commun, 1989. **158**(1): p. 251-6.
81. Bai, X.H., et al., *Structure of pneumococcal peptidoglycan hydrolase LytB reveals insights into the bacterial cell wall remodeling and pathogenesis.* J Biol Chem, 2014.
82. Perez-Dorado, I., et al., *Insights into pneumococcal fratricide from the crystal structures of the modular killing factor LytC.* Nat Struct Mol Biol, 2010. **17**(5): p. 576-81.
83. Garcia, P., et al., *The molecular characterization of the first autolytic lysozyme of* Streptococcus pneumoniae *reveals evolutionary mobile domains.* Mol Microbiol, 1999. **33**(1): p. 128-38.
84. Lopez, R., et al., *Biological roles of two new murein hydrolases of* Streptococcus pneumoniae *representing examples of module shuffling.* Res Microbiol, 2000. **151**(6): p. 437-43.
85. Eldholm, V., et al., *Pneumococcal CbpD is a murein hydrolase that requires a dual cell envelope binding specificity to kill target cells during fratricide.* Mol Microbiol, 2010. **76**(4): p. 905-17.
86. Kausmally, L., et al., *Choline-binding protein D (CbpD) in* Streptococcus pneumoniae *is essential for competence-induced cell lysis.* J Bacteriol, 2005. **187**(13): p. 4338-45.
87. Reinscheid, D.J., et al., *Identification and molecular analysis of PcsB, a protein required for cell wall separation of group B streptococcus.* J Bacteriol, 2001. **183**(4): p. 1175-83.
88. Reinscheid, D.J., et al., *Functional analysis of a PcsB-deficient mutant of group B streptococcus.* FEMS Microbiol Lett, 2003. **221**(1): p. 73-9.
89. Ng, W.L., et al., *Constitutive expression of PcsB suppresses the requirement for the essential VicR (YycF) response regulator in* Streptococcus pneumoniae *R6.* Mol Microbiol, 2003. **50**(5): p. 1647-63.

90. Barendt, S.M., et al., *Influences of capsule on cell shape and chain formation of wild-type and pcsB mutants of serotype 2* Streptococcus pneumoniae. J Bacteriol, 2009. **191**(9): p. 3024-40.
91. Ng, W.L., K.M. Kazmierczak, and M.E. Winkler, *Defective cell wall synthesis in* Streptococcus pneumoniae *R6 depleted for the essential PcsB putative murein hydrolase or the VicR (YycF) response regulator.* Mol Microbiol, 2004. **53**(4): p. 1161-75.
92. Ng, W.L., H.C. Tsui, and M.E. Winkler, *Regulation of the pspA virulence factor and essential pcsB murein biosynthetic genes by the phosphorylated VicR (YycF) response regulator in* Streptococcus pneumoniae. J Bacteriol, 2005. **187**(21): p. 7444-59.
93. Giefing, C., et al., *Discovery of a novel class of highly conserved vaccine antigens using genomic scale antigenic fingerprinting of pneumococcus with human antibodies.* J Exp Med, 2008. **205**(1): p. 117-31.
94. Giefing-Kroll, C., et al., *Absence of pneumococcal PcsB is associated with overexpression of LysM domain-containing proteins.* Microbiology, 2011. **157**(Pt 7): p. 1897-909.
95. Mills, M.F., M.E. Marquart, and L.S. McDaniel, *Localization of PcsB of* Streptococcus pneumoniae *and its differential expression in response to stress.* J Bacteriol, 2007. **189**(12): p. 4544-6.
96. Uehara, T., T. Dinh, and T.G. Bernhardt, *LytM-domain factors are required for daughter cell separation and rapid ampicillin-induced lysis in* Escherichia coli. J Bacteriol, 2009. **191**(16): p. 5094-107.
97. Uehara, T., et al., *Daughter cell separation is controlled by cytokinetic ring-activated cell wall hydrolysis.* EMBO J, 2010. **29**(8): p. 1412-22.
98. Yang, D.C., et al., *An ATP-binding cassette transporter-like complex governs cell-wall hydrolysis at the bacterial cytokinetic ring.* Proc Natl Acad Sci U S A, 2011. **108**(45): p. E1052-60.
99. Yang, D.C., et al., *A conformational switch controls cell wall-remodelling enzymes required for bacterial cell division.* Mol Microbiol, 2012. **85**(4): p. 768-81.
100. Meisner, J., et al., *FtsEX is required for CwlO peptidoglycan hydrolase activity during cell wall elongation in* Bacillus subtilis. Mol Microbiol, 2013. **89**(6): p. 1069-83.
101. Dominguez-Cuevas, P., et al., *Differentiated roles for MreB-actin isologues and autolytic enzymes in* Bacillus subtilis *morphogenesis.* Mol Microbiol, 2013. **89**(6): p. 1084-98.
102. Layec, S., B. Decaris, and N. Leblond-Bourget, *Characterization of proteins belonging to the CHAP-related superfamily within the Firmicutes.* J Mol Microbiol Biotechnol, 2008. **14**(1-3): p. 31-40.
103. Bateman, A. and N.D. Rawlings, *The CHAP domain: a large family of amidases including GSP amidase and peptidoglycan hydrolases.* Trends Biochem Sci, 2003. **28**(5): p. 234-7.

104. Berg, K.H., H.S. Ohnstad, and L.S. Havarstein, *LytF, a novel competence-regulated murein hydrolase in the genus Streptococcus.* J Bacteriol, 2012. **194**(3): p. 627-35.

105. Matsushita, M. and K.D. Janda, *Histidine kinases as targets for new antimicrobial agents.* Bioorg Med Chem, 2002. **10**(4): p. 855-67.

106. Hoch, J.A., *Two-component and phosphorelay signal transduction.* Curr Opin Microbiol, 2000. **3**(2): p. 165-70.

107. Parkinson, J.S., *Signal transduction schemes of bacteria.* Cell, 1993. **73**(5): p. 857-71.

108. Mascher, T., J.D. Helmann, and G. Unden, *Stimulus perception in bacterial signal-transducing histidine kinases.* Microbiol Mol Biol Rev, 2006. **70**(4): p. 910-38.

109. Fukuchi, K., et al., *The essential two-component regulatory system encoded by yycF and yycG modulates expression of the ftsAZ operon in* Bacillus subtilis. Microbiology, 2000. **146 (Pt 7)**: p. 1573-83.

110. Dubrac, S., et al., *A matter of life and death: cell wall homeostasis and the WalKR (YycGF) essential signal transduction pathway.* Mol Microbiol, 2008. **70**(6): p. 1307-22.

111. Lange, R., et al., *Domain organization and molecular characterization of 13 two-component systems identified by genome sequencing of* Streptococcus pneumoniae. Gene, 1999. **237**(1): p. 223-34.

112. Wayne, K.J., et al., *Involvement of WalK (VicK) phosphatase activity in setting WalR (VicR) response regulator phosphorylation level and limiting cross-talk in* Streptococcus pneumoniae *D39 cells.* Mol Microbiol, 2012. **86**(3): p. 645-60.

113. Fabret, C. and J.A. Hoch, *A two-component signal transduction system essential for growth of* Bacillus subtilis*: implications for anti-infective therapy.* J Bacteriol, 1998. **180**(23): p. 6375-83.

114. Bisicchia, P., et al., *The essential YycFG two-component system controls cell wall metabolism in* Bacillus subtilis. Mol Microbiol, 2007. **65**(1): p. 180-200.

115. Howell, A., et al., *Genes controlled by the essential YycG/YycF two-component system of* Bacillus subtilis *revealed through a novel hybrid regulator approach.* Mol Microbiol, 2003. **49**(6): p. 1639-55.

116. Dubrac, S. and T. Msadek, *Identification of genes controlled by the essential YycG/YycF two-component system of* Staphylococcus aureus. J Bacteriol, 2004. **186**(4): p. 1175-81.

117. Fukushima, T., et al., *A sensor histidine kinase co-ordinates cell wall architecture with cell division in* Bacillus subtilis. Mol Microbiol, 2008. **69**(3): p. 621-32.

118. Szurmant, H., et al., *YycH regulates the activity of the essential YycFG two-component system in* Bacillus subtilis. J Bacteriol, 2005. **187**(15): p. 5419-26.

119. Salzberg, L.I., et al., *The WalRK (YycFG) and sigma(I) RsgI regulators cooperate to control CwlO and LytE expression in exponentially growing and stressed* Bacillus subtilis *cells.* Mol Microbiol, 2013. **87**(1): p. 180-95.

120. Dubrac, S., et al., *New insights into the WalK/WalR (YycG/YycF) essential signal transduction pathway reveal a major role in controlling cell wall metabolism and biofilm formation in* Staphylococcus aureus*.* J Bacteriol, 2007. **189**(22): p. 8257-69.

121. Buist, G., et al., *LysM, a widely distributed protein motif for binding to (peptido)glycans.* Mol Microbiol, 2008. **68**(4): p. 838-47.

122. Mesnage, S., et al., *Molecular basis for bacterial peptidoglycan recognition by LysM domains.* Nat Commun, 2014. **5**: p. 4269.

123. Kadioglu, A., et al., *The MicAB two-component signaling system is involved in virulence of* Streptococcus pneumoniae*.* Infect Immun, 2003. **71**(11): p. 6676-9.

124. Mohedano, M.L., et al., *Evidence that the essential response regulator YycF in* Streptococcus pneumoniae *modulates expression of fatty acid biosynthesis genes and alters membrane composition.* J Bacteriol, 2005. **187**(7): p. 2357-67.

125. Wagner, C., et al., *Genetic analysis and functional characterization of the* Streptococcus pneumoniae *vic operon.* Infect Immun, 2002. **70**(11): p. 6121-8.

126. Wayne, K.J., et al., *Localization and cellular amounts of the WalRKJ (VicRKX) two-component regulatory system proteins in serotype 2* Streptococcus pneumoniae*.* J Bacteriol, 2010. **192**(17): p. 4388-94.

127. Howell, A., et al., *Interactions between the YycFG and PhoPR two-component systems in* Bacillus subtilis*: the PhoR kinase phosphorylates the non-cognate YycF response regulator upon phosphate limitation.* Mol Microbiol, 2006. **59**(4): p. 1199-215.

128. Ng, W.L. and M.E. Winkler, *Singular structures and operon organizations of essential two-component systems in species of Streptococcus.* Microbiology, 2004. **150**(Pt 10): p. 3096-8.

129. Taylor, B.L. and I.B. Zhulin, *PAS domains: internal sensors of oxygen, redox potential, and light.* Microbiol Mol Biol Rev, 1999. **63**(2): p. 479-506.

130. Echenique, J.R. and M.C. Trombe, *Competence repression under oxygen limitation through the two-component MicAB signal-transducing system in* Streptococcus pneumoniae *and involvement of the PAS domain of MicB.* J Bacteriol, 2001. **183**(15): p. 4599-608.

131. Wang, C., et al., *Mechanistic insights revealed by the crystal structure of a histidine kinase with signal transducer and sensor domains.* PLoS Biol, 2013. **11**(2): p. e1001493.

132. Aravind, L. and C.P. Ponting, *The cytoplasmic helical linker domain of receptor histidine kinase and methyl-accepting proteins is common to many prokaryotic signalling proteins.* FEMS Microbiol Lett, 1999. **176**(1): p. 111-6.

133. Airola, M.V., et al., *Architecture of the soluble receptor Aer2 indicates an in-line mechanism for PAS and HAMP domain signaling.* J Mol Biol, 2013. **425**(5): p. 886-901.

134. Huynh, T.N. and V. Stewart, *Negative control in two-component signal transduction by transmitter phosphatase activity.* Mol Microbiol, 2011. **82**(2): p. 275-86.

135. Turck, M. and G. Bierbaum, *Purification and activity testing of the full-length YycFGHI proteins of* Staphylococcus aureus. PLoS One, 2012. **7**(1): p. e30403.

136. Gutu, A.D., et al., *Kinetic characterization of the WalRKSpn (VicRK) two-component system of* Streptococcus pneumoniae: *dependence of WalKSpn (VicK) phosphatase activity on its PAS domain.* J Bacteriol, 2010. **192**(9): p. 2346-58.

137. Fukushima, T., et al., *A role for the essential YycG sensor histidine kinase in sensing cell division.* Mol Microbiol, 2011. **79**(2): p. 503-22.

138. Szurmant, H., et al., *YycH and YycI interact to regulate the essential YycFG two-component system in* Bacillus subtilis. J Bacteriol, 2007. **189**(8): p. 3280-9.

139. Galperin, M.Y., *Structural classification of bacterial response regulators: diversity of output domains and domain combinations.* J Bacteriol, 2006. **188**(12): p. 4169-82.

140. Martinez-Hackert, E. and A.M. Stock, *Structural relationships in the OmpR family of winged-helix transcription factors.* J Mol Biol, 1997. **269**(3): p. 301-12.

141. Firon, A., et al., *The Abi-domain protein Abx1 interacts with the CovS histidine kinase to control virulence gene expression in group B Streptococcus.* PLoS Pathog, 2013. **9**(2): p. e1003179.

142. Jung, K., et al., *Histidine kinases and response regulators in networks.* Curr Opin Microbiol, 2012. **15**(2): p. 118-24.

143. Wolfe, A.J., *Physiologically relevant small phosphodonors link metabolism to signal transduction.* Curr Opin Microbiol, 2010. **13**(2): p. 204-9.

144. Ramos-Montanez, S., et al., *Instability of ackA (acetate kinase) mutations and their effects on acetyl phosphate and ATP amounts in* Streptococcus pneumoniae *D39.* J Bacteriol, 2010. **192**(24): p. 6390-400.

145. Lukat, G.S., et al., *Phosphorylation of bacterial response regulator proteins by low molecular weight phospho-donors.* Proc Natl Acad Sci U S A, 1992. **89**(2): p. 718-22.

146. Feng, J., et al., *Role of phosphorylated metabolic intermediates in the regulation of glutamine synthetase synthesis in* Escherichia coli. J Bacteriol, 1992. **174**(19): p. 6061-70.

147. Laub, M.T. and M. Goulian, *Specificity in two-component signal transduction pathways.* Annu Rev Genet, 2007. **41**: p. 121-45.

148. Dhiman, A., et al., *Functional characterization of WalRK: A two-component signal transduction system from* Bacillus anthracis. FEBS Open Bio, 2014. **4**: p. 65-76.

149. Saskova, L., et al., *Eukaryotic-type serine/threonine protein kinase StkP is a global regulator of gene expression in* Streptococcus pneumoniae. J Bacteriol, 2007. **189**(11): p. 4168-79.

150. Agarwal, S., et al., *Strain-specific regulatory role of eukaryote-like serine/threonine phosphatase in pneumococcal adherence.* Infect Immun, 2012. **80**(4): p. 1361-72.

151. Ulijasz, A.T., S.P. Falk, and B. Weisblum, *Phosphorylation of the RitR DNA-binding domain by a Ser-Thr phosphokinase: implications for global gene regulation in the streptococci.* Mol Microbiol, 2009. **71**(2): p. 382-90.

152. Novakova, L., et al., *Characterization of a eukaryotic type serine/threonine protein kinase and protein phosphatase of* Streptococcus pneumoniae *and identification of kinase substrates.* FEBS J, 2005. **272**(5): p. 1243-54.

153. Sun, X., et al., *Phosphoproteomic analysis reveals the multiple roles of phosphorylation in pathogenic bacterium* Streptococcus pneumoniae. J Proteome Res, 2010. **9**(1): p. 275-82.

154. Pancholi, V., G. Boel, and H. Jin, Streptococcus pyogenes *Ser/Thr kinase-regulated cell wall hydrolase is a cell division plane-recognizing and chain-forming virulence factor.* J Biol Chem, 2010. **285**(40): p. 30861-74.

155. Agarwal, S., et al., *Role of serine/threonine phosphatase (SP-STP) in* Streptococcus pyogenes *physiology and virulence.* J Biol Chem, 2011. **286**(48): p. 41368-80.

156. Shah, I.M. and J. Dworkin, *Induction and regulation of a secreted peptidoglycan hydrolase by a membrane Ser/Thr kinase that detects muropeptides.* Mol Microbiol, 2010. **75**(5): p. 1232-43.

157. Kobir, A., et al., *Protein phosphorylation in bacterial signal transduction.* Biochim Biophys Acta, 2011. **1810**(10): p. 989-94.

158. Alves, R. and M.A. Savageau, *Comparative analysis of prototype two-component systems with either bifunctional or monofunctional sensors: differences in molecular structure and physiological function.* Mol Microbiol, 2003. **48**(1): p. 25-51.

159. Stewart, R.C., *Protein histidine kinases: assembly of active sites and their regulation in signaling pathways.* Curr Opin Microbiol, 2010. **13**(2): p. 133-41.

160. Gao, R. and A.M. Stock, *Biological insights from structures of two-component proteins.* Annu Rev Microbiol, 2009. **63**: p. 133-54.

161. Mascher, T., *Intramembrane-sensing histidine kinases: a new family of cell envelope stress sensors in Firmicutes bacteria.* FEMS Microbiol Lett, 2006. **264**(2): p. 133-44.

162. Mitrophanov, A.Y. and E.A. Groisman, *Signal integration in bacterial two-component regulatory systems.* Genes Dev, 2008. **22**(19): p. 2601-11.

163. Buelow, D.R. and T.L. Raivio, *Three (and more) component regulatory systems - auxiliary regulators of bacterial histidine kinases.* Mol Microbiol, 2010. **75**(3): p. 547-66.

164. Mascher, T., *Bacterial (intramembrane-sensing) histidine kinases: signal transfer rather than stimulus perception.* Trends Microbiol, 2014. **22**(10): p. 559-565.

165. Szurmant, H., et al., *An essential sensor histidine kinase controlled by transmembrane helix interactions with its auxiliary proteins.* Proc Natl Acad Sci U S A, 2008. **105**(15): p. 5891-6.

166. Chayen, N.E., *Turning protein crystallisation from an art into a science.* Curr Opin Struct Biol, 2004. **14**(5): p. 577-83.

167. Goehring, N.W. and J. Beckwith, *Diverse paths to midcell: assembly of the bacterial cell division machinery.* Curr Biol, 2005. **15**(13): p. R514-26.

168. Bartual, S.G., et al., *Structural basis of PcsB-mediated cell separation in* Streptococcus pneumoniae. Nat Commun, 2014. **5**: p. 3842.

169. Mavrici, D., et al., Mycobacterium tuberculosis *FtsX extracellular domain activates the peptidoglycan hydrolase, RipC.* Proc Natl Acad Sci U S A, 2014. **111**(22): p. 8037-42.

170. Gotoh, Y., et al., *Two-component signal transduction as potential drug targets in pathogenic bacteria.* Curr Opin Microbiol, 2010. **13**(2): p. 232-9.

171. Liu, M., et al., *Defects in ex vivo and in vivo growth and sensitivity to osmotic stress of group A Streptococcus caused by interruption of response regulator gene vicR.* Microbiology, 2006. **152**(Pt 4): p. 967-78.

172. Delaune, A., et al., *Peptidoglycan crosslinking relaxation plays an important role in* Staphylococcus aureus *WalKR-dependent cell viability.* PLoS One, 2011. **6**(2): p. e17054.

173. Santelli, E., et al., *The crystal structure of* Bacillus subtilis *YycI reveals a common fold for two members of an unusual class of sensor histidine kinase regulatory proteins.* J Bacteriol, 2007. **189**(8): p. 3290-5.

174. Fleurie, A., et al., *Mutational dissection of the S/T-kinase StkP reveals crucial roles in cell division of* Streptococcus pneumoniae. Mol Microbiol, 2012. **83**(4): p. 746-58.

175. Giefing, C., et al., *The pneumococcal eukaryotic-type serine/threonine protein kinase StkP co-localizes with the cell division apparatus and interacts with FtsZ in vitro.* Microbiology, 2010. **156**(Pt 6): p. 1697-707.

176. Beilharz, K., et al., *Control of cell division in* Streptococcus pneumoniae *by the conserved Ser/Thr protein kinase StkP.* Proc Natl Acad Sci U S A, 2012. **109**(15): p. E905-13.

177. Maestro, B., et al., *Recognition of peptidoglycan and beta-lactam antibiotics by the extracellular domain of the Ser/Thr protein kinase StkP from* Streptococcus pneumoniae. FEBS Lett, 2011. **585**(2): p. 357-63.

178. Shah, I.M., et al., *A eukaryotic-like Ser/Thr kinase signals bacteria to exit dormancy in response to peptidoglycan fragments.* Cell, 2008. **135**(3): p. 486-96.

179. Mir, M., et al., *The extracytoplasmic domain of the* Mycobacterium tuberculosis *Ser/Thr kinase PknB binds specific muropeptides and is required for PknB localization.* PLoS Pathog, 2011. **7**(7): p. e1002182.

Paper I

Journal of Microbiological Methods 92 (2013) 59–63

Contents lists available at SciVerse ScienceDirect

Journal of Microbiological Methods

journal homepage: www.elsevier.com/locate/jmicmeth

CHiC, a new tandem affinity tag for the protein purification toolbox

Gro Anita Stamsås, Leiv Sigve Håvarstein, Daniel Straume *

Department of Chemistry, Biotechnology and Food Science, Norwegian University of Life Sciences, P.O. Box 5003, NO-1432 Aas, Norway

ARTICLE INFO

Article history:
Received 28 August 2012
Received in revised form 30 October 2012
Accepted 5 November 2012
Available online 12 November 2012

Keywords:
Protein purification
Choline binding domain
TAP-tag
Affinity chromatography

ABSTRACT

In the present work we have constructed a new tandem affinity purification tag and used it to purify two different polypeptides, PcsB and ECL1 from *Streptococcus pneumoniae*. PcsB probably functions as a peptidoglycan hydrolase and is believed to be involved in splitting of the septum during cell division. ECL1 is the extracellular domain of the membrane spanning protein FtsX. Experimental evidence indicates that the ECL1 domain controls the activity of PcsB through direct interaction (Sham et al., 2011). The affinity tag consists of an N-terminal 6xHis-tag, a choline binding domain followed by a proteolytic site specific for the TEV (tobacco etch virus) endopeptidase. Based on the choline-binding His-tag combination the new 16.5 kDa tag was named CHiC. CHiC-tagged PcsB and ECL1 were expressed in *Escherichia coli* and sequentially purified by employing diethylaminoethyl-cellulose affinity chromatography and Ni^{2+} immobilized metal affinity chromatography. After TEV digestion, the CHiC-tag, TEV-protease and undigested fusion protein were easily separated from the target protein in a single purification step. By using this method, 4–7 mg of recombinant PcsB and ECL1 were obtained from one liter of cell culture with a purity estimated to be at least 95%. In addition, we found that the tag has the potential to function as a solubilisation partner as it markedly increased the solubility of PcsB. In sum, the CHiC-tag is a versatile tool that allows purification of milligram quantities of highly purified recombinant protein in only one or two steps.

1. Introduction

Biochemical and structural analysis of proteins require that they are obtained in nearly pure form and in relatively high amounts. This is also true for proteins used in the production of vaccines and the development of diagnostic tools. In cases where it for some reason is inconvenient or impossible to isolate the protein of interest from its natural source, a heterologous host is commonly used to express the protein. Purification of such recombinant proteins is often a challenging task. As proteins are inherently different from one another with respect to their physicochemical properties, they will differ with respect to solubility, stability, yield and host toxicity. Consequently, an optimized purification protocol will have to be developed in each case. The common approach to overcome this problem is to express the protein of interest with a polypeptide fusion partner called an affinity tag. Several different affinity tags with various properties have been developed for this purpose (Terpe, 2003; Walls and Loughran, 2011; Young et al., 2012). Some function as an epitope that is recognized by for example a specific antibody, while others, like the tag developed in this study, bind to small molecule ligands linked to a solid support.

The main reason for the popularity of affinity tags is that considerable purification can be obtained in just a single chromatography step. However, a single step is usually not sufficient to obtain the desired purity. In recent years it has therefore been developed dual affinity tags in which two different affinity tags are expressed in tandem. This method was originally developed in yeast and is called tandem affinity purification (TAP). After fusing the protein of interest to the TAP-tag, the recombinant protein can be purified by performing two sequential affinity chromatography steps. In general this gives better results than the use of a single affinity tag (Puig et al., 2001; Gully et al., 2003; Rubio et al., 2005; Arnau et al., 2006; Xu et al., 2010). Since the affinity tag in certain cases affects the natural function of the target protein, preventing functional and structural analysis, it is desirable to remove the tag after the last chromatography step. This is achieved by introducing a proteolytic site between the affinity tag and its passenger protein. Following proteolytic digestion of the recombinant fusion protein, additional purification steps are required to remove the free tag, the protease and undigested fusion protein. Since each step reduces the yield of the target protein it is important to keep the number of such steps at a minimum.

In the present work we have constructed a new TAP-tag for easy and reliable purification of recombinant proteins. As a proof of principle we chose to purify two polypeptides from *Streptococcus pneumoniae*, the PcsB protein and the extracellular domain (ECL1) of the membrane spanning protein FtsX. The putative peptidoglycan hydrolase PcsB is involved in septum placement and separation during cell division.

* Corresponding author at: Department of Chemistry, Biotechnology, and Food Science, Norwegian University of Life Sciences, P.O. Box 5003, N-1432 Ås, Norway. Tel.: +47 64965818; fax: +47 64965901.
E-mail address: daniel.straume@umb.no (D. Straume).

0167-7012/$ – see front matter © 2012 Elsevier B.V. All rights reserved.
http://dx.doi.org/10.1016/j.mimet.2012.11.003

Experimental evidence indicates that the muralytic activity of PcsB is controlled by FtsX through direct interaction with its extracellular ECL1 domain (Sham et al., 2011). The new TAP-tag consists of a conventional 6xHis-tag fused to the choline binding domain (CBD) of the pneumococcal CbpD protein followed by a TEV (tobacco etch virus) protease cleavage site. The resulting tag was given the name CHiC (choline-binding histidine combination tag). After proteolytic digestion of CHiC-PcsB and CHiC-ECL1, the free CHiC-tag, the His-tagged TEV protease and undigested fusion protein were separated from the respective passenger protein in a single step by Ni^{2+} affinity column chromatography resulting in recombinant PcsB and ECL1 proteins that were more than 95% pure. In sum, the CHiC-tag is easy to use and gives high yields of pure recombinant protein through a small number of purification steps. We think that this tag represents a valuable addition to the protein expression and engineering toolbox.

2. Materials and methods

2.1. Bacterial strains and growth conditions

The bacterial strains used in this study are listed in Table 1. *Escherichia coli* was grown in Luria Bertani (LB) medium at 37 °C with shaking. When expressing recombinant proteins *E. coli* was grown at 28 °C. When appropriate, ampicillin was added to the medium to a final concentration of 100 μg/ml. *S. pneumoniae* was grown in C medium (Lacks and Hotchkiss, 1960) at 37 °C without shaking.

2.2. Construction of the CHiC-tag and CHiC-fusions

All primers used in this study are listed in Table 2. The CHiC-tag consists of a conventional 6xHis-tag in combination with the choline binding domain (CBD) of the competence induced murein hydrolase CbpD from *S. pneumoniae* (Kausmally et al., 2005; Eldholm et al., 2009). CbpD contains four domains: an N-terminal cysteine, histidine-dependent aminohydrolase/peptidase (CHAP) domain, two successive SH3 domains and a C-terminal CBD domain (Fig. 1A). The CBD-encoding part, including the linker region between the CBD and the second proximal SH3 domain of CbpD, was amplified by PCR using the primer pair 27/29. Genomic DNA from *S. pneumoniae* strain RH1 (Johnsborg et al., 2008) served as template. Primer 27 contained a His-tag-encoding sequence giving rise to a DNA fragment encoding an N-terminal His-tag in frame with the SH3-linker and the CBD domain of CbpD. Next, by using the same genomic DNA template the sequence encoding the linker between the CHAP domain and the first SH3 domain of CbpD was amplified by PCR using the primer pair 28/30. A TEV proteolytic site was introduced in the C-terminal end of the CHiC-tag by including 21 bases, corresponding to ENLYFQG, at the 5′ end of primer 28. Primer 30 contained a stretch of 21 bases at its 5′ end that was complementary to primer 29. The two PCR products 27/29 and 28/30 were then fused together by overlap extension PCR as described by Higuchi et al. (1988), using primers 27 and 28 giving rise to fragment 27/28 which contained the complete CHiC-tag encoding sequence.

The fusion gene *CHiC-pcsB* was constructed by overlap extension PCR. The *pcsB* gene was amplified by PCR using the primer pair 49/58 with strain RH1 genomic DNA as template. The CHiC-tag encoding fragment was amplified by PCR using primer pair 56/57 with PCR product 27/28 serving as template. Fragment 49/58 (*pcsB*) and 56/57 (*CHiC-tag*) were then fused by overlap extension PCR using primer pair 56/58. The 56/58 fragment was cleaved with *Xba*I and *Eco*RI and cloned into the expression vector pRSET A (Invitrogen) giving rise to pGS01. To construct the *CHiC-ECL1* fragment, the sequence encoding the ECL1 domain was amplified using primer pair ds59/ds60 with genomic DNA from strain RH1 as template. The *CHiC-tag* fragment was amplified by PCR using primer pair 56/ds58 and PCR product 27/28 as template. Fragment ds59/ds60 (*ECL1*) and 56/ds58 (*CHiC-tag*) were fused by overlap extension PCR using primer pair 56/ds60. The 56/ds60 fragment was cleaved with *Xba*I and *Eco*RI and cloned into pRSET A giving rise to pGS02.

Table 1
Bacterial strains and plasmids used in this study.

Strains and plasmids	Genotype/relevant features	Reference/ source
S. pneumoniae		
RH1	R704, but *ebg*::*spc*; Ery^r Spc^r	(Johnsborg et al., 2008)
E. coli		
DH5α	Host strain	Invitrogen
BL21 (DE3)	Expression host	Invitrogen
Plasmids		
pRSET A	Expression vector carrying the *lacT7* promoter and an ampicillin resistance gene	Invitrogen
pGS01	pRSET A containing CHiC-fused *pcsB*	This study
pGS02	pRSET A containing CHiC-fused *ECL1*	This study

2.3. Expression and purification of CHiC-tagged PcsB and ECL1

The plasmids pGS01 and pGS02 were transformed into *E. coli* DH5α (Invitrogen) as described by Sambrook and Russell (2001). Vectors were then isolated from *E. coli* DH5α and transformed into the expression host *E. coli* BL21 (DE3) (Invitrogen). *E. coli* BL21 (DE3) containing pGS01 or pGS02 were grown to an OD_{600} of 0.3 before the cells were induced with 0.1 mM isopropyl-β-D-thiogalactopyranoside (IPTG, Promega) at 28 °C for 4 hours with shaking. The cells were collected by centrifugation and resuspended in 10 mM Tris–HCl (pH 7.4) containing 100 mM NaCl. The cells were lysed by treatment with a final concentration of 1 mg/ml lysozyme (Sigma Aldrich) at 37 °C for 15 minutes. DNase I (Sigma Aldrich) was added to a final concentration of 1 μg/ml to degrade DNA. Non-lysed cells and insoluble cell debris were removed by centrifugation at 20 000 *g* for 30 minutes.

CHiC-fused PcsB and ECL1 were purified on DEAE cellulose as described by Sanchez-Puelles et al. (1992). Briefly, the soluble protein extracts containing CHiC-PcsB or CHiC-ECL1 were passed through a 2 ml DEAE-cellulose column with a flow rate of 1 ml/minute. The CBD of the CHiC-tag binds DEAE with high affinity (Sanz et al., 1988). The DEAE-cellulose was then washed with 20 column volumes of 1.5 M NaCl in 10 mM Tris–HCl (pH 7.4) to remove contaminating proteins bound to the column via anionic interactions. The CHiC-tagged proteins were eluted by adding 0.14 M choline to the wash buffer. Fusion proteins were collected in 2 ml fractions and examined by SDS–PAGE. The purest fractions were pooled and further purified by immobilized metal affinity chromatography (IMAC) using a 1 ml Ni^{2+}-charged column (HisTrapHP, GE Healthcare) and the Äkta Prime Plus instrument from GE Healthcare. When bound to the Ni^{2+} column via the His-tag, the immobilized fusion proteins were washed with 20 ml of 10 mM Tris–HCl (pH 7.4) containing 20 mM imidazole, 500 mM NaCl and 0.14 M choline. The flow rate was set to 1 ml/min. CHiC-fused proteins were then eluted by gradually increasing the concentration of imidazole in the mobile phase from 20 mM to 500 mM in a time frame of 40 minutes. Eluted proteins were collected in 1 ml fractions and examined by SDS–PAGE. Choline was included in all buffers to stabilize and to increase the solubility of the CBD domain.

2.4. Removal of the CHiC-tag

The CHiC-tag was cleaved from its fusion partner by digestion with a His-tagged TEV protease (AcTEV™ Protease, Invitrogen). To optimize the reaction conditions for the TEV protease, salts and imidazole following the IMAC purification were removed by overnight dialysis against 10 mM Tris–HCl (pH 7.4) containing 0.14 M choline. The dialysed protein samples were concentrated to a final volume of 0.5 ml using

Table 2
Primers used in this study.

Primer	Oligonucleotide sequence (5′→3′)	Reference
27	GACTCCCGGGTTAAGAAGGAGATATACATATGCATCATCATCATCATCATGAGGGAGTGACTTCTTCACA	This study
28	AGTCCTGCAGACCTTGGAAGTACAGGTTCTCAGCTGAGGATTGACTATTCC	This study
29	TACTCGTTCTCCATCACTGTT	This study
30	ACAGTGATGGAGAACGAGTAAGTGGCAGTGTTGGGAATAG	This study
49	GAAACGACTGATGACAAAATTG	This study
56	GATC TCTAGA TTAAGAAGGAGATATACATATGC	This study
57	CAATTTTGTCATCAGTCGTTTCACCTTGGAAGTACAGGTTCT	This study
58	GATCGAATTCTTAATCTGCATAAATATATGTAAC	This study
ds58	ACCTTGGAAGTACAGGTTCTC	This study
ds59	GAGAACCTGTACTTCCAAGGTAAACTAGCTACAGATATTGAAAATAATG	This study
ds60	CGTAGAATTCTTACTTGAAGAGTCTTTCTGTATTG	This study

Millipore Amicon® Ultra Centrifugal Filters. The fusion proteins were then digested with AcTEV™ Protease (Invitrogen) at 30 °C for 3 hours as described by the manufacturer. Undigested fusion protein, free CHiC-tag and AcTEV™ Protease were separated from the target proteins by performing Ni^{2+} IMAC. The digested target protein was collected in the flow through, while uncut fusion protein, the free CHiC-tag and AcTEV™ Protease bound to the Ni^{2+}-charged column were eluted with 500 mM imidazole. The concentration of purified protein was calculated based on its extinction coefficient and absorbance at 280 nm.

2.5. SDS–PAGE and Western blotting

The molecular size and purity of recombinant proteins were examined by SDS–PAGE as described by Laemmli (1970). Proteins were separated in a 12% gel at 1.5 V/cm^2 for approximately 45 minutes. After electrophoresis the separated proteins were either stained with Coomassie blue (Thermo Scientific) or transferred onto an Immun-Blot™ PVDF Membrane (Bio-Rad) using the Trans-Blot®SD Semi-Dry Electrophoretic Transfer Cell from Bio-Rad at 0.25 V/cm^2 for 60 minutes. His-tagged proteins were detected by using the SuperSignal® West HisProbe™ Kit (Thermo Scientific) as described by the manufacturer, and developed on a CL-X Posure™ Film (Thermo Scientific).

3. Results and discussion

3.1. Design of the choline-binding histidine combination tag

The basis for the choline-binding histidine combination (CHiC) tag is a conventional 6xHis-tag and the C-terminal CBD domain of the pneumococcal murein hydrolase CbpD. CbpD is produced during competence and plays a key role in a mechanism called fratricide in which competent cells lyse their non-competent siblings in order to capture their DNA (Kausmally et al., 2005; Håvarstein et al., 2006; Eldholm et al., 2009, 2010). CbpD consists of an N-terminal cysteine, histidine-dependent amidohydrolase/peptidase (CHAP) domain, two consecutive SH3 domains and a C-terminal CBD domain composed of four choline binding repeats (Fig. 1A). The CHAP domain and the first SH3 domain are separated by a linker region termed linker 1, while the second SH3 domain and the CBD domain are separated by linker 2. The natural function of the choline binding repeats is to bind choline residues decorating the cell wall teichoic and lipoteichoic acids of *S. pneumoniae*. Hence, the CBD domain has strong affinity for tertiary amines, and will bind avidly to the diethylaminoethanol (DEAE) groups of DEAE-cellulose. The use of a single CBD-tag for purifying recombinant fusion proteins on DEAE-cellulose has been described previously by others (Ortega et al., 1992; Sanchez-Puelles et al., 1992; Caubin et al., 2001). The CBD-tag used by these investigators was derived from the pneumococcal major autolysin LytA, which possesses a somewhat larger CBD domain consisting of six choline binding repeats. The reason we based the construction of the CHiC-tag on the CBD domain of CbpD rather than the corresponding domain from LytA was that we already had good experience with the former. During our investigations of the fratricide mechanism we succeeded in purifying recombinant CbpD from a crude cell extract by exploiting the DEAE-binding property of its CBD domain (unpublished data). The high purity that was obtained after only one purification step (>90%) motivated us to use this CBD domain when constructing the CHiC-tag. The 6xHis-tag was added for two purposes: (i) to increase the purity of the target protein by introducing a second purification step and (ii) to separate the free CHiC-tag, His-tagged TEV-protease and undigested fusion protein from the target protein in a single step (see Section 3.3). To ensure sufficient flexibility between the three functional parts of the CHiC-tag, linkers were introduced. The linker 2 region of CbpD was inserted between the His-tag and the CBD domain, while the linker 1 region was introduced between the CBD domain and the TEV-protease cleavage site (ENLYFQG) resulting in a total size of 16.5 kDa for the complete tag (Fig. 1B). Since we used overlap extension PCR when constructing CHiC-fusions, the target protein is only left with an N-terminal Gly residue originating from the CHiC-tag after proteolytic digestion with TEV protease. In most cases, this residue will have no influence on the structure and functionality of the purified target protein. Nevertheless, to make the system more versatile, we also constructed a vector containing only the CHiC-tag with a multiple cloning site at its 3′ end allowing direct cloning of genes in frame with the tag (data not shown). These fusions, however, will contain two or more amino acids (depending on which restriction site that is used) between the tag and the target protein, which will append the recombinant protein after TEV digestion.

3.2. Expression and purification of CHiC-tagged proteins

As a proof of principle we chose to purify the PcsB protein and a polypeptide (ECL1) corresponding to the extracellular loop of the membrane protein FtsX. As mentioned above, both target proteins originate from *S. pneumoniae* and are involved in cell division and daughter cell separation (Reinscheid et al., 2001; Ng et al., 2004; Sham et al., 2011). PCR-fragments encoding the fusion proteins CHiC-PcsB or CHiC-ECL1 were cloned into the pRSET A vector (Invitrogen) downstream of the P_{lacT7} promoter giving rise to pGS01 and pGS02, respectively (Fig. 1C). After expression in *E. coli* BL21 (DE3), CHiC-PcsB (55.4 kDa) and CHiC-ECL1 (32.3 kDa) were purified from the crude protein extract by employing DEAE-cellulose affinity chromatography. This purification step yielded 5–8 mg of fusion protein from one liter of cell culture with a purity of ~90–95% as determined by visual inspection of the Coomassie blue stained gel (Fig. 2). Following DEAE-cellulose purification, additional impurities were removed from the samples by performing Ni^{2+} immobilized metal affinity chromatography (IMAC). This resulted in >95% pure fusion protein with negligible loss of target protein (Fig. 2). In cases when the purity is sufficient after the DEAE-cellulose purification step, this IMAC step could be omitted.

The CHiC-tag had a positive effect on the solubility of PcsB. Similar to Reinscheid et al. (2001), we experienced that when native PcsB was over-expressed in *E. coli* BL21, the majority of recombinant

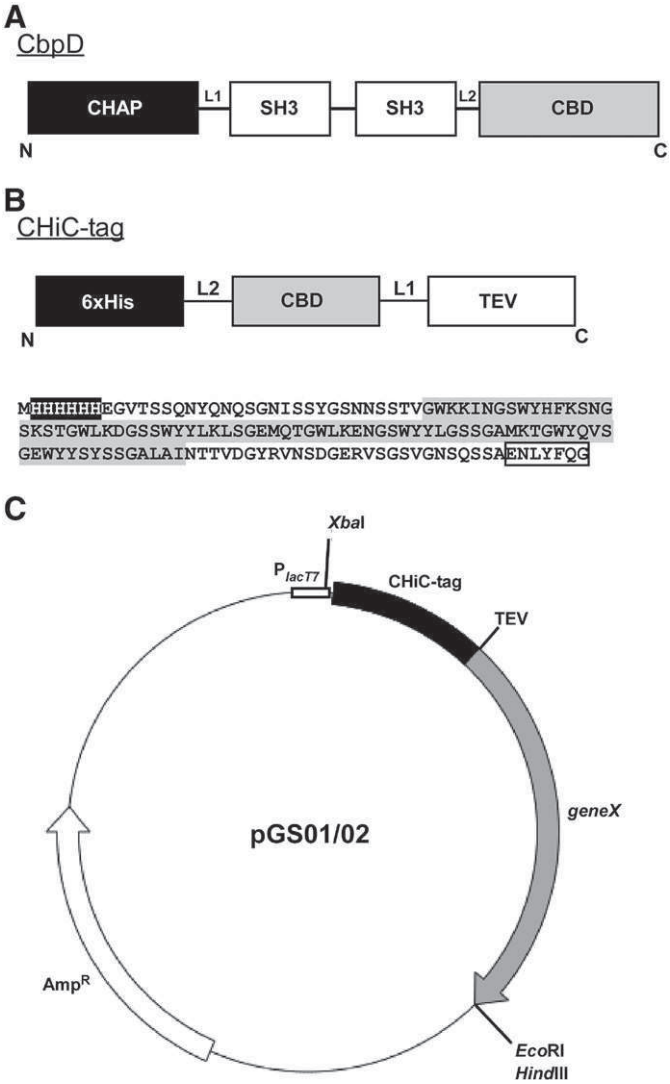

Fig. 1. A. Domain organization of the pneumococcal fratricin CbpD. The choline binding domain (CBD) and linker 1 and 2 (L1 and L2) were used in designing the CHiC-tag. B. Schematic presentation of the architecture of the CHiC-tag (upper) and its amino acid sequence (lower) is shown. The His-tag is indicated in black, the CBD domain in gray and the TEV proteolytic site is boxed. The TEV protease cleaves between the glutamine (Q) and glycine (G) residues leaving only an N-terminal Gly residue in the target protein. The two linkers L1 and L2 separating the functional parts of the tag are without markings. C. Schematic view of the plasmids pGS01 and pGS02 expressing CHiC-fused PcsB or ECL1. GeneX, representing *pcsB* or *ECL1* in the present study, was fused to the CHiC-tag and cloned immediately downstream of the *lacT7* promoter in pRSET A (Invitrogen).

protein ended up as insoluble aggregates that were difficult to refold. CHiC-PcsB, on the other hand, was expressed in a soluble form using the same host and induction parameters as for the non-tagged PcsB, and was easily obtained in milligram amounts from just one liter of cell culture. There are several examples of solubilisation partners that can increase the solubility of its fusion partner when over-expressed in *E. coli*, e.g., NusA (anti-termination factor), MBP (maltose-binding protein) or TrxA (thioredoxin) (Davis et al., 1999; Kapust and Waugh, 1999; LaVallie et al., 2000; Terpe, 2003; De Marco et al., 2004). Our results indicate that in addition to functioning as a tandem affinity tag, the CHiC-tag has the potential to increase the solubility of its fusion partner.

3.3. Removal of the CHiC-tag

To study structure, functionality and other properties of recombinant proteins purified by the use of tag technology, it is usually necessary to remove the affinity tag. More than 90% of the CHiC-tags were cleaved off

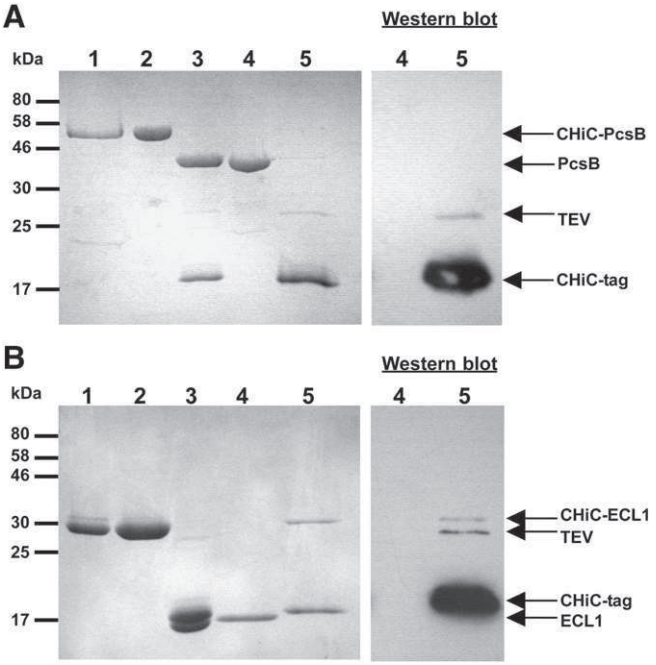

Fig. 2. CHiC-fused PcsB (A) and ECL1 (B) were examined by SDS–PAGE after each purification step. Purified fusion protein obtained after DEAE-cellulose affinity chromatography and the following Ni^{2+} IMAC is shown in lane 1 and lane 2, respectively. TEV protease digested samples of CHiC-PcsB and CHiC-ECL1 are shown in lane 3. After TEV protease treatment PcsB and ECL1 were separated from the free CHiC-tag, TEV protease and undigested fusion protein by doing a second Ni^{2+} IMAC. The flow-through from this step contained PcsB or ECL1 and is shown in lane 4. The three imidazol eluted His-tagged components, CHiC-tag, AcTEV™ Protease (Invitrogen) and undigested fusion protein, are shown in lane 5. Western analysis demonstrated that the CHiC-tag, TEV protease and undigested fusion protein were completely removed from the recombinant PcsB and ECL1.

CHiC-PcsB and CHiC-ECL1 by using the His-tagged AcTEV™ Protease. Addition of 0.14 M choline to the cleavage buffer in order to stabilize the CHiC-tag did not have any negative effect on the activity of the TEV protease (data not shown). After digestion, the free CHiC-tag, AcTEV™ Protease and undigested fusion protein were separated from PcsB and ECL1 in a single Ni^{2+} IMAC purification step. PcsB (38.9 kDa) or ECL1 (15.8 kDa) were collected in the flow-through while the three His-tagged components, the CHiC-tag, AcTEV™ protease and undigested fusion protein, were bound to the column (Fig. 2). Purified PcsB and ECL1 were obtained in amounts ranging from 4–7 mg with a purity of >95%.

4. Conclusion

The novel property of the CHiC-tag is that it combines a conventional 6xHis-tag with a CBD-domain and a TEV cleavage site. The CBD domain functions extremely well as an affinity tag as it provides good yield and a very pure product (>90%) in a single chromatography step. Furthermore, the DEAE-cellulose resin used is inexpensive and has high binding capacity. The presence of the His-tag and TEV cleavage site makes it easy to remove the CHiC-tag, the TEV protease and undigested target protein post-purification by running the digest through a metal chelate affinity column. If necessary, metal chelate chromatography may also be used as an extra purification step before digestion with the TEV protease. An additional advantage of the CHiC-tag is that it may increase the solubility of its fusion partner.

Acknowledgements

This work was funded by a grant from the Research Council of Norway. Cathrine Arnason Bøe is thanked for helpful discussions when writing the article. Kari Helene Berg is thanked for critical reading of the article.

References

Arnau, J., Lauritzen, C., et al., 2006. Current strategies for the use of affinity tags and tag removal for the purification of recombinant proteins. Protein Expr. Purif. 48 (1), 1–13.

Caubin, J., Martin, H., et al., 2001. Choline-binding domain as a novel affinity tag for purification of fusion proteins produced in *Pichia pastoris*. Biotechnol. Bioeng. 74 (2), 164–171.

Davis, G.D., Elisee, C., et al., 1999. New fusion protein systems designed to give soluble expression in *Escherichia coli*. Biotechnol. Bioeng. 65 (4), 382–388.

De Marco, V., Stier, G., et al., 2004. The solubility and stability of recombinant proteins are increased by their fusion to NusA. Biochem. Biophys. Res. Commun. 322 (3), 766–771.

Eldholm, V., Johnsborg, O., et al., 2009. Fratricide in *Streptococcus pneumoniae*: contributions and role of the cell wall hydrolases CbpD, LytA and LytC. Microbiology 155 (Pt 7), 2223–2234.

Eldholm, V., Johnsborg, O., et al., 2010. Pneumococcal CbpD is a murein hydrolase that requires a dual cell envelope binding specificity to kill target cells during fratricide. Mol. Microbiol. 76 (4), 905–917.

Gully, D., Moinier, D., et al., 2003. New partners of acyl carrier protein detected in *Escherichia coli* by tandem affinity purification. FEBS Lett. 548 (1–3), 90–96.

Håvarstein, L.S., Martin, B., et al., 2006. New insights into the pneumococcal fratricide: relationship to clumping and identification of a novel immunity factor. Mol. Microbiol. 59 (4), 1297–1307.

Higuchi, R., Krummel, B., et al., 1988. A general method of in vitro preparation and specific mutagenesis of DNA fragments: study of protein and DNA interactions. Nucleic Acids Res. 16 (15), 7351–7367.

Johnsborg, O., Eldholm, V., et al., 2008. A predatory mechanism dramatically increases the efficiency of lateral gene transfer in *Streptococcus pneumoniae* and related commensal species. Mol. Microbiol. 69 (1), 245–253.

Kapust, R.B., Waugh, D.S., 1999. *Escherichia coli* maltose-binding protein is uncommonly effective at promoting the solubility of polypeptides to which it is fused. Protein Sci. 8 (8), 1668–1674.

Kausmally, L., Johnsborg, O., et al., 2005. Choline-binding protein D (CbpD) in *Streptococcus pneumoniae* is essential for competence-induced cell lysis. J. Bacteriol. 187 (13), 4338–4345.

Lacks, S., Hotchkiss, R.D., 1960. A study of the genetic material determining an enzyme in Pneumococcus. Biochim. Biophys. Acta 39, 508–518.

Laemmli, U.K., 1970. Cleavage of structural proteins during the assembly of the head of bacteriophage T4. Nature 227 (5259), 680–685.

LaVallie, E.R., Lu, Z., et al., 2000. Thioredoxin as a fusion partner for production of soluble recombinant proteins in *Escherichia coli*. Methods Enzymol. 326, 322–340.

Ng, W.L., Kazmierczak, K.M., et al., 2004. Defective cell wall synthesis in *Streptococcus pneumoniae* R6 depleted for the essential PcsB putative murein hydrolase or the VicR (YycF) response regulator. Mol. Microbiol. 53 (4), 1161–1175.

Ortega, S., Garcia, J.L., et al., 1992. Single-step purification on DEAE-sephacel of recombinant polypeptides produced in *Escherichia coli*. Biotechnology 10 (7), 795–798.

Puig, O., Caspary, F., et al., 2001. The tandem affinity purification (TAP) method: a general procedure of protein complex purification. Methods 24 (3), 218–229.

Reinscheid, D.J., Gottschalk, B., et al., 2001. Identification and molecular analysis of PcsB, a protein required for cell wall separation of group B streptococcus. J. Bacteriol. 183 (4), 1175–1183.

Rubio, V., Shen, Y., et al., 2005. An alternative tandem affinity purification strategy applied to Arabidopsis protein complex isolation. Plant J. 41 (5), 767–778.

Sambrook, J., Russell, D.W., 2001. Molecular cloning: a laboratory manual. Cold Spring Harbor Laboratory Press, Cold Spring Harbor N.Y.

Sanchez-Puelles, J.M., Sanz, J.M., et al., 1992. Immobilization and single-step purification of fusion proteins using DEAE-cellulose. Eur. J. Biochem./FEBS 203 (1–2), 153–159.

Sanz, J.M., Lopez, R., et al., 1988. Structural requirements of choline derivatives for 'conversion' of pneumococcal amidase. A new single-step procedure for purification of this autolysin. FEBS Lett. 232 (2), 308–312.

Sham, L.T., Barendt, S.M., et al., 2011. Essential PcsB putative peptidoglycan hydrolase interacts with the essential FtsXSpn cell division protein in *Streptococcus pneumoniae* D39. Proc. Natl. Acad. Sci. U. S. A. 108 (45), E1061–E1069.

Terpe, K., 2003. Overview of tag protein fusions: from molecular and biochemical fundamentals to commercial systems. Appl. Microbiol. Biotechnol. 60 (5), 523–533.

Walls, D., Loughran, S.T., 2011. Tagging recombinant proteins to enhance solubility and aid purification. Methods Mol. Biol. 681, 151–175.

Xu, X., Song, Y., et al., 2010. The tandem affinity purification method: an efficient system for protein complex purification and protein interaction identification. Protein Expr. Purif. 72 (2), 149–156.

Young, C.L., Britton, Z.T., et al., 2012. Recombinant protein expression and purification: a comprehensive review of affinity tags and microbial applications. Biotechnol. J. 7 (5), 620–634.

Paper II

nature COMMUNICATIONS

ARTICLE

Received 28 Nov 2013 | Accepted 8 Apr 2014 | Published 8 May 2014

DOI: 10.1038/ncomms4842

Structural basis of PcsB-mediated cell separation in *Streptococcus pneumoniae*

Sergio G. Bartual[1,*], Daniel Straume[2,*], Gro Anita Stamsås[2], Inés G. Muñoz[3], Carlos Alfonso[4], Martín Martínez-Ripoll[1], Leiv Sigve Håvarstein[2] & Juan A. Hermoso[1]

Separation of daughter cells during bacterial cell division requires splitting of the septal cross wall by peptidoglycan hydrolases. In *Streptococcus pneumoniae,* PcsB is predicted to perform this operation. Recent evidence shows that PcsB is recruited to the septum by the transmembrane FtsEX complex, and that this complex is required for cell division. However, PcsB lacks detectable catalytic activity *in vitro*, and while it has been proposed that FtsEX activates PcsB, evidence for this is lacking. Here we demonstrate that PcsB has muralytic activity, and report the crystal structure of full-length PcsB. The protein adopts a dimeric structure in which the V-shaped coiled-coil (CC) domain of each monomer acts as a pair of molecular tweezers locking the catalytic domain of each dimeric partner in an inactive configuration. This suggests that the release of the catalytic domains likely requires an ATP-driven conformational change in the FtsEX complex, conveyed towards the catalytic domains through coordinated movements of the CC domain.

[1] Department of Crystallography and Structural Biology, Instituto de Química-Física Rocasolano, CSIC, Serrano 119, 28006 Madrid, Spain. [2] Department of Chemistry, Biotechnology and Food Science, Norwegian University of Life Sciences, N-1432 Ås, Norway. [3] Macromolecular Crystallography Group. Structural Biology and Biocomputing Programme, Spanish National Cancer Research Centre (CNIO), Melchor Fernández Almagro 3, 28029 Madrid, Spain. [4] Centro de Investigaciones Biológicas (CIB), Ramiro de Maeztu 9, 28040 Madrid, Spain. * These authors contributed equally to this work. Correspondence and requests for materials should be addressed to L.S.H. (email: sigve.havarstein@nmbu.no) or to J.A.H. (email: xjuan@iqfr.csic.es).

In order to divide, bacteria must synthesize a new septal cell wall, which must be split down the middle by one or more murein hydrolases to separate the resulting daughter cells. The precise molecular mechanism underlying this fundamental process is still poorly understood in most bacteria. In the present investigation, we have studied the septal cross wall splitting mechanism in the Gram-positive bacterium *Streptococcus pneumoniae*. In addition to its important biological implications, this process might be worthy for therapeutic targeting since *S. pneumoniae* is a major human pathogen that has become increasingly resistant to antibiotics in recent decades[1]. Thus, new drugs and new drug targets are urgently sought.

The peptidoglycan (PG), the major constituent of the cell wall, is essential for bacterial survival. Its synthesis and turnover involve a number of enzymes that must function in a coordinated manner. During the last decade it has become clear that a two-component regulatory system termed WalKR (also known as VicKR and YycGF) controls PG metabolism in low G + C Gram-positive bacteria[2]. Analysis of the WalKR regulons of *Bacillus subtilis* and *Staphylococcus aureus* have revealed their role in the control of the expression of a number of PG hydrolases, some of which are involved in the separation of daughter cells[3,4]. Similarly, genes encoding several putative and proven PG hydrolases are part of the pneumococcal WalKR regulon[5,6]. The product of one of these genes, PcsB (from protein required for cell wall separation of group B streptococcus), has been shown to be essential for viability in *S. pneumoniae* strains D39 and R6 (ref. 7). PcsB is a secreted putative murein hydrolase that localizes to the septal area. It has been characterized to various degrees in *S. pneumoniae*[8,9], *Streptococcus mutans* (where it is called GbpB)[10], and *Streptococcus agalactiae*[11]. In all cases, it has been shown to be required for normal growth and cell division. Homologues of PcsB are present in all members of the genera *Streptococcus* and *Lactococcus*.

Judging from its primary structure, PcsB consists of four parts: an amino-terminal signal peptide, a coiled–coil (CC) domain containing putative leucine zipper motifs, an alanine-rich linker region and a carboxy-terminal cysteine, histidine-dependent amidohydrolase/peptidase (CHAP) domain. Despite the presence of this putative catalytic domain in the PcsB sequence, attempts to demonstrate hydrolytic activity of full-length PcsB have been unsuccessful[8,11,12]. Recently, it was discovered that PcsB interacts with the membrane-embedded protein FtsX through its N-terminal CC domain. FtsX has two extracellular loops, ECL1 and ECL2, which are involved in this interaction[13,14]. At the cytoplasmic side of the membrane, FtsX, which has four transmembrane segments, interacts with FtsE. An increasing body of knowledge indicates that the FtsEX complex is an essential regulator of murein–hydrolase activity in Gram-positive as well as Gram-negative bacteria[15]. FtsE is an ATPase, and it is therefore believed that ATP hydrolysis drives a conformational change in the FtsEX/PcsB complex that activates PcsB.

Recently, PcsB has emerged as a leading candidate for a new-generation pneumococcal vaccine. Depending on the vaccine type, pneumococcal vaccine formulations in the current use contain a mixture of 7–23 capsular polysaccharides, making them costly to produce and with limited serotype coverage. In addition, since there are at least 90 different capsular varieties, serotype replacement and capsular switching will eventually enable pneumococci to evade capsule-based vaccines. A promising alternative is the use of conserved nonpolysaccharide antigens[16]. PcsB, which is a surface-exposed and exceptionally conserved protein (>99.5% identity) among clinical isolates of *S. pneumoniae*, has demonstrated its efficacy in lethal models of sepsis and pneumonia[17].

In the present report we show that depletion of PcsB in *S. pneumoniae* strain R6, inhibits daughter cell separation without affecting the synthesis of new septal cross walls. We also provide strong evidence that the C-terminal CHAP domain of PcsB exhibits muralytic activity. Furthermore, the full-length pneumococcal PcsB protein was expressed, purified to homogeneity, crystallized and its structure determined. The structure displays a striking arrangement of the CC and catalytic domains, which associate forming a dimer through three-dimensional domain swapping. In solution, the protein is present in a monomer–dimer equilibrium. Analysis of the structure, together with the biochemical and biophysical characterization, have provided new insights into the catalytic mechanism of PcsB, revealing the regulatory role played by the PcsB–FtsEX complex during daughter cell separation.

Results

Effect of PcsB depletion on cross wall separation. In Gram-negative bacteria, synthesis and splitting of the new cross wall take place in close succession, leading to a gradual constriction of the whole bacterial cell that culminates in separation. On the other hand, in Gram-positives, it has been reported that the complete cross wall is synthesized before muralytic enzymes cleave it[18]. To determine whether synthesis of the PG cross wall is independent of cross wall splitting, we performed transmission electron microscopy (TEM) studies of PcsB-depleted *S. pneumoniae* R6 cells. In intermediately depleted R6 cells, the first sign of PcsB deficiency is uncleaved cross walls. As seen in Supplementary Fig. 1, the original cell wall separating the first-generation daughter cells has not been cleaved, even though the second-generation daughter cells are separated by fully formed cross walls. In severely depleted cells, most new cross walls are misplaced. In these cells, synthesis of the next septum can start anywhere from the internal surface of the cell and, in many cases, it grows at a skewed angle relative to the cell's long axis. As shown in Supplementary Fig. 1C, a new cross wall can even assemble on top of and at a right angle to an old cross wall. Together, these results show three important facts about PcsB-depleted R6 cells: (i) splitting of PG cross walls are inhibited already in intermediately depleted cells, (ii) the lack of PcsB does not inhibit the synthesis of new cross walls, and (iii) strongly depleted cells lose their spatial orientation and initiates synthesis of new cross walls at random. The last effect may explain why PcsB is essential in the R6 strain. For reasons unknown, some pneumococcal strains are able to survive without PcsB. Deletion of the *pcsB* gene in these strains gives rise to very sick cells with phenotypes[17] that are highly similar to those depicted in Supplementary Fig. 1.

Overall structure of PcsB. The crystal structure of the wild-type PcsB was solved at 2.5 Å resolution by the SAD technique (see Methods). The asymmetric unit of PcsB consists of two monomers arranged in a 164-Å long dimer (Fig. 1a). Each monomer is composed of three distinct regions: a CC domain (residues 41–266), a linker region (residues 267–278) and a CHAP domain (residues 279–392) (Fig. 1b and Supplementary Fig. 2). Structures of the two monomers show C^{α} backbone root mean squared deviation (r.m.s.d.) of 1.82 Å; as the domains are nearly identical (C^{α} backbone r.m.s.d. of 1.09 Å and 0.16 Å for CC and CHAP domains, respectively) this value is due to a slight difference in modular arrangement between CC and CHAP domains for each monomer (Supplementary Fig. 3). Thus, hereafter, we limit our discussion to one PcsB molecule (Chain A). The whole structure can be roughly encased in an acute triangle of two long sides (~112 and ~118 Å) and a short side of ~66 Å. The CC domain

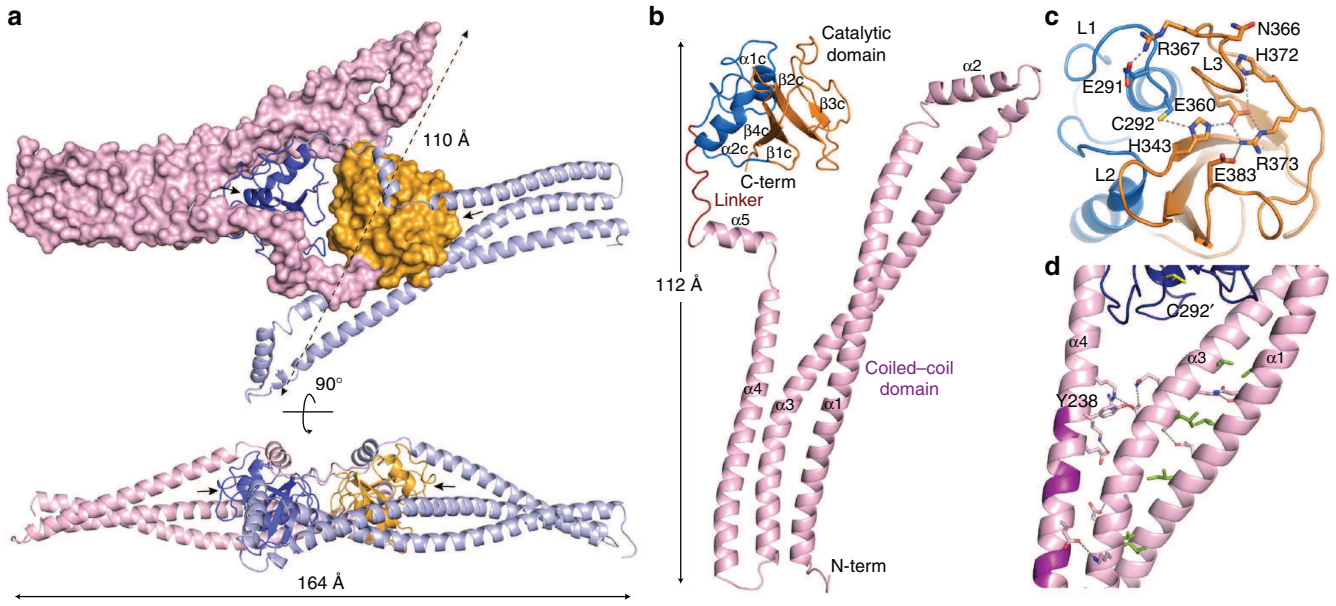

Figure 1 | Three-dimensional structure of PcsB. (**a**) Representation of the PcsB dimer showing the molecular surface for monomer A (CC domain coloured in pink and catalytic domain in orange) and the monomer B as a ribbon representation (CC domain coloured in light blue and catalytic domain in dark blue). Arrows indicate the active sites. (**b**) General structure of PcsB monomer. CC domain (pink) is formed by five helices. An eleven-residue linker region (dark red) connects to the catalytic CHAP domain. The CHAP domain is built by N-lobe (coloured in blue) and C-lobe (coloured in orange), the different secondary structural elements are labelled. (**c**) Active site of PcsB showing the catalytic residues (Cys292, His343 and Glu360) and the interaction network around the triad. Relevant loops in the active site (L1, L2 and L3) are labelled. The salt bridge interaction (E291-R367) connecting the L1 and L3 loops is also depicted. The previously predicted catalytic Asn366 is far from the active site and oriented outward. (**d**) Interactions connecting α1, α3 and α4 of the CC domain (pink cartoon). Leu and Ile residues involved in hydrophobic interactions are depicted as green sticks. Residues involved in salt links, and Tyr238, are drawn as pink capped sticks. The Ala-rich regions are coloured in magenta. The CHAP domain of the dimeric partner is represented as blue cartoon and the catalytic Cys292′ as yellow sticks.

is arranged in five helices, three long bent helices (α1, α3 and α4) composed of a large number of residues (66, 73 and 41 aa, respectively) and two short ones (α2 and α5). The electron density was of good quality for all of them except for the short α2 that also has the highest B factors. The linker region is composed of an alanine-rich region and the sequence comprises the stretch between Pro271 to Pro278 (266-AAAPVRAKVRP-279). This region connects the end of the α5 helix of the CC domain with the globular catalytic CHAP domain. The electron density for the linker unequivocally defines the connection between the modules of one of the chains (Supplementary Fig. 4), while in the other, the density is of less quality probably due to crystal contacts. The catalytic domain displays an α + β papain-like amidase fold, with two α-helices ($\alpha1_c$ and $\alpha2_c$) and an antiparallel β sheet built up by $\beta1_c$–$\beta4_c$ (Fig. 1b). The N-terminal lobe ($\alpha1_c$–$\alpha2_c$) folds together with the C-terminal lobe, comprising the β sheet, to build the active-site cleft (Fig. 1c). Similar to other amidases, the reactive cysteine of PcsB, Cys292, is positioned at the N-terminal end of $\alpha1_c$.

The architecture of the PcsB CC domain. The extended CC_{PcsB} is composed of residues arranged in a continuous helical arrangement. Only the first four residues (41–45) and those of the short turns do not follow this pattern. All the helices within the CC domain are located in the same plane except for the α5 helix. The CC domain is a V-shaped molecule formed by helices α1–α3 on one side and by α4 and α5 on the other, making an angle of ~40° (Fig. 1b). A search for the closest structural homologues of CC_{PcsB} with the DALI server[19] reveals that no similar structure for the complete CC has been reported previously. High structural homology is, however, found between the antiparallel α1α3 bundle of the CC domain and the human inter-SH2 domains of p85β and p85α, the regulatory subunits of phosphatidylinositol-4,5-biphosphate 3-kinase, the tower domain of the Lys-specific histone demethylase, the molecular chaperone prefoldin and the structures of CC domains from type III secretion system translocators (Supplementary Fig. 5).

Remarkably, interhelix interactions in the CC_{PcsB} differ depending on the helices in question: interactions between α1 and α3 are mainly mediated by hydrogen bonds and by the hydrophobic interactions of residues forming a leucine zipper (Fig. 1d), in contrast, α3 interacts with α4 through salt links and the hydrophobic contribution is less relevant, as a consequence of the presence of less bulky alanine residues (all the Ala-rich regions, except that of the linker, are located in α4) (Fig. 1d). Interestingly, Tyr238 is inserted at the bottom of the V-shaped conformation. Together with long-chain charged residues it opens the cavity in which the catalytic domain of the other paired monomer is located (Fig. 1d).

The catalytic machinery of the CHAP domain of PcsB. A search for proteins structurally related to the catalytic domain of PcsB was performed with the DALI server[19]. Papain-like proteins such as the *Staphylococcus saprophyticus* CHAP domain protein, the catalytic domain of endolysin PlyCA and the type VI amidase effector Tse1 from *Pseudomonas aeruginosa*, were found to be among the most closely related 3D structures (Supplementary Fig. 6a).

Papain-like hydrolytic enzymes form covalent intermediates with their substrates during the course of the reaction. A reactive cysteine acts as a catalytic nucleophile, promoted by the side chain of a histidine. The His-imidazole ring is further hydrogen

bonded to a third catalytic residue, usually an Asp or Asn. The Cys-His-Asp/Asn catalytic triad is positioned by the common structural core; the cysteine is located at the N terminus of the helix, and the histidine and the Asp/Asn are provided by the β-sheet and linking loops[20]. Sequence analysis suggested that Cys292, His343 and Asn366 are the catalytic residues in this triad. Mutations in the first two residues (Cys292Ala and His343Ala) are not tolerated in PcsB, whereas that of Asn366Ala is.[7] Our crystal structure indicates that Asn366 is far from the Cys292 (Fig. 1c) while the Glu360 is hydrogen bonded to His343 and superimposes with the Asn175 from the catalytic triad of the papain (Supplementary Fig. 6b). Therefore, the catalytic triad comprises Cys292, His343 and Glu360 (Fig. 1c). The corresponding triad positions are also seen in the secreted CHAP domain from *S. saprophyticus*[21] and were shown to be the proteolytic triad in pyroglutamyl peptidases, a family of cysteine peptidases[22]. Remarkably, a strong network of salt bridge and hydrogen-bond interactions is observed around the active site of PcsB (Fig. 1c). Besides the expected hydrogen bonds between the catalytic triad, Glu360 is making salt bridge interactions with both His372 and Arg373, and the last with Glu383. These interactions could modulate the PcsB activity depending on the protonation state of the corresponding amino acids.

Substrate binding in PcsB. The active site of PcsB is partially occluded by the presence of the α3 helix from the dimeric partner (Fig. 1a), a fact that provides interesting implications for the regulatory role of the CC domain in the PcsB dimer (see discussion below). Among the PG papain amidases, some, as for instance Spr from *E. coli,* have a closed active-site architecture with active-site loops blocking the active-site entrance. Others like Tse1 from *P. aeruginosa* present an exposed active site[23] (Supplementary Fig. 7). Similar to Tse1, $CHAP_{PcsB}$ has an open active site with loops L1-L3 (Fig. 1c and Supplementary Fig. 7) protruding outwards, creating a large groove ~31 Å long and ~7 Å wide. The active site of one monomer, chain A, showed an entrapped polyethylene glycol molecule, presumably mimicking binding of the substrate (Fig. 2a and Supplementary Fig. 8). This open active site, however, is partially occluded due to the dimeric arrangement. Very interestingly, the distance between the putative glycan strands is greater than 30 Å (ref. 24). Consequently, the active site of PcsB could get access to the peptide bridges that interconnect the glycan strands in the PG sacculus.

All attempts to obtain crystals of a complex between PcsB and PG analogues failed, very likely due to the occlusion created by the dimer arrangement. To gain insight into the substrate recognition by PcsB, we performed docking calculations with GOLD[25] using a peptide stem fragment, L-Ala-D-isoGln-L-Lys-D-Ala, present in pneumococcal PG. The top scoring positions nicely fit the polyethylene glycol molecule found at the active site of the crystal structure (Fig. 2a,b) and place the scissile bond between isoGln and L-Lys close to the catalytic Cys292 and His343. The ligand is strongly stabilized by many hydrogen bonds and salt links with residues in the active site (Supplementary Fig. 9). Remarkably, a very similar conformation for the substrate (L-Ala-D-Glu-mDAP) was found in Tse1 from *P. aeruginosa*[23] where mDAP is present in place of L-Lys. It has been shown that Tse1 exhibits a strong preference for the mDAP-type[23]. Our docking calculations reveal the presence of an acidic patch in the PcsB active site formed by Asp338 and Glu383 (Fig. 2b and Supplementary Fig. 9), responsible of stabilization of L-Lys in the cross-linked PG. This patch does not exist in Tse1, and consequently provides an explanation for the different substrate specificities of the two PG amidases.

$CHAP_{PcsB}$ displays murein–hydrolase activity. To investigate whether full-length PcsB has muralytic activity, we performed zymography with purified recombinant PcsB and pneumococcal cells mixed into the separating SDS–PAGE gel as substrate. Consistent with the results reported by others[8,11,12], no muralytic activity was detected. Next, we expressed only the C-terminal CHAP domain of PcsB. For purification purposes, a 6xHis tag was attached to the N-terminal end of the domain (see Methods). Zymography analysis performed with various amounts of the $CHAP_{PcsB}$ protein revealed distinct clearing zones in the opaque gel at the expected migration positions (Fig. 3a,b). As a negative control, we expressed a mutated version of the CHAP domain (His-$CHAP_{C292A}$) in which the catalytic cysteine was substituted

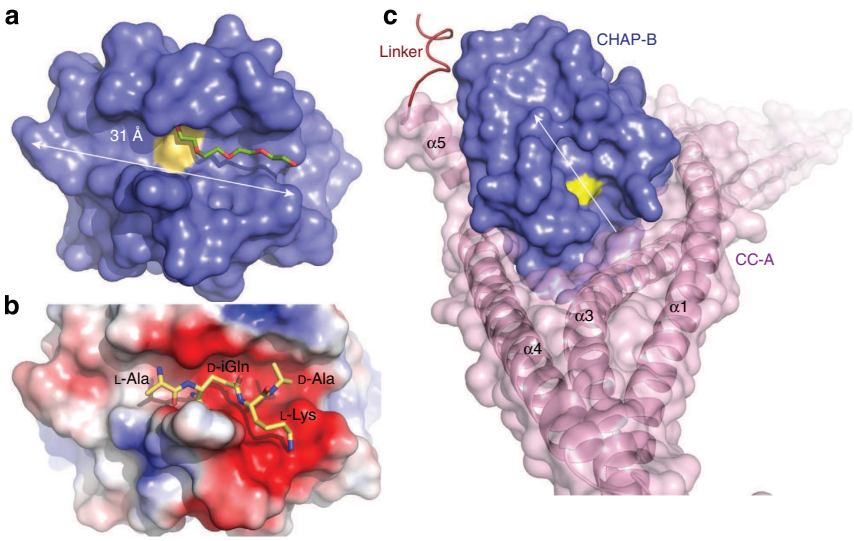

Figure 2 | The active site of PcsB. (**a**) Molecular surface representation of the CHAP domain of PcsB. The catalytic Cys292 is coloured in yellow. The PEG molecule attached to the active site is represented as capped sticks. The length of the active-site groove is indicated by an arrow. (**b**) Electrostatic potential on the $CHAP_{PcsB}$ molecular surface with the peptide L-Ala-D-isoGln-L-Lys-D-Ala docked in the active site. An acidic patch (coloured in red) stabilizes L-Lys. (**c**) Domain interactions between the CC domain in chain A (CC-A) with the CHAP domain of chain B (CHAP-B). Colour code as in Fig. 1. White arrow indicates, as in **a**, the active-site groove.

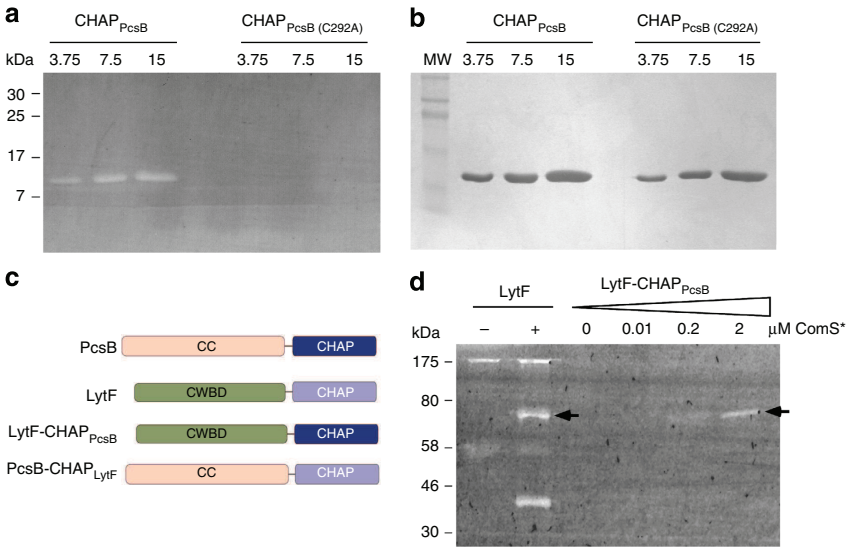

Figure 3 | Zymogram analysis demonstrating the PG-hydrolyzing activity of His-CHAP$_{PcsB}$ and the LytF-CHAP$_{PcsB}$ chimera. (**a**) Muralytic activity of His-CHAP$_{PcsB.}$ Different amounts of purified His-CHAP$_{PcsB}$ and its C292A-mutated counterpart (3.75, 7.5 and 15 μg indicated on top) were separated in an SDS–PAGE gel containing RH14 cells as substrate. The light bands are clearing zones showing degradation of the PG of the RH14 cells incorporated in the SDS–PAGE gel. (**b**) A parallel gel without RH14 cells was stained with Coomassie Blue to visualize the purified His-CHAP$_{PcsB}$ and His-CHAP$_{PcsB(C292A)}$ recombinant proteins loaded onto the gel in **a**. (**c**) Cartoon depicting the domain composition of PcsB and LytF, and the chimera (LytF-CHAP$_{PcsB}$ and PcsB-CHAP$_{LytF}$) constructed by swapping the domains of the parental proteins. The LytF-CHAP$_{PcsB}$ chimera was used in the zymogram analysis displayed below in **d**. The gene encoding the PcsB-CHAP$_{LytF}$ chimera was incorporated into the genome of *S. pneumoniae* strain R6 to determine whether the chimeric protein was able to replace the essential PcsB wild-type protein (see result section for details). (**d**) Zymogram analysis. Lanes: MW, molecular weight marker; LytF (−), extracts of *S. gordonii* cells; LytF (+), extracts of competence induced *S. gordonii* cells producing LytF; LytF-CHAP$_{PcsB}$ (0–2), extracts of pneumococci expressing increasing amounts of LytF-CHAP$_{PcsB}$ chimera from the ComS*-inducible P_{ComX} promoter[30]. ComS* is an 8 aa synthetic peptide that is added to the growth medium to induce transcription of genes inserted behind the P_{ComX} promoter. Maximum expression is reached at 2 μM ComS* (see text for details). The light bands in lanes containing cell extracts are clearing zones that result from degradation of the PG sacculus of *S. gordonii* cells that have been incorporated in the SDS–PAGE separating gel. Left arrow: clearing zone corresponding to wild-type LytF. Right arrow: clearing zone corresponding to the LytF-CHAP$_{PcsB}$ chimera.

with an alanine. No clearing zones were observed when the same amounts of the CHAP$_{PcsB(C292A)}$-mutant protein was subjected to zymography (Fig. 3a,b). Together, these results provide strong evidence that the catalytic domain has muralytic activity and further support the open conformation observed in the crystal structure of CHAP$_{PcsB}$. In order to identify the exact bond split by PcsB, purified PG was treated with CHAP$_{PcsB}$ in solution. Subsequent analysis of the digest by reverse phase HPLC, however, did not reveal any cleavage products. Thus, it remains for future studies to determine the cleavage specificity of PcsB.

Modular arrangement and oligomerization in PcsB. A dimeric arrangement of PcsB molecules was found in the crystal structure (Fig. 1a). This dimer is formed by three-dimensional domain swapping[26], in which both monomers exchange their catalytic domains in a similar way to that originally described for the dimeric structure of diphtheria toxin[27]. The dimer places both catalytic domains in the middle with their active sites oriented in opposite directions, and with the CC domain extending outwards on the same axis in a 164 Å long dimer. Analysis of the PcsB dimer by the PISA server[28], gave a high value for the complex formation significance score (0.915) and indicated that the buried area upon assembly formation is 7,040 Å^2. The calculated free energy of assembly dissociation (ΔG^{diss}) is 26.1 kcal M^{-1}. The ΔG^{diss} corresponds to the free energy difference between dissociated and associated states. Positive values of ΔG^{diss} indicate that an external driving force should be applied in order to dissociate the assembly. Consequently, the PcsB assembly is predicted to be thermodynamically stable.

The V-shaped CC domain of one monomer clamps the CHAP domain of the other in a narrow cavity. All the α helices of the CC domain, except for the α2 helix, are involved in the interaction with the CHAP domain. While there are few hydrogen bonds and no salt links between the two domains (Supplementary Table 1), about three-quarters of the CC/CHAP interactions are van der Waals contacts, most of which involve exposed hydrophobic side chains (Supplementary Fig. 10 and Supplementary Table 1).

In agreement with crystallographic results, analytical ultracentrifugation experiments over a broad range of protein concentrations (0.1–8.0 mg ml^{-1}) revealed that the protein exists as an equilibrium mixture of dimers and monomers in solution, with dimer favored at higher protein concentrations (over 4 mg ml^{-1}) and monomer at low concentrations (Supplementary Fig. 11). The monomer–dimer equilibrium presents an estimated K_d of 90 μM. Interestingly, while the experimental sedimentation coefficients for the dimer are compatible with that calculated for the crystallographic dimeric structure, those for the monomer are better described by a PcsB molecule with the CHAP domain inserted in its own CC domain rather than the protein monomer observed in the asymmetric unit of our crystal (Supplementary Fig. 11).

We explored whether the arrangement in the crystal is representative of PcsB in solution using small-angle X-ray scattering (SAXS). The overall molecular parameters derived from the scattering data are given in Supplementary Table 2. The scattering profiles at five different concentrations (0.29–9.40 mg ml^{-1}) (Fig. 4 and Supplementary Fig. 12) indicate the presence of a monomer–dimer equilibrium, being the monomer more abundant at lower concentrations whereas the dimer is the

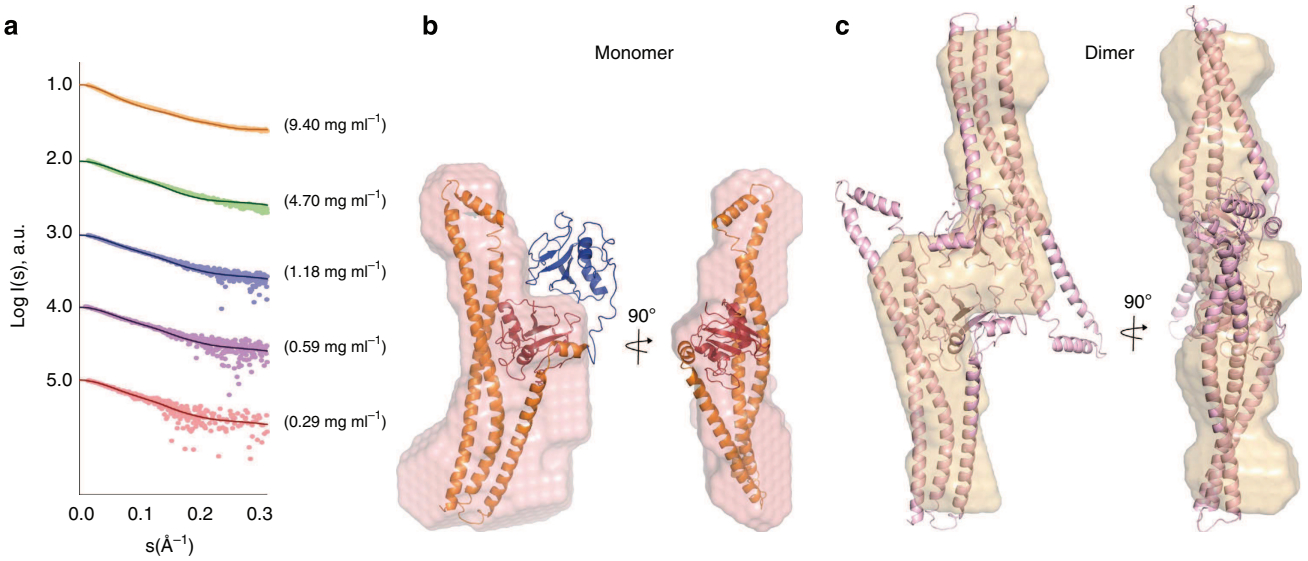

Figure 4 | Arrangement of PcsB in solution by SAXS. (**a**) SAXS experimental scattering curves (dots) and theoretical scattering computed from the models (smooth curves) at different concentrations of PcsB. The data for different concentrations were offset vertically for clarity. a.u., arbitrary units. (**b**) Rigid-body overlaying of the *ab initio* determined SAXS envelope and the PcsB crystallographic monomer. The elongated CC domain (coloured in orange) fits into the envelope but not the linker or the CHAP domain (coloured in blue). In red, a model where the catalytic domain belongs to the dimeric partner, that perfectly fits the SAXS envelope. (**c**) Rigid-body fitting of the PcsB crystallographic dimer inside the SAXS envelope. The region around the α2 helix presents the highest B factors in the crystal structure, and is not observed in the SAXS envelope of the dimer.

predominant form at higher concentrations. A molecular mass of 61 ± 6 kDa was deduced for the dimer, which is comparable with the expected dimer mass of 78 kDa (Supplementary Table 2). The radius of gyration (R_g) and the maximum dimension (D_{max}) with values of 45 ± 3 Å and 168 ± 7 Å, respectively, indicate a rather extended dimeric assembly in agreement with the dimensions observed in the crystal structure (D_{max} of 164 Å, see Fig. 1a). The *ab initio* models generated with DAMMIF and DAMMIN without symmetry constrains produced rather elongated shapes of PcsB at high concentration. Rigid-body modelling was performed using the dimer found in the crystal structure, showing that the envelope encases the main core of the dimer (Fig. 4c). It is worth to note that the α2 regions that present the highest B factors in the crystal structure are not observed in the SAXS envelope of the dimer. At low concentrations (0.29–1.18 mg ml^{-1}) PcsB appeared mostly as a monomer with a molecular mass and R_g between 35 ± 4/44 ± 4 kDa and 35 ± 6/41 ± 6 Å, respectively (Supplementary Table 2). The D_{max} for monomers (Supplementary Table 2) were also compatible with their associated crystallographic monomer (122 Å). Rigid-body modelling of the PcsB monomer extracted from the crystallographic dimer inside the SAXS envelope, fits well the elongated CC domain (coloured in orange in Fig. 4b) but not the linker or the CHAP domain (coloured in blue in Fig. 4b) indicating that a single-molecular conformation alone does not represent the experimental data fittingly. Remarkably, if the catalytic domain is replaced with the one corresponding to its dimeric partner (coloured in red in Fig. 4b) the model perfectly fits the SAXS envelope. Therefore, two relevant points can be derived from this analysis; first, in solution, the monomeric PcsB present an inactive conformation with the CHAP domain inserted in its own CC domain, and second, the PcsB dimer is generated by the three-dimensional domain swapping of their catalytic domains.

Evidence that PcsB muralytic activity is regulated by its modular arrangement. We have previously characterized a murein hydrolase termed LytF[29], which is produced by *Streptococcus gordonii* strain Challis during the competent state. LytF consists of an N-terminal cell wall binding domain and a C-terminal CHAP domain. The C-terminal CHAP domains of PcsB and LytF are the same size and 70% identical, while their N-terminal domains are unrelated. Considering that $CHAP_{PcsB}$ and $CHAP_{LytF}$ are highly similar (Supplementary Fig. 13), we wondered whether $CHAP_{PcsB}$ would become active if fused to the N-terminal domain of LytF. To test this idea, we replaced the CHAP domain of LytF with the CHAP domain of PcsB. The resulting LytF-$CHAP_{PcsB}$ chimera was expressed in pneumococcal cells from the ComS*-inducible P_{comX} promoter[30]. Extracts from pneumococcal cultures grown in the presence of 0, 0.01, 0.2 and 2 μM ComS* were subjected to zymography with *S. gordonii* cells incorporated in the separating gel (Fig. 3c,d). The analysis revealed a clearing zone corresponding to the expected molecular weight of LytF-$CHAP_{PcsB}$ in the sample induced with 2 μM ComS*. The fact that the LytF-$CHAP_{PcsB}$ chimera gives rise to clearing zones in gels containing *S. gordonii* cells as substrate shows that the structure and composition of the peptide cross bridges of *S. pneumoniae* and *S. gordonii* must be similar. Available data indicate that the pentapeptide stem L-Ala-D-isoGln-L-Lys-D-Ala-D-Ala is the same in the two species. In *S. pneumoniae* interpeptide bridges are either absent or predominantly L-Lys-L-Ser-L-Ala-D-Ala, while they are predominantly L-Lys-L-Ala-L-Ala-D-Ala in *S. gordonii*[31,32].

To further verify that the function of PcsB depends on the muralytic activity of its CHAP domain, we constructed a chimera in which the CHAP domain of PcsB was replaced by the corresponding domain of LytF. LytF, which is produced by *S. gordonii* cells during the competent state, lyses susceptible streptococcal cells by disrupting their cell wall[29]. The gene encoding this PcsB-$CHAP_{LytF}$ chimera was inserted into the native *pcsB* locus in a strain that expressed the wild-type PcsB ectopically from the P_{comX} promoter. Next, the wild-type gene was deleted from the ectopic locus giving rise to strain SPH250. Surprisingly, the SPH250 strain was viable. A homology model for the PcsB-$CHAP_{LytF}$ chimera was constructed (Supplementary

Fig. 13). This model indicates that the main determinants for catalytic activity and substrate recognition were conserved between both CHAP domains. Despite some of the interactions stabilizing CC and CHAP domains in PcsB (such as a poly-Ala region) could be disturbed in the chimera (Supplementary Fig. 13) the strain SPH250 is viable. Its doubling time of 45 min was somewhat longer than the 35 min generation time of the parental strain. In addition, inspection of the SPH250 cultures by light microscopy revealed some enlarged misshapen cells, morphological changes reminiscent of those seen in pneumococcal cells that have been subjected to light PcsB depletion (Supplementary Fig. 14). Together, these results provide strong evidence that the CHAP domain of PcsB has muralytic activity that is regulated by the CC domain.

Discussion

The crystal structure of the PG amidase PcsB reveals a surprising arrangement of its different domains. The CC domain is a unique V-shaped molecule built by three long bent α-helices and two short ones. A flexible and extended 11-aa linker connects the CC domain with the catalytic CHAP domain. Remarkably, the crystal structure of the full-length PcsB is a dimer formed by three-dimensional domain swapping in which the entire catalytic domain of one monomer is inserted in the internal cavity of the CC domain of the other (Figs 1a and 2c), a pattern that is also observed for the monomer in solution as deduced from AUC and SAXS experiments. The PISA server further confirmed the stability of this dimer formation, as well as by analytical ultracentrifugation and by SAXS experiments. In this unique oligomeric arrangement, the CC domain of one monomer acts as molecular tweezers clamping the catalytic domain of its dimeric partner. The implications of this arrangement are profound; active sites are partially occluded (roughly half of the active-site groove) by the α3 helix of the partner resulting in an inactive dimer. This point was confirmed by our experiments with the $CHAP_{PcsB}$ domain and a LytF-$CHAP_{PcsB}$ chimera in which the $CHAP_{LytF}$ domain of the LytF fratricine was replaced by the closely related $CHAP_{PcsB}$ domain of PcsB. When separated from the CC domain, the $CHAP_{PcsB}$ domain turned out to be active on its own in zymography assays. Similarly, when fused to the cell wall binding domain of LytF, the CHAP domain of PcsB displayed muralytic activity (Fig. 3). In contrast, muralytic activity was not observed with the full-length PcsB protein. The functional homology of the $CHAP_{PcsB}$ and $CHAP_{LytF}$ domains was demonstrated by showing that replacement of PcsB in strain R6 with a chimera consisting of the CC domain of PcsB and the CHAP domain of LytF gave rise to viable R6 cells.

The role of the CC domain, however, goes beyond its inhibitory function. The structural framework provided by the CC domain is also required for activation of PcsB, that is, for cross wall splitting and daughter cell separation. It has been reported that a temperature sensitive (Ts) mutant containing two amino-acid changes (L79S and L218P, R6 strain numbering) in the CC domain of PcsB showed mild or severe defects in cell morphology and division at 32 °C or 41.4 °C, respectively[13]. At the non-permissive temperature, the double mutant formed spherical cells that phenocopied the defect caused by severe depletion of PcsB[13]. The three-dimensional structure of PcsB shows that these mutations are located in the leucine zipper regions and are involved in the interaction between α1 and α3 (Leu 79) and in the interaction between α4 and α3 (Leu218) (Supplementary Fig. 15). Thus, the alteration in the CC architecture caused by these amino-acid changes probably perturbs the activation mechanism of PcsB and locks the mutant protein in an inactive state, although we cannot discard other possibilities such as the mutant is unstable and degraded, or that mutations in the CC domain could alter the length of the protein or its orientation relative to the cytoplasmic membrane.

The conserved FtsEX complex recently emerged as a major regulator of PG hydrolysis during bacterial cell division[13,15,33]. FtsEX is essential or conditionally essential in a great variety of bacterial species[14,34]. FtsEX structurally resembles an ABC transporter[35], but recent studies indicate that FtsEX acts as a signal transduction system rather than as a transporter of an unknown substrate[34]. The 3D structure of PcsB provides clues to how regulation/activation by the FtsEX complex can take place (Fig. 5). The dimeric arrangement of PcsB precludes any lytic activity unless the CHAP domain is released, in a controlled way, from the CC domain. To release the CHAP domain, the 'molecular tweezers', which consists of α1–α3 on one side and α4–α5 on the other, must be opened on both sides. Previous studies involving Ts and suppressor mutants of PcsB and FtsX, respectively, revealed mutations in the large (ECL1) and small (ECL2) extracellular loops of FtsX that indicate that the FtsX–PcsB interaction occurs between these loops and the CC domain of PcsB[13,14]. The Ts mutations in CC_{PcsB} are located just in the middle of α1 and α3 helices and at the base of α4 helix (Supplementary Fig. 15), while the connecting regions in FtsX involve the distal portion of the ECL1 and ECL2 loops[14]. These results point to a specific interaction between the FtsX loops and both sides of the 'molecular tweezers'. The energy required for the coordinated movement of α-helices in the CC_{PcsB} domain is in all likelihood produced by hydrolysis of ATP by FtsE. In agreement with this, it has been shown that the conserved amino acids in the ATP binding site of FtsE are essential for pneumococcal growth, supporting the idea that ATPase activity by FtsE is required for FtsEX→PcsB signalling and coordination of cell separation[14]. Once released, the catalytic domain would not require further opening of the active-site loops. We have demonstrated that CHAP alone exhibits hydrolytic activity and presents a pre-formed 31-Å groove that can accommodate the cross-linked peptide stems (Fig. 5c). Our docking calculations allowed us to map the different subsites of substrate-peptide recognition for PcsB. Especially relevant is the presence of an acidic patch that could explain PcsB's specificity for L-Lys containing stem peptides (Fig. 2b and Supplementary Fig. 9). Further studies on hydrolytic activity of PcsB are, however, required to precisely identify the cleavage site of this enzyme.

Our TEM studies of intermediately and severely PcsB-depleted cells show that the synthesis of new cross walls continues unimpeded in the absence of PcsB, suggesting that the cross wall splitting machinery operates independently of the septal PG synthesis machinery. What controls the activity of the cross wall splitting machinery to ensure that it acts at the right time and place? As discussed above, evidence strongly supports that ATP hydrolysis by FtsE provides the energy needed to activate PcsB. However, as ATP is abundant in the cytoplasm throughout the cell cycle, the availability of this nucleotide cannot be a factor that controls splitting of the cross wall. In principle, the level of PcsB, FtsX, FtsE or possibly other hitherto unknown members of the cell wall splitting machinery could be tightly regulated in a cell cycle dependent manner, but so far no evidence of such regulation has been reported. In our view, the unusual dimeric structure of PcsB is a striking characteristic that must serve a critical function in the *in vivo* regulation of this murein hydrolase. A pertinent question is: Why is the dimer linear with CHAP domains in the middle and CC domains at each end? An intriguing possibility is that dimers form *in vivo* when a monomer (in the inactive configuration observed in the analytical ultracentrifugation and SAXS experiments) from each of the daughter cells meet in the middle of the cross wall. As shown in

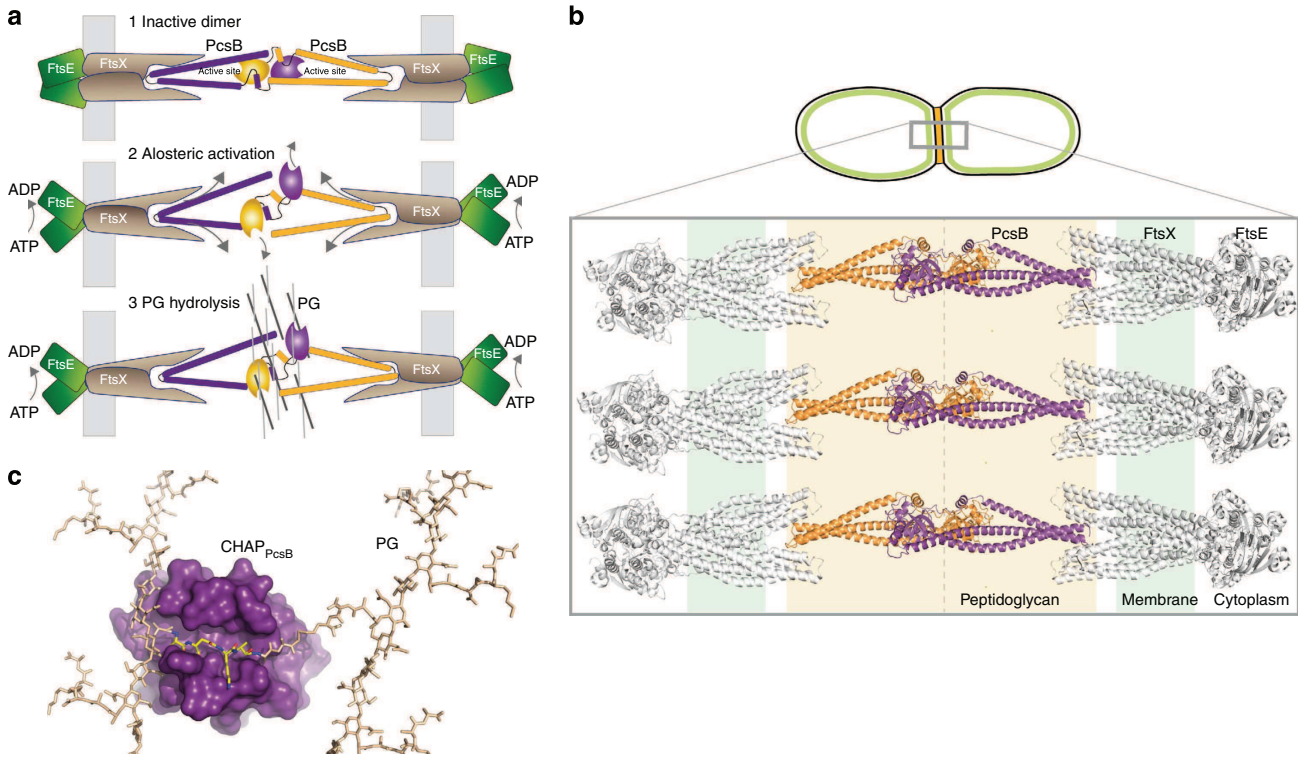

Figure 5 | Activation and regulation in PcsB. (**a**) Proposed model for regulation of hydrolytic activity of PcsB. The inactive dimer is located at the septum by FtsX (1). The ATPase activity of FtsE induces an allosteric change on PcsB through FtsX producing the release of the CHAP domains (2). The catalytic domains start the PG hydrolysis (3). (**b**) Possible spatial location of PcsB dimers (yellow and magenta ribbon) on the pneumococcal septum. The structure of the FtsEX complex resembles that of an ABC transporter (PDB code 2ONJ, is coloured in white ribbons representing FtsEX). (**c**) Model of the cross-linked PG chains (capped sticks) bound at the molecular surface of the CHAP$_{PcsB}$ (magenta). The peptide substrate used in docking calculations is highlighted (with C atoms in yellow, N atoms in blue and O atoms in red).

Fig. 5, this implies that the PcsB dimer extends across the cross wall and interacts with FtsEX complexes at both ends. Measurements from TEM micrographs showed that the thickness of the pneumococcal cross wall is in the range of 17–25 nm. It is reasonable to assume that the periplasmic part of FtsX will add a few nanometres to each end of the 16.4 nm long PcsB dimer. Consequently, the estimated thickness of the cross wall is consistent with the model depicted in Fig. 5b. The appealing feature of this model is that splitting of the shared cross wall involves active participation of both daughter cells. Presumably, this introduces an additional level of control in the division process. If PcsB can only function as a dimer, it means that it can only be active in cleaving cross walls and not ordinary cell walls. Only cross walls have membranes on both sides that make it possible to insert PcsB from the compartment of each daughter cell so that the molecules will meet in the middle and dimerize. This would represent an ingenious control mechanism. Due to the net-like polymeric structure of PG, the mobility of PcsB dimers is probably restricted. Thus, it is likely that PcsB, which is a moderately abundant protein in the pneumococcal cell (about ~5,000 monomers per cell[12]), only acts locally and is then discarded. This is supported by the fact that relatively large amounts of PcsB are released to the medium during growth[12]. In sum, our results indicate that the unique modular structure and dimeric organization of PcsB have evolved to allow precise splitting of the septum during cell division, while avoiding damage to other parts of the PG sacculus.

Methods

Bacterial growth and transformation. Strains of *Escherichia coli* were grown in Luria Bertani medium at 37 or 28 °C with shaking in the presence of 100 μg ml^{-1} ampicillin when appropriate. *E. coli* was transformed by heat shock as described by Sambrook and Russell[36]. *S. pneumoniae* strain R6 and *S. gordonii* strain Challis were grown without shaking at 37 °C in C medium[37] and Todd–Hewitt medium (Difco), respectively. Construction of *S. pneumoniae* mutants was performed by natural transformation. Briefly, pneumococcal cultures were cultivated at 37 °C until they reached OD_{550} = 0.05–0.1. Then, transforming DNA and 250 ng ml^{-1} of synthetic competence stimulating peptide were added. After further incubation at 37 °C for 120 min, transformants were selected on Todd–Hewitt plates containing the appropriate antibiotic; kanamycin (400 μg ml^{-1}) or streptomycin (200 μg ml^{-1}).

Expression and purification of mature PcsB. PcsB was purified by using the tandem affinity tag called CHiC-tag as previously described by Stamsås *et al.*[38] followed by ion exchange chromatography. In brief, *pcsB* fused to the CHiC-tag by overlap extension PCR[39] was cloned into the expression vector pRSET A (Invitrogen) resulting in pGS01 (ref. 38). *E. coli* BL21 (DE3) (Invitrogen) containing the plasmid pGS01 (strain gs32, see Supplementary Table 3) was grown at 37 °C with shaking. When reaching OD_{600} = 0.3 expression of CHiC-fused PcsB was induced by adding isopropyl-β-D-thiogalactopyranoside (IPTG) to a final concentration of 0.1 mM. After incubation for 4 h at 28 °C cells from 2 l of cell culture were harvested at 5,000*g* and resuspended in 40 ml 10 mM Tris-HCl (pH 7.4) containing 100 mM NaCl. The cells were lysed by adding lysozyme to a final concentration of 1 mg ml^{-1}. CHiC-PcsB was purified from the soluble protein fraction by DEAE-cellulose affinity chromatography as described by Sanchez-Puelles *et al.*[40] The CHiC-tag was then separated from PcsB by digestion with AcTEV Protease (Invitrogen) at 30 °C for 3 h. The free CHiC-tag, undigested CHiC-PcsB and AcTEV Protease, all of which contains a 6xHis tag, were removed by Ni(2+)-NTA affinity chromatography. The flow through which contained PcsB in 10 mM Tris-HCl (pH 7.4) was then bound onto an anion exchanger (Sepharose Q, GE Healthcare) and eluted by gradually increasing the NaCl concentration from 0–500 mM in a 25 ml gradient. The flow rate was set to 1 ml min^{-1}. The fractions containing >99% pure PcsB were pooled and concentrated by using Amicon Ultra-15 Centrifugal Filter Units (Millipore).

Cloning and production of SeMet-PcsB. A SeMet derivative of PcsB was produced in order to solve the phase problem associated with the structure determination of native PcsB. Since mature PcsB only contains two methionines per 365

residues (M140 and M150), we introduced two additional methionines by replacing the residues Q180 and L250 with M. Methionine codons were introduced at codon 180 and 250 by overlap extension PCR[39]. For the CAA180 to ATG180 (Q180M) substitution, base pairs 535–1179 of *pcsB* were amplified using the forward primer ds85 and the T7 reverse primer producing PCR product 1 (Primers are listed in Supplementary Table 4). The region corresponding to base pairs 1–559 of *pcsB* fused 5′ to the CHiC-tag was amplified using the T7 forward primer and reverse primer ds86 producing PCR product 2. The plasmid pGS01 (ref. 38) served as template in both reactions. Since primer ds85 is complementary to primer ds86, PCR product 1 and 2 were fused in an overlap extension PCR by using the flanking primers T7 forward and T7 reverse generating PCR product 3. To introduce the additional CTT250 to ATG250 (L250M) substitution, base pairs 748–1179 of *pcsB* were amplified using forward primer ds79 and T7 reverse primer producing PCR product 4. Similarly region 1–773 of *pcsB* fused 5′ to the CHiC-tag was amplified using the T7 forward primer and reverse primer ds80 to generate PCR product 5. PCR product 3 was used as template in both reactions. PCR fragment 4 and 5 were fused in an overlap extension PCR using the T7 forward and T7 reverse primers. This generated PCR fragment 6 that contained a Q180M and L250M version of PcsB fused N-terminally to the CHiC-tag. This mutated version of PcsB will be referred to as $PcsB_{mut}$. Fragment 6 was cleaved with *Xba*I and *Eco*RI and ligated immediately downstream of the *T7lac* promoter in pRSET A giving rise to plasmid pGS214.

For production of SeMet-$PcsB_{mut}$, *E. coli* BL21 (DE3) harbouring pGS214 (strain ds122, see Supplementary Table 3) was grown in M9 minimal medium containing 0.4% glucose[36] and 50 mM choline chloride. Choline was supplemented to M9 to improve the solubility of CHiC-$PcsB_{mut}$. At $OD_{600} = 0.3$ methionine production in *E. coli* BL21 (DE3) was blocked by adding the following cocktail of amino acids: L-lysine (0.1 mg ml^{-1}), L-phenylalanine (0.1 mg ml^{-1}), L-threonine (0.1 mg ml^{-1}), L-isoleucine (0.05 mg ml^{-1}), L-leucine (0.05 mg ml^{-1}) and L-valine (0.05 mg ml^{-1}). After 10 min, the production of selenomethionine-derivatized CHiC-PcsBmut was induced by adding a final concentration of 0.1 mM IPTG and 0.05 mg selenomethionine (Acros Organics) per ml growth medium. The cells were grown at 28 °C for 4 h before SeMet-derivatized CHiC-$PcsB_{mut}$ was purified as described above for native PcsB.

Construction of His-CHAP and *pcsB/lytF* chimeras. To construct the *pcsB-CHAP$_{lytF}$* chimeric gene, pneumococcal *pcsB* without its CHAP-encoding part (bp 1–858) was amplified using the primer pair 216/52 and genomic DNA from strain RH1 (ref. 41) as template. The CHAP-encoding part of *lytF* (bp 1260–1578) was amplified using the primer pair 53/217 and genomic DNA from *S. gordonii* (Challis) as template. These two fragments were fused by overlap extension PCR using the primer pair 216/217 producing the fragment *pcsB-CHAP$_{lytF}$*. Next, ~1,000-bp fragments corresponding to the 5′ and 3′ flanking regions of *pcsB* were amplified with the primer pairs 37/218 and 219/38, respectively. Genomic DNA from the RH1 strain was used as template. By overlap extension PCR the 5′ flanking region was fused to the 5′ end of the *pcsB-CHAP$_{lytF}$* gene using the primer pair 37/217. Similarly, the 3′ flanking region was fused to the 3′ end of *pcsB-CHAP$_{lytF}$* using the primer pair 216/38. Finally, these two fragments were fused using the primers 37 and 38.

To test if PcsB-$CHAP_{lytF}$ could substitute for wild-type PcsB in *S. pneumoniae* we wanted to replace the native *pcsB* gene with the chimeric *pcsB-CHAP$_{lytF}$* gene. As *pcsB* is an essential gene in *S. pneumoniae* R6, an extra copy of the wild-type gene had to be expressed ectopically before the native *pcsB* gene could be removed and replaced by a Janus cassette[42]. For ectopic expression of *pcsB*, we employed the R6 derivative SPH131, which has the ComRS expression/depletion system integrated in its genome[30]. First, the *pcsB* gene was amplified with the primers 35 and 36 and DNA from strain RH1 as template. Next, fragments corresponding to the ~1,000-bp upstream and downstream regions of the Janus cassette in strain SPH131 were amplified using the primer pairs khb31/khb36 and khb33/khb34, respectively. Then, by the use of overlap extension PCR with the primers khb31 and 36, the *pcsB* fragment was fused to the upstream fragment. Similarly, the *pcsB* fragment was fused to the downstream fragment by using the primers 35 and khb34. Finally, these two fragments were fused using the primer pair khb31/khb34. By replacing the Janus cassette in SPH131 with the resulting PCR product strain SPH246 was generated.

Before the *pcsB-CHAP$_{lytF}$* gene could be introduced into the native *pcsB* locus, the native *pcsB* gene was replaced with the Janus cassette. The Janus cassette was amplified with the primers Kan484.F and RpsL41.R and genomic DNA from strain RH426[32] as template. Fragments (~1,000 bp) corresponding to the 5′ and 3′ regions of the native *pcsB* gene was amplified using the primer pairs 37/39 and 40/38, respectively. DNA from strain RH1 was used as template. The resulting fragments were then fused to the Janus cassette in separate PCR reactions. The 5′ flanking region was fused to the Janus cassette using the primers 37 and RpsL41.R, while the 3′ flanking region was fused to the Janus cassette with the primers Kan484.F and 38. Finally, these two fragments were fused together using the primers 37 and 38. By transforming strain SPH246 with a PCR fragment corresponding to the Janus cassette flanked by the upstream and downstream regions of the *pcsB* gene, strain SPH247 was obtained. Transformants of SPH247 was grown in the presence 1 μM ComS* to drive ectopic expression of PcsB. Next, the Janus cassette in SPH247 was replaced with the *pcsB-CHAP$_{lytF}$* fragment described above, giving rise to strain SPH248. For removal of the ectopically expressed copy of WT *pcsB* in strain SPH248, this gene and its P_{comX} promoter was replaced by a Janus cassette. Genomic DNA from strain SPH154 (ref. 43), which contains a Janus cassette inserted in the ectopic locus, served as template to amplify a PCR fragment consisting of the Janus cassette plus ~1,000 bp flanking regions. The PCR reaction was carried out with the primers khb31 and khb34. The resulting fragment was transformed into strain SPH248, generating strain SPH249. Finally, the Janus cassette was removed by transforming strain SPH249 with a fragment containing only the flanking regions of the Janus cassette. The 5′ and the 3′ region of the Janus cassette were amplified using the primer pairs khb31/khb32 and 154/khb34, respectively. DNA from SPH154 served as template. These two fragments were fused by overlap extension PCR using the primer pair khb31/khb34. The resulting fragment was transformed into strain SPH249, giving rise to strain SPH250.

To construct *lytF-CHAP$_{pcsB}$*, the region (bp 76–1332) encoding the cell wall binding domain of LytF (without its 25 aa leader sequence) was amplified using the primer pair ds95/ds96 and DNA from *S. gordonii* strain Challis as template. The CHAP-encoding region of PcsB (bp 859–1179) was amplified using the primer pair ds97/ds98 and DNA from *S. pneumoniae* RH1 as template. These two fragments were fused in an overlap extension PCR with the flanking primers ds95 and ds98 resulting in a *lytF-CHAP$_{pcsB}$* chimera. LytF-$CHAP_{PcsB}$ was expressed in *S. pneumoniae* by using the ComRS system described by Berg *et al.*[30] The 5′ and 3′ regions of the Janus cassette in strain SPH131 (see above) were amplified by the primer pairs khb31/khb36 and khb33/khb34, respectively, and then fused to the 5′ and 3′ ends of the *lytF-CHAP$_{pcsB}$* fragment by overlap extension PCR using the primers khb31 and khb34. The resulting fragment was transformed into strain SPH131, replacing the Janus cassette and giving rise to strain SPH252.

To construct His-$CHAP_{PcsB}$, we amplified the CHAP-encoding part of *pcsB* using the primers ds147 and T7 reverse primer and the plasmid pGS01 (ref. 38) as template. The C292A-mutated version of $CHAP_{PcsB}$ was amplified using the same primers but with genomic DNA from SPH258 as template. Primer ds147 contains a 6xHis encoding part. The PCR products were cleaved with *Xba*I and *Eco*RI and ligated into pRSET A immediately downstream of the *T7lac* promoter. The resulting plasmids were transformed into *E. coli* BL21 (DE3) giving rise to strain ds179 and ds189.

Zymogram analysis. The muralytic activity of LytF-$CHAP_{PcsB}$, His-$CHAP_{PcsB}$ and His-$CHAP_{PcsB(C292A)}$ was examined in zymogram gels. For LytF-$CHAP_{PcsB}$ strain SPH252 was grown in the presence of 0, 0.01, 0.2 and 2 μM ComS* inducer for 1 h to drive LytF-$CHAP_{PcsB}$ expression. Competence induced *S. gordonii* (Challis) was used as control for native LytF activity[29]. The cells were collected at $OD_{550} = 0.25$ by centrifugation and lysed in SDS sample buffer. Total protein extracts were separated by SDS–PAGE using a 12% separation gel containing *S. gordonii* (Challis) cells as substrate. The cell substrate was collected from a 300 ml *S. gordonii* (Challis) culture at $OD_{550} = 0.3$. The cells were suspended in 1.25 ml separation gel buffer (1.5 M Tris–HCl, pH 8.8) and heat inactivated at 95 °C for 10 min before they were mixed into the resolving gel. After gel electrophoresis the gel was washed two times for 30 min in distilled water before protein refolding was initiated by submerging the gels in 50 mM NaCl, 20 mM $MgCl_2$, 0.5% Triton X-100 and 20 mM Tris–HCl, pH 7.4. The gels were incubated in refolding buffer until muralytic activity was observed as clear bands in the opaque gel.

Similarly, the activity of His-$CHAP_{PcsB}$ and its C292A-mutated counterpart were examined in zymogram gels containing *S. pneumoniae* strain RH14 as substrate. His-$CHAP_{PcsB}$ and His-$CHAP_{PcsB(C292A)}$ were expressed in *E. coli* strain ds179 and ds189, respectively by adding a final concentration of 0.1 mM IPTG at $OD_{600} = 0.3$ followed by incubation at 28 °C for 4 h. A volume of 500 ml-induced ds179 cells were collected by centrifugation at 5,000 *g* for 5 min. The cells were then resuspended in 5 ml of 10 mM Tris–HCl, pH 7.4 containing 100 mM NaCl. The cells were lysed by adding lysozyme to a final concentration of 1 mg ml^{-1} followed by 10 min at 37 °C. His-$CHAP_{PcsB}$ and His-$CHAP_{PcsB(C292A)}$ were purified from the soluble protein fraction by using Protino Ni-TED150 (Macherey–Nagel) columns as described by the manufacturer. The purified proteins were then separated by SDS–PAGE in 13% zymogram gels before the gels were incubated in refolding buffer.

Transmission electron microscopy. SPH247 cells were grown to an $OD_{550} = 0.3$ in the presence of 1 μM ComS*, harvested by centrifugation and washed once in C medium to remove excess ComS*. To start depletion of *pcsB*, the washed cells were resuspended in C medium containing 0 μM ComS* to an $OD_{550} = 0.025$. Cells were collected for TEM 1 h before their growth rate was affected by PcsB starvation and 45 min after the cell growth was severely inhibited by *pcsB* depletion. Cells were fixed by mixing cell culture and fix solution (2% paraformaldehyde [v/v] and 2.5% glutardialdehyde [w/v] in 0.1 M sodium cacodylate buffer pH 7.4) in a 1:1 ratio. After incubation at room temperature for 1 h, the cells were fixed overnight at 4 °C. The fixed cells were washed three times in sodium cacodylate buffer (0.1 M, pH 7.4).

For TEM, fixed cells were post fixed for 1 h at room temperature using 1% OsO_4 (w/v) and 1.5% $K_3[Fe(CN)_6]$ (w/v) dissolved in dH_2O. Following three washing steps in dH_2O (3 × 10 min), cells were prestained for 30 min using 1% uranyl

acetate. Next, cells were washed for 3 × 10 min in water, and dehydrated with a gradient series of ethanol comprising 10 min sequential incubations in 70, 90 and 100% ethanol. Finally, the cells were stepwise infiltrated in LR white resin as follows: LR white resin: EtOH in ratios 1:3 for 30 min, 1:1 overnight, 3:1 for 4 h and finally 100% LR white resin overnight followed by embedding in 100% LR white resin at 60 °C overnight. Thin sections were cut with a diamond knife mounted on an ultramicrotome (LEICA, EM UC 6). The sections were counterstained with 1% $KMnO_4$ for 10 min. After staining, the grids were washed thoroughly in dH_2O. The sections were examined in a FEI MORGAGNI 268 electron microscope.

PcsB crystallization. Crystals of native PcsB were obtained using the sitting-drop vapour diffusion method at 4 °C. Crystals grew in 2 µl droplets formed by mixing 1 µl of protein solution at 10 mg ml^{-1} (buffered in 20 mM Tris-HCl pH 7.5) and 1 µl of precipitant solution formed by 12% (v/v) polyethylenglycol 4000, 0.1 M Hepes pH 7.5, 0.2 M Magnesium Acetate in 1:1 volume ratio drops supplemented with 115,38 mM Guanidinium chloride and 33.5 mM n-octyl β-D-Glucopyranoside. Crystals belong to the $P3_121$ hexagonal space group ($a = b = 125.8$ Å, $c = 126.6$ Å). PcsB SeMet derivative crystals were obtained in the same way as the native PcsB crystals but replacing magnesium acetate by zinc acetate in the reservoir solution. SeMet derivative crystals belong to the $P3_121$ hexagonal space group ($a = b = 127.2$ Å, $c = 126.3$ Å).

X-ray data collection and structural determination. Crystals were harvested in a proper reservoir solution supplemented with 23% ethylene glycol, mounted into nylon loops and flash cooled in liquid nitrogen. Native and SAD experiments were carried out on beamline ID29 at the European Synchrotron Radiation Facility (ESRF) (Grenoble, France). All X-ray data sets were processed and scaled with XDS[44] and Aimless[45], respectively. PcsB structure was solved by SAD technique. Due to the low content of methionine residues (2 Met residues) in the wt PcsB sequence, four different constructions were produced having two additional methionine residues. Among them only the PcsB-Q180M-L250M construct could be expressed in the presence of SeMet, purified and crystallized. PcsB-Q180M-L250M crystals diffracted up to at 2.71 Å resolution. The initial selenium sites were located with SHELX[46] using the HKL2MAP GUI[47] and refined within AUTOSHARP[48]. Solvent flattening was calculated with Parrot[49] followed by density modification with Pirate programme[50]. Initial model was obtained with Buccaneer[51] followed by manual modelling with COOT[52]. Two monomers were found in the asymmetric unit yielding a Matthews's coefficient of 3.97 Å^3/Da and a solvent content of 69.07%. All X-ray data sets presented anisotropy, the best of the native PcsB being collected at 2.55 Å resolution. The PcsB-SeMet derivative structure was used as initial model in the molecular replacement method using Phaser[53]. Structure of native PcsB was subjected to alternate cycles of refinement with Refmac5[54] and COOT. Geometry of the final models was checked with MOLPROBITY[55]. In all cases, the good quality of all electron density maps allowed modelling the most part of the polypeptide chain, ligands and solvent molecules (see Table 1). The first 40 amino acids from the N-terminal tail were disordered and were not visible in the structure and the short helix α2 presented a poor electron density especially in one of the monomers. In the crystal structure of the native PcsB, the electron density map clearly defines a polyethylene glycol moiety attached to the active site of chain B. The figures were generated by using PyMol (Molecular Graphics System, Version 1.5.0.4 Schrödinger, LLC.).

Docking calculations. The structure of the pneumococcal PG peptide stem fragment L-Ala-D-isoGln-L-Lys-D-Ala was modelled using PyMol. Charges assignment and optimization were carried in chimera[56]. Molecular docking was carried using GOLD (Genetic Optimization for Ligand Docking) software[25], using the genetic algorithm (GA). The PEG ligand found in the crystal structure was used as starting point for cavity detection. For each of the 25 independent GA runs, a maximum number of 100,000 GA operations were performed on a set of five groups with a population size of 100 individuals. Default cut-off values of 2.5 Å (dH-X) for hydrogen bonds and 4.0 Å for van der Waals distance were employed. When the top three solutions attained r.m.s.d. values within 1.5 Å, GA docking was terminated. The r.m.s.d. values for the docking calculations are based on the r.m.s.d. matrix of the ranked solutions. Best-ranked solutions were always among the first 10 GA runs, and the conformation of molecules based on the best fitness score was further analysed.

Analytical ultracentrifugation. Sedimentation velocity was used in combination with sedimentation equilibrium to determine the association state of protein PcsB over a broad range of concentrations (0.1–8.0 mg ml^{-1}). Sedimentation velocity runs were carried out at 171,600 g and 20 °C in an XL-I analytical ultracentrifuge (Beckman–Coulter) equipped with ultraviolet-Vis and Raleigh interference detection system, using an An50Ti rotor and 3 and 12 mm double sector centerpieces (sample in the range of 0.1–1.0 mg ml^{-1} were loaded in normal 12 mm centrepiece and samples in the range of 2.0–8.0 mg ml^{-1} in narrow 3 mm centerpieces). The sedimentation coefficient distributions were calculated by least squares boundary modelling of sedimentation velocity data using the $c(s)$ method[57] as implemented in the SEDFIT programme. Calculated s-values were corrected to standard conditions (water, 20 °C, and infinite dilution) using the SEDNTERP programme[58] and the concentration dependence of s, to get the corresponding standard s-values. Short column (21–85 µl, depending of the centerpieces) equilibrium runs were carried out at multiple speeds (5,426 g, 11,394 g and 17,804 g) and the corresponding scans were measured at the appropriate wavelength. Whole cell apparent weight-average buoyant molecular weight of the protein samples were determined by fitting a single-species model to the experimental data using the HeteroAnalysis programme[59]. The corresponding protein molecular weights were calculated from the experimental buoyant values using 0.722 cm^3 g^{-1} as the protein partial specific volume. Several models of self-association were globally fitted to multiple sedimentation equilibrium using the HeteroAnalysis programme.

To assign the most probable structure of the main protein species present, the standard s-values experimentally obtained were compared with the s-values determined for given structural models using the shell model calculation implemented in HYDROPRO[60].

Table 1 | Diffraction data collection and refinement statistics.

	PcsB-Q180M-L250M SeMet	PcsB
Data collection		
	$P3_121$	$P3_121$
a, b, c (Å)	127.2, 127.2, 126.3	125.8, 125.8, 126.6
T (K)	100	100
X-ray source	Synchrotron	Synchrotron
Wavelength (Å)	0.9792	0.9792
Resolution (Å)	44.80 (3.10–2.97)	44.63-(2.66–2.55)
Total no. of reflections	562,550	404,398
No. unique reflections	32,228	38,172
R_{sym}	0.10 (0.76)	0.08 (0.64)
$I/\sigma(I)$	18.2 (3.3)	11.9 (2.9)
CC (1/2)	1 (0.99)	1 (0.99)
Completeness (%)	99.1 (99.9)	99,9 (99.8)
Redundancy	17.5 (14)	10.6 (11)
Refinement		
Resolution (Å)		44.63–2.55
R_{work}/R_{free}		0.23/0.27
No. atoms		
Protein		5231
Ethylene glycol		8
Polyethylene glycol		13
Magnesium		1
Chloride		7
Solvent		450
B-factor (Å^2)		
Protein		76.20
Ligands		82.90
Solvent		59.60
R.m.s. deviations		
Bond length (Å)		0.005
Bond angles (°)		0.83
PDB CODE		4CGK

*Highest resolution shell is shown in parenthesis.

SAXS experiments. SAXS data were collected at the EMBL beamline BM29 at the ESRF (Grenoble, France), using a robotic sample changer, from six sample solutions of PcsB at concentrations ranging from 0.29–9.40 mg ml^{-1} in 10 mM Tris-HCl pH 7.4 and 5% glycerol at 277 K. Data were recorded using a photon-counting Pilatus 1 M pixel detector (DECTRIS, Switzerland) at a sample detector distance of 2.7 m and a wavelength of $\lambda = 1$ Å. The scattering intensity $I(q)$ was recorded in a range of the momentum transfer $0.01 < q < 0.6$ Å^{-1} (where $q = 4\pi \sin\theta/\lambda$, and 2θ is the scattering angle). Sample solutions were circulated in a thermostatic flow mode during the measurement to minimize radiation damage effects. Ten frames of 1-s exposures were collected for each sample, normalized to the transmitted intensity and subsequently averaged using AUTOSUB. In PRIMUS, the forward scattering $I(0)$ and the radii of gyration Rg were estimated using the Guinier approximation $I(q) = I(0) \exp(-(qRg)^2/3)$ with $qRg < 1.3$. These parameters were also computed from the entire scattering patterns using the indirect transform package GNOM, providing also the pair-distance distribution function $P(r)$, from which the maximum particle dimension, $Dmax$, was estimated. The molecular weight was calculated from excluded volume of the hydrated particle (the Porod

volume, *Vp*). The *ab initio* modelling programs DAMMIN and DAMMIF were used for low-resolution shape generation, and 10 models were calculated in the slow mode, and averaged with DAMAVER, which also provides a value of normalized spatial discrepancy representing a measure of similarity among different models. The theoretical profile from the high-resolution structure of PcsB was computed with CRYSOL. The *ab initio* model was superimposed with the high-resolution structure using the programme SUPCOMB. All the SAXS programs and calculation modules are included in the ATSAS programs package[61].

References

1. Norrby, R. P., M. *et al.* The bacterial challenge, time to react: a call to narrow the gap between multidrug-resistant bacteria in the EU and the development of new antibacterial agents. (ECDC/EMEA) (2009).
2. Dubrac, S., Bisicchia, P., Devine, K. M. & Msadek, T. A matter of life and death: cell wall homeostasis and the WalKR (YycGF) essential signal transduction pathway. *Mol. Microbiol.* **70,** 1307–1322 (2008).
3. Salzberg, L. I. *et al.* The WalRK (YycFG) and sigma(I) RsgI regulators cooperate to control CwlO and LytE expression in exponentially growing and stressed Bacillus subtilis cells. *Mol. Microbiol.* **87,** 180–195 (2013).
4. Delaune, A. *et al.* The WalKR system controls major staphylococcal virulence genes and is involved in triggering the host inflammatory response. *Infect. Immun.* **80,** 3438–3453 (2012).
5. Ng, W. L., Tsui, H. C. & Winkler, M. E. Regulation of the pspA virulence factor and essential pcsB murein biosynthetic genes by the phosphorylated VicR (YycF) response regulator in *Streptococcus pneumoniae*. *J. Bacteriol.* **187,** 7444–7459 (2005).
6. Dubrac, S. & Msadek, T. Identification of genes controlled by the essential YycG/YycF two-component system of *Staphylococcus aureus*. *J. Bacteriol.* **186,** 1175–1181 (2004).
7. Ng, W. L., Kazmierczak, K. M. & Winkler, M. E. Defective cell wall synthesis in *Streptococcus pneumoniae* R6 depleted for the essential PcsB putative murein hydrolase or the VicR (YycF) response regulator. *Mol. Microbiol.* **53,** 1161–1175 (2004).
8. Giefing-Kroll, C., Jelencsics, K. E., Reipert, S. & Nagy, E. Absence of pneumococcal PcsB is associated with overexpression of LysM domain-containing proteins. *Microbiology* **157,** 1897–1909 (2011).
9. Sham, L. T., Tsui, H. C., Land, A. D., Barendt, S. M. & Winkler, M. E. Recent advances in pneumococcal peptidoglycan biosynthesis suggest new vaccine and antimicrobial targets. *Curr. Opin. Microbiol.* **15,** 194–203 (2012).
10. Duque, C. *et al.* Downregulation of GbpB, a component of the VicRK regulon, affects biofilm formation and cell surface characteristics of *Streptococcus* mutans. *Infect. Immun.* **79,** 786–796 (2011).
11. Reinscheid, D. J., Gottschalk, B., Schubert, A., Eikmanns, B. J. & Chhatwal, G. S. Identification and molecular analysis of PcsB, a protein required for cell wall separation of group B streptococcus. *J. Bacteriol.* **183,** 1175–1183 (2001).
12. Barendt, S. M. *et al.* Influences of capsule on cell shape and chain formation of wild-type and pcsB mutants of serotype 2 *Streptococcus pneumoniae*. *J. Bacteriol.* **191,** 3024–3040 (2009).
13. Sham, L. T., Barendt, S. M., Kopecky, K. E. & Winkler, M. E. Essential PcsB putative peptidoglycan hydrolase interacts with the essential FtsXSpn cell division protein in *Streptococcus pneumoniae* D39. *Proc. Natl Acad. Sci. USA* **108,** E1061–E1069 (2011).
14. Sham, L. T., Jensen, K. R., Bruce, K. E. & Winkler, M. E. Involvement of FtsE ATPase and FtsX extracellular loops 1 and 2 in FtsEX-PcsB complex function in cell division of *Streptococcus pneumoniae* D39. *MBio* **4,** e00431–e00513 (2013).
15. Yang, D. C. *et al.* An ATP-binding cassette transporter-like complex governs cell-wall hydrolysis at the bacterial cytokinetic ring. *Proc. Natl Acad. Sci. USA* **108,** E1052–E1060 (2011).
16. Bogaert, D., Hermans, P. W., Adrian, P. V., Rumke, H. C. & de Groot, R. Pneumococcal vaccines: an update on current strategies. *Vaccine* **22,** 2209–2220 (2004).
17. Giefing, C. *et al.* Discovery of a novel class of highly conserved vaccine antigens using genomic scale antigenic fingerprinting of pneumococcus with human antibodies. *J. Exp. Med.* **205,** 117–131 (2008).
18. Goehring, N. W. & Beckwith, J. Diverse paths to midcell: assembly of the bacterial cell division machinery. *Curr. Biol.* **15,** R514–R526 (2005).
19. Holm, L. & Rosenstrom, P. Dali server: conservation mapping in 3D. *Nucleic Acids Res.* **38,** W545–W549 (2010).
20. Yao, Q. *et al.* A bacterial type III effector family uses the papain-like hydrolytic activity to arrest the host cell cycle. *Proc. Natl Acad. Sci. USA* **106,** 3716–3721 (2009).
21. Rossi, P. *et al.* Structural elucidation of the Cys-His-Glu-Asn proteolytic relay in the secreted CHAP domain enzyme from the human pathogen *Staphylococcus saprophyticus*. *Proteins* **74,** 515–519 (2009).
22. Sokabe, M. *et al.* The X-ray crystal structure of pyrrolidone-carboxylate peptidase from *hyperthermophilic archaea Pyrococcus horikoshii*. *J. Struct. Funct. Genomics* **2,** 145–154 (2002).
23. Chou, S. *et al.* Structure of a peptidoglycan amidase effector targeted to Gram-negative bacteria by the type VI secretion system. *Cell Rep.* **1,** 656–664 (2012).
24. Kern, T. *et al.* Toward the characterization of peptidoglycan structure and protein-peptidoglycan interactions by solid-state NMR spectroscopy. *J. Am. Chem. Soc.* **130,** 5618–5619 (2008).
25. Verdonk, M. L., Cole, J. C., Hartshorn, M. J., Murray, C. W. & Taylor, R. D. Improved protein-ligand docking using GOLD. *Proteins* **52,** 609–623 (2003).
26. Liu, Y. & Eisenberg, D. 3D domain swapping: as domains continue to swap. *Protein Sci.* **11,** 1285–1299 (2002).
27. Bennett, M. J., Choe, S. & Eisenberg, D. Domain swapping: entangling alliances between proteins. *Proc. Natl Acad. Sci. USA* **91,** 3127–3131 (1994).
28. Krissinel, E. & Henrick, K. Inference of macromolecular assemblies from crystalline state. *J. Mol. Biol.* **372,** 774–797 (2007).
29. Berg, K. H., Ohnstad, H. S. & Håvarstein, L. S. LytF, a novel competence-regulated murein hydrolase in the genus Streptococcus. *J. Bacteriol.* **194,** 627–635 (2012).
30. Berg, K. H., Biornstad, T. J., Straume, D. & Håvarstein, L. S. Peptide-regulated gene depletion system developed for use in *Streptococcus pneumoniae*. *J. Bacteriol.* **193,** 5207–5215 (2011).
31. Bizzini, A. *et al.* Effects of alpha-phosphoglucomutase deficiency on cell wall properties and fitness in *Streptococcus gordonii*. *Microbiology* **153,** 490–498 (2007).
32. Berg, K. H., Stamsås, G. A., Straume, D. & Håvarstein, L. S. Effects of low PBP2b levels on cell morphology and peptidoglycan composition in *Streptococcus pneumoniae* R6. *J. Bacteriol.* **195,** 4342–4354 (2013).
33. Johnsborg, O. & Håvarstein, L. S. Pneumococcal LytR, a protein from the LytR-CpsA-Psr family, is essential for normal septum formation in *Streptococcus pneumoniae*. *J. Bacteriol.* **191,** 5859–5864 (2009).
34. Meisner, J. *et al.* FtsEX is required for CwlO peptidoglycan hydrolase activity during cell wall elongation in Bacillus subtilis. *Mol. Microbiol.* **89,** 1069–1083 (2013).
35. Arends, S. J., Kustusch, R. J. & Weiss, D. S. ATP-binding site lesions in FtsE impair cell division. *J. Bacteriol.* **191,** 3772–3784 (2009).
36. Schmidt, K. L. *et al.* A predicted ABC transporter, FtsEX, is needed for cell division in Escherichia coli. *J. Bacteriol.* **186,** 785–793 (2004).
37. Sambrook, J. & Russell, D. W. *Molecular Cloning: A Laboratory Manual* (Cold Spring Harbor Press, 2001).
38. Lacks, S. & Hotchkiss, R. D. A study of the genetic material determining an enzyme in Pneumococcus. *Biochim. Biophys. Acta.* **39,** 508–518 (1960).
39. Stamsås, G. A., Håvarstein, L. S. & Straume, D. CHiC, a new tandem affinity tag for the protein purification toolbox. *J. Microbiol. Methods* **92,** 59–63 (2013).
40. Higuchi, R., Krummel, B. & Saiki, R. K. A general method of *in vitro* preparation and specific mutagenesis of DNA fragments: study of protein and DNA interactions. *Nucleic Acids Res.* **16,** 7351–7367 (1988).
41. Sanchez-Puelles, J. M., Sanz, J. M., Garcia, J. L. & Garcia, E. Immobilization and single-step purification of fusion proteins using DEAE-cellulose. *Eur. J. Biochem.* **203,** 153–159 (1992).
42. Johnsborg, O., Eldholm, V., Bjornstad, M. L. & Håvarstein, L. S. A predatory mechanism dramatically increases the efficiency of lateral gene transfer in *Streptococcus pneumoniae* and related commensal species. *Mol. Microbiol.* **69,** 245–253 (2008).
43. Sung, C. K., Li, H., Claverys, J. P. & Morrison, D. A. An *rpsL* cassette, Janus, for gene replacement through negative selection in *Streptococcus pneumoniae*. *Appl. Environ. Microbiol.* **67,** 5190–5196 (2001).
44. Kabsch, W. XDS. *Acta. Crystallogr. D Biol. Crystallogr.* **66,** 125–132 (2010).
45. Evans, P. R. An introduction to data reduction: space-group determination, scaling and intensity statistics. *Acta. Crystallogr. D Biol. Crystallogr.* **67,** 282–292 (2011).
46. Sheldrick, G. M. Experimental phasing with SHELXC/D/E: combining chain tracing with density modification. *Acta. Crystallogr. D Biol. Crystallogr.* **66,** 479–485 (2010).
47. Pape, T. & Schneider, T. R. HKL2MAP: a graphical user interface for phasing with SHELX programs. *J. Appl. Cryst.* **37,** 843–844 (2004).
48. Vonrhein, C., Blanc, E., Roversi, P. & Bricogne, G. Automated structure solution with autoSHARP. *Methods Mol. Biol.* **364,** 215–230 (2007).
49. Cowtan, K. Recent developments in classical density modification. *Acta. Crystallogr. D Biol. Crystallogr.* **66,** 470–478 (2010).
50. Cowtan, K. General quadratic functions in real and reciprocal space and their application to likelihood phasing. *Acta. Crystallogr. D Biol. Crystallogr.* **56,** 1612–1621 (2000).
51. Cowtan, K. Fitting molecular fragments into electron density. *Acta. Crystallogr D Biol. Crystallogr.* **64,** 83–89 (2008).
52. Emsley, P., Lohkamp, B., Scott, W. G. & Cowtan, K. Features and development of Coot. *Acta. Crystallogr. D Biol. Crystallogr.* **66,** 486–501 (2010).
53. McCoy, A. J. *et al.* Phaser crystallographic software. *J. Appl. Crystallogr.* **40,** 658–674 (2007).
54. Murshudov, G. N. *et al.* REFMAC5 for the refinement of macromolecular crystal structures. *Acta. Crystallogr. D Biol. Crystallogr.* **67,** 355–367 (2011).

55. Chen, V. B. *et al.* MolProbity: all-atom structure validation for macromolecular crystallography. *Acta. Crystallogr. D Biol. Crystallogr.* **66,** 12–21 (2010).
56. Pettersen, E. F. *et al.* UCSF Chimera–a visualization system for exploratory research and analysis. *J. Comput. Chem.* **25,** 1605–1612 (2004).
57. Schuck, P. Size-distribution analysis of macromolecules by sedimentation velocity ultracentrifugation and lamm equation modeling. *Biophys. J.* **78,** 1606–1619 (2000).
58. Laue, T. M., Shah, B. D., Ridgeway, T. M. & Pelletier, S. L. *Analytical Ultracentrifugation in Biochemistry and Polymer Science* 90–125 (The Royal Society of Chemistry, 1992).
59. Cole, J. L. Analysis of heterogeneous interactions. *Methods Enzymol.* **384,** 212–232 (2004).
60. Ortega, A., Amoros, D. & Garcia de la Torre, J. Prediction of hydrodynamic and other solution properties of rigid proteins from atomic- and residue-level models. *Biophys. J.* **101,** 892–898 (2011).
61. Petoukhov, M. V. *et al.* New developments in the ATSAS program package for small-angle scattering data analysis. *J. Appl. Cryst.* **45,** 342–350 (2012).

Acknowledgements

We thank the ESRF beam lines ID29 and BM29 for access to synchrotron radiation. We thank Petra Pernot (ESRF) for assistance on SAXS experiments, Germán Rivas (CIB-CSIC) for advice on analytical ultracentrifugation assays, Zhian Salehian for technical assistance and Shahriar Mobashery (Univ. Notre Dame, USA) for critical reading of the manuscript. This work was supported by grants BFU2011-25326 and S2010/BMD-2457 and grants from the Research Council of Norway.

Author contributions

S.G.B. performed crystallization, crystal structure determination, docking calculations and SAXS data collection; D.S. performed purification of PcsB, cloning and purification of SeMet-PcsB$_{mut}$, and His-CHAP$_{pcsB}$. D.S. also constructed the LytF-CHAP$_{pcsB}$ chimera and performed the zymogram assays. G.A.S. constructed the CHiC-PcsB fusion and performed the PcsB depletion and TEM microscopy experiments. G.A.S. also constructed the PcsB-CHAP$_{LytF}$ mutant, I.G.M. performed SAXS data analysis and structural determination, C.A. performed analytical ultracentrifugation experiments, M.M.-R. wrote the manuscript, L.S.H. and J.A.H. conceived the study and wrote the manuscript.

Additional information

Accession codes: Atomic coordinates and structure factors for native PcsB have been deposited in the Protein Data Bank with accession code 4CGK.

Supplementary Information accompanies this paper at http://www.nature.com/naturecommunications

Competing financial interests: The authors declare no competing financial interests.

Reprints and permission information is available online at http://npg.nature.com/reprintsandpermissions/

How to cite this article: Bartual, S. G. *et al.* Structural basis of PcsB-mediated cell separation in *Streptococcus pneumoniae*. *Nat. Commun.* 5:3842 doi: 10.1038/ncomms4842 (2014).

Supplementary Fig. 1: Transmission electron micrographs showing the effect of PcsB depletion

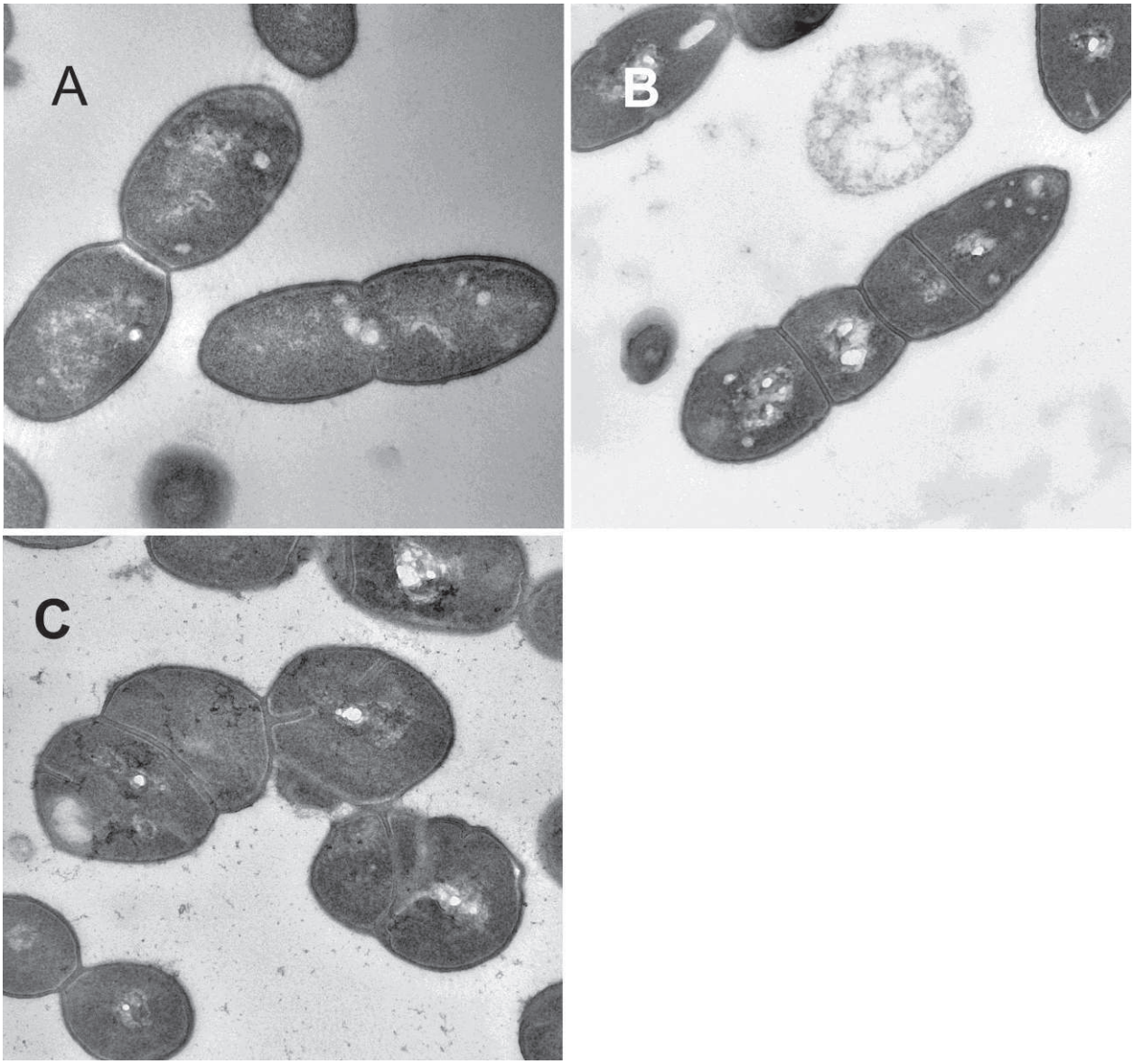

Transmission electron micrographs (TEM) showing the effect of PcsB depletion in S. pneumoniae R6 cells. A: Non-depleted control. B: Cells subjected to intermediate PcsB depletion. C: Cells subjected to severe PcsB depletion.

Supplementary Fig. 2: Electron density for the PcsB monomer

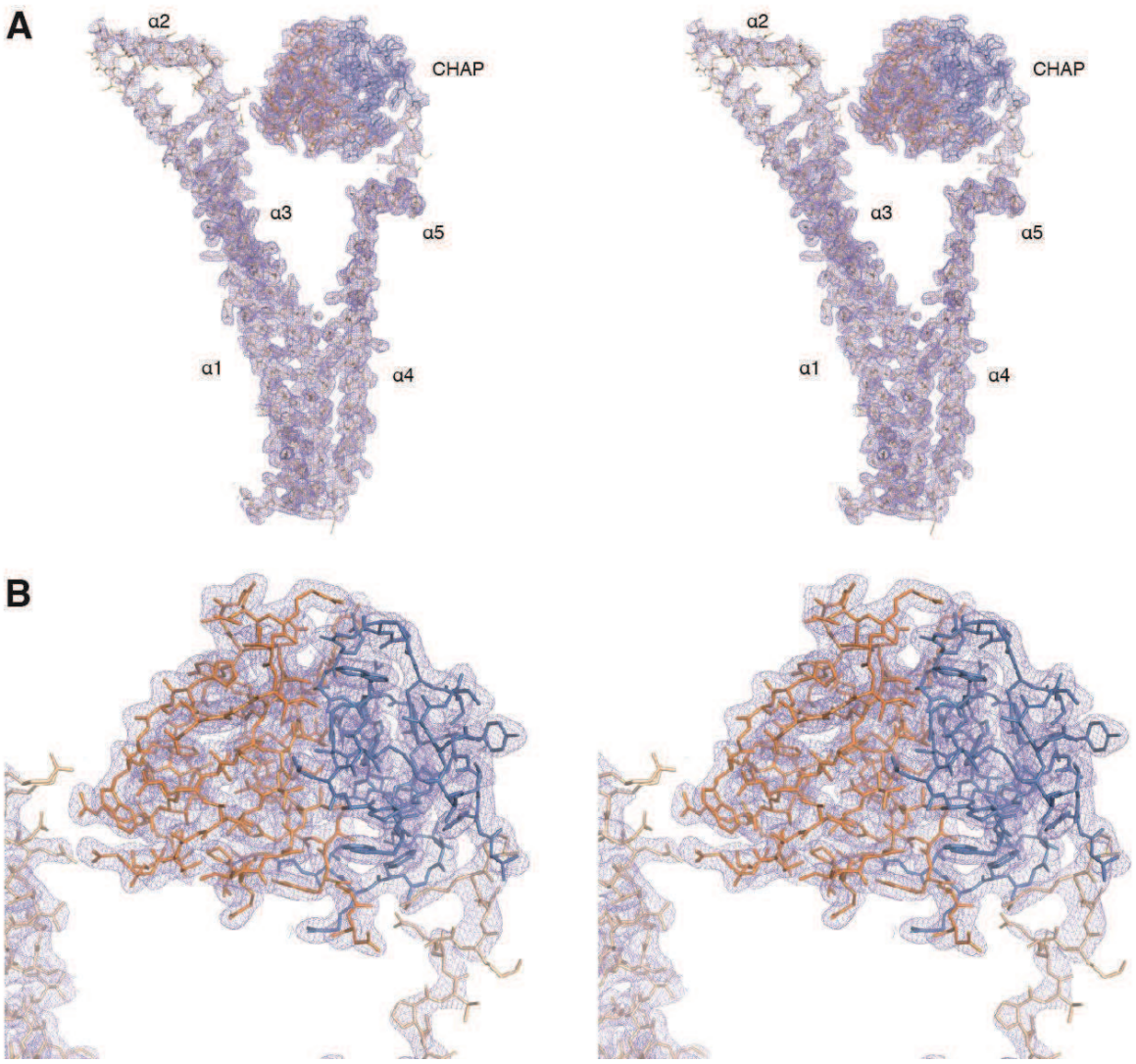

Electron density in PcsB. (A) Stereo view of the electron density map for the full-length PcsB monomer. (B) Stereo view of the electron density map of the CHAP domain. Residues are represented as capped sticks and colored in blue for the Lobe1, in orange for Lobe2 and the remaining part in light brown. Electron density map corresponds to the σ-weighted 2Fo-Fc electron density map contoured at 1.0 σ.

Supplementary Fig. 3: Structural superimposition of PcsB monomers

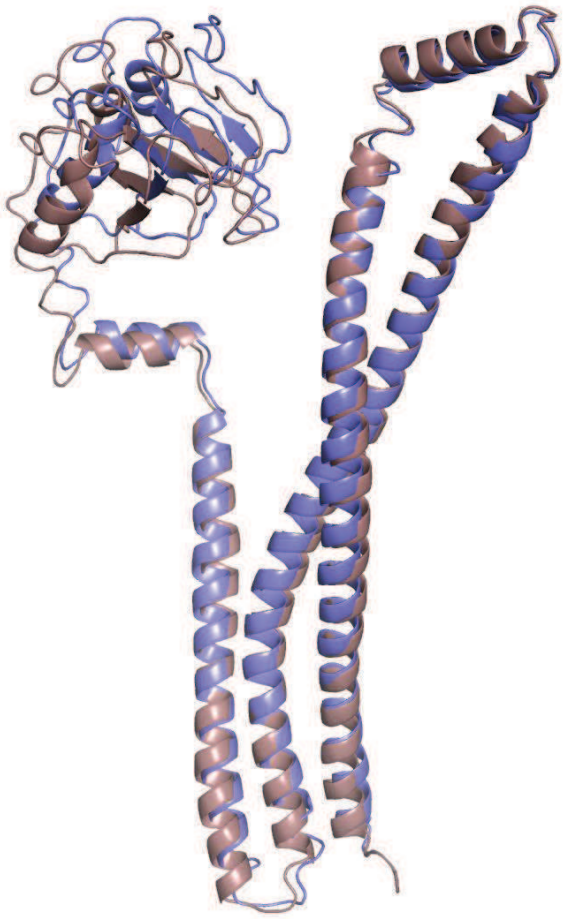

Structural comparison of chains A (brown) and B (blue) of PcsB. Structures of the two monomers present C^{α} backbone rmsd of 1.82 Å; as domains are nearly identical (C^{α} backbone rmsd of 1.09 Å and 0.16 Å for CC and CHAP domains respectively) this value is due to a slight difference in modular arrangement between CC and CHAP domains for each monomer.

Supplementary Fig. 4: Electron density for the linker region

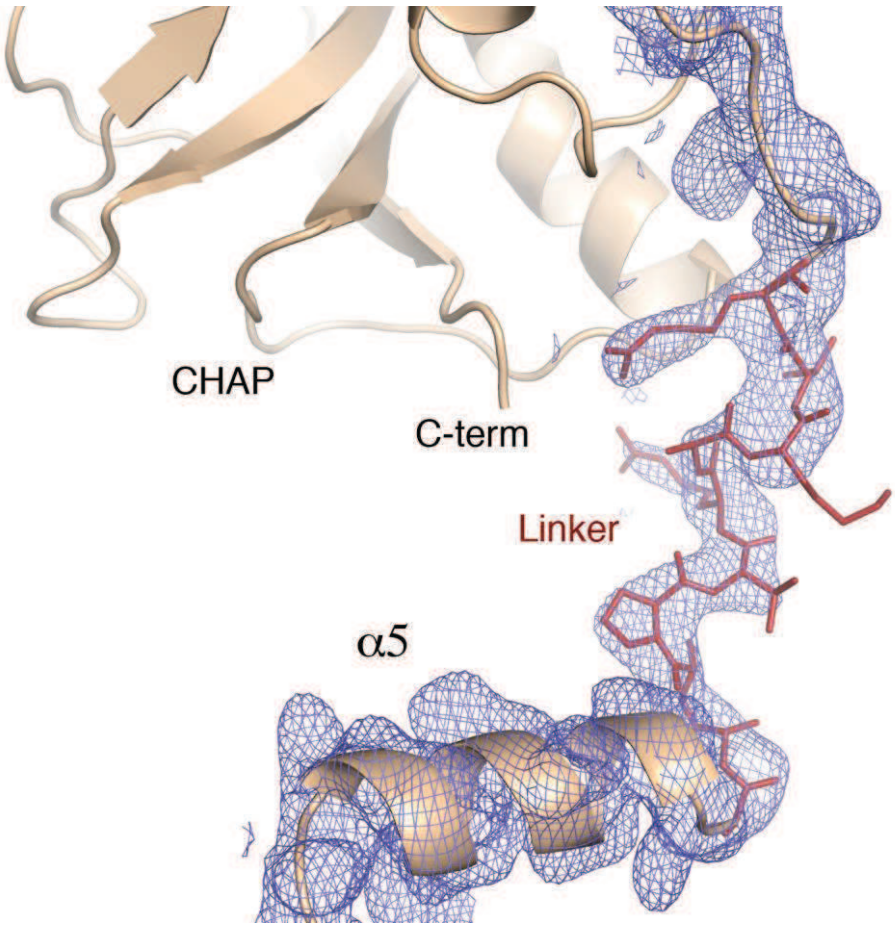

Electron density map of the linker region of PcsB. Linker (red sticks) connects the α5 of the coiled coil domain to the CHAP domain. Electron density map corresponds to the σ-weighted 2Fo-Fc electron density map contoured at 1.0 σ.

Supplementary Fig. 5: Structural comparison of $PcsB_{CC}$

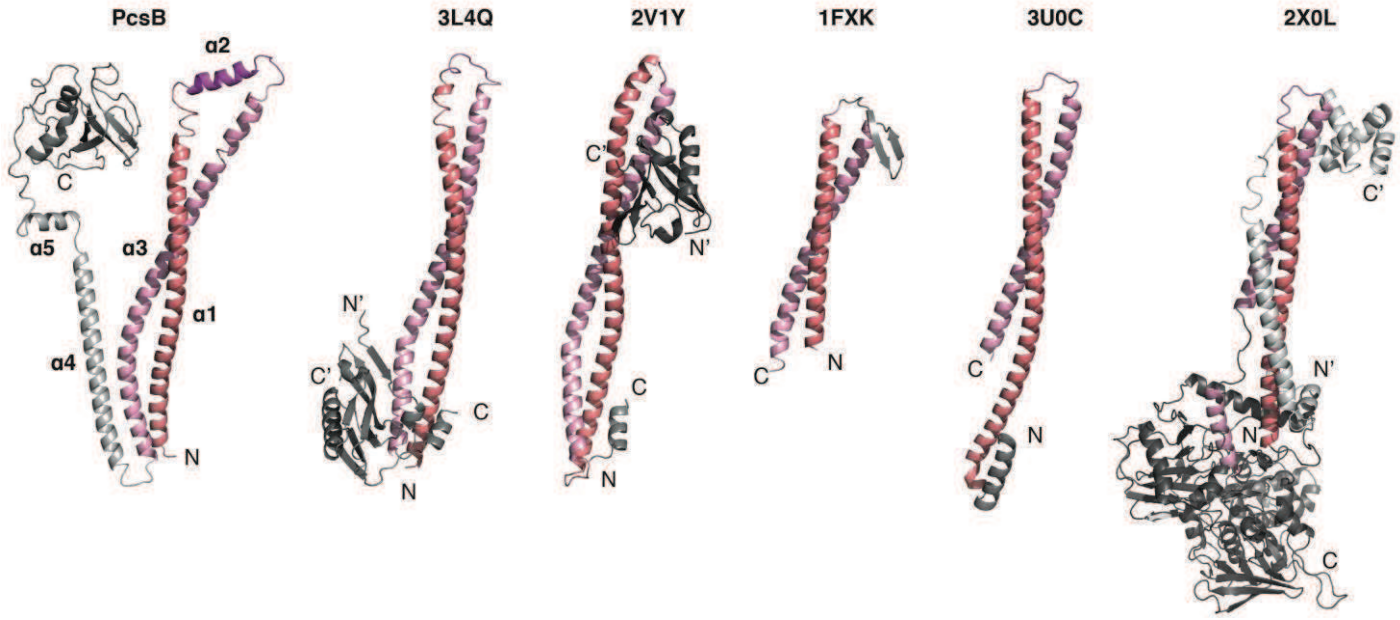

Structural comparison of $PcsB_{CC}$ with its closest homologues. The similar $PcsB_{CC}$ regions are highlighted in colour. Salmon for α1, magenta for α2 and light pink for α3 helices. A high structural homology is found for the antiparallel α1α3 bundle of the CC domain with the human inter-SH2 domains of p85β and p85α, regulatory subunits of Phosphatidylinositol-4,5-biphosphate 3-Kinase (PI3K), (PDB code 3L4Q, Z score of 10.2 and rmsd of 3.6 Å for 133 C^{α} atoms and PDB code 2V1Y, Z score of 10.1 and rmsd of 4.6 Å for 136 C^{α} atoms), the tower domain of the Lys-specific Histone dimethylase (PDB code 2X0L, Z score of 9.7 and rmsd of 4.4 Å for 133 C^{α} atoms) and also with the molecular chaperone prefoldin (PDB code 1FXK, Z score of 9.4 and rmsd of 1.9 Å for 91 C^{α} atoms) and the structures of coiled-coil domains from type III secretion system translocators (PDB code 3U0C, Z score of 9.4 and rmsd of 4.3 Å for 124 C^{α} atoms).

Supplementary Fig. 6: Structural homologues of PcsB

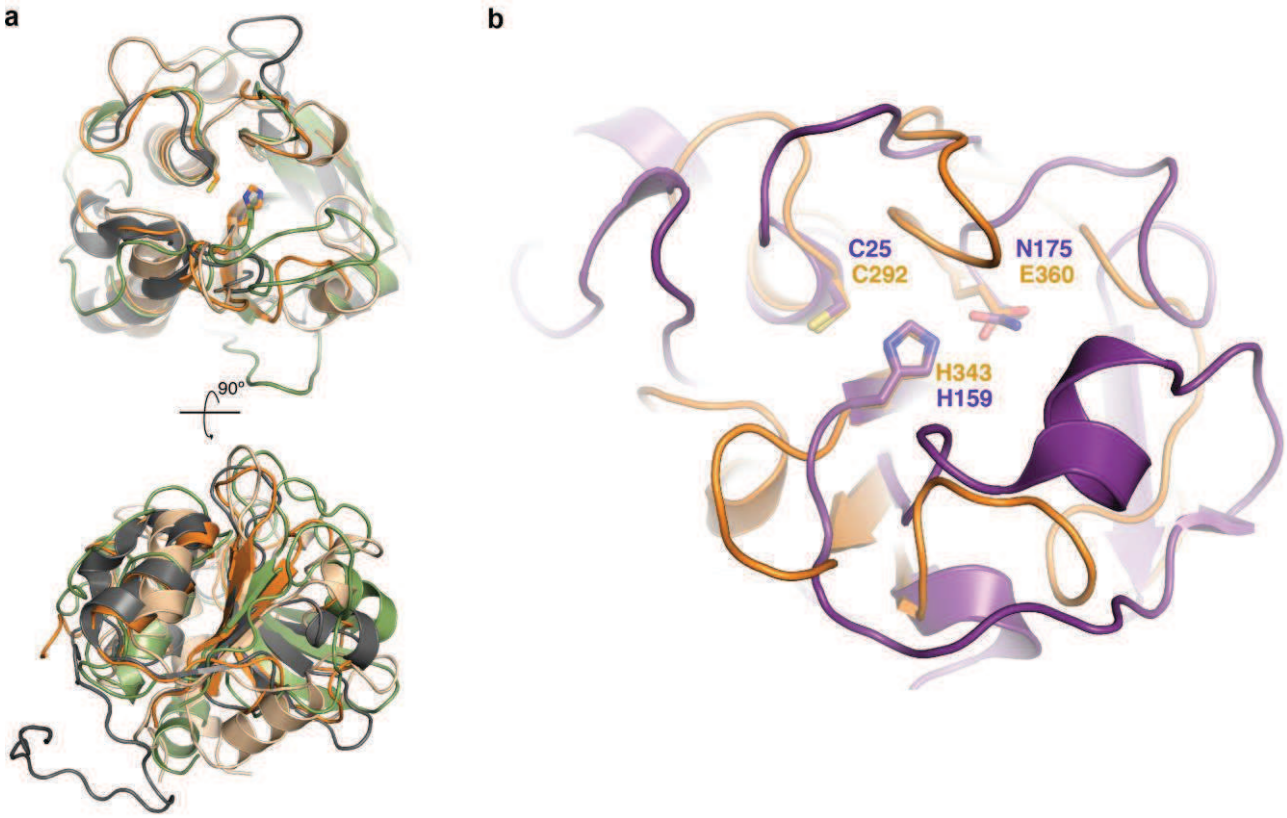

CHAP$_{PcsB}$ comparison with papain-like proteins. (**a**) Structural superimposition of CHAP$_{PcsB}$ (orange cartoon) with the *Staphylococcus saprophyticus* CHAP domain protein (PDB code 2K3A, Z score of 11.4 and rmsd of 2.7 Å for 105 C$^{\alpha}$ atoms) (gray cartoon), the type VI peptidoglycan amidase effector Tse1 from *Pseudomonas aeruginosa* (PDB code 4EOB, Z score of 7.5 and rmsd of 3.1 Å for 98 C$^{\alpha}$ atoms) (light brown) and the CHAP domain of the streptococcal specific phage lysin PlyC (PDB code 4F88, Z score of 7.9 and rmsd of 2.5 Å for 95 C$^{\alpha}$ atoms) (green cartoon). The catalytic Cys292 and His343 from pneumococcal PcsB are represented as capped sticks. Other related 3D structures are the staphyloxanthin Biosyntesis Protein (PDB code 2LRJ, Z score of 12.1 and rmsd of 2.7 Å for 103 C alpha atoms) and the CHAP domain of the Bifunctional Glutathionylspermidine

(PDB code 2IO9, Z score of 9.9 and rmsd of 2.5 Å for 104 C^{α} atoms), that are omitted for clarity. (**b**) The three-dimensional structure of papain (PDB code 1PPN) (magenta) with its catalytic triad (Cys25, His159 and Asn175) is superimposed onto the catalytic domain of PcsB (orange) with its catalytic triad (Cys292, His343 and Glu360).

Supplementary Fig. 7: Active sites of bacterial amidase structures

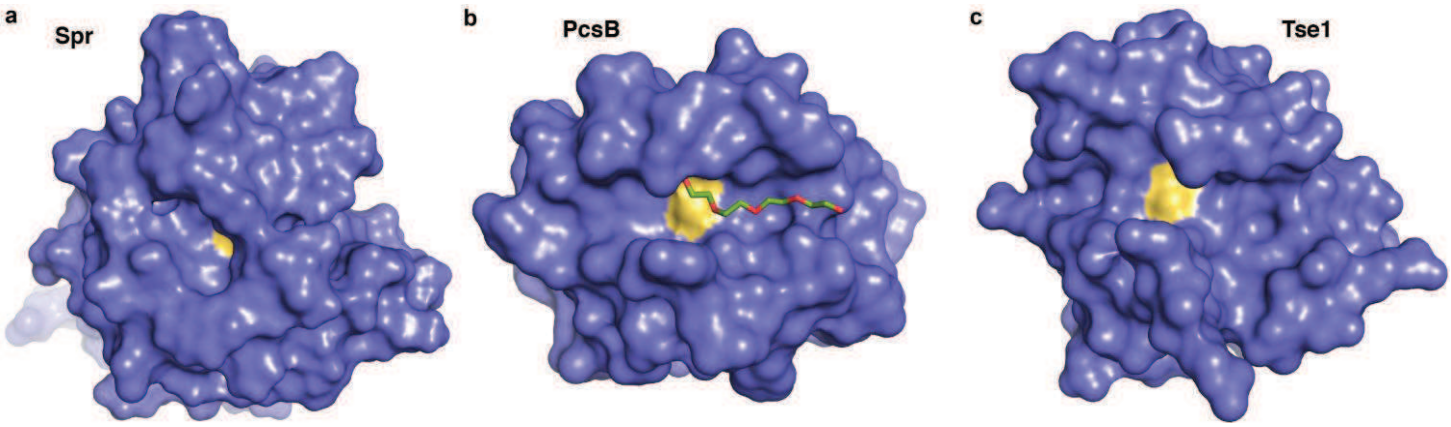

Different conformations of bacterial amidases. Surface representation of the *E. coli* Spr (PDB code 2K1G) (a), the CHAP domain of pneumococcal PcsB (b) and Tse1, a type VI secretion bacteriolytic amidase effector of *Pseudomonas aeruginosa* (c). The catalytic Cys residue is shown in yellow. The Polyethylene glycol molecule attached to the active site of PcsB is represented in capped sticks. Active-site loops cover the catalytic Cys residue in Spr providing a closed conformation for the enzyme while Tse presents en exposed active site with highly accessible catalytic residues. The PcsB structure also presents an open active site as confirmed by the presence of a substrate-mimicking ligand attached to it.

Supplementary Fig. 8: Electron density for the PEG

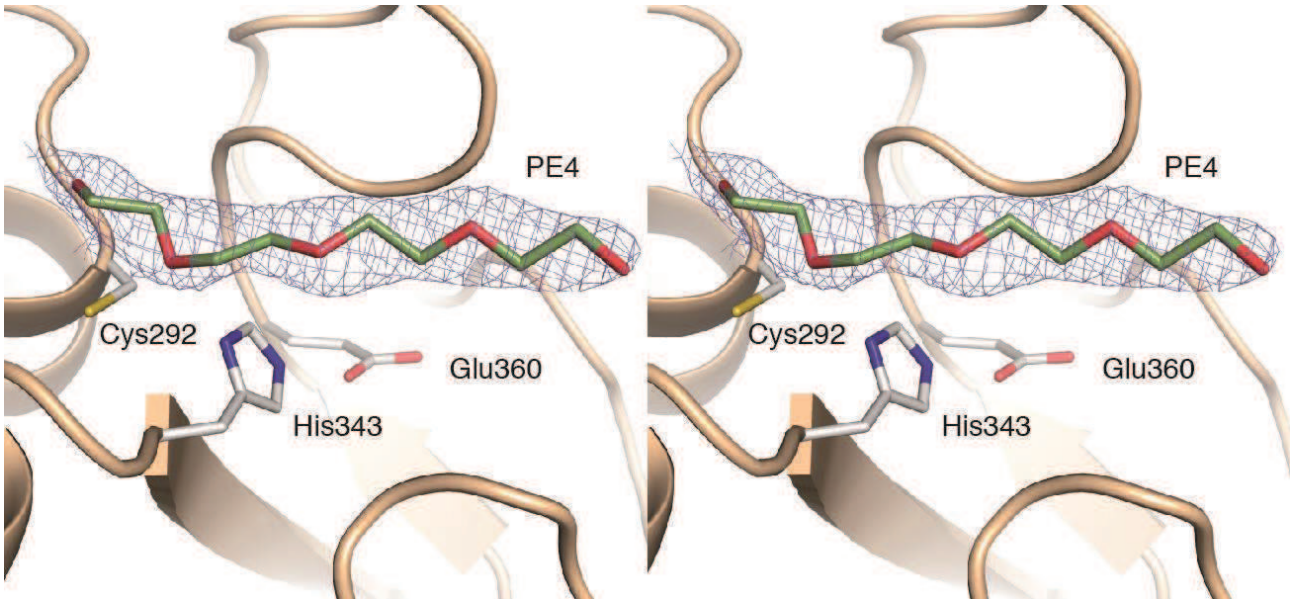

Electron density map for the PEG molecule attached to the active site of chain B.

Electron density map corresponds to the σ-weighted 2Fo-Fc electron density map contoured at 1.0 σ.

Supplementary Fig. 9: Peptide stem stabilization at the PcsB active site.

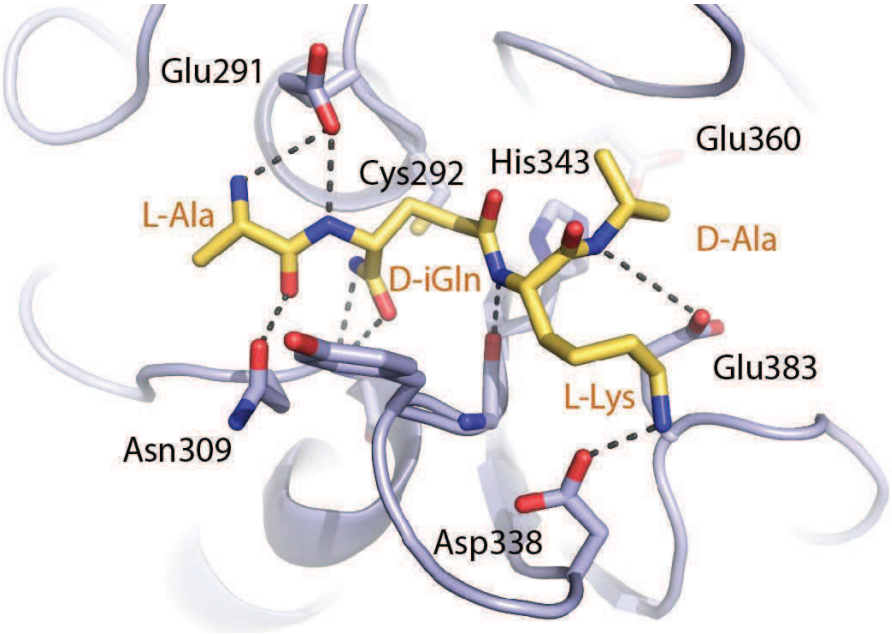

Substrate recognition in PcsB as obtained by docking calculations. Tetrapeptide (L-Ala-D-isoGln-L-Lys-D-Ala) (yellow sticks) interactions at the substrate-binding site of PcsB. Relevant residues lining the cavity are drawn as blue sticks and labeled. H-bond interactions and salt links between ligand and PcsB are depicted as dotted lines.

Supplementary Fig. 10: Dimer stabilization in PcsB.

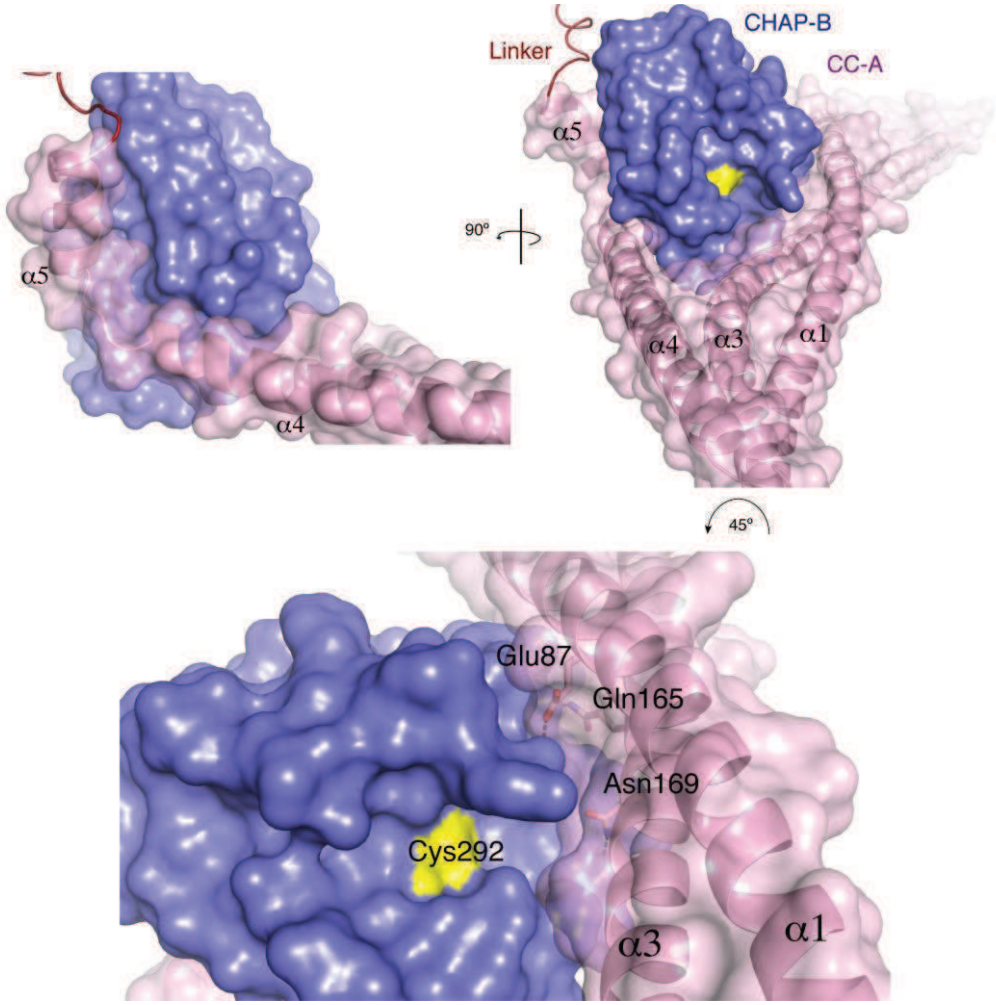

CC domain clamps the CHAP domain. Three views showing interactions between coiled coil domain of chain A (CC-A colored in pink) and the CHAP domain of chain B (CHAP-B colored in blue). About three-quarters of the CC/CHAP interactions are van der Waals contacts, and most of them involve exposed hydrophobic side chains. A few hydrogen bonds are found (see **Supplementary Table 3**) but no salt links between both domains.

Supplementary Fig. 11: Analytical ultracentrifugation experiments

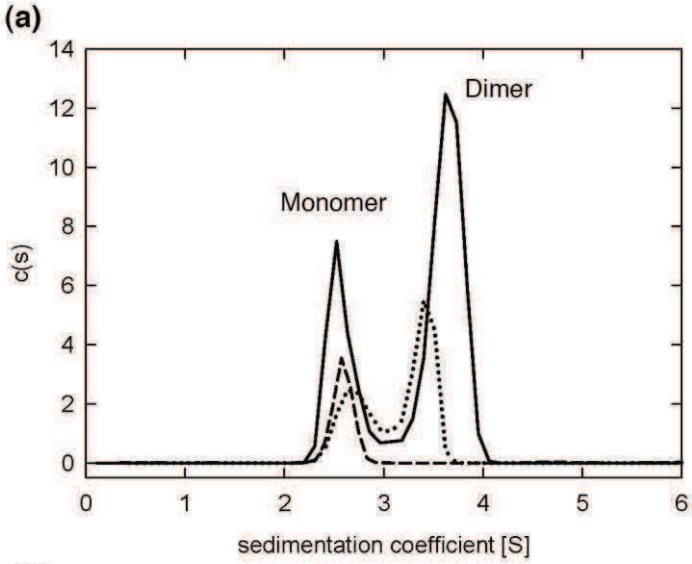

(b)

Experimental S values	
Dimer	**3.8**
Monomer	**2.7**

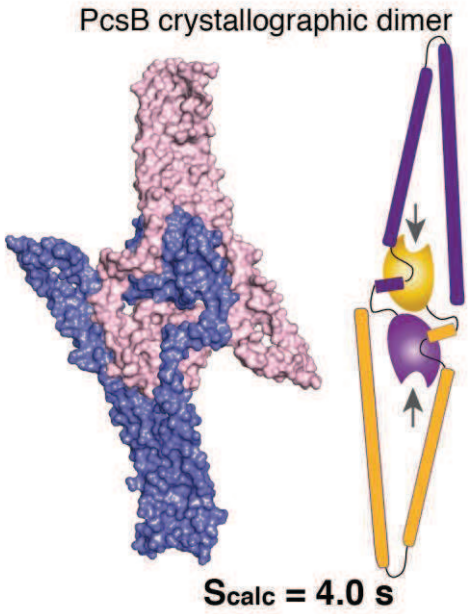

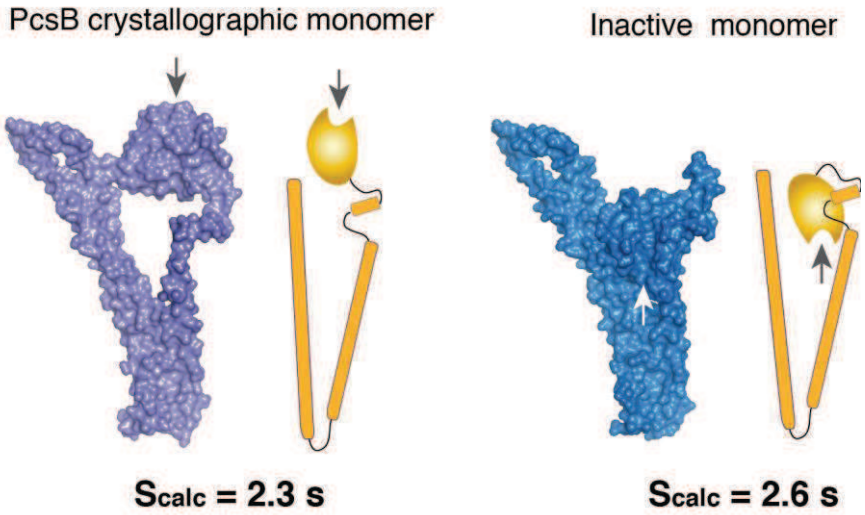

Sedimentation velocity analysis of PcsB. (**a**) Normalized sedimentation velocity distributions of PcsB at concentrations of 0.3 (dashed line), 4.0 (dotted line) and 8.0 (solid line) mg/ml. The sedimentation velocity profiles of PcsB at low protein concentration (0.1-0.3 mg/ml) corresponds to a single peak in the sedimentation coefficient distributions with a standard s-value of 2.7 ± 0.1 S, compatible with the behavior of a protein monomer, as further confirmed by molecular weight determination by sedimentation equilibrium (37500 +/- 1500 Da *vs.* 38916 Da, calculated from sequence). At high protein concentrations (4.0-8.0 mg/ml), the velocity data showed a biphasic behavior, leading to two separated peaks with standard s-values 2.7 ± 0.1 and 3.8 ± 0.1 S. The faster species is compatible with a protein dimer with a frictional ratio of f/f0 of 1.8, suggesting that the overall conformation of the dimer deviates from the expected for a globular rigid protein dimer. (**b**) HYDROPRO analysis allowed determining/establishing the most probable structure of monomers and dimers compatible with the experimental s-values of these species. The monomer is well described by a PcsB molecule with the CHAP domain inserted in its own CC domain –the calculated s-value for this structure was 2.6 S – almost the same as the experimental value 2.7 S and higher than the calculated s-value (2.3 S) for the alternative, less compact structure of the protein monomer observed in the asymmetric unit. The dimer corresponded to dimeric structure observed in the crystal (calculated s-value for this structure was 4.0 S, while the experimental s-value was 3.8S). Structural models for each arrangement are represented as molecular surface and in cartoons. Arrows indicate active sites. Sedimentation equilibrium analysis of protein in the range of 0.1-4.0 mg/ml confirmed the existence of a monomer-dimer equilibrium, with a quite high dissociation constant (K_d = 90 μM; data not shown).

Suplementary Fig. 12: SAXS analysis of PcsB.

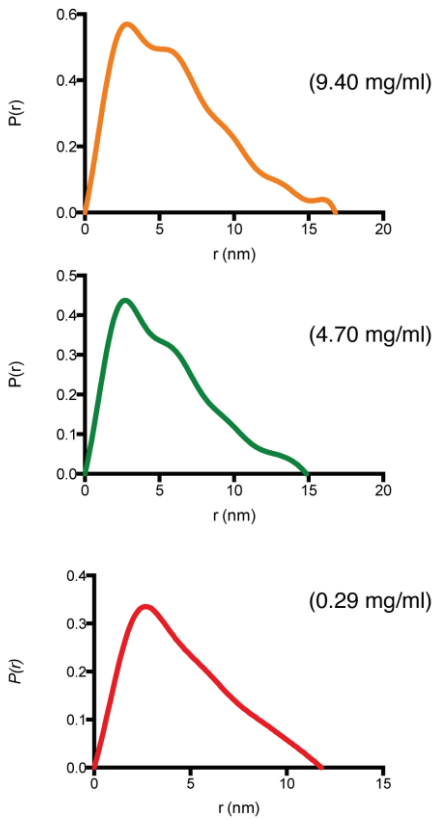

SAXS analysis of PcsB. The figures show the normalized pair-distance distribution function P(r) for the monomer (red graph) and dimer (green-yellow graphs). The tail in the P(r) function reveals the elongated shape of both monomer and dimer. Volume fractions of the corresponding models were further re-confirmed by the program OLIGOMER (Konarev et al. 2006 J. App. Cryst). The Dmax values suggest an equilibrium between the monomeric and dimeric species in solution.

Suplementary Fig. 13: PcsB Chimera homology model.

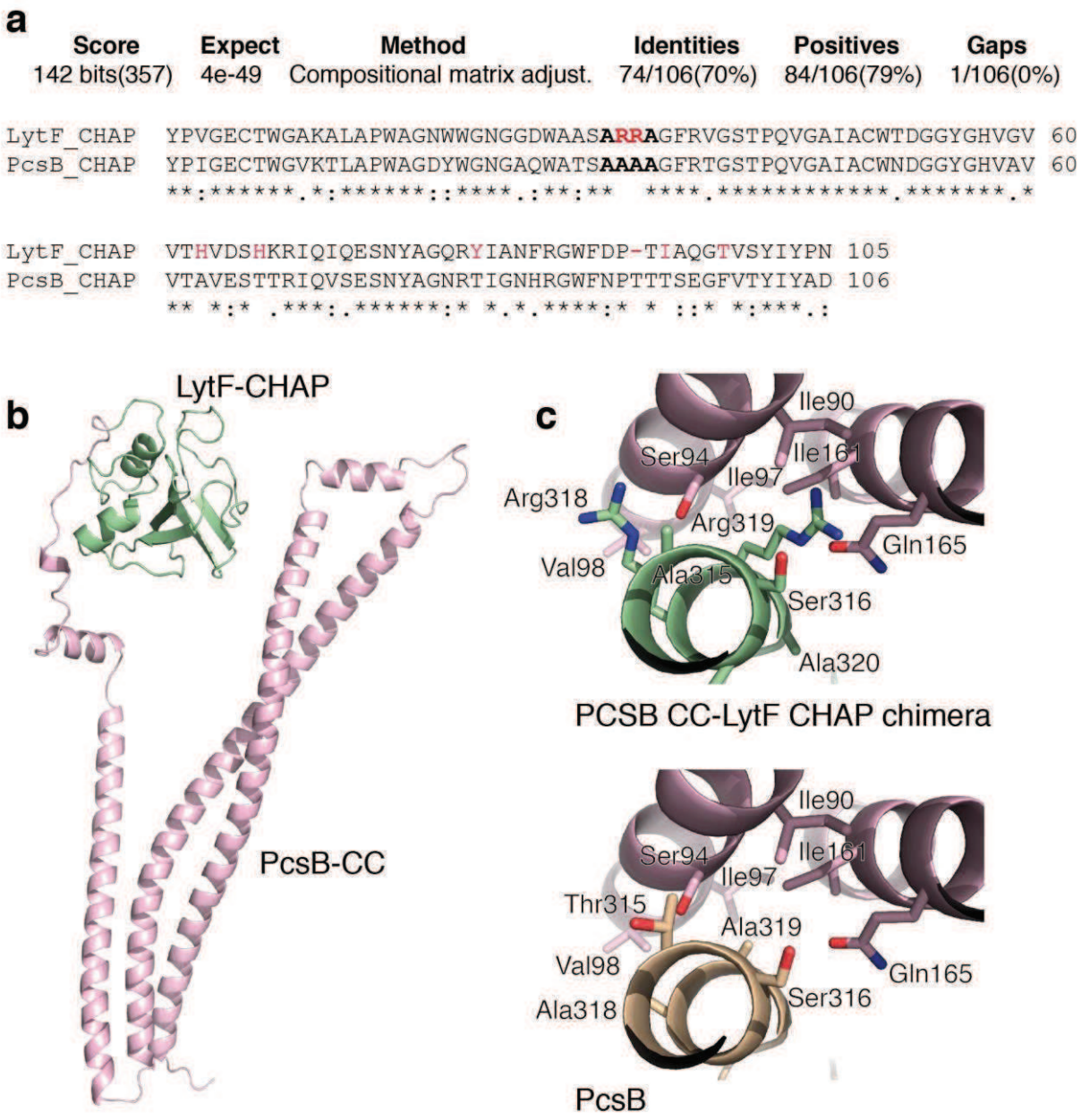

In silico model of PcsB-CHAP$_{LytF}$ chimera. (**a**) Sequence alignment between CHAP$_{LytF}$ and CHAP$_{PcsB}$ domains. The non-conservative changes are marked in red. One of the poli-Ala regions in PcsB is replaced in the chimera by ($_{317}$ASARRAG$_{321}$) (shown in bold letters). (**b**) *in silico* 3D model of the PcsB-CHAP$_{LytF}$ chimera. The model was calculated by homology comparison with the Swiss-Model server[1] using PcsB crystal structure as template. PcsB$_{CC}$ domain is colored light pink and LytF$_{CHAP}$ domain in light green. (**c**)

Zoomed detail of the $PcsB_{cc}$-$LytF_{CHAP}$ ($_{317}$ASARRAG$_{321}$) region (up) and the equivalent region of PcsB involved in the dimer stabilization (down). The $PcsB_{CC}$ domain of one dimer molecule (light pink) interacts with the CHAP domain of the other molecule (light green for $LytF_{CHAP}$ and weat for $PCSB_{CHAP}$ domains).

Suplementary figure 14: Growth and morphology of the pneumococci expressing the PcsB-CHAP$_{LytF}$ chimera.

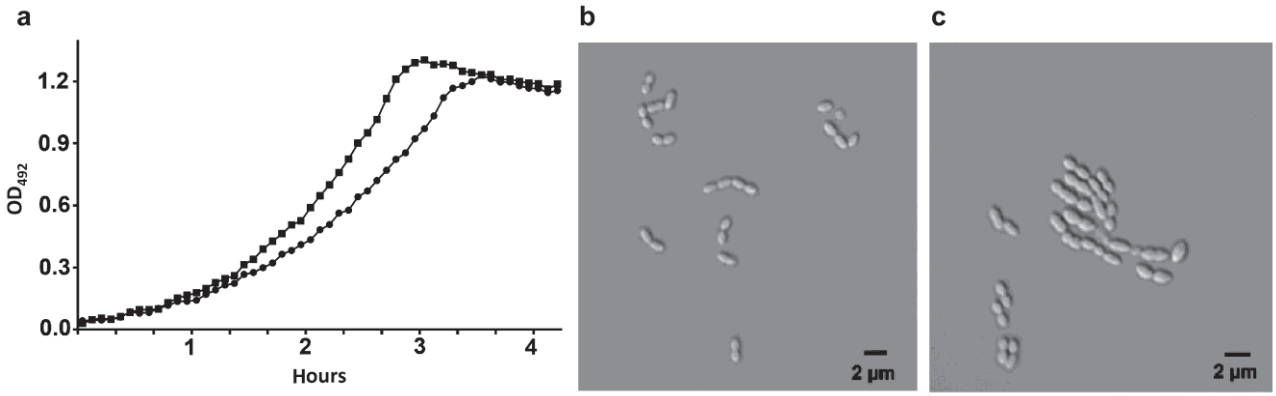

Comparison of a wild type and PcsB-mutant strain with respect to growth rate and morphology. In the mutant strain (SPH250), the native pcsB gene has been replaced by a gene encoding the PcsB-CHAP$_{LytF}$ chimera. Panel a: Growth curves of wild type cells (RH1) (■) and cells expressing the PcsB-CHAP$_{LytF}$ chimera (●). Panels b and c: Examination of RH1 (**b**) and SPH250 (**c**) cells by DIC microscopy revealed that some cells in the population expressing the PcsB-CHAP$_{LytF}$ chimera are morphologically abnormal.

Supplementary Fig. 15: Mutations on CC_{PcsB}.

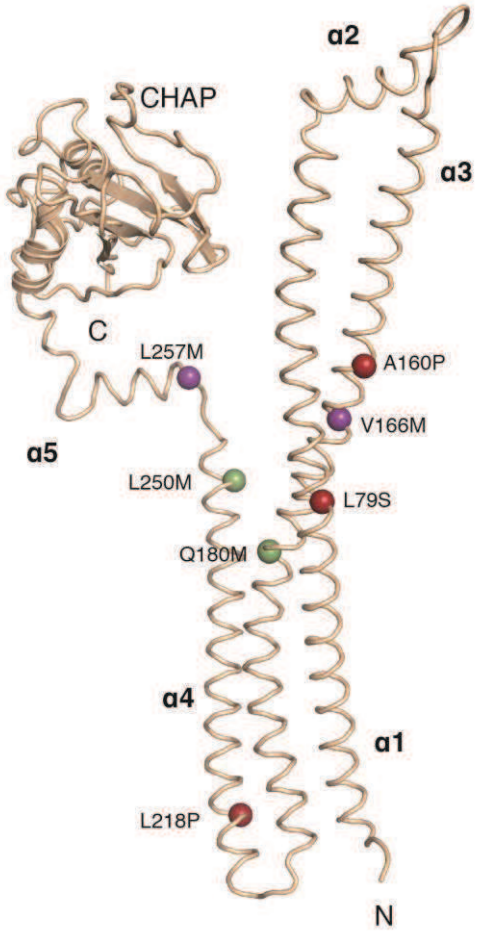

Mutations affecting CC stability. Three temperature sensitive mutants containing amino acid changes in L79S, L218P and A160P (numbering in D39 strain) (red spheres) have been reported [2,3] showing mild or severe defects in cell morphology and division. All of them disrupting stability of the CC domain: two of them (A160P and L79S) affecting α1- α3 interactions and the other (L218P) disrupting α3- α4 interactions. Due to the low content of methionine residues in the wt PcsB sequence, four different constructions were produced having two additional methionine residues in the CC domain. Mutations at Q180 and L250 (green spheres) were tolerated, whereas mutations at V166 and/or L257 residues (magenta spheres) resulted in misfolding of the protein.

Supplementary Table 1: Interactions in the PcsB dimer.

CHAIN B	HSDC	ASA	BSA	ΔiG
B:GLN80		89.17	15.31||	-0.11
B:SER83		11.20	1.10|	-0.01
B:LYS84		145.93	17.52||	-0.55
B:GLU87	H	74.46	52.41||||||||	-0.15
B:ILE90		30.63	24.27||||||||	0.39
B:THR91	H	89.48	29.09||||	-0.02
B:SER94	H	45.91	41.93||||||||||	-0.04
B:ILE97		22.60	17.74||||||||	0.28
B:VAL98		85.42	33.12||||	0.53
B:ASN101		71.07	31.02|||||	-0.36
B:GLU105		42.17	3.91|	-0.05
B:ASN114		154.67	3.35|	-0.02
B:LYS158		111.17	38.72||||	-0.64
B:ILE161		23.59	13.72||||||	0.22
B:SER162		58.12	1.97|	-0.02
B:GLN165	H	90.15	69.32||||||||	-0.20
B:VAL166		92.07	36.50||||	0.58
B:ASN168		17.48	12.52||||||||	-0.14
B:ASN169	H	82.62	80.42||||||||||	-0.69
B:ASP170		84.26	7.01|	-0.08
B:ILE172		62.70	39.65|||||||	0.63
B:ASN173	H	80.73	44.89||||||	-0.39
B:ILE176		86.17	60.76||||||||	0.97
B:GLN180		111.11	14.23||	-0.24
B:GLN246		114.10	18.82||	0.02
B:SER248		66.05	12.45||	-0.06
B:VAL249		103.65	92.60|||||||||	1.38
B:LEU250		99.60	34.07||||	0.55
B:SER252		79.85	52.60|||||||	0.27
B:ALA253		73.41	46.89|||||||	0.51
B:THR255		68.42	25.24||||	0.23
B:ASN256		91.52	10.55||	0.17
B:LEU257		140.21	96.58|||||||	1.38
B:GLN260		96.80	70.58||||||||	0.08
B:VAL261		83.14	35.36|||||	0.57
B:VAL264		83.39	71.42|||||||||	1.14
B:ALA269		68.91	14.41|||	-0.07
B:ALA270		48.00	33.94||||||||	0.33
B:PRO271		92.85	25.78|||	0.41
B:ARG273	H	151.41	80.74||||||	0.20
B:VAL276		125.31	12.74||	0.20
B:SER285		97.29	0.25|	-0.00
B:SER286	H	50.22	28.17||||||	-0.20
B:TYR287		12.62	6.59||||||	0.11
B:PRO288		87.47	58.22|||||||	0.92
B:ILE289		126.09	65.67||||||	0.95
B:GLY290		2.85	2.51||||||||	0.04
B:GLU291		59.51	27.38|||||	-0.10
B:TRP294		50.64	39.69||||||||	0.64
B:THR298		70.17	33.66|||||	0.41
B:LEU299		81.33	72.99|||||||||	0.70
B:ALA300		1.85	0.84|||||	0.01
B:TRP302		72.75	1.74|	-0.02
B:ASP305	H	13.26	0.60|	-0.01
B:TYR306		192.28	97.85||||||	0.94
B:TRP307		20.37	13.66|||||||	0.06
B:GLY308		44.81	41.82||||||||||	0.64
B:ASN309	H	77.20	56.85||||||||	-0.67
B:GLN312	H	82.10	54.76|||||||	0.20
B:THR315	H	89.27	56.07|||||||	0.76
B:SER316	H	37.71	35.36||||||||||	-0.12
B:ALA318		55.53	26.43|||||	0.13

B:ALA319		91.26	79.89|||||||||	0.70
B:ARG323	H	118.43	101.94||||||||||	-0.89
B:THR324		49.96	7.72||	-0.09
B:GLY325		23.10	11.71||||||	0.19
B:SER326	H	81.99	23.71|||	-0.27
B:THR327	H	68.60	67.08||||||||||	0.39
B:PRO328	H	1.72	1.72||||||||||	-0.02
B:GLN329	H	109.23	73.87|||||||	-0.37
B:ILE330		119.15	29.87|||	0.47
B:GLY331		31.35	18.46||||||	0.26
B:GLY339	H	79.56	16.34|||	-0.18
B:GLY340		40.37	13.13||||	0.04
B:TYR341	H	168.67	32.54||	-0.33
B:VAL346		17.25	17.25|||||||||||	0.28
B:VAL347		1.35	1.35||||||||||	-0.02
B:THR348		62.63	61.48||||||||||	-0.25
B:ALA349		26.76	24.58||||||||||	0.39
B:VAL350		48.71	33.57|||||||	0.12
B:GLU351	H	99.12	89.69||||||||||	-0.28
B:SER352		49.62	16.52||||	0.26
B:THR353		62.36	14.92|||	-0.17
B:ARG355		30.62	2.33|	-0.09
B:GLN357		37.82	26.89||||||||	-0.35
B:SER359		24.59	23.33||||||||||	-0.02
B:ARG367		108.94	35.83||||	0.09
B:THR368		91.16	53.15||||||	0.84
B:ILE369	H	56.80	43.91||||||||	0.28
B:GLY370		24.77	10.21|||||	0.16
B:ASN371		80.64	7.76|	0.04
B:TRP375		84.63	41.92|||||	0.16
B:TYR390	H	24.41	16.33|||||||	0.12
B:ASP392		138.89	2.64|	-0.03

CHAIN A	HSDC	ASA	BSA	ΔiG
A:GLN80	H	87.65	24.40|||	-0.12
A:SER83		10.91	2.21|||	-0.03
A:LYS84	H	147.86	27.91||	-0.80
A:GLU87	H	73.91	56.78||||||||	-0.15
A:ILE90		30.29	24.28|||||||||	0.39
A:THR91	H	89.67	30.90||||	0.01
A:SER94	H	45.81	41.62||||||||||	-0.06
A:ILE97		22.93	18.58|||||||||	0.30
A:VAL98		85.24	34.48|||||	0.55
A:ASN101		62.96	13.10|||	-0.15
A:GLU105		69.06	18.84|||	-0.31
A:ARG109		115.42	3.62|	-0.01
A:LYS158		108.45	20.79||	-0.41
A:ILE161		23.24	13.02||||||	0.21
A:GLN165	H	90.59	67.48||||||||	-0.17
A:VAL166		93.65	34.31||||	0.55
A:ASN168		17.61	13.42||||||||	-0.15
A:ASN169	H	81.39	78.88||||||||||	-0.65
A:ASP170		85.87	4.22|	-0.05
A:ILE172		63.80	44.14|||||||	0.71
A:ASN173	H	80.30	40.32||||||	-0.33
A:VAL175		13.21	0.67|	0.01
A:ILE176		84.42	60.91||||||||	0.97
A:GLN179		87.86	1.11|	-0.02
A:GLN180		112.18	23.08|||	-0.26
A:GLN246		111.58	18.38||	0.04
A:SER248		74.07	13.91||	0.01
A:VAL249		100.90	91.38||||||||||	1.40
A:LEU250		102.29	35.56||||	0.57
A:SER252	H	75.00	49.34|||||||	0.26

A:ALA253		72.17	41.72||||||	0.47
A:THR255		71.25	24.84||||	0.23
A:ASN256		88.25	10.88||	0.17
A:LEU257		136.08	92.52|||||||	1.30
A:GLN260		95.54	71.22||||||||	0.09
A:VAL261		89.19	45.16||||||	0.72
A:VAL264		80.58	72.19|||||||||	1.15
A:ALA268		113.51	3.30|	0.05
A:ALA269		65.96	10.54||	-0.09
A:ALA270		50.84	40.03||||||||	0.37
A:PRO271		95.74	35.30||||	0.56
A:ARG273	H	156.91	85.85|||||	-0.01
A:VAL276		98.65	23.27|||	0.37
A:PRO278		89.63	2.01|	0.03
A:SER285		98.47	0.86|	-0.01
A:SER286	H	48.55	28.76||||||	-0.19
A:TYR287		13.42	7.37|||||	0.12
A:PRO288		86.56	59.68|||||||	0.94
A:ILE289		128.75	64.50||||||	0.96
A:GLY290		3.76	3.51||||||||||	0.06
A:GLU291		56.16	24.74|||||	-0.06
A:TRP294		49.69	39.03||||||||	0.62
A:THR298		70.12	33.12|||||	0.41
A:LEU299		77.58	67.94|||||||||	0.66
A:ALA300		2.01	0.33||	0.01
A:ASP305	H	13.46	0.74|	-0.01
A:TYR306		191.38	102.93||||||	1.01
A:TRP307		20.90	13.92|||||||	0.05
A:GLY308		44.75	41.17||||||||||	0.63
A:ASN309	H	76.11	55.18||||||||	-0.64
A:GLN312	H	82.70	52.06|||||||	0.17
A:THR315	H	88.21	55.02|||||||	0.75
A:SER316	H	37.33	35.60||||||||||	-0.14
A:ALA318		54.65	25.76|||||	0.20
A:ALA319		92.84	83.82||||||||||	0.69
A:ARG323	H	122.69	114.41|||||||||||	-0.89
A:THR324		48.97	10.72|||	-0.12
A:GLY325		22.53	11.60||||||	0.19
A:SER326	H	78.09	16.87|||	-0.19
A:THR327	H	64.92	61.74||||||||||	0.68
A:PRO328	H	5.52	5.52||||||||||	-0.03
A:GLN329	H	103.41	78.48||||||||	-0.44
A:ILE330		118.77	24.61|||	0.39
A:GLY331		31.70	18.36||||||	0.28
A:GLY339		80.86	8.96||	-0.10
A:GLY340		40.42	8.87|||	0.08
A:TYR341		169.09	16.49|	-0.19
A:VAL346		12.20	12.20||||||||||	0.20
A:VAL347		0.98	0.98||||||||||	-0.01
A:THR348		61.28	59.25||||||||||	0.43
A:ALA349		27.71	26.54||||||||||	0.42
A:VAL350		49.35	30.65|||||||	0.17
A:GLU351	H	95.35	62.39|||||||	0.05
A:SER352		48.22	9.46||	0.15
A:THR353		64.73	13.68|||	-0.16
A:GLN357		39.89	29.30||||||||	-0.36
A:SER359		16.00	15.17||||||||||	0.18
A:ARG367		108.28	31.64|||	0.13
A:THR368		89.97	55.64|||||||	0.89
A:ILE369		57.65	44.51||||||||	0.30
A:GLY370		24.77	11.21|||||	0.18
A:ASN371		85.09	9.93||	0.03
A:TRP375		74.39	43.11||||||	0.21
A:TYR390		19.18	14.48||||||||	0.15
A:ASP392		138.23	11.11|	-0.03

HSDC: Residues making Hydrogen/Disulphide bond, Salt bridge or Covalent link.

ASA: accessible surface area ($Å^2$)

BSA: Buried Surface Area ($Å^2$)

ΔiGdiss: dissociation barrier, kcal/mol

||||: Buried area percentage, one bar per 10%

Supplementary Table 2: SAXS Data Collection and derived parameters for PcsB

Data collection parameters					
Instrument	EMBL beamline BM29 (ESRF, France)				
Wavelength (Å)	1				
s-range ($Å^{-1}$)	0.01–0.6				
Exposure time (s)	1×10				
Concentration range (mg ml^{-1})	0.29-9.40				
Temperature (K)	277				
Structural parameters					
Concentration (mg ml^{-1})	0.29	0.59	1.18	4.70	9.40
R_g (Å) (from Guinier)	35±6	41±6	39±4	42±4	45±4
R_g (Å) (from P(r))	36±6	41±6	39±4	43±4	48±5
D_{max} (Å)	118±12	146±15	136±14	148±15	168±17
Molecular mass determination					
MM (kDa) from Porod volume	44±4	35±4	35±4	48±5	61±6
Calculated MM (kDa) from sequence (Monomer / Dimer)	39 / 78				
Software employed					
Data processing	PRIMUS, GNOM				
Ab initio analysis	DAMMIF, DAMMIN				
Validation and averaging	SUPCOMB, DAMAVER				
Computation of model intensities	CRYSOL				
3D graphics representations	PYMOL				

Supplementary Table 3. Bacterial strains used in this study.

Strain	Characteristics	Source
E. coli		
DH5α	Cloning host	Invitrogen
BL21 (DE3)	Expression host	Invitrogen
gs32	BL21 (DE3) containing *pcsB* cloned downstream of the *T7lac* promoter in the pRSET A vector	[4]
ds122	BL21 (DE3) containing $pcsB_{mut}$ cloned downstream of the *T7lac* promoter in the pRSET A vector	This work
ds179	BL21 (DE3) containing $His\text{-}CHAP_{pcsB}$ cloned downstream of the *T7lac* promoter in the pRSET A vector	This work
ds189	BL21 (DE3) containing $His\text{-}CHAP_{pcsBC292A}$ cloned downstream of the *T7lac* promoter in the pRSET A vector	This work
S. pneumoniae		
R704	R6 derivative, *comA*::*ermAM*; Ery^r	J. P. Claverys[a]
RH1	R704, but *ebg*::*spc*; Ery^r Spc^r	[5]
RH14	RH1, but Δ*lytA*::*kan*; Ery^r Spc^r Kan^r	[6]
RH426	Δ*comA* ΔIS*1167*::Janus[b]; Ery^r Kan^r	[7]
SPH131	Δ*comA,* P1::P_{comR}::*comR*, P_{comX}::Janus. Ery^r, Kan^r	[8]
SPH154	Δ*comA,* P1::P_{comR}::*comR*, *cpsO*::Janus::*cpsN*. Ery^r, Kan^r	[9]
SPH246	SPH131, but ΔJanus::P_{comX}-*pcsB*; Ery^r Sm^r	This work
SPH247	SPH246, but Δ$pcsB_{wt}$.::Janus; Ery^r Kan^r	This work
SPH248	SPH247, but ΔJanus::*pcsB-CHAP*$_{lytF}$; Ery^r Sm^r	This work
SPH249	SPH248, but ΔP_{comX}-*pcsB*::Janus; Ery^r Kan^r	This work
SPH250	SPH249, but ΔJanus::DEL; Ery^r Sm^r	This work
SPH252	SPH131, but ΔJanus::P_{comX}-*lytF-CHAP*$_{pcsB}$; Ery^r Sm^r	This work
SPH258	SPH247, but ΔJanus::$pcsB_{C292A}$; Ery^r Sm^r	This work

[a] Gift from Jean-Pierre Claverys.
b Janus indicates the presence of a *kan*::*rpsL*+ cassette.

Supplementary Table 4. Primers used in this study.

Primer name	Sequence (5' ---> 3')	Source
ds79	[a]ATGGCTTCAGCAAACACTAACTTAAC	This work
ds80	GTTAAGTTAGTGTTTGCTGAAGCCATTACTGATTGTTGTTGGCTAGC	This work
ds85	ATGCAAAAATTGGCTGATGATGCTC	This work
ds86	GAGCATCATCAGCCAATTTTTGCATATTAGCAATTACAGTATTGATAGC	This work
ds95	ATTTATATTTATTATTGGAGGTTCAATGAATGAACAGTTTAGCCCATCC	This work
ds96	AGTATTACTTGGGTCGGTCG	This work
ds97	CGACCGACCCAAGTAATACTTATCCAATTGGAGAATGTACATG	This work
ds147	TACGTCTAGAAATAATTTTGTTTAACTTTAAGAAGGAGATATACATATGCATCATCATCATCATCATGCAAAAGTTCGTCCAACATAC	This work
ds98	ATTGGGAAGAGTTACATATTAGAAATTAATCTGCATAAATATATGTAAC	This work
khb31	ATAACAAATCCAGTAGCTTTGG	8
khb32	GGTCTAGAGATGATTTTAATTAC	8
khb33	TTTCTAATATGTAACTCTTCCCAAT	8
khb34	CATCGGAACCTATACTCTTTTAG	8
khb36	TGAACCTCCAATAATAAATATAAAT	8
35	ATTTATATTTATTATTGGAGGTTCAATGAAGAAAAAAATCTTAGCGTC	This work
36	ATTGGGAAGAGTTACATATTAGAAATTAATCTGCATAAATATATGTAACA	This work
37	TCAAAAGGTGCTTCTGAGAAC	This work
38	CTTCTACAACTTCAACGATTTC	This work
39	CACATTATCCATTAAAAATCAAACATTACGTAGATACTCCTTCTTTT	This work
40	CTAAACGTCCAAAAGCATAAGGAAAGTTTACAGAGGGACTCGAATAG	This work
52	GTGCATTCACCAACAGGGTAACTTGAAGCGTTTGTACTGTATG	This work
53	TACCCTGTTGGTGAATGCAC	This work
154	GTAATTAAAATCATCTCTAGACCTTTCTAATATGTAACTCTTCCCAAT	This work
216	AAAAGAAGGAGTATCTACGTAATATGAAGAAAAAAATCTTAGCGTC	This work
217	CTATTCGAGTCCCTCTGTAAATTAATTTGGGTAGATATAGGAAAC	This work
218	ATTACGTAGATACTCCTTCTTTT	This work
219	TTTACAGAGGGACTCGAATAG	This work
Kan4	GTTTGATTTTTAATGGATAATGTG	5
84.F		
RpsL 41.R	CTTTCCTTATGCTTTTGGAC	5
T7 F	TAATACGACTCACTATAGGG	Invitrogen
T7 R	CTAGTTATTGCTCAGCGGTGG	Invitrogen

[a] Bases introducing Met codons are underlined.

Supplementary References

1 Kiefer, F., Arnold, K., Kunzli, M., Bordoli, L. & Schwede, T. The SWISS-MODEL Repository and associated resources. *Nucleic acids research* **37**, D387-392, doi:10.1093/nar/gkn750 (2009).

2 Sham, L. T., Barendt, S. M., Kopecky, K. E. & Winkler, M. E. Essential PcsB putative peptidoglycan hydrolase interacts with the essential FtsXSpn cell division protein in Streptococcus pneumoniae D39. *Proceedings of the National Academy of Sciences of the United States of America* **108**, E1061-1069, doi:10.1073/pnas.1108323108 (2011).

3 Sham, L. T., Jensen, K. R., Bruce, K. E. & Winkler, M. E. Involvement of FtsE ATPase and FtsX extracellular loops 1 and 2 in FtsEX-PcsB complex function in cell division of Streptococcus pneumoniae D39. *mBio* **4**, doi:10.1128/mBio.00431-13 (2013).

4 Stamsas, G. A., Havarstein, L. S. & Straume, D. CHiC, a new tandem affinity tag for the protein purification toolbox. *Journal of microbiological methods* **92**, 59-63, doi:10.1016/j.mimet.2012.11.003 (2013).

5 Johnsborg, O., Eldholm, V., Bjornstad, M. L. & Havarstein, L. S. A predatory mechanism dramatically increases the efficiency of lateral gene transfer in Streptococcus pneumoniae and related commensal species. *Molecular microbiology* **69**, 245-253, doi:10.1111/j.1365-2958.2008.06288.x (2008).

6 Eldholm, V. *et al.* Pneumococcal CbpD is a murein hydrolase that requires a dual cell envelope binding specificity to kill target cells during fratricide. *Molecular microbiology* **76**, 905-917, doi:10.1111/j.1365-2958.2010.07143.x (2010).

7 Johnsborg, O. & Havarstein, L. S. Pneumococcal LytR, a protein from the LytR-CpsA-Psr family, is essential for normal septum formation in Streptococcus pneumoniae. *Journal of bacteriology* **191**, 5859-5864, doi:10.1128/JB.00724-09 (2009).

8 Berg, K. H., Biornstad, T. J., Straume, D. & Havarstein, L. S. Peptide-regulated gene depletion system developed for use in Streptococcus pneumoniae. *Journal of bacteriology* **193**, 5207-5215, doi:10.1128/JB.05170-11 (2011).

9 Berg, K. H., Stamsas, G. A., Straume, D. & Havarstein, L. S. Effects of low PBP2b levels on cell morphology and peptidoglycan composition in Streptococcus pneumoniae R6. *Journal of bacteriology* **195**, 4342-4354, doi:10.1128/JB.00184-13 (2013).

Paper III

The single transmembrane segment of pneumococcal WalK is required for the perception of an intramembrane or extracellular signal.

Gro Anita Stamsås, Daniel Straume, Zhian Salehian and Leiv Sigve Håvarstein*

Department of Chemistry, Biotechnology and Food Science, Norwegian University of Life Sciences, NO-1432 Ås, Norway.

The *Streptococcus pneumoniae* genome encodes 13 two-component regulatory systems plus an orphan repsonse regulator. Only one of these systems, WalRK, is essential for viability under laboratory conditions. Despite its importance, the biological role of the WalRK system is not well understood. However, previous studies have shown that it regulates expression of the cross wall splitting enzyme PcsB, and consequently has a crucial role in pneumococcal cell division. Considerable efforts have been made to understand how the system is regulated, but no signal(s) sensed by the WalK histidine kinase has been identified so far. WalK orthologs in most low-GC Gram-positive bacteria are attached to the cytoplasmic membrane via two transmembrane segments separated by a large extracellular loop believed to function as a sensor domain. In contrast, members of the genus *Streptococcus* have WalK histidine kinases that are anchored to the cytoplasmic membrane by a single transmembrane segment. It has been a long standing question whether this transmembrane segment still serves as a signal-sensing domain, or if it only functions as a membrane anchor. Here, we present data that strongly suggest that the transmembrane segment senses or relays an extracellular or intramembrane signal that regulates the activity of WalK. Moreover, in contrast to what was previously believed, we provide evidence suggesting that the serine/threonine protein kinase StkP upregulates PcsB expression by stimulating the kinase activity or inhibiting the phosphatase activity of WalK rather than by direct phosphorylation of the WalR response regulator.

S. pneumoniae is a leading cause of morbidity and mortality worldwide, especially in children, the elderly and in immunocompromised patients (Mehr and Wood, 2012). In most cases, pneumococcal infections lead to transient colonization of the upper respiratory tract, but for reasons not fully understood they occasionally give rise to local or invasive disease. Regardless of whether *S. pneumoniae* lives as a commensal in multispecies biofilms in the nasopharynx or causes disease, it must regulate its gene expression to adapt to the local environment within the human host. Two-component regulatory systems represent one of several mechanisms used by bacteria to regulate cellular functions in response to changing environments (for reviews see Jordan et al., 2008; Gao and Stock, 2009; Capra and Laub, 2012; Salazar and Laub, 2015). They sense specific environmental signals and respond by regulating the expression of the appropriate set of genes. Since most two-component systems are involved in niche adaptation, they are not required for growth

* Corresponding author: Leiv Sigve Håvarstein. Department of Chemistry, Biotechnology, and Food Science, Norwegian University of Life Sciences, P.O. Box 5003, NO-1432 Ås, Norway. Tlf: 47-67232493. Fax:47-64965901.E-mail: sigve.havarstein@nmbu.no

in the laboratory. In contrast, the WalRK (also called VicKR and YycGF) two-component regulatory system, which is highly conserved among low-GC Gram-positive bacteria, is essential (Lange et al., 1999; Throup et al., 2000). For this reason the WalRK system is attracting increasing attention as a possible new antibacterial drug target. It consists of the multi-domain transmembrane histidine kinase, WalK, and its cognate response regulator WalR. In addition, the *walRK* operon includes a gene, *walJ* (*yycJ*), of unknown function, which is predicted to encode a member of the metallo-β-lactamase superfamily (Dubrac et al., 2008). With the exception of *Streptococcus pyogenes* (Liu et al., 2006), WalR is essential in all species tested. WalK, on the other hand, has been shown to be dispensable in several streptococcal species, including *S. pneumoniae*. The growth rate and virulence of *walK* mutants, however, are significantly reduced (Wagner et al., 2002). The genes controlled by the WalRK system varies between species, but a common theme is that they all regulate expression of peptidoglycan hydrolases involved in bacterial growth and division (Dubrac and Msadek, 2004; Ng et al., 2005; Bisicchia et al., 2007; Dubrac et al., 2008; Delauné et al., 2012). In *S. pneumoniae* R6, depletion of WalR in a Δ*walK* background gives rise to cells with a grossly abnormal morphology (Ng et al., 2003). Ng and co-workers (2003) show that these changes in morphology are, at least in part, due to downregulation of *pcsB*, one of the genes positively regulated by the WalRK system. Recently, it was shown that PcsB is a murein hydrolase that splits the septal cross wall during pneumococcal cell division (Bartual et al., 2014). Hence, a major function of WalRK must be to control cross wall splitting during daughter cell separation by sensing and responding to specific extracellular and/or intracellular signals. Unfortunately, the nature and number of signals sensed by WalK is not known.

S. pneumoniae WalK consists of the following domains in order from its N-terminus: a small extracellular domain of about 12 amino acids, a transmembrane segment, a HAMP domain (commonly found in histidine kinases, adenylyl cyclases, methyl-accepting chemotaxis, and phosphatase proteins), a PAS domain (acronym for Per, Arnt, and Sim), a DHp domain (dimerization and histidine phosphorylation domain) and a CA domain (C-terminal catalytic and ATP-binding domain) (Dubrac et al., 2008; Wang et al., 2013). HAMP domains are found in many bacterial signaling molecules. They function as signal relay modules that convert input signals into an output response (Dunin-Horkawicz and Lupas, 2010; Parkinson, 2010; Stewart, 2014). PAS domains function as sensor domains that respond to signals such as alterations in light, redox potential, oxygen levels and various small molecules (Henry and Crosson, 2011). However, some PAS domains, seem to function solely in intramolecular signal conversion or amplification (Mascher, 2014). It is not known if the cytoplasmic PAS domain of pneumococcal WalK has a sensory role, but if it does, it must sense an intracellular signal. In addition to the cytoplasmic PAS domain, the WalK histidine kinase of most low-GC Gram-positive bacteria contains a large extracellular loop believed to function as a sensor domain (Ng and Winkler, 2004; Dubrac et al., 2008). This domain, which is predicted to adopt a PAS-like fold, consists of about 150 amino acids and is flanked by two transmembrane segments (Santelli et al., 2007). In contrast, the WalK kinases of streptococci are anchored to the cytoplasmic membrane via a single N-terminal transmembrane segment and lack the extracellular loop (Ng and Winkler, 2004; Dubrac et al., 2008). It has therefore been

proposed that streptococcal WalK kinases have lost the ability to sense external signals, and only respond to internal stimuli (Wagner et al., 2002). This would imply that the remaining transmembrane segment only serves to anchor WalK to the cytoplasmic membrane. Alternatively, it is possible that the transmembrane segment and/or the small remaining extracellular domain could still function as a signal sensing or signal transfer domain. To discriminate between these alternatives we introduced point mutations within or in the regions flanking the transmembrane segment, and constructed chimeras between pneumococcal WalK and the corresponding kinase from *Streptococcus thermophilus*. In sum, our results strongly indicate that the single transmembrane segment of streptococcal WalK kinases are not merely anchoring devices, but are required for the perception or transfer of intramembrane or extracellular signals. In addition, we obtained evidence suggesting that the serine/threonine protein kinase StkP does not phosphorlylate WalR directly as previously suggested (Sasková et al., 2007). Judging from our results, it is more likely that StkP activates WalR-dependent gene expression by influencing the kinase or phosphatase activity of WalK.

MATERIALS AND METHODS

Cultivation and transformation of* S. pneumoniae *R6. All transformations and experiments were carried out in C medium (Lacks and Hotchkiss, 1960) at 37ºC. When constructing mutant strains, DNA was introduced into the recipient strain by natural genetic transformation. Bacterial cultures were grown to an $OD_{550} = 0.05$ and induced to competence by adding 250 ng ml^{-1} CSP-1 peptide together with the transforming DNA (Håvarstein et al., 1995). After incubation at 37°C for 120 minutes transformants were selected on Todd-Hewitt agar containing kanamycin (400 µg ml^{-1}) or streptomycin (200 µg ml^{-1}). When required, PCR fragments used for transformation were "stitched" together by overlap extension PCR (Higuchi et al., 1988). Genes were inserted at specific sites in the pneumococcal chromosome by double-crossover homologous recombinantion. For this purpose ~ 1000 bp sequences corresponding to the upstream and downstream regions of the gene/fragment to be replaced were added to the 5' and 3' ends of the gene/fragment to be inserted. The counter selectable Janus cassette was used to make clean deletions of target genes or to replace one DNA fragment with another. Janus is a *kan-rpsL*$^{+}$ DNA cassette that confers resistance to kanamycin and dominant sensitivity to streptomycin in a streptomycin-resistant background (Sung et al., 2001). Thus, transformants in which the cassette has been inserted are selected for by kanamycin, while transformants in which the cassette has been deleted are selected for by streptomycin. To drive ectopic gene expression from the P_{comX} promoter, 0.2 µM of an inducer peptide called ComS (NH_2-LPYFAGCL-COOH) was added to the medium during transformation, selection of transformants and growth (Berg et al., 2011). Details regarding the construction of the various streptococcal mutant strains are described in the accompanying supplementary material. All strains and plasmids used in this study are listed in Table 1, while the sequences of all primers used are given in Table S1.

Luciferase reporter assays. All strains assayed for P_{pcsB}-driven luciferase (*luc*) reporter activity were grown in C medium to an $OD_{550} \sim 0.3$. Then the bacterial cultures were diluted to $OD_{550} = 0.05$ in the same medium and added to a 96-well Corning NBS clear-bottom plate. D-luciferin (Thermo Scientific) was added to the wells to a final concentration of 10 mM. The plate was incubated in a Synergy H1 Hybrid Reader (BioTek®) at 37ºC, and OD_{492} and luminescence were measured automatically every 5 min throughout the experiment.

SDS-PAGE and Western blotting. Cells were grown to an $OD_{550} = 0.3$ before they were collected at 4000 xg and lysed in SDS sample buffer. Proteins from whole cell extracts were

Table 1

Strains	Genotype/relevant features[1]	References
S. pneumoniae		
R704	R6 derivative, *comA::ermAM*; Ery^r	J. P. Claverys[2]
RH1	R704 but *ebg::spc*; Ery^r Spc^r	Johnsborg et al. (2008)
RH426	RH425 but ΔIS*1167*::Janus[3]; Ery^r Kan^r	Johnsborg and Håvarstein (2009)
SPH259	RH426 but replacement of Janus with P_1P_{comR}::*comR*; Ery^r Sm^r	This work
SPH260	SPH259 but replacement of *spr0324* with Janus; Ery^r Kan^r	This work
SPH261	SPH260 but replacement of Janus with P_{pcsB}::*luc*, Sm^r	This work
SPH262	SPH261 but Janus inserted between *cpsO* and *cpsN*; Ery^r Kan^r	This work
SPH263	SPH262 but replacement of Janus with P_{comX}::*walK*; Ery^r Sm^r	This work
SPH264	SPH263 but replacement of *walK* with Janus; Ery^r Kan^r	This work
SPH265	SPH261 but replacement of *walK* with Janus; Ery^r Kan^r	This work
Strains carrying point mutations in WalK		
SPH266	SPH264 but replacement of Janus with $walK^{T222A}$; Ery^r Sm^r	This work
SPH267	SPH266 but replacement of P_{comX}::*walK* with Janus; Ery^r Kan^r	This work
SPH268	SPH267 but deletion of Janus; Ery^r Sm^r	This work
SPH269	SPH264 but replacement of Janus with $walK^{E33A}$; Ery^r Sm^r	This work
SPH270	SPH269 but replacement of P_{comX}::*walK* with Janus; Ery^r Kan^r	This work
SPH271	SPH270 but deletion of Janus; Ery^r Sm^r	This work
SPH272	SPH264 but replacement of Janus with $walK^{E33A/\ N34A}$; Ery^r Sm^r	This work
SPH273	SPH272 but replacement of P_{comX}::*walK* with Janus; Ery^r Kan^r	This work
SPH274	SPH273 but deletion of Janus; Ery^r Sm^r	This work
SPH275	SPH264 but replacement of Janus with $walK^{F23A}$; Ery^r Sm^r	This work
SPH276	SPH275 but replacement of P_{comX}::*walK* with Janus; Ery^r Kan^r	This work
SPH277	SPH276 but deletion of Janus; Ery^r Sm^r	This work
SPH278	SPH264 but replacement of Janus with $walK^{G22A}$; Ery^r Sm^r	This work
SPH279	SPH278 but replacement of P_{comX}::*walK* with Janus; Ery^r Kan^r	This work
SPH280	SPH279 but deletion of Janus; Ery^r Sm^r	This work
SPH281	SPH264 but replacement of Janus with $walK^{R12A/\ D13A}$; Ery^r Sm^r	This work

SPH282	SPH281 but replacement of P_{comX}::*walK* with Janus; Ery^r Kan^r	This work
SPH283	SPH282 but deletion of Janus; Ery^r Sm^r	This work
SPH284	SPH264 but replacement of Janus with $walK^{R36A/D37A}$; Ery^r Sm^r	This work
SPH285	SPH284 but replacement of P_{comX}::*walK* with Janus; Ery^r Kan^r	This work
SPH286	SPH285 but deletion of Janus; Ery^r Sm^r	This work
SPH287	SPH264 but replacement of Janus with $walK^{R12A/\ D13A/R36A/\ D37A}$; Ery^r Sm^r	This work
SPH288	SPH287 but replacement of P_{comX}::*walK* with Janus; Ery^r Kan^r	This work
SPH289	SPH288 but deletion of Janus; Ery^r Sm^r	This work
SPH305	SPH264 but replacement of Janus with *walK* ΔTM; Ery^r Sm^r	This work
SPH306	SPH305 but replacement of P_{comX}::*walK* with Janus; Ery^r Kan^r	This work

Strains with WalK chimeric proteins

SPH290	SPH264 but replacement of Janus with *walK* encoding the extracellular region of *S. thermophilus walK*; Ery^r Sm^r	This work
SPH291	SPH290 but replacement of P_{comX}::*walK* with Janus; Ery^r Kan^r	This work
SPH292	SPH291 but deletion of Janus; Ery^r Sm^r	This work
SPH293	SPH264 but replacement of Janus with *walK* encoding the transmembrane region of *S. thermophilus walK*; Ery^r Sm^r	This work
SPH294	SPH293 but replacement of P_{comX}::*walK* with Janus; Ery^r Kan^r	This work
SPH295	SPH294 but deletion of Janus; Ery^r Sm^r	This work
SPH296	SPH264 but replacement of Janus with *walK* encoding the extracellular and transmembrane regions of *S. thermophilus walK*; Ery^r Sm^r	This work
SPH297	SPH296 but replacement of P_{comX}::*walK* with Janus; Ery^r Kan^r	This work
SPH298	SPH297 but deletion of Janus; Ery^r Sm^r	This work
SPH299	SPH264 but replacement of Janus with *walK* containing the HAMP-encoding part of *S. thermophilus walK*; Ery^r Sm^r	This work
SPH300	SPH299 but replacement of P_{comX}::*walK* with Janus; Ery^r Kan^r	This work
SPH301	SPH300 but deletion of Janus; Ery^r Sm^r	This work
SPH302	SPH264 but replacement of Janus with *walK* encoding the	This work

	extracellular + transmembrane + HAMP regions of *S. thermophilus walK*; Ery^r Sm^r	
SPH303	SPH302 but replacement of P_{comX}::*walK* with Janus; Ery^r Kan^r	This work
SPH304	SPH303 but deletion of Janus; Ery^r Sm^r	This work

Strains carrying StkP mutations

SPH307	SPH261 but replacement of *stkP* with Janus; Ery^r Kan^r	This work
SPH308	SPH307 but deletion of Janus; Ery^r Sm^r	This work
SPH309	SPH308 but replacement of *walK* with Janus; Ery^r Kan^r	This work
SPH310	SPH268 but replacement of *stkP* with Janus; Ery^r Kan^r	This work
SPH311	SPH261 but replacement of *pnpR* with Janus; Ery^r Kan^r	This work
SPH312	SPH311 but deletion of Janus; Ery^r Sm^r	This work
SPH313	SPH312 but replacement of *walK* with Janus; Ery^r Kan^r	This work
SPH314	SPH312 but replacement of *stkP* with Janus; Ery^r Kan^r	This work
SPH315	SPH314 but deletion of Janus; Ery^r Sm^r	This work
SPH316	SPH315 but replacement of *walK* with Janus; Ery^r Kan^r	This work
SPH317	SPH307 but replacement of Janus with *stkP*^{K42M}; Ery^r Sm^r	This work

Plasmid

pR424	ColE1 (pEVP3) derivative; Cm^r; contains the *luc* gene	Chastanet et al., (2001)

[1] Ery; erythromycin, Spc; spectinomycin, Kan; kanamycin, Sm; streptomycin

[2] Gift from Jean-Pierre Claverys

[3] Janus contains a *kan::rpsL*$^+$ cassette (Sung et al., 2001)

separated by SDS-PAGE using a 4 % stacking gel and a 12 % separation gel at 1.5 V/cm^2. The proteins were then transferred onto an Immuno-Blot™ PVDF Membrane (Bio-Rad) using a semi dry transfer cell system from Bio-Rad at 0.25 V/cm^2 for 60 minutes. Proteins containing phosphorylated threonine residues were detected by sequential incubations with the primary antibody Phospho-Threonine Antibody P-Thr-Polyclonal from Cell Signaling Technology® (1:1000 in TBS-T) and HRP conjugated anti-rabbit from Sigma (1:4000 in TBS-T) as secondary antibody. The immunoblot was developed using a 50:50 mixture of luminol and peroxide solution (Thermo Scientific) as substrate for the HRP. Chemiluminescence was visualized in a C400 imaging system from Azure biosystems.

RESULTS

Amino acid comparison of streptococcal WalK sequences. Alignment of the 120 N-terminal amino acids of WalK from 30 different streptococcal species uncovered three different patterns of conserved amino acids in the parts corresponding to the predicted transmembrane segments and their immediate flanking regions (groups I-III, Fig. 1). Comparison of group I - III sequences between positions 10 and 40 (see amino acid numbering in Fig. 1) shows that each of them contains several conserved amino acid positions that are group specific. Group I and II sequences, which share three conserved amino acid positions (Y26, F27 and R33) are more similar to each other than they are to the corresponding group III sequences. Group III sequences do not share any fully conserved positions with group I and II sequences, neither within the transmembrane segments nor in the regions bordering them. *S. pneumoniae* and other mitis-group streptococci belong to WalK group III. The group III transmembrane segments contain two conserved amino acid residues (F14 and F16) located close to the external face of the membrane, and two conserved residues (G22 and F23) situated in the middle of the transmembrane domain (Fig. 1). Furthermore, three fully conserved residues, E33, R36 and D37, are located at the interface between the membrane and the cytoplasm. In addition, the interfacial zone on the outside of the membrane often contains a negatively charged amino acid residue in position 13. The strong conservation of the above described amino acid residues in group III sequences suggests that they play an important functional role. Since the conserved residues are located within the transmembrane segment, and at the interface between membrane and the aqueous phase, it also suggests that the function of the transmembrane segment extends beyond that of a simple anchoring device. To test the functional importance of the conserved residues, we replaced several of them with alanine and compared the properties of the resulting mutant proteins with wild type WalK.

Alanine substitution mutagenesis of conserved amino acid residues in the transmembrane region of pneumococcal WalK. Since G22 and F23 are fully conserved in group III, and are predicted to be situated in the middle of the transmembrane segments, we hypothesized that these residues might be important for signal transfer through the transmembrane segment or for sensing a signal within the membrane. To test this hypothesis we constructed two strains, SPH277 and SPH280, carrying the $WalK^{F23A}$ and $WalK^{G22A}$ mutations, respectively. To avoid exposing the pneumococcal cells to a selection pressure when deleting the native *walK* gene, an ectopically expressed wild-type *walK* gene was inserted into a neutral region of the *S. pneumoniae* R6 genome under control of the inducible P_{comX} promoter (see Materials and Methods for details). Thus, during the two transformation steps required to replace the native *walK* gene with the mutated version, wild-type WalK was expressed ectopically from the P_{comX} promoter by growing the cells in the presence of the ComS inducer peptide (Fontaine et al., 2010; Berg et al., 2011). Following replacement of the native *walK* gene with the mutated counterpart, the ectopic *walK* gene was deleted. To be able to measure and compare the activity of wild-type WalK and the WalK mutants constructed in this study, a luciferase (*luc*) reporter gene under control of the *pcsB* promoter was inserted into the non-functional *spr0324* gene. Light emission and growth rate were monitored by growing the various mutant strains in 96-well plates at 37° C inside a microplate reader (BioTek Synergy H1 Hybrid Reader). The results presented in Fig. 2B show that the light emitted [relative

luminescence units (RLU)/ OD_{492}] by the strains tested increased the first 15-20 minutes after the experiment was started, and then leveled off to reach a maximal plateau. After 60-80 minutes at this maximal level, light emission started to fall while the pneumococcal cultures were still in their early exponential growth phase. When the cultures entered stationary phase, light emission had dropped close to the detection limit of the Synergy H1 luminometer. Comparison of the light emitted by the SPH277 and SPH280 strains with the parental wild-type strain SPH261, revealed that both $WalK^{F23A}$ and $WalK^{G22A}$ are considerable less active that wild-type WalK in stimulating transcription of the *pcsB* gene. When the Δ*walK* background activity is subtracted, the maximum reporter activity of the strains producing the $WalK^{F23A}$ and $WalK^{G22A}$ kinases are reduced by about 48% and 36%, respectively, compared to the wild type strain (Fig. 2). These results strongly indicate that the transmembrane segment is involved in signal sensing, and that the G22 and F23 residues are important for perceiving the signal or transducing it across the membrane.

Following the same procedure as outlined above, we also tested the effect of substituting the conserved amino acid residues immediately flanking the WalK transmembrane segment with alanine. The following substitutions were made: R12A/D13A, E33A, E33A/N34A, R36A/D37A and R12A/D13A/R36/A/D37A. As shown in Fig. 2, single and double substitutions of conserved residues on the cytoplasmic side (E33A, E33A/N34A and R36A/D37A) all caused significant reduction i light emission compared to wild-type. Substitution of the external semi-conserved R12 and D13 residues, on the other hand, had no significant effect. However, interestingly, a substantial increase in reporter activity relative to wild type was obtained with the mutant strain SPH289 in which both the external R12 and D13 residues and the internal R36 and D37 residues of WalK had been substituted by alanine. A comparison of reporter gene expression in strain SPH289 ($WalK^{R12A/D13A/R36/A/D37A}$) with strain SPH286 ($WalK^{R36/A/D37A}$), showed that the maximum level of light emission in the former is about 1.8-fold higher. In other words, the addition of the two external substitutions had a dramatic effect on WalK that either stimulated its kinase activity or reduced its phosphatase activity. This result suggests that introduction of the R12A/D13A substitutions in a R36A/D37A background, mimics sensing of an external or intramembrane signal.

Domain swapping between* S. pneumoniae *and* S. thermophilus *WalK proteins. The results from the alanine substitution study showed that the small extracellular domain and/or the transmembrane segment are involved in signal sensing. To attempt to determine which part is important for this function we decided to swap domains between the WalK proteins of *S. pneumoniae* and *S. thermophilus*. WalK from *S. thermophilus* was chosen for this purpose because the patterns of conserved amino acid positions in the transmembrane segments and flanking regions of group II (*S. thermophilus*) and III (*S. pneumoniae*) sequences are very different (Fig. 1). The only similarity between these groups is the conserved negatively charged amino acid at the interface between the membrane and extracellular solution. This is a fully conserved glutamate in the case of group II sequences, and a semi-conserved glutamate/aspartate in the case of group III sequences (Fig. 1). Hence, on account of the large differences in their primary structures, it is highly unlikely that the extracellular or transmembrane domain of *S. thermophilus* WalK will function

```
                          1        10        20        30        40        50
                          |         |         |         |         |         |
S. ferus                 --MTNFFSTTPFLLRLVFGGLLFLLFLYFIFLNYREYKNNKQIKAINKKVRSLIAGDYSD
S. macacae               --MTNIFESTPLLLRLLLASLIILLFLYFIFLNYREYKNTNQIKLLNTKVRSLITGEYTD
S. mutans                --MTNVFESSPLFLRILLAVLIILLFFYFIFLNYREYKNNNQVKQLNAKVRSLITGHYTD I
S. devriesei             --MTNTFDSSPLFLRILLAVLLILLFIYFVFLNYREYKNNNHIKLLNAKVRSLIAGDYTE
S. ratti                 --MTNTFESSPLFLRILLAVLLILLFIYFVFLNYREYKNNNHIKLLNAKVRSLIAGDYTE
S. sobrinus              MNNNPVVEN-LNTFELALLILLALVALYFIYQAVREYRNAKTIRAISQKVTSLIAGDYTE
S. thermophilus          --MTSIGLN-ITSFELALLFMLLFVAFYFIFLAYRDYQQVKNIRKLTKRVKSLMAGNYNE
S. salivarius            --MTSIGLN-ITSFELALLFTLLFVAFYFIFLAYRDYRQVKNIRKLTKRVKSLMAGNYNE
S. pyogenes              -MTRDIIGN-LSTFELAILILLVFVAFYFIHLAVRDYRNARIIRMMSHKIRDLINGRYTD
S. equi                  -MTKDIIGN-LSAFELAILLLLVFVAFYFIHLAIRDYRNARIIRLMSHKIRDLINGRYTD
S. iniae                 -MTKDIIGN-LSLFELAILSLLIFVAVYFVHLALRDYRNAKIIRQMSHKIRDLINGRYTD
S. uberis                -MTENLIGN-LSLFELSILLLLIFVAAYFIYLAVRDYRNAKIIRQMSHKIRDLINGRYTD II
S. agalactiae            --MNNSAAN-IRSFELALLFLLVFVAVYFVYLAVRDFKMSKNIRLLNWKVRDLIAGNYSD
S. caballi               --MNNIFAN-LRAFELALLCLLAFVAVYFVYLAFRDFRTSRNIKLLSNKVRELITGNYSD
S. infantarius           -MNDTIVQN-QYLFEQAILFLLAFVAIYFIHLAIRDYRTSVNIRRLSGKVRELITGKYTE
S. macedonicus           -MNDTMLQN-LTYFEQAILFLLAFVAVYFVYLAIREYQTSANIRRLSGKVRELITGKYTE
S. gallolyticus          -MNDTMLQN-LTYFEQAILFLLAFVAVYFVYLAIRDYRTSVNIRRLSGKVRELITGKYTE
S. pasteurianus          -MNDTMLQN-LTYFEQAILFLLAFVAVYFVYLAIRDYRTSVNIRRLSGKVRELITGKYTE
S. merionis              --MIEKLKLFIFSQGFVFTIIVIGFVAIIVFLLLENYKDNKQIKLLNKKVQELIHGDYSE
S. suis                  --MINQLRYLMTTAEFWFVVILIGFLIALTVLLIENYRDNKQIKQLNQKVNALIEGNYAD
S. ovis                  --MINQLRYLVTTTEFWFVAILVGFVVALSFMLIENYRDNKQIKILNQKVKELIAGDYSD
S. minor                 --MINQLRYLLTTAEFWFVIIIIGFVIALSFMVLENHRDSKQIKVLNQKVKDLIAGDYSD
S. pneumoniae            --MLDLLKQTIFTRDFIFILILLGFILVVTLLLLENRRDNIQLKQINQKVKDLIAGDYSK
S. infantis              --MINIIKQTILTRDFIFVLILIGFIMLVSFLLLEGRRDNIRLKQLNQKVKDLIAGDYSQ III
S. intermedius           --MIDNIRQFVVSKDFVFVLLILGFILVITLLSLENRRDNVRIRQLNQKVKDLIAGDYSE
S. gordonii              --MIENIRQFVFSVDFVFVLIVLGFILVVALLFLENRRDNRQLRLLNQKIKDLIAGDYSE
S. sanguinis             --MIEAIKQFVISADFVFAIIIIGFIVVVALLLLENRRDNQKLVQLNQKVKDLIAGDYSE
S. cristatus             --MIETLKEFVLSPDFVFSLIVVGFIIVVALLLLENRRDTQKLVQLNQKIKGLIAGDYSE
S. parasanguinis         --MIDQLKQFVMSSNFVFVLITVGFIIVVALLLLENRRDNIKLRQLNSKIKDLIAGDYSE
S. australis             --MINHIKEVMTSYNFVFILLTLGFIIVVALLILENRRDNMKLRLLNDKIKSLIAGEYSD
                                          :      .   .     .  :    :  :. ::  *: * * .

                         60        70        80        90        100       110
                          |         |         |         |         |         |
S. ferus                 KLDIKSNPELTDLVNNINDLSEVFRLTHENLAQETNRLTNVLTYMTDGVLATDRQGKIVL
S. macacae               KLEMKSNPELSDLVSNINDLSEVFRLTHENLEQEKNRLTSILSYMTDGVLATDRSGKITM
S. mutans                KLKVEDNSDLSELVNNVNDLSEVFRLTHENLAQEKNRLTSILSYMTDGVLATDRSGKITV I
S. devriesei             KLKIKANPELSELVRNVNDLSEVFRLTHENLAQEKNRLTSILAYMTDGVLATDRSGKITM
S. ratti                 KLKFKANPELSELVRNVNDLSEVFRLTHENLAQEKNRLTSILAYMTDGVLATDRSGKITM
S. sobrinus              DLHLKGDSELIELGTNLNDLSDVLHLTHENLSQERNRLASVLSYMSDGVLATNRVGKITM
S. thermophilus          KLCIKGDSELLELANSLNDLSDVFRLTHENLIQEKNRLSSVLSYMSDGVIATNRLGQITM
S. salivarius            ELRLKGDSELLELANSLNDLSDVFRLTHENLAQEKNRLSSVLSYMSDGVIATNRRGQITM
S. pyogenes              IIDEKADIELMELSDQLNDLSDVFRLTHENLAQEKNRLASILAYMSDGVLATDRSGKIIM
S. equi                  TINEKADIELMELSEQLNDLSDVFRLTHENLAQEKNRLASILAYMTDGVLATNRSGKIIM
S. iniae                 DINQKADIELMELSEQLNDLSDVFRLTHENLAQEKNRLASILAYMSDGVLATDRSGQILM
S. uberis                EINEKADIELIELSEQLNDLSDVFRLTHENLAQEKNRLASILAYMSDGVLATDRTGQIMM II
S. agalactiae            SILIQGDADLVELGESLNDLSDVFRMAHDNLEQEKNRLASILTYMTDGVLATDRSGKIVM
S. caballi               DITIQRDPDLAELAEHLNDLSKVFRLTHENLEQEKNRLASILAYMTDGVLATDRAGNITM
S. infantarius           DIIIEKDRDLAELAGQLNDLSTVFRLAQENLAQEKNRLASILSYMTDGVLATDRSGNITM
S. macedonicus           DIIIEKDRDLAELADQLNDLSKVFRLAQENLAQEKNRLASILSYMTDGVLATDRAGNIIM
S. gallolyticus          DIIIEKDRDLAELADQLNDLSTVFRLAQENLAQEKNRLASILSYMTDGVLATDRAGNITM
S. pasteurianus          DIIIEKDRDLAELADQLNDLSTVFRLAQENLAQEKNRLASILSYMTDGVLATDRAGNITM
S. merionis              VLDVLGSPEITDMTNNLNDLSEVIRLTQDSLEQEKNRLSSILTYMSDGVVATDRLGRIIL
S. suis                  VLDMRGSPEITDMANSLNDLSEVIRLTHDNLEQEKTRLTSILSYMSDGVIATDRIGRIIM
S. ovis                  ILDMRGSPEITDMTNSLNDLSEVIRLTHDSLEQEKTRLSSILAYMSDGVIATDRMGRIIM
S. minor                 VLDMRGSPEITDMTNSLNDLSEVIRLTHDSLEQEKTRLSSILSYMSDGVIATDRMGRVIM
S. pneumoniae            VLDMQGGSEITNITNNLNDLSEVIRLTQENLEQESKRLNSILFYMTDGVLATNRRGQIIM
S. infantis              VLDMQGNSEITNITNNLNDLSEVIRLTQENLEQESKRLHSILSYMTDGVLATNRRGQITM III
S. intermedius           VLDMQGGPEITDITNSINDLSEVIRLTHENLEQETKRLSSILSYMTDGVLATNRRGQIIM
S. gordonii              VLDMQGSPEITDMTNSINDLSEVTRLTQENLEQETKRLTSILSYMTDGVLATNRRGQIIM
S. sanguinis             VLDMQGSPEITDMTNSINDLSEVIRLTHENLEQETKRLSSILSYMTDGVLATNRRGQIIT
S. cristatus             VLDMQGSPEITDMTNSINDLSEVIRLTHENLEQETKRLSSILSYMTDGVLATNRRGQIIT
S. parasanguinis         VVDMQGSPELTDMTNSINDLSEVIRLTHENLEQETKRLTSILSYMTDGVLATNRRGQIIM
S. australis             IIDLQGGPELTEISNNINDLSEVIRLTHENLEQETKRLTSILSYMTDGVLATNRRGQIIL
                          :      :: ::   :**** * ::::::.* ** .** .:* **:***:**:* *.:
```

Fig. 1. Alignment of the 120 N-terminal amino acid residues of WalK from 30 different species in the genus *Streptococcus*. The shaded area represents transmembrane regions predicted using the SPOCTOPUS algorithm

(Viklund et al., 2008). Members of groups I-III possess different patterns of conserved amino acids in the part of their sequences corresponding to the predicted transmembrane segments and their immediate flanking regions.

normally when replacing the corresponding parts of pneumococcal WalK. Five different WalK chimeras were constructed and tested (Fig. 3A). In addition to the the extracellular and transmembrane domains, we also constructed chimeras involving the HAMP domains. The HAMP domain lies near the cytoplasmic side of the membrane, and is presumably part of the membrane associated sensory unit. By analogy with similar systems, it probably relays the sensory input perceived by the extracellular and/or transmembrane domain to the C-terminal catalytic domain (Parkinson, 2010). The results presented in Fig. 3C clearly show that all mutant strains carrying chimeras containing the transmembrane segment from *S. thermophilus* WalK have reduced reporter gene expression compared to the wild type strain. In contrast, replacement of the extracellular domain of pneumococcal WalK with the corresponding domain from *S. thermophilus* WalK did not significantly alter its properties (Fig. 3C). These results strongly indicate that the transmembrane segment constitutes the key component of the membrane-associated input domain, while the extracellular domain has no signal-sensing function. It is possible, however, that the transmembrane segment from *S. thermophilus* functions poorly or differently when fused to the HAMP domain of pneumococcal WalK. This could in principle explain the reduced light emission observed with the SPH295 and SPH298 strains (Fig. 3C). To clarify this question, we tested the effect of replacing the HAMP domain of pneumococcal WalK with the corresponding domain from *S. thermophilus*. The properties of this chimeric WalK protein was indentical to wild type (see strain SPH301, Fig. 3C), demonstrating that the two HAMP domains are interchangeable. In conclusion, the results from the alanine substitution and domain swapping experiments clearly show that the transmembrane segment of WalK senses or relays a signal that regulates the activity of the WalK kinase.

Evidence that WalR is not directly phosphorylated by StkP. The eukaryotic-type serine/threonine protein kinase StkP is a global regulator of gene expression in *S. pneumoniae* (Sasková et al., 2007). Deletion of the *stkP* gene affects competence development, stress management, autolysis and virulence (Echenique et al., 2004; Sasková et al., 2007). Recently, analyses of the function of StkP have shown that it plays an important role in pneumococcal cell division (Beilharz et al., 2012; Fleurie et al., 2012). While wild type pneumococci grow in short chains consisting of 2-5 cells, *stkP* mutants form significantly longer chains. Furthermore, they have unsplit cross walls and a more spherical cell shape (Fleurie et al., 2012). Most likely, the altered morphology observed in pneumococci lacking the *stkP* gene is, at least in part, caused by reduced levels of the cross wall splitting murein hydrolase PcsB. Similar to the WalRK system, StkP regulates the expression of PcsB and two LysM domain-containing proteins believed to be involved in pneumococcal cell wall metabolism. In a *stkP* mutant, expression of the genes encoding these proteins are reduced 5-10 fold (Sasková et al., 2007). In accordance with previous studies, we found that deletion of the *stkP* gene strongly reduces PcsB expression in *S. pneumoniae*. In fact, if the basal reporter activity observed in a Δ*walK* mutant is subtracted, the activity in the *stkP* mutant is reduced by 50% relative to wild

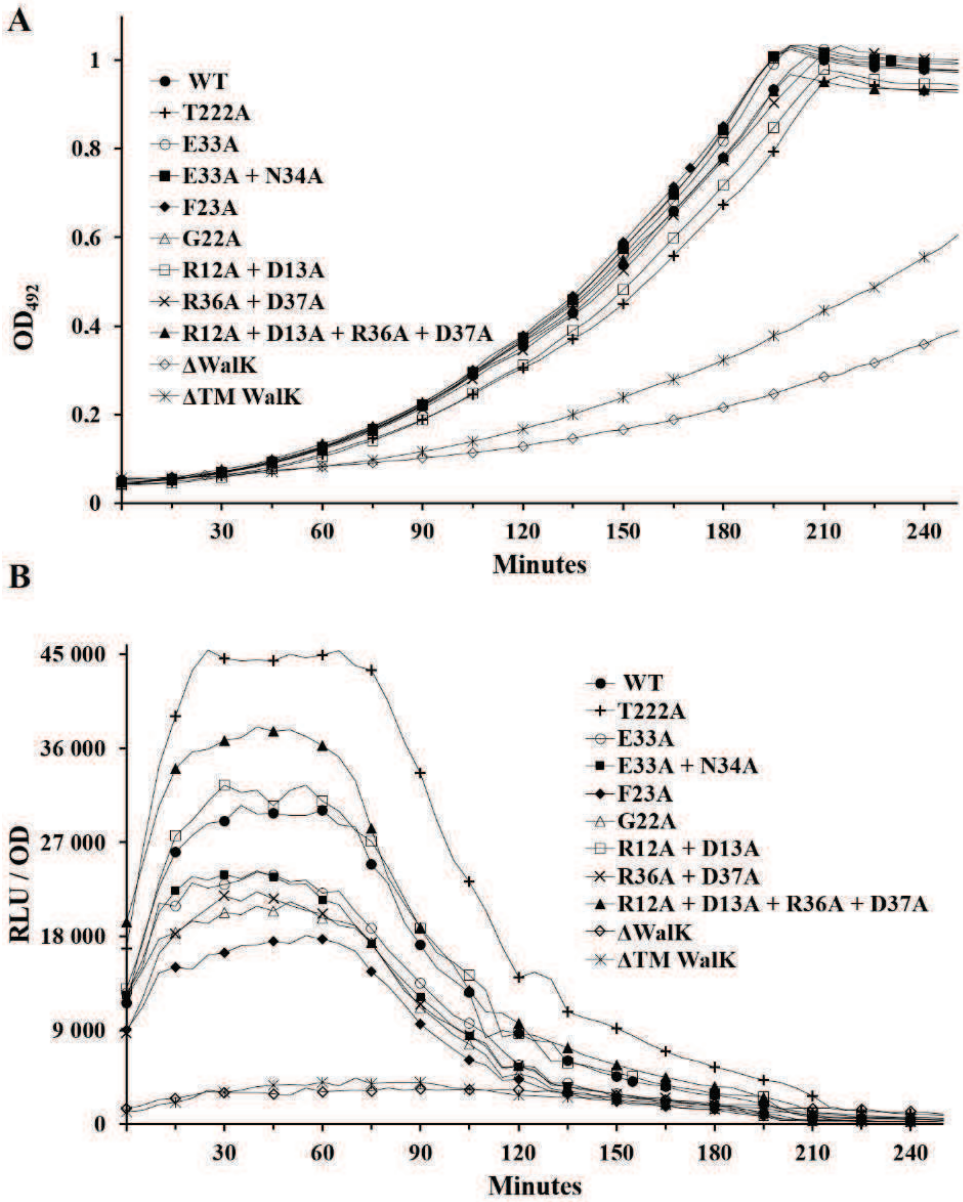

Fig. 2. Growth rate **(A)** and PcsB expression **(B)** in various WalK mutant strains. To monitor PcsB expression, a firefly luciferase gene (*luc*) driven by a P_{pcsB} promotor was inserted into a neutral site in the chromosome of all strains investigated. Light emission was measured automatically by growing the bacteria in 96-well microplates inside a luminometer. WT, wild type strain; ΔWalK, strain lacking the *walK* gene; ΔTMWalK, strain expressing a WalK protein lacking the transmembrane and extracellular part. The other strains tested are named according to the amino acid substitutions introduced in their WalK proteins. The numbering used is the same as in Fig. 1. The experiment was repeated three times with highly similar results.

type (Fig. 4). It has been speculated in the literature that StkP stimulates PcsB expression by direct phosphorylation of WalR (Sasková et al., 2007). Experimental evidence supporting this hypothesis has been reported by Agarwal and co-workers (2011). They studied the orthologous WalRK system of *Streptococcus pyogenes,* and showed that StkP phosphorylates WalR *in vitro* at a threonine residue (Agarwal et al., 2011). In *S.*

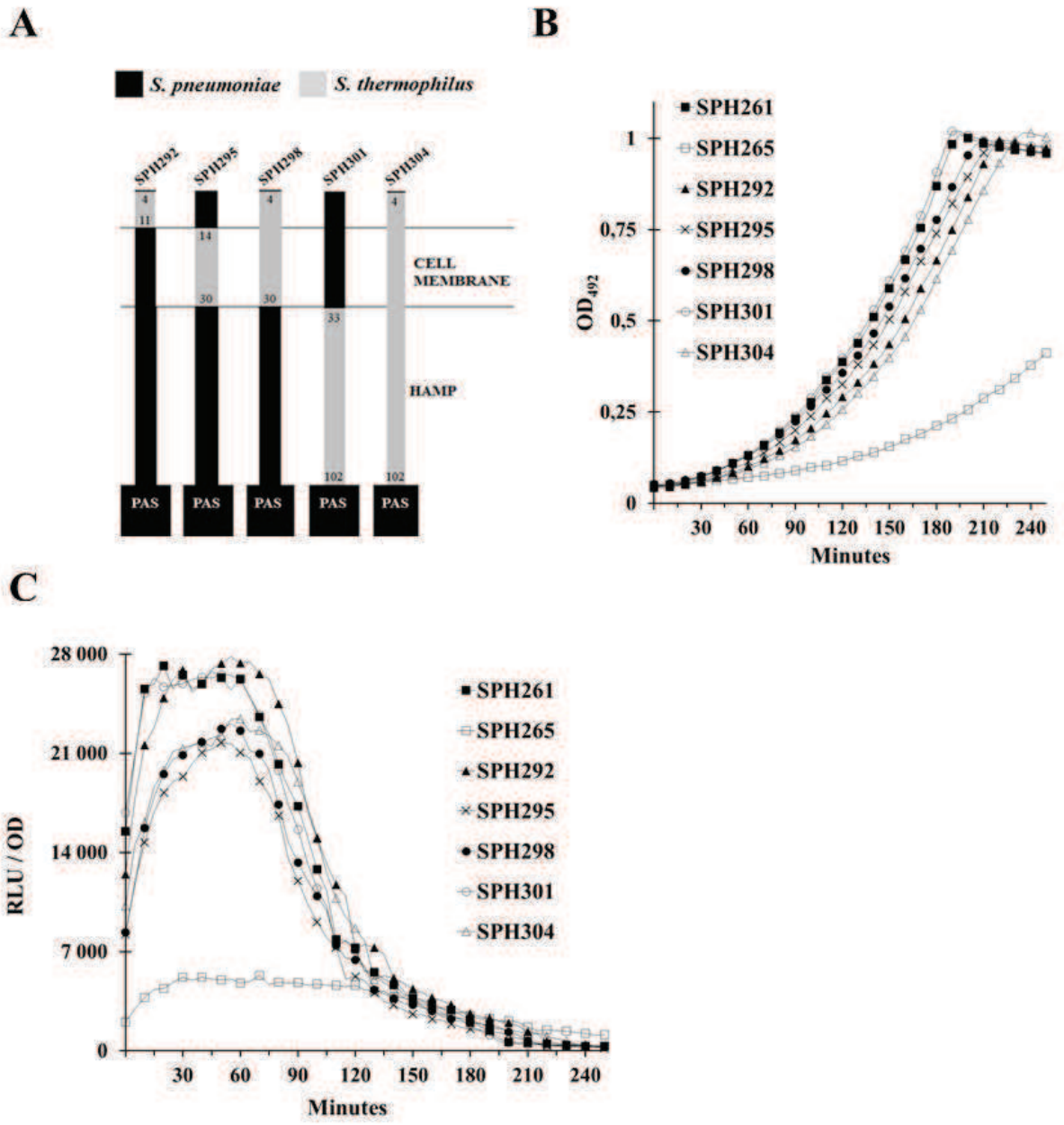

Fig. 3. Analysis of different WalK chimeras for their ability to activate transcription from the *pcsB* promoter. (**A**) Schematic representation of the different WalK chimeras investigated. Amino acid positions at the junctions of the swapped domains are indicated. The amino acid numbering used is the same as in Fig. 1. (**B**) Growth rate and (**C**) P_{pcsB}-driven *luc* reporter activity of chimeras and control strains. The chimeras were constructed by exchanging the extracellular, transmembrane and HAMP domains in pneumococcal WalK with the corresponding domains in *S. thermophilus* WalK. SPH261, wild type strain; SPH265, Δ*walK* mutant; SPH292, WalK with extracellular domain from *S. thermophilus*; SPH295, WalK with transmembrane domain from *S. thermophilus*; SPH298, WalK with extracellular and transmembrane domains from *S. thermophilus*; SPH301, WalK with HAMP domain from *S. thermophilus*; SPH304, WalK with extracellular, transmembrane and HAMP domains from *S. thermophilus.* The experiment was repeated three times with highly similar results.

pneumoniae it has been demonstrated that StkP phosphorylates the response regulators RR06 and RitR. RR06 is part of a two-component system (RR06/HK06) regulating expression of the pneumococcal surface adhesin CbpA, while the orphan response regulator RitR is a repressor of iron transport (Agarwal et al., 2012; Ulijasz et al., 2009). Based on these results we considered it likely that StkP modulates PcsB expression in *S. pneumoniae* by the same mechanism, i.e. by phosporylating WalR. To gain further insight into these matters, we deleted the *stkP* gene in a Δ*walK* strain (SPH309) and compared it to the parental strain (SPH261). The *walK* single and *walK/stkP* double mutants displayed the same low level of reporter activity (Fig. 4). If StkP stimulates PcsB expression through direct phosphorylation of WalR, a lower reporter activity would have been expected in the *stkP/walK* double mutant. Similarly, we deleted the *stkP* gene in a strain carrying the $walK^{T222A}$ mutation. This mutation does not affect the kinase activity of WalK, but abolishes or greatly reduces its phosphatase activity (Wayne et al., 2012). Consequently, reporter gene expression is very high in the $walK^{T222A}$ mutant. Our results showed that the amount of light emitted by cultures of the $stkP/walK^{T222A}$ double mutant (SPH310) and the $walK^{T222A}$ single mutant (SPH268) is the same (Fig. 4). The fact that deletion of the *stkP* gene in the $walK^{T222A}$ strain does not reduce reporter activity was unexpected as it does not seem to be in accordance with the idea that StkP stimulates PcsB expression by phosphorylating WalR.

In a recent study of the pneumococcal WalRK system, Wayne et al. (2012) used Western-blots of Phos-tag gels to show that the histidine kinase PnpS (HK04) cross-phosphorylates WalR only when its cognate response regulator PnpR (RR04) and WalK have been deleted. Using our reporter gene assay, we observed a strong increase in light emission when deleting the *pnpR* gene in a *walK* mutant, confirming the result of Wayne and co-workers (Fig. 4). Light emission increased to nearly wild type levels and the growth rate was also greatly improved in the *walK/pnpR* double mutant relative to the *walK* single mutant. To determine whether StkP-mediated phosphorylation of WalR contributes to reporter gene expression in the *walK/pnpR* double mutant (SPH313), we deleted the *stkP* gene in this strain. No change in light emission was observed in the *walK/pnpR/stkP* triple-mutant relative to the parental strain. In sum, our results suggest that StkP does not directly phosphorylate WalR. They also suggest that the observed stimulatory effect of StkP on PcsB expression depends on the presence of wild type WalK.

StkP-mediated stimulation of PcsB expression only partly depends on its kinase activity. Based on the data described in the above paragraph we speculated that StkP might stimulate PcsB expression indirectly by stimulating the kinase activity of WalK. If this was the case, the stimulatory effect of StkP might not depend on its kinase activity. Instead it could result from a direct interaction between StkP and WalK that stimulates the kinase activity of the latter. To investigate this possibility, we constructed a mutant strain in which the kinase activity of StkP was inactivated by substituting the invariant catalytic lysine residue (K42) with methionine (Fleurie et al., 2012). The reporter activity observed with this strain (SPH317) was partly reduced compared to the wild type parental strain (SPH261), but much higher than observed with the Δ*stkP* strain (Fig. 5A). Hence, deletion of StkP has a much stronger negative effect on PcsB-expression than inactivation of its kinase activity. To verify that the mutant expressing the $StkP^{K42M}$ protein has no kinase activity, immunoblotting with a phosphothreonine-specific antibody was performed with whole cell extracts from the SPH317 ($StkP^{K42M}$),

SPH307 (ΔStkP) and SPH261 (WT) strains. The results clearly show that the StkP^{K42M} mutant protein is inactive with respect to its kinase activity (Fig. 5B). Taken together, these findings indicate that the presence of the StkP protein has, in itself, a stimulatory effect on PcsB expression.

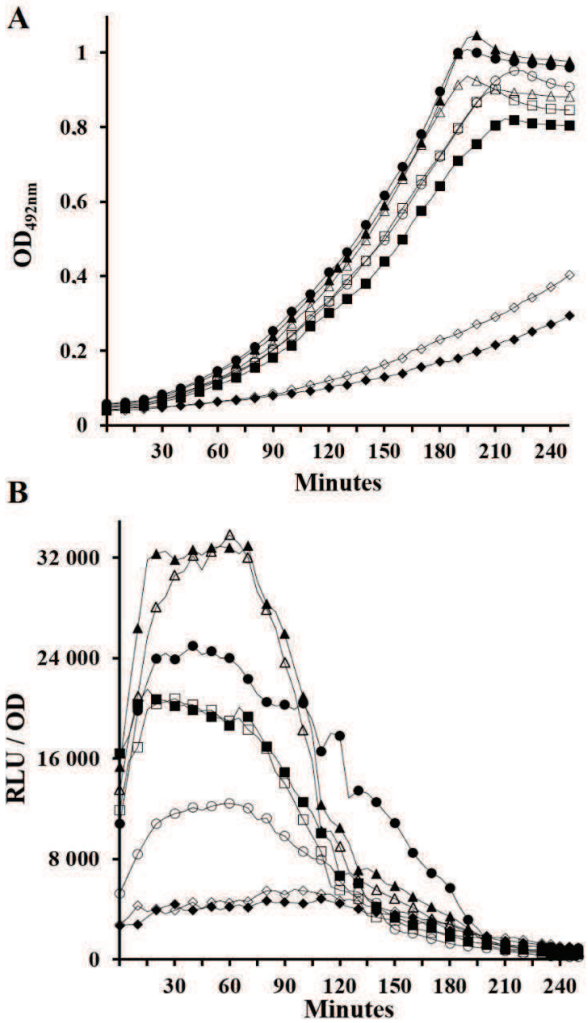

Fig. 4. The positive effect of StkP on PcsB expression seems to require the presence of wild-type WalK. **(A)** Growth rate, and **(B)** luciferase light emission representing transcription from the *pcsB* promoter in the strains investigated. (●), wild type; (○), Δ*stkP*; (♦), Δ*walK*; (◊), Δ*stkP* Δ*walK*; (▲), *walK*^{T222A}; (Δ), *walK*^{T222A} Δ*stkP*; (■), Δ*walK* Δ*pnpR*; (□),Δ*walK* Δ*pnpR* Δ*stkP*. The experiment was repeated three times with highly similar results.

DISCUSSION

WalK belongs to the HisKA subfamily of histidine kinases. Members of this subfamily are bifunctional, i.e. they are able to phosphorylate as well as dephosphorylate their cognate response regulators (Gutu et al., 2010; Huynh et al., 2010; Huynh and Stewart, 2011). Recently, the bifunctionality of WalK was confirmed by experimental data (Wayne et al., 2012). In the present work we have studied the activity of various WalK mutants by using a reporter gene assay to measure the rate of transcription from the *pcsB* promoter. As the assay measures WalK activity indirectly, it cannot discriminate between changes in kinase versus phosphatase activity. However, the assay makes it possible to automatically measure whether the introduced mutations increases or decreases the ability of WalK to activate expression of its target genes. Thus, it is well suited to answer our main quesition: Does the degenerated membrane associated domain of pneumococcal WalK have a signal-sensing function or is it merely an anchoring device? The finding that the G22A and F23A mutations, which were introduced in the middle of the WalK transmembrane segment, both have a large impact on reporter gene expression, strongly indicates that this segment is involved in signal sensing. It might be argued that the introduction of these mutations prevents or negatively affects attachment of WalK to the cytoplasmic membrane. This is unlikely, however, as the substitutions are conservative. Alanine is commonly found in the membrane-spanning regions of transmembrane proteins, and consequently should not affect correct membrane insertion of the WalK transmembrane segment. Besides, our results show that reporter gene expression in a strain producing an anchor-less version of WalK is much lower than in the strains producing WalK^{G22A} and WalK^{F23A}. In fact, it is at the

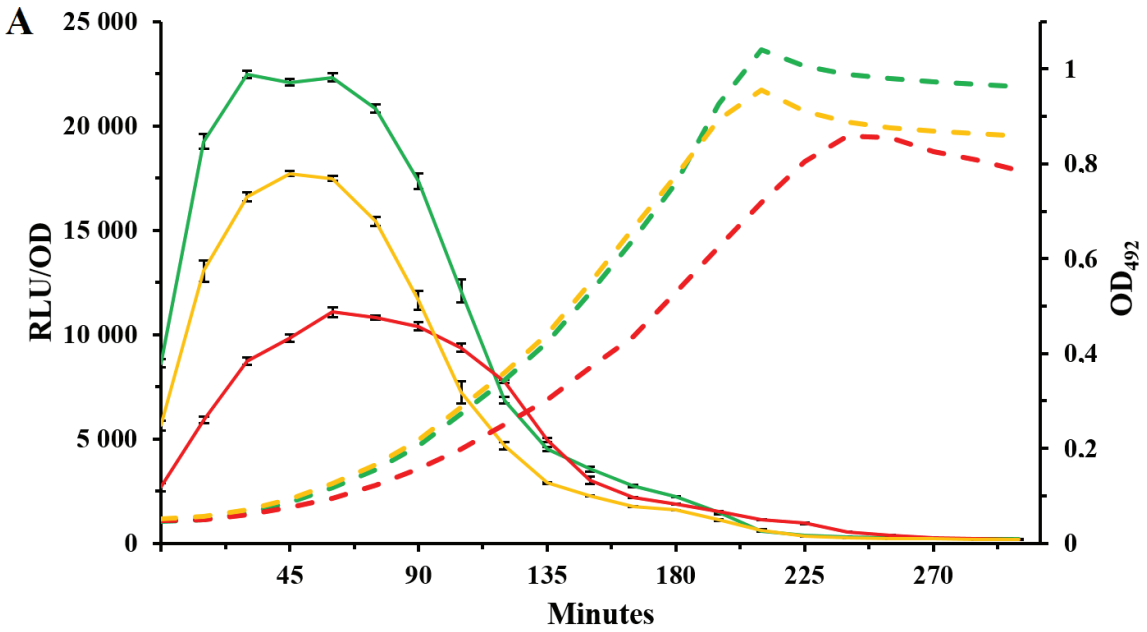

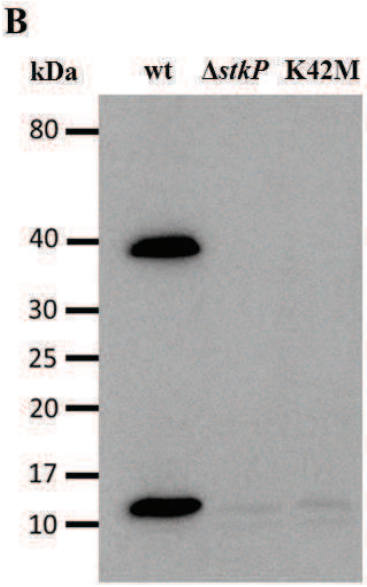

Fig. 5. The presence of kinase-inactive StkP has a strong positive effect on PcsB expression. Panel **A:** Growth kinetics (stippled lines) and P_{pcsB}-driven *luc* reporter activity (solid lines) in the strains investigated. Green lines, wild type; red lines, Δ*stkP*; yellow lines, $stkP^{K42M}$. Mean estimates (n = 4) together with their standard errors are shown. Panel **B:** Immunoblot detection of *in vivo* phosphorylated proteins in wild type, Δ*stkP* and $stkP^{K42M}$ strains using a phosphothreonine-specific antibody. Phosphorylation of proteins on threonine is StkP dependent in *S. pneumoniae* (Nováková et al., 2010)

same level as in a Δ*walK* mutant (Fig. 2). Thus, our results strongly indicate that the transmembrane segments of the $WalK^{G22A}$ and $WalK^{F23A}$ are inserted normally into the cytoplasmic membrane, and that the reduced activity of these mutant proteins is due to impared sensing of an extracellular or intramembrane signal. Further evidence that the transmembrane segment is involved in signal-sensing was obtained by introducing substitutions on either side of the transmembrane segment, and by constructing various WalK chimeras (Figs. 2 and 3). The finding that reporter gene expression in strain

SPH289 (WalK$^{R12A/D13A/R36A/D37A}$) is about 1.8 times higher than in strain SPH286 (WalK$^{R36A/D37A}$), is hard to explain unless it is assumed that the membrane-associated part of WalK perceives a signal that is relayed to the DHp and CA domains.

In principle, the transmembrane domain of WalK might function in two different ways. Either it could sense the primary signal itself, or it could relay a signal sensed by another protein. In case of the former, it might sense a physico-chemical parameter of the membrane, such as membrane composition, membrane tension or membrane curvature, or, alternatively, the presence of another membrane protein. Mohedano and co-workers (2005) reported that overexpression of WalR in *S. pneumoniae* resulted in a change in the ratio of C_{18}/C_{16} fatty acids, suggesting that the WalKR system regulates the fatty acid composition of the cytoplasmic membrane. Further evidence for this hyphothesis comes from the work of Ng et al. (2005). They showed that the defective growth of a Δ*walR* mutant, which expressed PcsB from an ectopic promoter in order to be viable, can be reversed by addition of linoleic or oleic acid to the growth medium. However, the expression of fatty acid biosynthetic genes in this mutant was not significantly affected, ruling out direct regulation of fatty acid biosynthesis by WalR (Ng et al., 2005). Using the same procedure as Ng et al. (2005), we added different concentrations of linoleic or oleic acid to the growth medium of the WalK^{wt} and WalK^{F23A} strains to determine whether this would alter the P_{pcsB}-driven transcription of the luciferase reporter gene. No effect was observed, suggesting that WalK does not directly sense the fatty acid composition of the cytoplasmic membrane (data not shown).

In our view, it is more likely that the transmembrane domain of WalK senses the presence of another membrane-spanning protein. In *Bacillus subtilis*, this has been shown to be the case (Szurmant et al., 2008). YycG, the ortholog of WalK in *B. subtilis*, is anchored to the cytoplasmic membrane by two transmembrane segments separated by an extracytoplasmic domain predicted to adopt a PAS-like fold (Santelli et al., 2007). Two proteins,YycH and YycI, which are co-transcribed with YycG, have been shown to regulate the activity of the kinase (Szurmant et al., 2007). YycH and YycI are localized outside the plasma membrane, but are attached to the membrane by N-terminal transmembrane sequences. Interestingly, truncation studies of YycH and YycI showed that the presence of their transmembrane segments is sufficient to alter the activity of YycG (Szurmant et al., 2008). This strongly indicates that the putative signal(s) sensed by YycH and YycI is transferred to YycG through the interaction of their transmembrane segments. No homologs of YycH and YycI are encoded in the pneumococcal genome. However, it is possible that a signal perceived by an unknown membrane-anchored extracytoplasmic protein could be relayed to WalK via alterations in the interactions of their transmembrane segments.

As stated in the result section, we found that deletion of the *stkP* gene in a wild-type genetic background reduces the luciferase activity, i.e. transcription from the *pcsB* promoter, by about 50%. This shows that the presence of StkP has a stimulatory effect on PcsB expression under the growth conditions used in the current study. It would therefore have been expected that deletion of the *stkP* gene in the Δ*walK* and *walK*^{T222A} genetic backgrounds would have reduced the luciferase activity as well. This was not observed. The T222A mutation changes the properties of WalK by apparently locking it permanently into the kinase mode. Hence, WalK^{T222A} might drive expression from the PcsB promoter at maximum rate regardless of

whether StkP is present or not. This may explain why we did not see a reduction in reporter activity when *stkP* is deleted in a *walK*^{T222A} background. In contrast, reporter gene activity in the *walK* mutant is low, but still well above the detection limit of the assay. Thus, if it is assumed that StkP stimulates PcsB expression by phosphorylating WalR, deletion of the *stkP* gene in a *walK* mutant should further reduce light emission by the luciferase reporter. The same logic holds true for the experiment that involves the PnpRS system. If StkP phosphorylates WalR, deletion of *stkP* in the *walK*/*pnpR* double mutant should have reduced the reporter activity relative to the parental strain.

The finding that StkP only reduces PcsB expression when deleted in a wild-type (*walK*$^{+}$) genetic background, led us to speculate that StkP acts through WalK rather than WalR. In principle StkP could stimulate the kinase activity of WalK through direct physical interaction with one of its sensory domains. To explore this possibility we substituted a catalytic lysine residue in StkP with a methionine, resulting in an inactive kinase (Fig. 5B). The reporter activity measured in cultures of the StkP^{K42M} mutant strain was somewhat lower than in the wild-type parental strain, but much higher than in the Δ*stkP* mutant (Fig. 5A). This result complicates the overall picture, as it shows that StkP stimulates PcsB expression by to different mechanisms. Additional evidence that the kinase-inactive StkP protein plays a significant biological role comes from other interesting traits specific for the StkP^{K42M} mutant. Whereas the growth rate of a Δ*stkP* strain is clearly retarded, it is virtually identical to wild-type in the StkP^{K42M} strain (Fig. 5A). Futhermore, Fleurie et al. (2012) have shown that cells of the ΔStkP and StkP^{K42M} strains have very different morphologies. The former grows in chains made of spherical cells, while the latter forms elongated and unchained cells. Only a few targets of StkP phosphorylation have been identified (Nováková et al., 2010). Two of them, DivIVA and MapZ (also called LocZ), are known to be involved in cell division in *S. pneumoniae* (Fleurie et al., 2014; Holecková et al., 2015). Hence, it is possible that StkP stimulates PcsB expression by phosphorylating one or both of these proteins. This question should be addressed in future studies. The stimulatory effect of StkP that is independent of its kinase activity, presumably involves protein-protein interactions with other proteins. As mentioned above, it is conceivable that WalK could detect the presence of StkP trough its transmembrane or cytoplasmic sensory domains. This interaction could either stimulate the kinase activity of WalK or inhibit its phosphatase activity resulting in increased phosphorylation of WalR. If this supposition is correct, StkP would represent the first known signal sensed by WalK. It is also possible that StkP is part of a larger protein complex which does not form properly in the absence of StkP. This could influence PcsB expression indirectly. Further studies are required to elucidate these matters.

ACKNOWLEDGEMENTS

This work was supported by The Research Council of Norway.

REFERENCES

Agarwal, S., Agarwal, S., Pancholi, P., and Pancholi, V. (2011) Role of serine/threonine phosphatase (SP-STP) in *Streptococcus pyogenes* physiology and virulence. *J Biol Chem* **286:** 41368-41380.

Agarwal, S., Agarwal, S., Pancholi, P., and Pancholi, V. (2012) Strain-specific regulatory role of eukaryote-like serine/threonine phosphatase in pneumococcal adherence. *Infect Immun* **80:** 1361-1372.

Bartual, S. G., Straume, D., Stamsås, G. A., Muñoz, I. G., Alfonso, C., Martínez-Ripoll, M., Håvarstein, L. S., and Hermoso, J. A. Structural basis of PcsB-mediated cell separation in *Streptococcus pneumoniae*. *Nature Commun* **5:** 3842

Beilharz, K., Nováková, L., Fadda, D., Branny, P., Massidda, O., and Veening, J. W. (2012) Control of cell division in *Streptococcus pneumoniae* by the conserved Ser/Thr protein kinase StkP. *Proc Natl Acad Sci USA* **109:** E905-E913.

Berg, K. H., Biørnstad, T. J., Straume, D., and Håvarstein, L. S. (2011) Peptide-regulated gene depletion system developed for use in *Streptococcus pneumoniae. J Bacteriol* **193:** 5207-5215.

Bisicchia, P., Noone, D., Lioliou, E., Howell, A., Quigley, S., Jensen, T., Jarmer, H., and Devine, K. M. (2007) The essential YycFG two-component system controls cell wall metabolism in *Bacillus subtilis*. *Mol Microbiol* **65:** 180-200.

Capra, E. J., and Laub, M. T. (2012) Evolution of two-component signal transduction systems. *Annu Rev Microbiol* **66:** 325-347.

Chastanet, A., Prudhomme, M., Claverys, J. P., and Msadek, T. (2001) Regulation of *Streptococcus pneumoniae clp* genes and their role in competence development and stress survival. *J Bacteriol* **183:** 7295-7307.

Delauné, A., Dubrac, S., Blanchet, C., Poupel, O., Mäder, U., Hiron, A., Leduc, A., Fitting, C., Nicolas, P., Cavaillon, J. M., Adib-Conquy, M., and Msadek, T. (2012) The WalKR system controls major staphylococcal virulence genes and is involved in triggering the host inflammatory response. *Infect Immun* **80:** 3438-3453.

Dubrac, S., and Msadek, T. (2004) Identification of genes controlled by the essential YycG/YycF two-component system of *Staphylococcus aureus*. *J Bacteriol* **186:** 1175-1181.

Dubrac, S., Bisicchia, P., Devine, K. M., and Msadek, T. (2008) A matter of life and death: cell wall homeostasis and the WalKR (YycGF) essential signal transduction pathway. *Mol Microbiol* **70:** 1307-1322.

Dunin-Horkawicz, S., and Lupas, A. N. (2010) Comprehensive analysis of HAMP domains: Implications for transmembrane signal transduction. *J Mol Biol* **397:** 1156-1174.

Echenique, J., Kadioglu, A., Romao, S., Andrew, P. W., and Trombe, M. C. (2004) Protein serine/threonine kinase StkP positively controls virulence and competence in *Streptococcus pneumoniae*. *Infect Immun* **72:** 2434-2437.

Fleurie, A., Cluzel, C., Guiral, S., Freton, C., Galisson F., Zanella-Cleon, I., Di Guilmi, A. M., and Grangeasse, C. (2012) Mutational dissection of the S/T-kinase StkP reveals crucial roles in cell division of *Streptococcus pneumoniae*. *Mol Microbiol* **83:** 746-758.

Fleurie, A., Lesterlin, C., Manuse, S., Zhao, C., Cluzel, C., Lavergne J. P., Franz-Wachtel, M., Macek, B., Combet, C., Kuru, E., VanNieuwenhze, M. S., Brun, Y. V., Sherratt, D., and Grangeasse, C. (2014) MapZ marks the division sites and positions FtsZ rings in *Streptococcus pneumoniae*. *Nature* **516:** 259-262.

Fontaine, L., Boutry, C., de Frahan, M. H., Delplace, B., Fremaux, C., Horvath, P., Boyaval, P.,and Hols, P. **(**2010) A novel pheromone quorum-sensing system controls the development of natural competence in *Streptococcus thermophilus* and *Streptococcus salivarius. J Bacteriol* **192:**1444-1454.

Gao, R., and Stock, A. M. (2009) Biological insights from structures of two-component proteins. *Annu Rev Microbiol* **63:** 133-154.

Gutu, A. D., Wayne, K. J., Sham, L. T., and Winkler M. E. (2010) Kinetic characterization of the WalRK$_{Spn}$ (VicRK) two-component system of *Streptococcus pneumoniae*: Dependence of WalK$_{Spn}$ (VicK) phosphatase activity on its PAS domain. *J Bacteriol* **192:** 2346-2358.

Henry, J. T., and Crosson, S. (2011) Ligand binding PAS domains in a genomic, cellular, and structural context. *Annu Rev Microbiol* **65:** 261-286.

Higuchi, R., Krummel, B., and Saiki, R. K. (1988) A general method of *in vitro* preparation and specific mutagenesis of DNA fragments: study of protein and DNA interactions. *Nucleic Acids Res* **16:** 7351-7367.

Holecková, N., Doubravová, L., Massidda, O., Molle, V., Buriánková, K., Benada, O., Kofronová, O., Ulrych, A., and Branny, P. (2015) LocZ is a new cell division protein involved in proper septum placement in *Streptococcus pneumoniae*. *mBio* **6:** e01700-14.

Huynh, T. N., Noriega, C. E., and Stewart, V. (2010) Conserved mechanism for sensor phosphatase control of two-component signaling revealed in the nitrate sensor NarX. *Proc Natl Acad Sci USA* **107:** 21140-21145.

Huynh, T. N., and Stewart, V. (2011) Negative control in two-component signal transduction by transmitter phosphatase activity. *Mol Microbiol* **82:** 275-286.

Håvarstein, L. S., Coomaraswami, G., and Morrison D. A. (1995) An unmodified heptadekapeptide pheromone induces competence for genetic transformation in *Streptococcus pneumoniae*. *Proc Natl Acad Sci USA* **92:**11140-11144.

Johnsborg, O., Eldholm, V., Bjørnstad, M. L., and Håvarstein, L. S. (2008) A predatory mechanism dramatically increases the efficiency of lateral gene transfer in *Streptococcus pneumoniae. Mol Microbiol* **69:** 245-253.

Johnsborg, O., and Håvarstein, L. S. (2009) Pneumococcal LytR, a protein from the LytR-CpsA-Psr family, is essential for normal septum formation in *Streptococcus pneumoniae. J Bacteriol* **191:** 5859-5864.

Jordan, S., Hutchings, M. I., and Mascher, T. (2008) Cell envelope stress response in Gram-positive bacteria. *FEMS Microbiol Rev* **32:** 107-146.

Lacks, S., and Hotchkiss, R. D. (1960) A study of the genetic material determining an enzyme in Pneumococcus. *Biochim Biophys Acta* **39:** 508-518.

Lange, R., Wagner, C., de Saizieu, A., Flint, N., Molnos, J., Stieger, M., Caspers, P., Kamber, M., Keck, W., and Amrein, K. E. (1999) Domain organization and molecular characterization of 13 two-component systems identified by genome sequencing of *Streptococcus pneumoniae*. *Gene* **237:** 223-234.

Liu, M., Hanks, T. S., Zhang, J., McClure, M. J., Siemsen, D. W., Elser, J. L., Quinn, M. T., and Lei, B. (2006) Defects in *ex vivo* and *in vivo* growth and sensitivity to osmotic stress of group A *Streptococcus* caused by interruption of response regulator gene *vicR*. *Microbiology* **152:** 967-978.

Mascher, T. (2014) Bacterial (intramembrane-sensing) histidine kinases: signal transfer rather than stimulus perception. *Trends Microbiol* **22:** 559-565.

Mehr, S., and Wood, N. (2012) *Streptococcus pneumoniae* – a review of carriage, infection, serotype replacement and vaccination. *Ped Respir Rev* **13:** 258-264.

Mohedano, M. L., Overweg, K., de la Fuente, A., Reuter, M., Altabe, S., Mulholland, F., de Mendoza, D., López, P., and Wells, J. M. (2005) Evidence that the essential response regulator YycF in *Streptococcus pneumoniae* modulates expression of fatty acid biosynthesis genes and alters membrane composition. *J Bacteriol* **187:** 2357-2367.

Ng, W. L., Robertson, G. T., Kazmierczak, K. M., Zhao, J., Gilmour, R., and Winkler, M. E. (2003) Constitutive expression of PcsB suppresses the requirement for the essential VicR (YycF) response regulator in *Streptococcus pneumoniae* R6. *Mol Microbiol* **50:** 1647-1663.

Ng, W. L., and Winkler, M. E. (2004) Singular structures and operon organizations of essential two-component systems in species of *Streptococcus*. *Microbiology* **150:** 3096-3098.

Ng, W. L., Tsui, H. C. T., and Winkler M. E. (2005) Regulation of the *pspA* virulence factor and essential *pcsB* murein biosynthetic genes by the phosphorylated VicR (YycF) response regulator in *Streptococcus pneumoniae*. *J Bacteriol* **187:** 7444-7459.

Nováková, L., Bezousková, S., Pompach, P., Spidlová, P., Sasková, L., Weiser, J., and Branny P. (2010) Identification of multiple substrates of the StkP Ser/Thr protein kinase in *Streptococcus pneumoniae. J Bacteriol* **192:** 3629-3638.

Parkinson, J. S. (2010) Signaling mechanisms of HAMP domains in chemoreceptors and sensor kinases. *Annu Rev Microbiol* **64:** 101-122.

Salazar, M. E., and Laub, M. T. (2015) Temporal and evelutionary dynamics of two-component signaling pathways. *Curr Opin Microbiol* **24:** 7-14.

Santelli, E., Liddington, R.C., Mohan, M. A., Hoch, J., and Szurmant, H. (2007) The crystal structure of *Bacillus subtilis* YycI reveals a common fold for two members of an unusual class of sensor histidine kinase regulatory proteins. *J Bacteriol* **189:** 3290-3295.

Sasková, L., Nováková, L., Basler, M., and Branny, P. (2007) Eukaryotic-type serine/threonine protein kinase StkP is a global regulator of gene expression in *Streptococcus pneumoniae*. *J Bacteriol* **189:** 4168-4179.

Stewart, V. (2014) The HAMP signal-conversion domain: static two-state or dynamic three-state? *Mol Microbiol* **91:** 853-857.

Sung, C. K., Li, H., Claverys, J.P., and Morrison, D. A. (2001) An *rpsL* cassette, Janus, for gene replacement through negative selection in *Streptococcus pneumoniae*. *Appl Environ Microbiol* **67:** 5190-5196.

Szurmant, H., Mohan, M. A., Imus, P. M., and Hoch J. A. (2007) YycH and YycI interact to regulate the essential YycFG two-component system in *Bacillus subtilis*. *J Bacteriol* **189:** 3280-3289.

Szurmant, H., Bu, L., Brooks III, C. L., and Hoch, J. A. (2008) An essential sensor histidine kinase

controlled by transmembrane helix interactions with its auxiliary proteins. *Proc Natl Acad Sci USA* **105:** 5891-5896.

Throup, J. P., Koretke, K. K., Bryant, A. P., Ingraham, K. A., Chalker, A. F., Ge, Y., Marra, A., Wallis, N. G., Brown, J. R., Holmes, D. J., Rosenberg, M., and Burnham, M. K. R. (2000) A genomic analysis of two-component signal transduction in *Streptococcus pneumoniae*. *Mol Microbiol* **35:** 566-576.

Ulijasz, A. T., Falk, S. P., and Weisblum, B. (2009) Phosphorylation of the RitR DNA-binding domain by a Ser-Thr phosphokinase: implications for global gene regulation in the streptococci. *Mol Microbiol* **71:** 382-390.

Viklund, H., Bernsel, A., Skwark, M., and Elofsson, A. (2008) SPOCTOPUS: a combined predictor of signal peptides and membrane protein topology. *Bioinformatics* **24:** 2928-2929.

Wagner, C., de Saizieu, A., Scönfeld, H. J., Kamber, M., Lange, R., Thompson, C. J., and Page, M. G. (2002) Genetic analysis and functional characterization of the *Streptococcus pneumoniae* vic operon. *Infect Immun* **70:** 6121-6128.

Wang, C., Sang, J., Wang, J., Su, M., Downey, J. S., Wu, Q., Wang, S., Cai, Y., Xu, X., Wu, J., Senadheera, D. B., Cvitkovitch, D. G., Chen, L., Goodman, S. D., and Han, A. (2013) Mechanistic insights revealed by the crystal structure of a histidine kinase with signal transducer and sensor domains. *PLoS Biol* **11:** e1001493

Wayne, K. J., Li, S., Kazmierczak, K. M., Tsui, H. C. T., and Winkler, M. E. (2012) Involvement of WalK (VicK) phosphatase activity in setting WalR (VicR) response regulator phosphorylation level and limiting cross-talk in *Streptococcus pneumoniae* D39 cells. *Mol Microbiol* **86:** 645-660.

SUPPLEMENTARY MATERIAL

Construction of* S. pneumoniae *mutant strains. To construct strain SPH259, the counter selectable Janus cassette (Sung et al., 2001) present in strain RH426 was replaced with the *comR* gene. Expression of the *comR* gene is driven by a constitutive promoter termed P_1, which is situated upstream of the native *comR* promoter (Johnsborg and Håvarstein, 2009). The fragment used for transformation was amplified with the primers AmiF and TreR using genomic DNA from strain SPH130 (Berg et al., 2011) as template.

Strain SPH260 was derived from strain SPH259 by replacing the *spr0324* gene, which encodes a truncated transposase, with the Janus cassette. The cassette and *spr0324* flanking regions was amplified from the genome of strain SPH127 (Berg et al., 2011) using the primers KHB50 and KHB53. Next, the Janus cassette was replaced with P_{pcsB}::*luc* through natural transformation giving rise to strain SPH261. The P_{pcsB} promoter was amplified from genomic RH1 DNA (Johnsborg et al., 2008) using the primer pair 89/90, while the gene encoding firefly luciferase (*luc*) was amplified from the pR424 plasmid (Chastanet et al., 2001), using the primers KHB78 and 91. These two PCR fragments were fused together by overlap extension PCR (Higuchi et al., 1988), using the primer pair 89/91. Two approximately 1000-bp fragments immediately flanking upstream and downstream regions of *spr0324* was amplified using the primer pairs KHB50/KHB51 and KHB52/KHB53, respectively, with genomic DNA from the RH1 strain as template. These two flanking regions were fused to the 5` and 3`ends of the P_{pcsB}::*luc* fragment by overlap extension PCR using the primers KHB50 and KHB53. The resulting fragment was used to transform strain SPH260 giving rise to strain SPH261.

In order to express *walK* ectopically from the P_{comX} promoter, a Janus cassette was first inserted between the *cpsO* and *cpsN* genes in SPH261, giving rise to strain SPH262. *S. pneumoniae* strain R6 does not produce a polysaccharide capsule, because part of the capsule locus has been deleted. Hence, the *cpsO* and *cpsN* capsule genes serve no function in the R6 strain. The Janus cassette plus flanking regions was amplified from genomic DNA from strain SPH154 (Berg et al., 2013) using the primers KHB31 and KHB34. Next, we set out to replace the Janus cassette in strain SPH262 with the P_{comX}::*walK* fragment. This was done by using primers 151 and 152 to amplify *walK* using genomic DNA from RH1 as template. Then, an ~1000-bp upstream fragment containing parts of *cpsO* and the P_{comX} promoter was amplified from genomic SPH158 DNA (Berg et al., 2013) using the primer pair KHB31 and KHB147. The P_{comX} promoter contains a modified Shine-Dalgarno sequence as described in Berg et al. (2013). Next, a ~1000-bp downstream fragment containing parts of *cpsN* was amplified using the primer pair KHB33/KHB34 and genomic DNA derived from RH1 as template. The upstream and downstream fragments were fused to the 5`and 3`end of the *walK* gene, respectively, using overlap extension PCR and the primers KHB31 and KBH34. The resulting DNA

fragment was used to transform strain SPH262 giving rise to strain SPH263.

To construct strain SPH264, we replaced the native *walK* gene of strain SPH263 with a Janus cassette. The cassette was amplified using the primers Kan484.F and KHB108 and genomic DNA from RH426 as template. Primer KHB108 contains the constitutive P_1 promoter, which ensures transcription of the downstream *walJ* gene. The ~1000-bp upstream and downstream regions flanking native *walK* was amplified using the primer pairs 78/76 and 153/79. Genomic DNA from strain RH1 was used as template. The upstream and downstream fragments were fused to the 5`and 3`ends of the Janus cassette, respectively, using the primers 78 and 79. The resulting DNA fragment was used to transform strain SPH263 giving rise to strain SPH264. This Janus cassette-construct was also used to replace the native *walK* gene in strain SPH261, giving rise to strain SPH265.

All strains containing a mutated or chimeric version of *walK* were constructed in a similar way. First, the Janus cassette, which replaces the native *walK* gene in strain SPH264, was exchanged with the mutated *walK* gene in question. Then, the Janus cassette previously used in the construction of strain SPH262 was used to replace P_{comX}::*walK* at the ectopic site. This Janus cassette was subsequently removed by transformation with a PCR construct containing only the flanking *cpsO/cpsN* regions. The *cpsO* and *cpsN* fragments were amplified using the primer pairs KHB31/KHB32 and 154/KHB34, respectively, with genomic DNA from RH1as template. The two fragments were fused by overlap extension PCR using the primer pair KHB31/KHB34.

Strain SPH302 was derived from SPH264 by replacing its Janus cassette with a chimeric *walK* gene containing the extracellular, transmembrane and HAMP coding regions from *S. thermophilus*. Genomic DNA from *S. thermophilus* LMG18311 (Blomqvist et al., 2006) was used as template. A fragment corresponding to base pairs 10-306 of the *walK* coding sequence was amplified using the primer pair 125/254. Next, a ~1000-bp fragment corresponding to the immediate upstream region of pneumococcal *walK* was amplified using the primers 78 and 124. The 3' part of the pneumococcal *walK* gene (starting at bp 307), including ~1000-bps downstream of the *walK* stop codon, was amplified using the primer pair 255/79. Finally, these three PCR fragments were fused by overlap extension PCR using the primers 78 and 79. The resulting DNA fragment was used to transform strain SPH264, giving rise to strain SPH302. The ectopic P_{comX}::*walk* fragment was then replaced by the Janus cassette (strain SPH303), which was subsequently deleted as explained above, resulting in strain SPH304.

When constructing strain SPH299, we followed the same procedure as in the above paragraph. The Janus cassette of strain SPH264 was replaced with the pneumococcal *walK* gene containing only the HAMP coding part of *S. thermophilus walK*. A PCR fragment corresponding to the ~1000-bp upstream region including the N-terminal region (bp 1-96 of the *walK* coding sequence)

of pneumococcal *walK* was amplified using the primers 78 and 168 and genomic DNA from RH1 as template. Next, a fragment encoding the HAMP domain from *S. thermophilus* fused to pneumococcal *walK* was amplified from genomic SPH302 DNA using the primers 169 and 79. These two fragments were then fused using the primer pair 78/79, giving rise to strain SPH299. The ectopic P_{comX}::*walk* fragment was then replaced by the Janus cassette (strain SPH300), which was subsequently deleted as explained above, resulting in strain SPH301.

Strain SPH296 was constructed by replacing the Janus cassette in SPH264 with a chimeric *walK* gene containing the extracellular and transmembrane coding regions of *S. thermophilus walK* fused to the rest of the pneumococcal *walK* gene. Base pairs 1-90 of the chimeric *walK* gene in strain SPH302 including the upstream ~1000-bp region was amplified using the primers 78 and 250. Base pairs 91-1347 of pneumococcal *walK* including the ~1000-bp downstream part was amplified with the primers 251 and 79 using genomic DNA from RH1 as template. The two fragments were fused using the primer pair 78/79. Finally, the ectopic P_{comX}::*walk* fragment was then replaced by the Janus cassette (strain SPH297), which was subsequently deleted as explained above, resulting in strain SPH298.

Genomic DNA from strain SPH296 was used as starting point when constructing SPH290 and SPH293. To make strain SPH290, the Janus cassette in strain SPH264 was replaced with a chimeric *walK* gene encoding the extracellular domain of WalK from *S. thermophilus*. A fragment containing the ~1000-bp upstream region and the sequence coding for the N-terminal part of the chimeric WalK in SPH296 (bp 1-33) were amplified using the primers 78 and 268. The DNA sequence encoding the C-terminal part of WalK (bp 34-1347) plus the ~1000-bp downstream from the *walK* gene was amplified using the primers 269 and 79 with genomic DNA from RH1 as template. These two fragments were fused using the primer pair 78/79. The resulting fragment was used to transform strain SPH264, giving rise to strain SPH290. Then, the ectopic P_{comX}::*walk* fragment was replaced by the Janus cassette (strain SPH291), which was subsequently deleted as explained above, resulting in strain SPH292.

In strain SPH293, the Janus cassette in SPH264 was replaced with a chimeric *walK* gene encoding a pneumococcal WalK in which the transmembrane domain had been replaced by the corresponding sequence from the *S. thermophilus walK*. The ~1000 upstream region and the first 39 base pairs of *walK* was amplified using the primers 78 and 266 and genomic DNA from RH1 as template. Then, a fragment corresponding to the 3'region of the chimeric *walK* gene in strain SPH296 (from bp 40) and ~1000-bp downstream of the gene was amplified using the primers 267 and 79. The two fragments were fused using the primer pair 78/79. Finally, the ectopic P_{comX}::*walk* fragment was then replaced by the Janus cassette (strain SPH294), which was subsequently deleted as explained above, resulting in strain SPH295.

Strain SPH266 was constructed by replacement of the Janus cassette in SPH264 with *walK*^{T222A}. The DNA sequence encoding aa 1-222 of WalK plus the 1000 bp stretch upstream of *walK* was amplified using the primers 78 and 159 and genomic DNA from RH1 as template. The DNA sequence encoding the C-terminal part of WalK (aa 216 - 449) and the ~1000-bp downstream region was amplified using the primers 160 and 79, also with genomic DNA from RH1 as template. The overlapping primers 159 and 160 both contain the base substitutions giving rise to the T222A mutation. The two PCR fragments were fused together using the primer pair 78/79. The resulting fragment was used to transform strain SPH264, giving rise to strain SPH266. Then, the ectopic P_{comX}::*walk* fragment was replaced by the Janus cassette (strain SPH267), which was subsequently deleted as explained above, resulting in strain SPH268.

Strain SPH269 was constructed by replacing the Janus cassette in strain SPH264 with *walK*^{E33A}. First a PCR fragment was generated by amplifying the upstream ~1000-bp and the sequence encoding aa 1-33 of WalK using primers 78 and 311 and genomic DNA from RH1 as template. The sequence encoding the C-terminal part of WalK (aa 27-449) plus ~1000-bp downstream of *walK* was amplified using the primers 312 and 79 from the genome of RH1. The overlapping primers 311 and 312 both contain the base substitutions giving rise to the E33A mutation. The two PCR fragments were fused using the primer pair 78/79. The resulting fragment was used to transform strain SPH264, giving rise to strain SPH269. Then, the ectopic P_{comX}::*walk* fragment was replaced by the Janus cassette (strain SPH270), which was subsequently deleted as explained above, resulting in strain SPH271.

SPH272 was derived from SPH264 by replacing the Janus cassette with *walK*$^{E33A, N34A}$. First a PCR fragment was generated by amplifying ~1000-bp upstream of *walK* and the first 102 bp of the *walK* gene from the RH1 genome using the primers 78 and 313. The remaining part of *walK* (bp 81-1347) plus a ~1000-bp stretch downstream of *walK* was amplified using primers 314 and 79 and genomic DNA from RH1 as template. The overlapping primers 313 and 314 both contain the base substitutions giving rise to the E33A and N34A mutations. The two PCR fragments were fused using the primer pair 78/79. The resulting fragment was used to transform strain SPH264, giving rise to strain SPH272. Finally, the ectopic P_{comX}::*walk* fragment was replaced by the Janus cassette (strain SPH273), which was subsequently deleted as explained above, resulting in strain SPH274.

To construct strain SPH275 the Janus cassette in strain SPH264 was replaced with *walK*^{F23A}. A PCR product comprising ~1000-bp upstream of *walK* and the first 69 bp of the *walK* gene was amplified using the primer pair 78/315. The remaining part of *walK* (bp 47-1347) plus ~1000 bp downstream of the gene was amplified using the primer pair 316/79. Genomic DNA form RH1 served as template in both PCR reactions. The overlapping primers 315 and 316 both contain the base substitutions giving rise to the F23A mutation. The two PCR fragments

were fused using the primer pair 78/79. The resulting fragment was used to transform strain SPH264, giving rise to strain SPH275. Finally, the ectopic P_{comX}::*walk* fragment was replaced by the Janus cassette (strain SPH276), which was subsequently deleted as explained above, resulting in strain SPH277.

Strain SPH278 was made by replacing the Janus cassette with *walK*^{G22A} in strain SPH264. A DNA fragment starting ~1000-bp upstream of *walK* and ending at bp 66 in the *walK* gene was amplified using the primers 78 and 317. Base pairs 43-1347 of *walK* plus the ~1000-bp downstream region was amplified using the primer pair 318/79. Genomic DNA from RH1 was used as template in both PCR reactions. The overlapping primers 317 and 318 both contain the base substitutions giving rise to the G22A mutation. The two PCR fragments were fused using the primer pair 78/79. The resulting fragment was used to transform strain SPH264, giving rise to strain SPH278. Finally, the ectopic P_{comX}::*walk* fragment was replaced by the Janus cassette (strain SPH279), which was subsequently deleted as explained above, resulting in strain SPH280.

Strain SPH281 was constructed by replacing the Janus cassette in strain SPH264 with *walK*$^{R12A, D13A}$. To make the whole *walK*$^{R12A, D13A}$ gene fragment, a PCR product consisting of bp 1-64 of *walK* and its ~1000 bp upstream region (amplified using primers 78/187) was fused to a fragment consisting of bp 34-1347 of *walK* plus the ~1000 bp downstream region (amplified using primers 186/79) using the primer pair 78/79. Genomic DNA from RH1 served as template. The overlapping primers 187 and 186 both contain the base substitutions giving rise to the R12A and D13A mutations. The resulting fragment was used to transform strain SPH264, giving rise to strain SPH281. Finally, the ectopic P_{comX}::*walk* fragment was replaced by the Janus cassette (strain SPH282), which was subsequently deleted as explained above, resulting in strain SPH283.

The SPH284 strain was made from strain SPH264 by replacing its Janus cassette with *walK*$^{R36A, D37A}$. A *walK*$^{R36A, D37A}$ construct was made by amplifying the upstream ~1000-bp and the first 135 bp of *walK* from the RH1 genome using primers 78 and 189. This fragment was fused to a PCR product consisting of bp 106-1347 of *walK* plus ~1000 bp downstream from this gene (amplified using the primer pair 188/79) by using the primer pair 78/79. The overlapping primers 188 and 189 both contain the base substitutions giving rise to the R36A and D37A mutations. The resulting fragment was used to transform strain SPH264, giving rise to strain SPH284. Finally, the ectopic P_{comX}::*walk* fragment was replaced by the Janus cassette (strain SPH285), which was subsequently deleted as explained above, resulting in strain SPH286.

To construct strain SPH287, the Janus cassette of strain SPH264 was replaced with *walK*$^{R12A, D13A, R36A, D37A}$. A fragment corresponding to the ~1000 bp upstream region of *walK* including the first 135 bp of *walK*$^{R12A, D13A}$ was amplified from the genome of strain SPH281 using the primers 78 and 189. This fragment was fused to a fragment comprising bp 106-1347 of *walK*

plus ~1000 bp downstream of the *walK* gene (amplified from the RH1 genome using primers 188 and 79) using primer 78 and 79. The overlapping primers 188 and 189 both contain the base substitutions giving rise to the R36A and D37A mutations. The resulting fragment was used to transform strain SPH264, giving rise to strain SPH287. Finally, the ectopic P_{comX}::*walk* fragment was replaced by the Janus cassette (strain SPH288), which was subsequently deleted as explained above, resulting in strain SPH289.

SPH305 was constructed by replacing the Janus cassette in SPH264 with *walK*ΔTM. In *walK*ΔTM, the sequence coding for the most of the extracellular domain and the transmembrane segment (aa 4-32) has been removed. First, a PCR fragment consisting of bp 1-9 of *walK* and ~1000-bp of the immediate upstream region was amplified using primers 78/124 and genomic DNA from strain RH1 as template. This fragment was fused to a fragment consisting of bp 97-1347 of *walK* plus ~1000 bp of the downstream region (amplified using primers 129/79) using overlap extension PCR and the primer pair 78/79. Finally, the ectopic P_{comX}::*walk* fragment was replaced by the Janus cassette as explained above, resulting in strain SPH306.

The SPH307 strain was constructed from strain SPH261 by replacing the *stkP* gene with the Janus cassette. The Janus cassette was amplified from strain RH426 with the primers Kan484.F and RpsL41.R. This fragment was fused with flanking PCR fragments corresponding to the ~1000 bp immediate upstream region of *stkP* (amplified using primers KHB410 and 321 with genomic DNA from strain RH1) and the ~1000 bp immediate downstream region of *stkP* (amplified using primers 322 and KHB411 with genomic DNA from RH1) using the primer pair KHB410/KHB411.

Strain SPH308 was derived from strain SPH307 by removal of the Janus cassette. This was done by transformation with a PCR fragment containing only the flanking regions of the *stkP* gene. First, a fragment consisting of ~1000 bp immediately upstream of *stkP* was amplified using the primers KHB410 and 323 with genomic DNA from strain RH1 as template. This fragment was fused to a PCR fragment comprising the ~1000 bp downstream region of *stkP* (amplified using primers 324 and KHB411 and genomic DNA from strain RH1), using the primer pair KHB410/KHB411. The resulting fragment was used to transform strain SPH307, giving rise to strain SPH308. Strain SPH309 was made from strain SPH308 by replacing its *walK* gene with a Janus cassette. The fragment used to transform strain SPH308 was amplified from strain SPH264 using primers 78 and 79.

SPH310 was constructed by replacing the *stkP* gene in strain SPH268 with a Janus cassette. This fragment used for transformation of strain SPH268 was amplified using the primers KHB410 and KHB411 and genomic DNA from strain SPH307 as template.

Strain SPH311 was derived from strain SPH261 by replacing its *pnpR* gene with the

Janus cassette. The Janus cassette in strain RH426 (amplified with primers Kan484.F and Rpsl41.R.) was fused to PCR fragments consisting of ~1000 bp immediately upstream and downstream of *pnpR* (amplified from RH1 genomic DNA with the primer pairs 270/272 and 273/271, respectively). Next, the Janus cassette of SPH311 was removed by transformation with a fragment consisting only of the flanking regions of *pnpR*, giving rise to strain SPH312. This fragment was made by fusing the ~1000 bp upstream (primer 270 and 274) and downstream (primer 271 and 275) regions of *stkP* using the primers 270 and 271. Genomic DNA from RH1 was used as template.

Strain SPH313 was derived from strain SPH312 by replacing its *walK* gene with the Janus cassette. The fragment used for transforming strain SPH312 was amplified from the genome of strain SPH264 using the primers 78 and 79.

To construct strain SPH314, *stkP* in strain SPH312 was replaced by a Janus cassette. The fragment containing the Janus cassette and the ~1000 bp flanking regions of *stkP* was amplified from strain SPH307 using primers KHB410 and KHB411. Next, strain SPH315 was obtained by deleting the Janus cassette in SPH314 with a fragment corresponding to only the flanking regions of *stkP*. This fragment was amplified with primers KHB410 and KHB411and genomic DNA from strain SPH308 as template. Strain SPH316 was derived from SPH315 by replacing its *walK* gene with a Janus cassette. The fragment used for transformation of SPH315 consisted of the Janus cassette and the ~1000 bp regions flanking *walk.* The fragment was amplified from genomic SPH264 DNA with the primers 78 and 79.

Strain SPH317 was constructed from strain SPH307 by replacing its Janus cassette with the $stkP^{K42M}$ gene. A fragment consisting of ~1000 bp upstream and the first 126 bp of *stkP* was amplified with the primers KHB410 and 320. This fragment was fused to a fragment consisting of bp 107-1980 of *stkP* plus its downstream ~1000 bp region using primers 319 and KHB411. Genomic DNA from RH1 served as template in both PCR reactions. The overlapping primers 319 and 320 both contain the base substitutions giving rise to the K42M mutation in StkP. The two fragments were fused using primer pair KHB410 and KHB411.The resulting fragment was used to transform strain SPH307, giving rise to strain SPH317.

Table S1

Primers	Oligonucleotide sequence (5` → 3`)	References
KHB31	ATAACAAATCCAGTAGCTTTGG	Berg et al., 2011
KHB32	GGTCTAGAGATGATTTTAATTAC	Berg et al., 2011
KHB33	TTTCTAATATGTAACTCTTCCCAAT	Berg et al., 2011
KHB34	CATCGGAACCTATACTCTTTTAG	Berg et al., 2011
KHB50	CCGATGCAGAAATGGTTGAG	Berg et al., 2011
KHB51	GATAATCGTACATCTGAAGCTC	Berg et al., 2011
KHB52	TTGGTAAACTACGAACCGCTAG	Berg et al., 2011
KHB53	TCATTGTAAGCGCCCAATAAC	Berg et al., 2011
KHB78	ATGAGATCCGCCAAAAACATA	This work
KHB108	AATGGAACCTCCACAAGTATTTTCTAGTATTATAGC ACATTTAACTTTCCTTATGCTTTTGGAC	Berg et al., 2013
KHB147	TGAACCTCGAATAATAAATATAAATTCTGTAATTAG	Berg et al., 2013
KHB410	AGAAATATTAGGTAGTGTTTGTC	This work
KHB411	CCAGACAGTCATGCCCAAAATC	This work
Kan484.F	GTTTGATTTTTAATGGATAATGTG	Johnsborg et al., 2008
RpsL41.R	CTTTCCTTATGCTTTTGGAC	Johnsborg et al., 2008
AmiF	CGGTGAAGGAAGTAAGAAGTTT	Johnsborg and Håvarstein, 2009
TreR	GTGACGGCAGTCACATTCTC	Johnsborg and Håvarstein, 2009
76	CACATTATCCATTAAAAATCAAACTCAAGCATTATTT CTCATGTAATA	This work
78	TTGTGTCTTCTGACTATTTTTTG	This work
79	ATATCTCTGTCAATGGTGTTG	This work
89	CAGATGTACGATTATCGCTTGGTACCGACGATGATT	This work
90	TATGTTTTTGGCGGATCTCATATTACGTAGATACTCCTTCTTTT	This work
91	CTAGCGGTTCGTAGTTTACCAATTACAATTTGGGCTTTCCGC	This work
124	ATCAAGCATTATTTCTCATGTAATA	This work
125	ATTACATGAGAAATAATGCTTGATATTGGCTTAAATA TTACAAGCTTT	This work
129	TATTACATGAGAAATAATGCTTGATGAAAATAGACGT GATAATATTCA	This work

151	ATTTATATTTATTATTCGAGGTTCAATGCTTGATTTAC TGAAACAAAC	This work
152	ATTGGGAAGAGTTACATATTAGAAACTAGTCTTCTAC TTCATCCTC	This work
153	AAATACTTGTGGAGGTTCCATTATGCAGTGAAAGAAG AAGTATG	This work
154	GTAATTAAAATCATCTCTAGACCTTTCTAATATGTAAC TCTTCCCAAT	This work
159	TGCCCGTAACTCATGGCTAACATT	This work
160	GTTAGCCATGAGTTACGGGCACCTCTGACTAGCGTAAAATC	This work
168	CAGTAATAAGAGGGTCACAAC	This work
169	GTTGTGACCCTCTTATTACTGCGTGATTATCAACAGGTCAAA	This work
186	GCAGCATTTATCTTTATCCTGATTTTGTTAG	This work
187	CTAACAAAATCAGGATAAAGATAAATGCTGCGGTAAAAAT GGTTTGTTTCAGTA	This work
188	GCAGCAAATATTCAGTTGAAGCAAATCAAT	This work
189	ATTGATTTGCTTCAACTGAATATTTGCTGCTCTATTTTCCAG TAATAAGAGG	This work
250	TAGAAAAATGAAATAGAAAGCAAC	This work
251	GTTGCTTTCTATTTCATTTTTCTATTACTGGAAAATAG ACGTGATAA	This work
254	GTACGAAAGAACAGATGATAAG	This work
255	CTTATCATCTGTTCTTTCGTACATGACAGATGGGGTTCTTGC	This work
266	ATCTCTGGTAAAAATGGTTTGTT	This work
267	AACAAACCATTTTTACCAGAGATCTGGCCTTACTCTTTATGCTC	This work
268	TTCAAAGCTTGTAATATTTAAGCC	This work
269	GGCTTAAATATTACAAGCTTTGAATTTATCTTTATCCTGATT TTGTTAG	This work
270	CAACCTTGCTTCTTTCCTTAG	This work
271	CGTCCATTGTATAGGCATTTG	This work
272	CACATTATCCATTAAAAATCAAACCTATTATCTCCTATTGGTAACAT	This work

273	CGTCCAAAAGCATAAGGAAAGATGAAACGCTACCTTCAATTTTG	This work
274	CTATTATCTCCTATTGGTAACAT	This work
275	ATGTTACCAATAGGAGATAATAGATGAAACGCTACCTTCAATTTTG	This work
311	TGCCAGTAATAAGAGGGTCACAAC	This work
312	GTGACCCTCTTATTACTGGCAAATAGACGTGATAATATTCAGTTG	This work
313	TGCTGCCAGTAATAAGAGGGTCACAAC	This work
314	ACCCTCTTATTACTGGCAGCAAGACGTGATAATATTCAGTTGAA	This work
315	TGCACCTAACAAAATCAGGATAAAGA	This work
316	TATCCTGATTTTGTTAGGTGCAATCCTTGTTGTGACCCTCTTA	This work
317	TGCTAACAAAATCAGGATAAAGATAAAA	This work
318	TCTTTATCCTGATTTTGTTAGCATTCATCCTTGTTGTGACCCTC	This work
319	GGAAGAAGTGGCAGTGATGGTTCTGAGGACCAACTACC	This work
320	CATCACTGCCACTTCTTCCCCA	This work
321	AATTGCACATCTCAAATAACTACTCATTCTGCATCCTCCTCGT	This work
322	CGTCCAAAAGCATAAGGAAAGAAGCAGATGGATAATCAAAATGA	This work
323	TCATTCTGCATCCTCCTCGT	This work
324	ACGAGGAGGATGCAGAATGAAAGCAGATGGATAATCAAAATGA	This work

REFERENCES

Berg, K. H., Biørnstad, T. J., Straume, D., and Håvarstein, L. S. (2011) Peptide-regulated gene depletion system developed for use in *Streptococcus pneumoniae. J Bacteriol* **193:** 5207-5215.

Berg, K.H., Stamsås, G.A., Straume, D., and Håvarstein LS. (2013) Effects of low PBP2b levels on cell morphology and peptidoglycan composition in *Streptococcus pneumoniae* R6. *J Bacteriol* **195:** 4342-4354.

Blomqvist, T., Steinmoen, H., and Håvarstein, L. S. (2006) Natural genetic transformation: a novel tool for efficient genetic engineering oft he dairy bacterium *Streptococcus thermophilus*. *Appl Environ Microbiol* **72:** 6751-6756.

Chastanet, A., Prudhomme, M., Claverys, J. P., and Msadek, T. (2001) Regulation of *Streptococcus pneumoniae clp* genes and their role in competence development and stress survival. *J Bacteriol* **183:** 7295-7307.

Higuchi, R., Krummel, B., and Saiki, R. K. (1988) A general method of *in vitro* preparation and specific mutagenesis of DNA fragments: study of protein and DNA interactions. *Nucleic Acids Res* **16:** 7351-7367.

Johnsborg, O., Eldholm, V., Bjørnstad, M. L., and Håvarstein, L. S. (2008) A predatory mechanism dramatically increases the efficiency of lateral gene transfer in *Streptococcus pneumoniae. Mol Microbiol* **69:** 245-253.

Johnsborg, O., and Håvarstein, L. S. (2009) Pneumococcal LytR, a protein from the LytR-CpsA-Psr family, is essential for normal septum formation in *Streptococcus pneumoniae. J Bacteriol* **191:** 5859-5864.

Sung, C. K., Li, H., Claverys, J.P., and Morrison, D. A. (2001) An *rpsL* cassette, Janus, for gene replacement through negative selection in *Streptococcus pneumoniae*. *Appl Environ Microbiol* **67:** 5190-5196.